OROGRAPHIC PRECIPITATION MODEL FOR HYDROMETEOROLOGICAL USE

BY
J. OWEN RHEA

Atmospheric Science
PAPER NO.
287

US ISSN 0067-0340

DEPARTMENT OF ATMOSPHERIC SCIENCE
COLORADO STATE UNIVERSITY
FORT COLLINS, COLORADO

OROGRAPHIC PRECIPITATION MODEL FOR HYDROMETEOROLOGICAL USE

by

J. Owen Rhea

Research report supported by the

Rocky Mountain Forest and Range Experiment Station
Forest Service
U.S. Department of Agriculture
Under Cooperative Agreements
16-332-CA and 16-547-CA

Department of Atmospheric Science

Colorado State University

Fort Collins, Colorado

March, 1978

Atmospheric Science Paper No. 287

NOTICE

This report consists in its entirety of a Ph. D. dissertation by the author, completed and accepted in July, 1977.

ABSTRACT

OROGRAPHIC PRECIPITATION MODEL FOR HYDROMETEOROLOGICAL USE

Research was performed to determine the ability to diagnose the effect of topography on winter precipitation for western Colorado over various time periods for differing wind regimes, employing upper air data and a fine-mesh topographic grid.

To accomplish the objectives, a simple, operationally-oriented orographic precipitation model was developed. The model is two-dimensional, steady state, and multi-layer. It follows parcels at layer mid-points through topographically-induced moist adiabatic ascents and descents. Layer budgets of water substance are calculated by (a) allowing precipitation of a constant fraction of total cloud water (i. e., local condensation plus imported cloud water), (b) carrying the remainder downstream where it and additional condensate can partially precipitate, and (c) permitting evaporation of cloud water upon descent and of precipitation falling into subsaturated layers. A key feature of this approach is its representation of precipitation shadowing by upstream barriers (when used with a different topographic grid for each wind direction).

Airflow is constrained to two dimensions and the complications of topographic effects on the flow are minimized by using a set of stability-dependent damping factors to adjust the vertical displacement of layers. Effects of large-scale vertical motion are added to those of topography.

The model was tested for western Colorado using 13 winter seasons of twice daily upper air measurements as input. Results were summed

and compared to observed spring and summer runoff from watersheds of varying size. Correlation coefficients between seasonally-summed model watershed precipitation and observed runoff range mainly between 0.75 and 0.94. On a daily basis large discrepancies between model and observation sometimes exist, but model frequency distribution of daily precipitation totals appears realistic.

A 13 year model mean precipitation map was found to agree quite well in mountainous areas with an isohyetal map constructed by ESSA of the U.S. Department of Commerce using precipitation and snow-course data with empirical correlation to topographic features. The model underestimated broad valley precipitation in most cases.

Test quantitative precipitation forecasts (QPF's) were made (and communicated daily to the U. S. Forest Service) from November, 1975, to March, 1976, using wind direction-dependent model pattern maps as objective aids. Isohyets on these pattern maps were calibrated using forecast wind speed, moisture depth, duration, areal coverage, and cloud temperature. Skill scores for 24 hour QPF's ranged from 0.56 to 0.87.

The derived method has utility (a) in assessing the average magnitude and the inter-season variation of topographic effects on winter precipitation in western Colorado and (b) as an objective aid for quantitative precipitation forecasting. It has substantial potential utility as input to hydrologic process models for streamflow forecasting. The basic approach should be transferable to other topographically complex areas which are dominated by stratiform precipitation.

John Owen Rhea
Department of Atmospheric Science
Colorado State University
Fort Collins, Colorado 80523
Summer, 1977

ACKNOWLEDGMENTS

A note of thanks is due a number of individuals and organizations for their help and support during the course of this research. Without the efforts by Dr. Pete Martinelli, Jr. and the funding by the U.S. Forest Service, this research would not have occurred. Mr. Arthur Judson provided constant moral support by his sense of humor and his interest in the project. I am grateful for the helpful suggestions and constructive criticism provided by my graduate committee members and my advisor, Professor Lewis O. Grant. In particular, Drs. Charles Leaf and James Meiman were helpful in indicating points of importance and applicability of the research to snow hydrology.

I am especially grateful for the support of my wife, Rosemary, who provided both the majority of the required data management programming and constant encouragement.

Ms. Lucy McCall drafted the figures for the text, while a variety of people, principally Ms. Janis Davis and Ms. Janet Lytton, typed the manuscript.

The great majority of computer time was supplied by the National Center for Atmospheric Research, which is sponsored by the National Science Foundation. Without this support, the study would have been greatly limited.

This research was sponsored by the Rocky Mountain Forest and Range Experiment Station, Forest Service, U. S. Department of Agriculture under Cooperative Agreements 16-332-CA and 16-547-CA with Colorado State University, and was supported in part by the National Science Foundation under Grant ERT 71-01885-A03.

TABLE OF CONTENTS

LIST OF TABLES

LIST OF TABLES (Continued)

LIST OF FIGURES

LIST OF SYMBOLS

ΔC	Increment of adiabatic condensation
E	Precipitation efficiency
e_s	Saturation vapor pressure
g	Gravitational acceleration
Δh	Vertical displacement of streamline
L	Latent heat of vaporization
1	Subscript denoting layer computations
P	Pressure
Q	Cloud water mixing ratio
q	Water vapor mixing ratio
q_s	Water vapor saturation mixing ratio
R_T	Total precipitation
R_d	Precipitation due to large-scale vertical motion, also gas constant for dry air
R_c	Precipitation due to convection
R_o	Precipitation due to orographic lifting
r	Precipitation: also, relative humidity
$\dot{r}$	Precipitation rate
S	Scorer parameter
T	Temperature
T_o	Base state temperature
T_c	Unlifted "cloud top" temperature
t	Time
V	Horizontal wind speed

V_o	Undisturbed current flow speed
w_{os}	Surface value of orographic vertical velocity
ΔX	Distance increment along direction of flow
z	Height
$\Delta z_{l.s.}$	Vertical displacement due to large-scale vertical motion
α	Specific volume of air
β	Static stability parameter for unsaturated air
β_E	Static stability parameter for cloudy air
γ_d	Dry adiabatic lapse rate
γ_m	Moist adiabatic lapse rate
ε	Ratio of molecular weights of water and dry air
θ	Potential temperature
$\theta_{\equiv}$	Equivalent potential temperature
ρ_w	Density of liquid water

1.0 INTRODUCTION

1.1 Problem Description

Accurate diagnostic and predictive knowledge of winter precipitation distribution in mountainous regions is of considerable importance to a wide range of the population. It is particularly significant for avalanche prediction, highway maintenance, and water supply forecasting.

The influence of terrain on precipitation in mountainous regions is readily recognized but quantifying the effect remains difficult, and this constitutes the main problem addressed in this paper. Specifically, the main goal of this research is to determine the ability to diagnose the magnitude of topographic effects on winter precipitation for Colorado under varying wind regimes, using routinely available upper air data and a fine mesh topographic grid as computational input.

In mountainous terrain, total precipitation, R_T, can be symbolically expressed in terms of component processes as

$$R_T = R_d + R_c + R_o \tag{1-1}$$

Where

R_d = Large-Scale Vertical Motion Precipitation Component

R_c = Convective Precipitation Component

R_o = Orographic (Forced Lifting) Precipitation Component

These component processes have been discussed by Elliott and Shaffer (1962), Hjermstad (1970), Chappell (1970), and others.

Without specifying the exact area of deposition, a generalized precipitation formula can be written as

$$R = \frac{E}{\rho_w g} \int_o^t \int_{P_1}^{P_2} \frac{dq_s}{dz} \, w dP dt \tag{1-2}$$

where

$\frac{dq_s}{dz}$ = the height change of saturation specific humidity following a parcel

w = the vertical motion, $\frac{dz}{dt}$

$\int_{P_1}^{P_2} dP$ = pressure depth of potentially precipitating saturated air column

$\int_{o}^{t} dt$ = duration of the process

ρ_w = density of water (1g cm^{-3})

g = gravitational acceleration

E = precipitation efficiency (proportion of the condensate which precipitates)

For air with horizontal velocity $\frac{dx}{dt}$, moving across terrain having slope $\frac{\partial z}{\partial x}$, the forced orographic vertical motion, w_{os}, (at the surface is given by

$$w_{os} = (\frac{\partial z}{\partial x}) \frac{dx}{dt} . \qquad (1\text{-}3)$$

This vertical motion changes with height as a function of stability (the more stable the air the more the resistance to vertical motion), but it is true in general that a most favorable condition for substantial orographic precipitation consists of strong winds moving deep layers of moist air up steeply sloping terrain. Consequently, the passage of closed low centers across mountainous areas may result in only small amounts of precipitation despite the favorable field of large-scale rising motion. In fact, orographic and large scale vertical motion may be of opposite signs depending on the orientation of topographic barriers.

Orographic vertical motion is frequently an order of magnitude larger than that associated with baroclinic waves (i. e., 10-100 cm sec^{-1} compared to 1-10 cm sec^{-1}), while vertical motion in embedded convection may even exceed 100 cm sec^{-1}. However, both orographic and convective element vertical motions are small scale phenomena, implying action on a given air parcel for only a short time, whereas the large-scale vertical motion field slowly displaces a given parcel for an extended period. Thus each may have a considerable influence on the total precipitation process.

In many complex terrain areas, the terrain influence exerts the dominant control because it provides (1) a more persistent orographic vertical motion field and (2) a forced lifting zone for release of convection. Evidence of this topographic dominance is clearly seen in ridge-to-valley winter precipitation ratios in the mountainous western U.S. which are observed to range mainly between 2 and 10/1 (Hjermstad, 1970; Roger, 1970; Rhea, 1967; Elliott and Shaffer, 1962; Peck and Williams, 1962). These ratios show large variability, however, over short time periods due partially (a) to the passage of meso-scale convergence bands (with a periodicity of 3 to 5 hours) as observed by Elliott and Hovind (1964) in California and by Rhea, et al. (1969) in Colorado at much higher altitudes and (b) to varying wind direction effects on orographic precipitation patterns.

Numerous other important factors complicate the specification of point precipitation, especially for snowfall, including (1) the "precipitation shadowing" effects of upstream topography, (2) the probable complex variability of precipitation efficiency for converting condensate to precipitation, and (3) increasingly large errors in snowfall

measurement as wind increases, thus precluding accurate knowledge of historical values of precipitation for calibrating precipitation models.

Despite these complexities, mountain precipitation regimes can be studied systematically with the objective of assessing the importance of a given precipitation contributing factor. This paper concentrates on orographic factors.

1.2 Background

Many hydrologic studies have used the observational fact that precipitation in many mountainous areas (e.g., much of the western U.S.) increases with elevation to develop local linear regression relationships between precipitation and elevation. Interesting examples of this approach can be found in studies by Peck and Brown (1962) for Utah, Hounam (1958) for a part of Australia, and Schermerhorn (1967) for Washington and Oregon. A frequent observational comment from such studies is that the relationships hold only for a relatively localized area and work particularly well for areas with similar terrain aspect.

Spreen (1947) indirectly accounted for variations in orographic precipitation production and explained up to 88% of the variance in winter precipitation between selected stations over western Colorado through graphical multiple correlation to the terrain factors of elevation, maximum terrain slope within 5 miles of the station, exposure (relative freedom from obstructing barriers within 20 miles), and orientation of exposure. He did not attempt to directly relate these factors to any causal meteorological flow features, and thus his work is not transferable for use on a year-by-year basis.

Elliott and Shaffer (1962) used a formulation for orographic precipitation and California coastal soundings for data input. They obtained

single correlation coefficients between 0.44 and 0.63 for observed versus calculated hourly precipitation in the San Gabriel and Santa Ynez Mountains. Higher r-values of 0.5 to 0.8 were obtained when replacing the theoretical equation with a multiple regression formula with parameters of stability, temperature (and therefore condensate supply rate), and wind speed and direction as the independent variables. Finally when empirically accounting for the non-orographic precipitation component, r-values ranged from 0.67 to 0.94.

In the last fifteen years a number of orographic precipitation numerical models have been developed. Most of these are two dimensional in nature (in the x, z plane), e.g., (Myers, 1962; Sarker, 1967; Willis, 1970; Fraser et al., 1973; Plooster, 1974; and Young, 1974), but a few are three dimensional (Colton, 1975; Nickerson and Chappell, 1975). At least one (Elliott, 1969) consists of both two-dimensional and three-dimensional versions.

Most of the two-dimensional models are steady state and obtain a flow solution (and thus streamline configuration) by invoking perturbation theory, assuming adiabatic (except for latent heat), frictionless flow over an ideal mountain of sinusoidal form, and requiring that the lower boundary streamline follow the surface of the ideal mountain. Such flow perturbations are periodic with strong winds, decreasing vertical shear aloft and small values of stability contributing to large values of vertical wave length. Exceptions to this usual flow solution for the two-dimensional models are found in those by Myers (1962) and Elliott (1969), who invoke the Bernoulli, mass continuity, hydrostatic, and thermodynamic energy equations to arrive at streamline configurations across a mountain of arbitrary shape (thus adding the advantage of using

realistic topography). The terrain-induced perturbation amplitude in their solution also varies in the vertical with the altitude of the first horizontal streamline (nodal surface) again shown to be positively related to windspeed and inversely dependent on static stability. The three-dimensional models have the advantage of more realistic simulation of the overall topographic effects on the flow but the serious operational disadvantage (with present computer speeds) of requiring 10 to 100 times more computational time to obtain a flow solution as compared to the simpler two-dimensional types.

Treatment of atmospheric water substance in these models varies from the assumption that all water which condenses precipitates (Myers, 1962; Sarker, 1967; Colton, 1975) to rather complex cloud physics considerations (e.g., Young, 1974; Nickerson and Chappell, 1975).

With the exception of those by Sarker (1967), Myers (1962, and Colton (1975), these models were primarily constructed as aids to cloud physics or weather modification research.

In a test (over a winter season) of the model by Myers (1962) linear correlation of model computations to the average six hourly precipitation for a group of stations on the western (upwind) slope of the Sierra Nevada mountains was 0.69 when using the observed Oakland, California, upper air sounding as input.

Sarker (1967) also obtained good agreement between model and observed rainfall profiles over the western Ghats of India using observed upwind sounding data as input.

In preliminary tests by Colton (1976), the two-dimensional version of the model depicted the precipitation amounts observed over a watershed rather well.

More details of these various models are discussed throughout the text as they apply to this current study.

In other empirical studies, Wilson and Atwater (1972) showed the importance of wind direction at hill-top level on precipitation patterns in Connecticut. Similar results were obtained by Rhea (1973) for a part of mountainous southwest Colorado.

An earlier study by Rhea, et al. (1969) for all of western Colorado and extreme eastern Utah implied rather severe "rain-shadowing" effects of upstream barriers on downstream mountains and valleys for certain 700-mb level (near mountain top) wind directions.

Finally, a preliminary study (Rhea and Grant, 1974) showed that for 28 snowcourse sites scattered throughout western Colorado (at elevations $\geq$ 9000 ft (2700 m MSL)), 80% of the inter-station variance in long term average 1 April water equivalent could be explained when considering (a) the average topographic slope over the first twenty kilometers upwind of each station for each 30° wind direction class, (b) the long term frequency of "wet" 700-mb wind occurrence by direction for November-March, and (c) the number of upstream "shadowing" barriers (relative to each station) within the bounds of Colorado, for each direction class.

As a result of the above research (Rhea and Grant, 1974), a wholly objective method of quantitatively considering the effects of upstream barriers, nearby topographic slope, and the inherent wind direction dependence of these factors was sought, leading to the present study.

2.0 OBJECTIVES

The objectives of the research were to (1) determine the ability to assess the average magnitude (and the inter-season variations) of topographic effects on winter season precipitation in the mountainous section of Colorado using only routinely available upper air information and a fine mesh topographic grid, (2) evaluate the agreement between precipitation computed by the method and spring and summer runoff from mountain watersheds of varying size, and (3) test the applicability of the derived method for short term forecasting of orographic snowfall.

3.0 RESEARCH APPROACH

3.1 Guidelines and Limitations

3.1.1 Key Considerations

Since the objective was to develop an operationally-oriented computation scheme for orographic precipitation for hydrological and/or climatological usage, simplicity, fast-running time, and usage of routinely available data as model input were key considerations in planning the research. Also, since where observations are available, it is evident that marked variations of average precipitation occur over distances of just a few kilometers in regions of complex terrain, a high degree of realism in the topography to be used is required.

3.1.2 Choice of Coordinate System and Computational Grid

The phenomenon of "rain-shadowing" is obvious in many arid to semi-aird regions of the world situated in the lee of major mountain massifs. From an atmospheric water budget viewpoint this phenomenon must exist, though perhaps not quite as extremely, on successive mountain barriers located downwind from other barriers of similar height. To consider this effect it is convenient to keep tract of the atmospheric water budget by adopting a Lagrangian coordinate framework and assuming straight steady state two-dimensional flow (i.e., flow only along the major current direction, but with vertical displacement by underlying topography permitted). While following the parcels in this manner simplifies the water budget-keeping task, it imposes the requirement for a topography grid unique to each wind direction and restricts computations to the use of only one wind direction over the whole of the computational grid for any given period. In effect, this reduces the model-building task to one of two-dimensions, with a unique topographic profile considered for each

grid line. Due to its computational efficiency and a lack of routinely available better resolution of the upper flow pattern, this procedure was chosen.

3.1.3 Period of Testing

In mountainous areas characterized by winter-long buildups of snowpack, the bulk of the runoff occurs from snowmelt during late spring and summer. If one is to evaluate the hydrologic usefulness of a precipitation model in such regions a number of years of model precipitation computations must be made. For this study a data base of upper air information covering 13 years was available as input data. This data source consisted of rawinsonde information at 12 hourly intervals. It was decided to make computations for each available measurement and then sum the values over each winter snowpack accumulation season.

To test the derived method for short term prediction of snowfall, the period November 1975 - March 1976 was chosen.

3.1.4 Model Validation

Throughout the computational area selected ($\approx$ 60,000 mi^2) only a handful of precipitation stations representative of high mountain precipitation regimes have existed for the 13 years chosen for computations. Thus other comparative data sources for model validation had to be sought. Available measurements suitable to this purpose are (1) snowcourse water equivalent values obtained monthly from 1 February through 1 May by the Soil Conservation Service of the U.S. Dept. of Agriculture and (2) USGS streamflow records from numerous streamgauges within the computational area. The research was planned to make extensive use of both these information sources.

3.2 Model Description

Consistent with the objectives and guidelines as put forth above, an orographic precipitation model was developed and is briefly described below. It is designed to run with highly realistic topography. It has the flexibility of using topographic grid meshes as small as 2.5 km on a side, but the testing has been with either a 10-km or 5-km grid interval.

The model follows the interactions of air layers with the underlying topography by allowing forced vertical displacement of the air column. It keeps track of the condensate or evaporation resulting from these vertical displacements. As the layers flow across the region, part of the condensate precipitates. That which does not moves downstream to the next grid point where a fraction of it and the condensate generated as a result of topographic lift precipitates. In the case of sinking motion, part or all of the parcel cloud water evaporates. Precipitation falling into a layer from above partially (or totally) evaporates when encountering subsaturated conditions. Eventually, precipitation generated in the highest layers reaches the ground provided it does not totally evaporate.

With the foregoing stipulations plus a coordinate framework which follows the parcels, and the further assumptions of steady-state, two-dimensional flow and spatially constant precipitation efficiency, E, the computational formula for precipitation rate, $\bar{\dot{r}}_{I,I+1}$, along grid interval, Δx, is, from an atmospheric water budget viewpoint,

$$(\bar{\dot{r}}_{I,I+1})_{\ell} = \frac{EV_{\ell}\Delta P_{\ell}}{\rho_w g \Delta x} (Q_I + \Delta C_{I,I+1})_{\ell} , \qquad (3\text{-}1)$$

where

ℓ = computational layer in question

V = the horizontal wind speed in the x direction at the upwind edge of the computational area

ΔP = pressure thickness of the inflowing layer at the upwind edge of the computational grid

Q_I = cloud water content (mixing ratio) of liquid or solid at grid point I

$\Delta C_{I,I+1}$ = additional condensation (or evaporation) due to vertical displacement between points I and I+1. (In the event that $\Delta C_{I,I+1}$ is evaporation and is numerically greater than Q_I, precipitation is zero.)

E = precipitation efficiency

ρ_w = density of water (1 g cm^{-3})

This formulation provides for the shadowing effects of upstream topography when combined with the requirement for a separate topographic grid for each prevailing wind direction. Model examples of shadowing are shown for western Colorado in Figures 1 and 2. The above and all model equations are derived in Section 4.

Model sophistication was designed to be consistent with the operationally available input data resolution. Input requirements are flexible and provision is made for considering variable moisture profiles across the computation area.

The primary objective is to maintain sufficient simplicity (and therefore fast running time) to (a) allow thousands of historical cases to be processed and summed over various time and space intervals for climatological and hydrological purposes, and (b) permit the use of model excerpts as objective short term forecast aids.

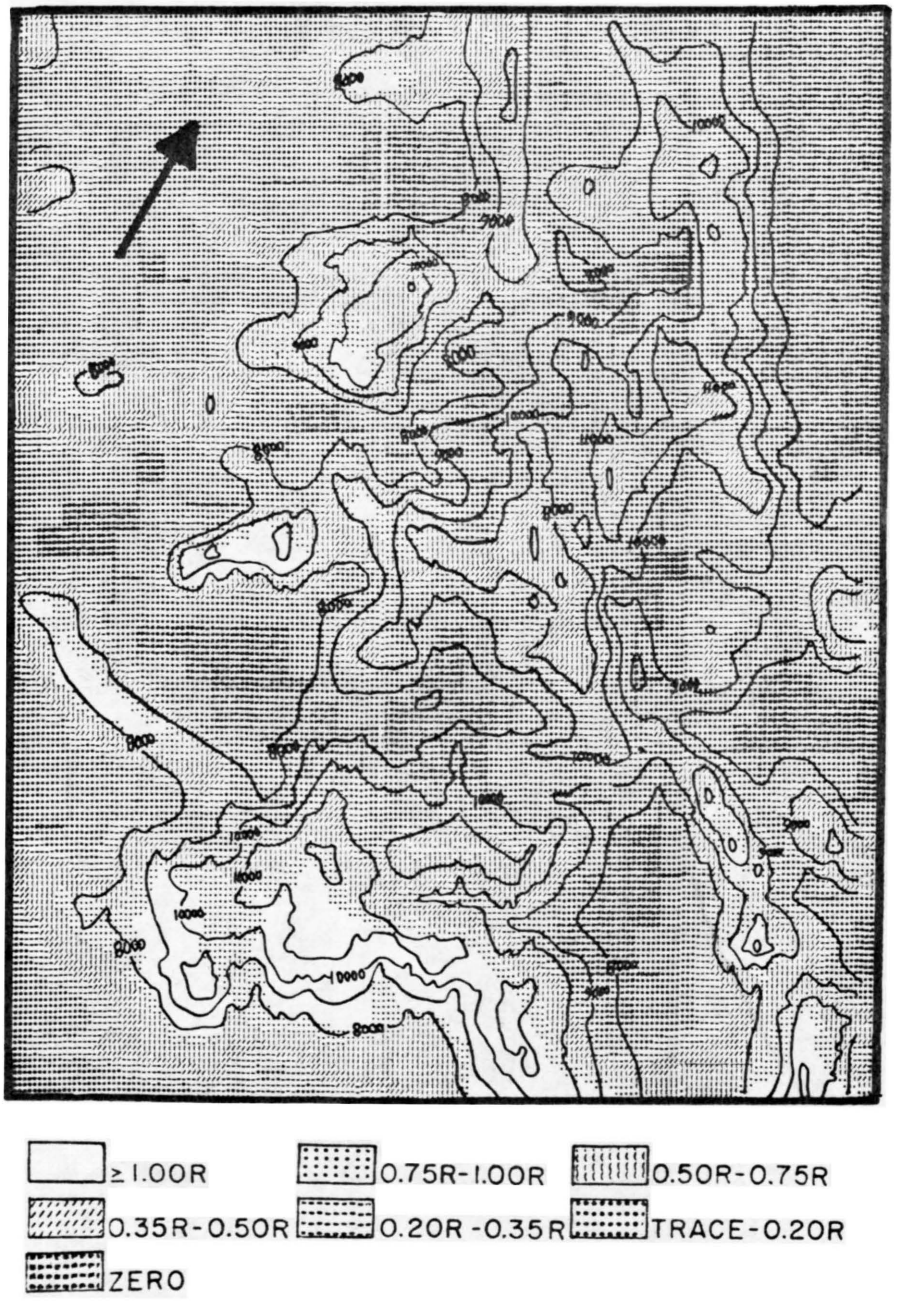

Figure 1. Example of model relative precipitation pattern for south-southwest (210°) flow over western Colorado with elevation contours also indicated

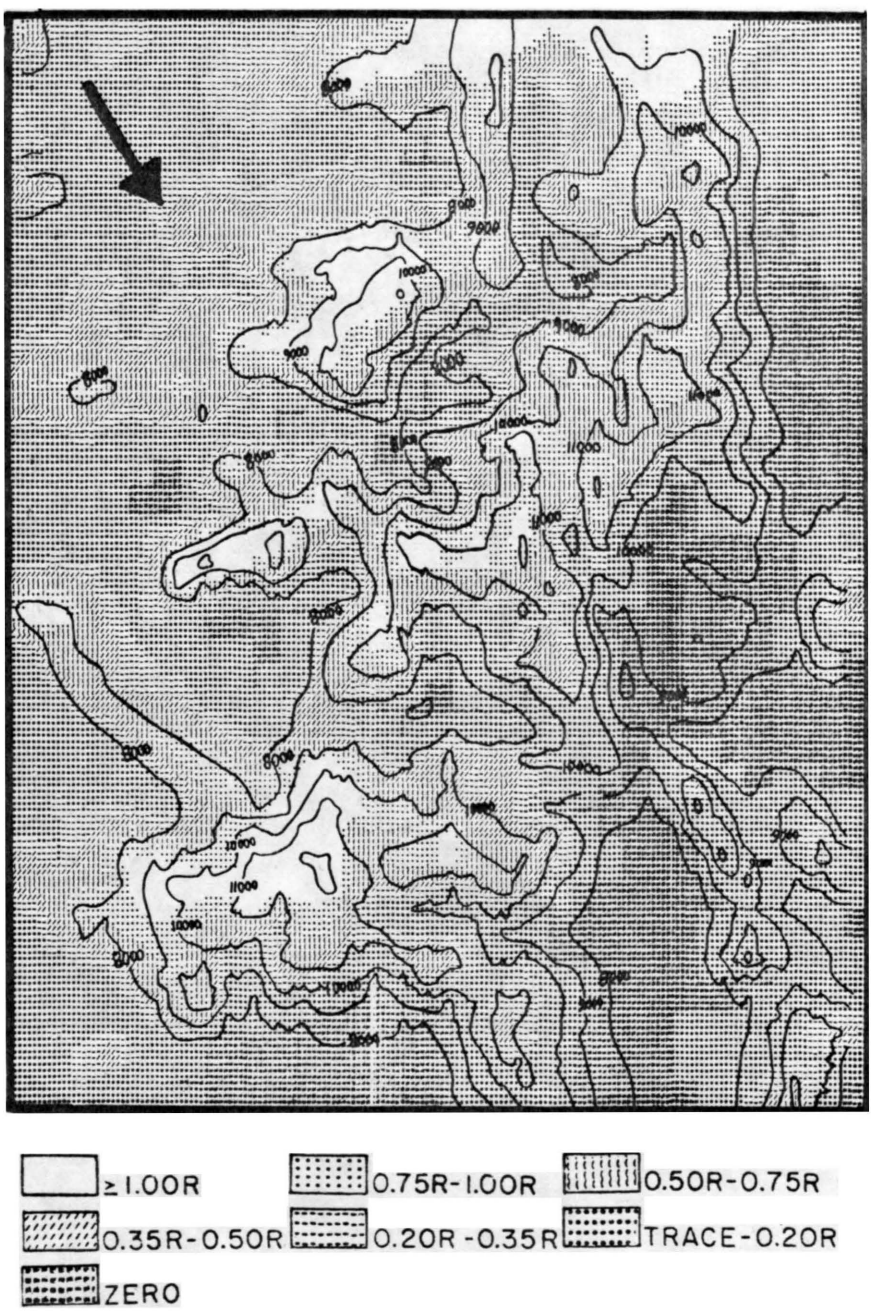

Figure 2. Example of model relative precipitation pattern for north-northwest (330°) flow over western Colorado with elevation contours also indicated

3.3 Topography and Study Area

The study area was confined to the mountainous portion of Colorado west of 105°W longitude (Figure 3).

Topography used in the computations was derived as follows:

1. From either 1/500,000 or 1/250,000 scale topographic maps the elevation values were estimated (to the nearest 100 ft.) at 2.5 km horizontal grid interval locations for typical x, y grid orientation.
2. Rotated grids (representing each 10° wind direction class) were then overlaid on the original 2.5 x 2.5 km elevation grid, and elevation values were generated at each grid point of the rotated overlay grid by interpolation (using inverse distance squared weighting) from the original x, y elevation grid (see Figure 4).
3. From each rotated elevation grid, average elevation was computed using a 10 x 10 km grid interval by averaging the 25 values of elevation at the surrounding 2.5 km grid points as in Figure 5a. Similarly, topography on a 5 x 5 km grid interval was generated as in Figure 5b, using the 9 values of elevation at the 2.5 km grid points. This gives 35 separate gridded arrays of topography (1 for each 10° wind direction class, for each choice of grid interval).

Figure 6 gives an example of the topographic detail obtained by using a 5 km grid interval while Figure 7 shows the same area using the 10 km interval.

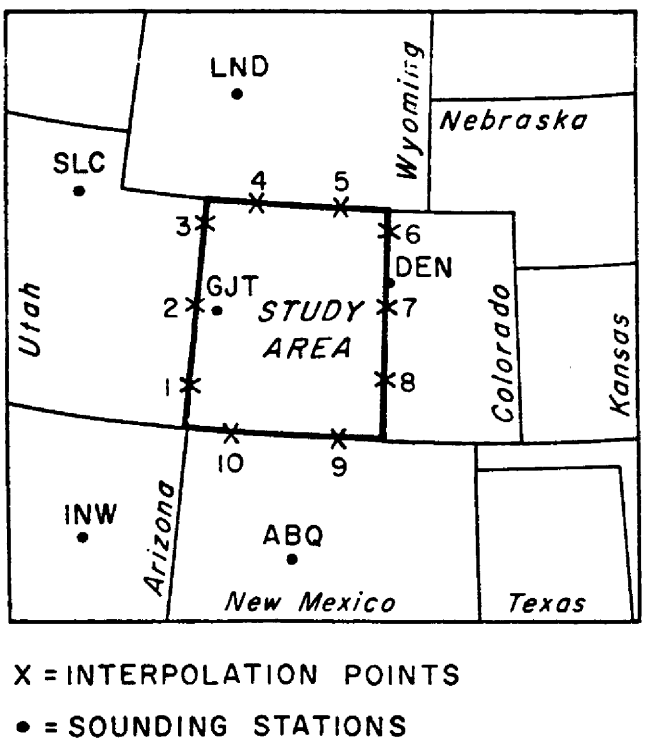

Figure 3. The study area and available upper air stations

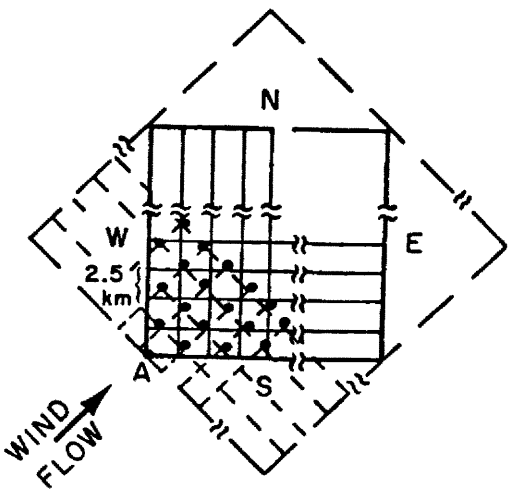

Figure 4. Illustration of method for obtaining the model topography

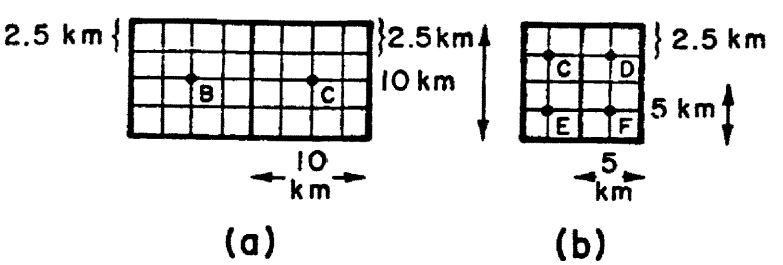

Figure 5. The averaging method for generating 10 x 10 km and 5 x 5 km elevation grids

Figure 6. Model topography with 5 km grid interval

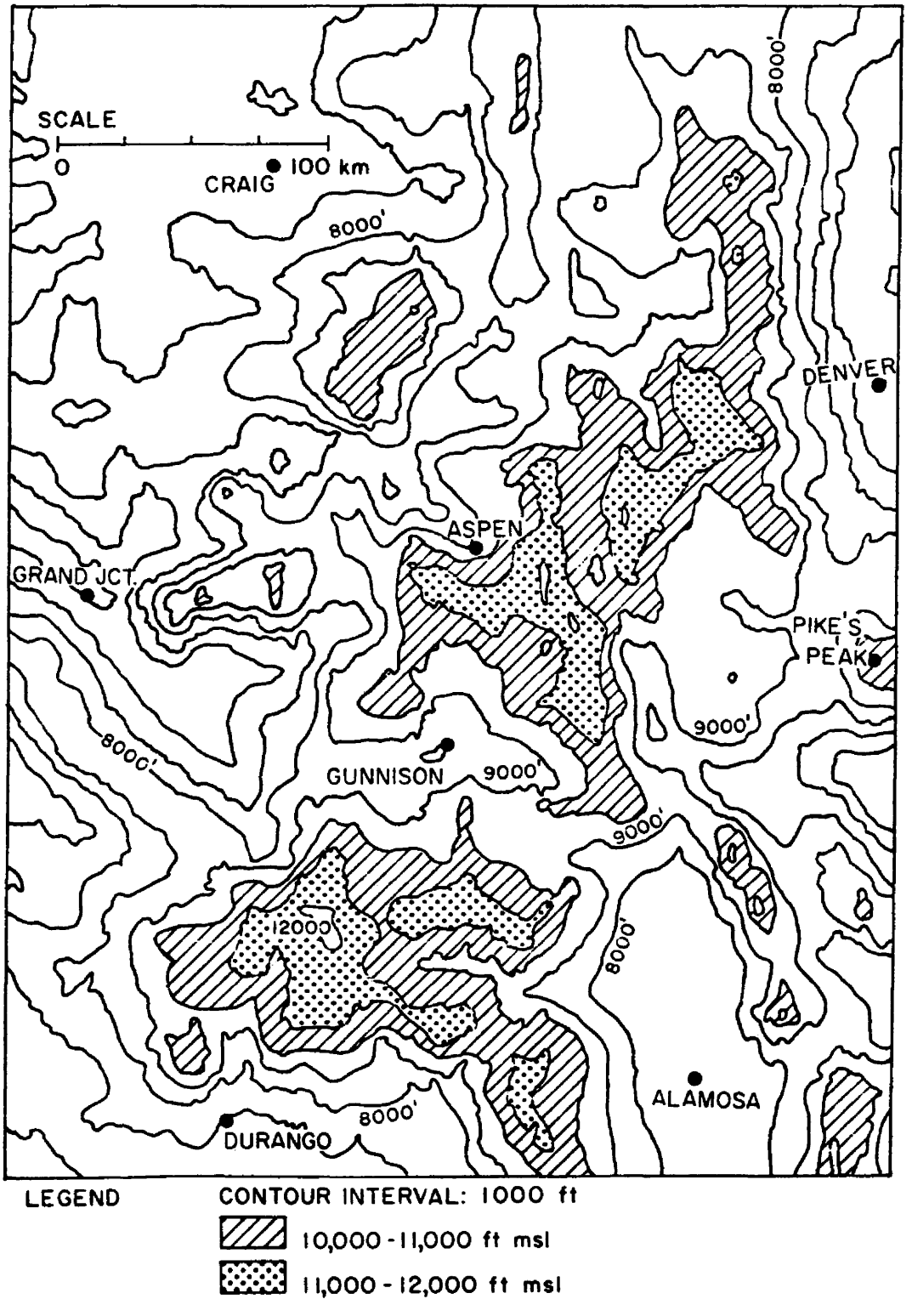

Figure 7. Model topography with 10 km grid interval

3.4 Data

3.4.1 Input

Routine twice-daily upper air soundings (with 50 mb vertical resolution) were available from the locations shown in Figure 3. To use this information for computing orographic precipitation, interpolated values were required at the indicated points along the border of the study area (Figure 3). To accomplish this, the method of Panofsky (1949) was employed. First, however, it was necessary to make corrections to the relative humidity profiles arising from lag effects of the various sensing elements used over the 13-year period.

Total precipitation at a point is composed of components from orographic effects, convective release, and large scale vertical motion. Thus, an estimate of large scale vertical motion is desirable. To obtain this the Bellamy technique (Bellamy, 1949) was applied to each of the five triangles formed by the 6 sounding stations in Figure 3. Resulting vertical motion profiles were corrected by the method of O'Brien (1968).

Appendix B gives details of obtaining all required input data for model computations.

3.4.2 Evaluation

To evaluate model performance the following three data sets were available:

1) Daily and Hourly Precipitation Gauges
2) USDA Soil Conservation Service Snow Survey snowcourse water equivalent records (with measurements for 1 February, 1 March, 1 April, and 1 May)
3) U.S.G.S. Streamgauge Records

Due to only a very small number of high mountain precipitation gauges, only very limited use could be made of this data set and therefore little model evaluation was made for integration intervals shorter than a season. Snowcourses, however, are located in higher mountain zones by design and represent a ready source of data for monthly or particularly seasonal evaluation or model performance. Only those snowcourses located above 9000 ft MSL (2743 m) were used. The general locations of snowcourses used are indicated in Figure 8.

While snowcourse values have been successfully used routinely as spring and summer runoff predictors, they can only be considered as indices of area precipitation rather than areally integrable values of such. Model calculations can be areally integrated to yield drainage basin volume precipitation estimates, and these values can be correlated to observed basin runoff. Thus streamgauge records are useful for this endeavor.

The watersheds listed in Table 1 and shown in Figure 9 were used in various combinations to evaluate model performance.

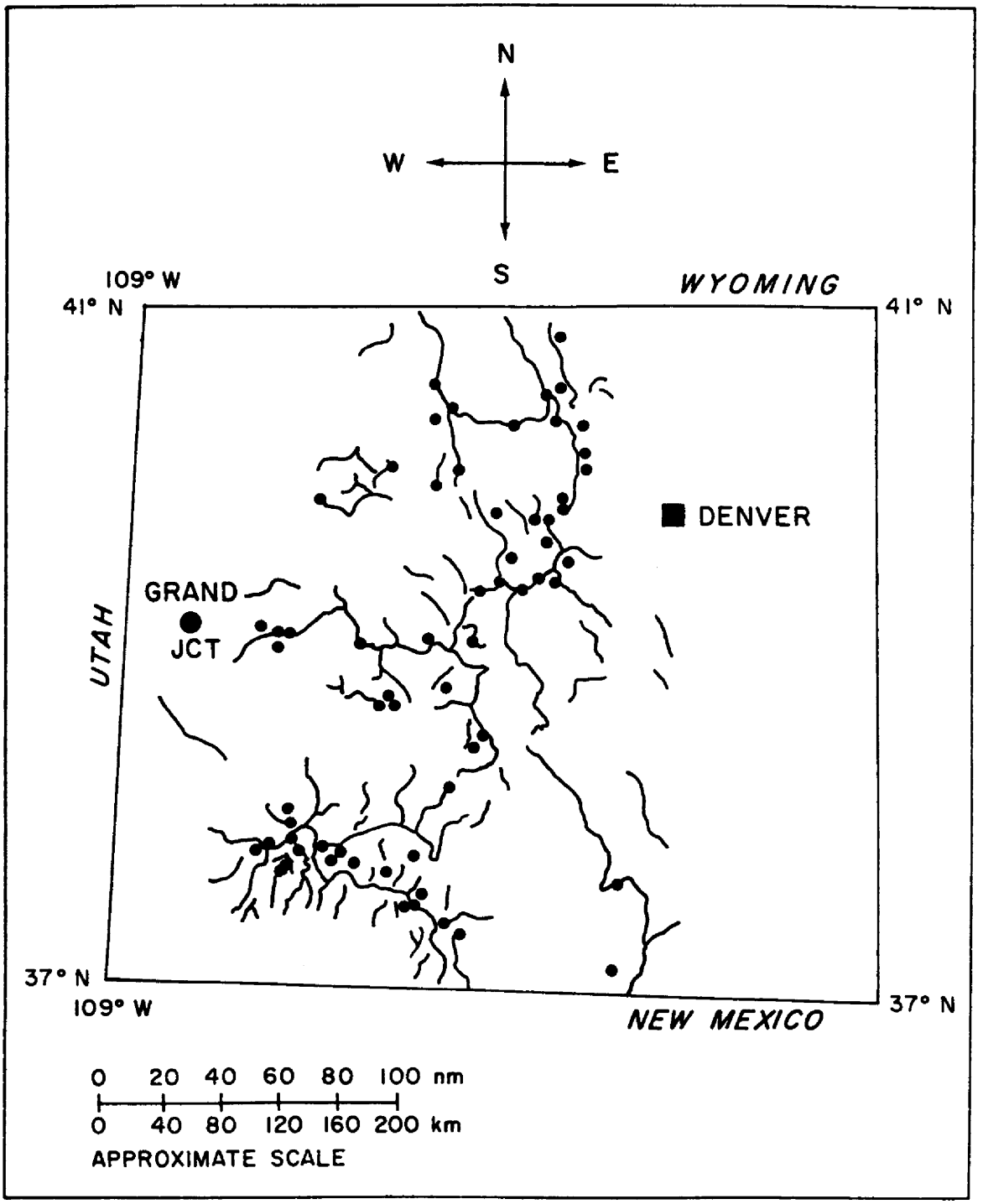

Figure 8. Locations of general group of Soil Conservation Service snowcourses used for model evaluation

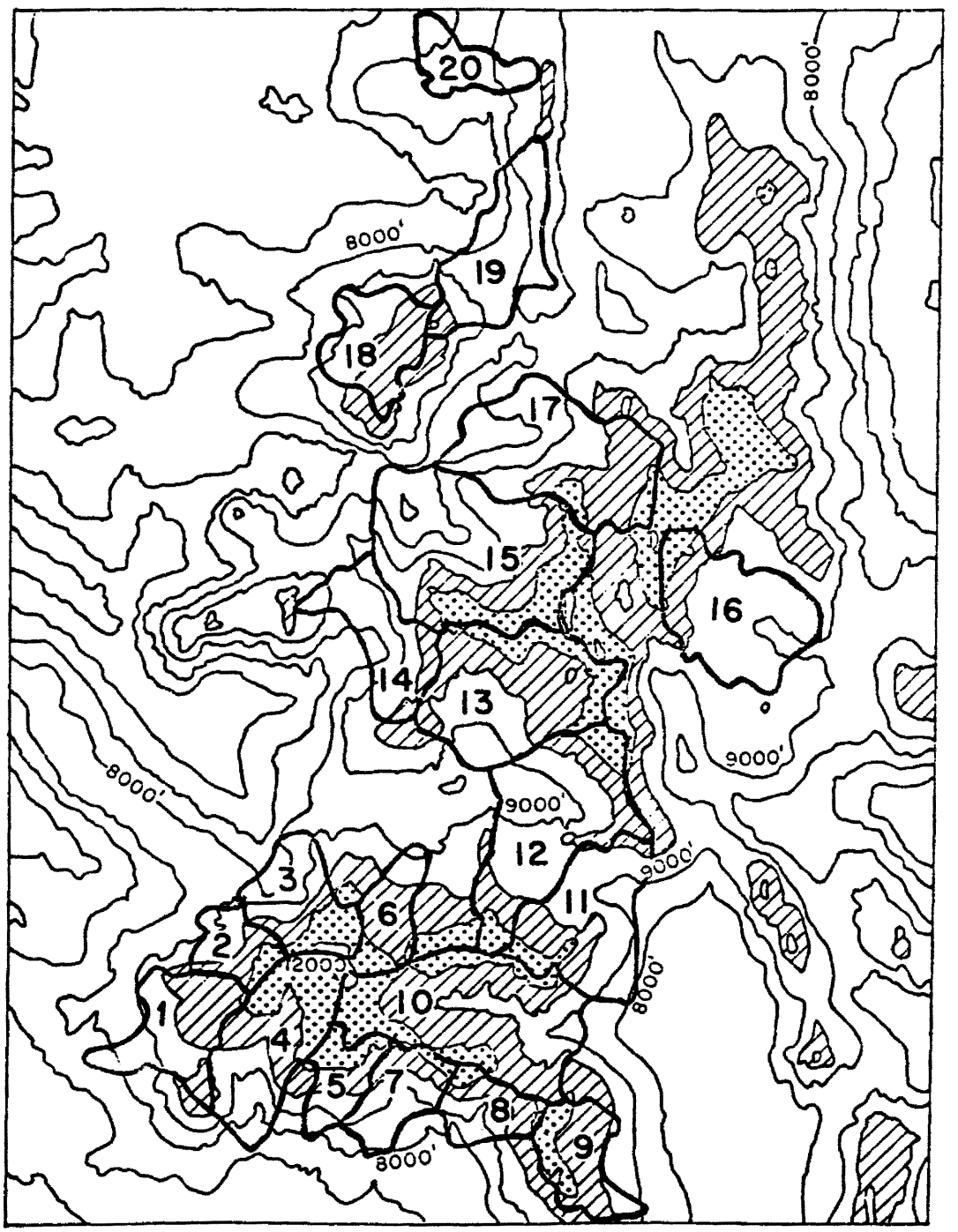

Figure 9. Locations of watersheds used for model evaluation

Table 1

List of Streamgauges Used for Model Validation

Small Basin #	Streamgauge Name
1	Dolores at Dolores
2	San Miguel at Placerville
3	Uncompahgre at Colona
4	Animas at Durango
5	Los Pinos near Bayfield
6	Lake Fork of Gunnison at Gateview
7	Piedra near Piedra
8	San Juan at Pagosa Springs
9	Conejos at Mogote and Alamosa Creek above Terrace Res.
10	Rio Grande near Del Norte
11	La Garita Creek, Saquache Creek and Carnero Creek
12	Tomichi Creek at Gunnison
13	Gunnison near Gunnison
14	North Fork of Gunnison near Somerset
15	Roaring Fork below Glenwood
16	South Platte near Hartsel
17	Eagle below Gypsum
18	South Fork White and North Fork White near Buford
19	Yampa at Steamboat
20	Elk at Clark, Elkhead Creek at Elkhead and Slater Fork at Slater

4.0 MODEL DEVELOPMENT

A general description of the orographic model developed for this study was given in Section 3.2. This section gives details of the model development.

4.1 Model Airflow

4.1.1 Flow Direction

The elevation grid to be used is selected by rounding the 700 mb wind direction at the center of the experimental area to the nearest 10°. It is assumed that the air streams along grid lines with no cross-current deflection (i.e., the horizontal projections of all streamlines are parallel and aligned with one axis of the topography grid selected). To account for directional shear with height, only the component of the wind at each level along the direction of the 700 mb wind at the center of the experimental area is considered in all model calculations.

4.1.2 Blocking

When a stable air mass flows toward a major barrier, flow in the lower layers is frequently observed to turn and flow more or less parallel to the ridge without climbing it. Reverse flow is also sometimes observed to develop in these lower layers. Both of these phenomena have the effect of producing a stagnant or "blocked" layer with respect to the trans-barrier wind component in the two-dimensional flow. To the extent that these lower layers of air are actually flowing parallel to the barrier, the blocking phenomenon is a problem which arises primarily in two-dimensional flow models due to the imposed constraints on the flow (Fraser et al., 1973).

Elliott (1969) referred to this blocked zone as the "dead" layer and defined it to exist in those lowest strata where either inversions existed over a 50 mb layer or the transbarrier wind component was zero or negative. In the current study, slightly more liberal criteria were invoked to designate "dead layers." Strata were defined as "dead" if either the mean layer transbarrier wind was less than 2.5 m/s or $\frac{\partial T}{\partial P} < 0.4$ K/50 mb, provided that all lower layers also met these criteria. Tests for this condition were made for each 25 mb thick layer starting with the surface-based layer and working upward.

An additional phenomenon which presents a similar problem to specifying the flow over complex topography is cold air pooling in local valleys from terrestrial radiation and subsequent drainage effects. This undoubtedly influences the effective topography "felt" by the main free air flow, particularly near the beginning of precipitation events following a period of clear nocturnal skies. However, it is beyond the scope of this study to make systematic and reasonable corrections for such. Thus it will not be further considered.

4.1.3 Streamline Vertical Displacement

It is well known qualitatively that when stable air is forced to rise over up-sloping terrain, the induced vertical motion decreases with height, and perhaps even eventually reverses in sign due to the wave disturbance created. At much higher levels it may again increase. Various formulations have been derived to quantitatively estimate the vertical displacement of streamlines under such circumstances (Berkofsky, 1964; Elliott, 1969; Myers, 1962; Fraser et al., 1973). All are found to be quite sensitive to slight differences in the static stability profile, and consequently on whether the air stream is dry or saturated. This

sensitivity is critical because moderately moist winter air masses flowing across complex terrain are typified by lapse rates not far from the moist adiabatic (i.e., with moist static stability near zero), frequently even exhibiting slight conditional instability. In cases of conditional instability, lifting over the higher terrain may release convection, thus invalidating the forced wave mode equations describing vertical displacement of the streamlines. From an operational viewpoint, the rather gross temporal and areal sampling frequency of upper air conditions further amplifies the importance of this sensitivity of streamline displacement to static stability, but at the same time precludes adequate consideration of it in models designed to use real data as input.

In view of the above described complications and the operationally-oriented nature of the present study, some very simple criteria for streamline vertical displacement were adopted. Three classes of streamline displacement were defined based upon certain stability and humidity characteristics of the "undisturbed" air stream.

Consider first a comparison of values of the Scorer parameter, S, for unsheared flow in the form developed by Fraser et al. (1973) for saturated and non-saturated flow. For non-saturated air, the Scorer parameter, S, is $g\beta/V_o^2$ while for saturated flow it is $gb\beta_E/V_o^2$, where

$$\beta = \frac{1}{\theta}\frac{\partial\theta}{\partial Z}$$

$$\beta_E = \frac{1}{\theta}\frac{\partial\theta_E}{\partial Z}$$

$$b = 1 - (1 - \gamma_m/\gamma_d)/(1 - c_p T_o/\varepsilon L)$$

For typical mid-latitude 700 mb and 500 mb temperatures, $0.4<b<0.9$ and averages $\approx$ 0.75. However, for typical observed winter air mass stratifications between 500 mb and 700 mb over the Colorado Rockies,

$\beta_E \tilde{\sim} 0.1\beta$ to 0.3β. Thus for saturated air, the Scorer parameter is only approximately 1/12 to 1/4 as large as for dry air. For broad mountains (> 20 km half-width) the height, H, at which the vertical motion first becomes zero is inversely related to $\sqrt{s}$. Thus H is typically between 2 and 3.5 times as far above the mountain for cloudy as for non-cloudy airflow across complex terrain. In the case of moist adiabatic lapse rate conditions for cloud air, $\beta_E = 0$, and $H \to \infty$.

Since it is the moist (or at least relatively moist) air which is of interest in this study, criteria for the fall-off with height of the terrain-induced vertical motion were defined for application only to the layers which could become cloudy upon lifting over the higher terrain. To help develop these criteria, a winter season (1970-71) of upper air and precipitation data (October - April) was studied for Colorado. It was found that virtually no precipitation occurred even at high mountain locations if the maximum relative humidity on the Grand Junction (GJT) (elev. 4540 ft. or 1384 m MSL) sounding was less than 65%. The amount of terrain relief between the typical top of the blocked layer and mountain top level is approximately 1500 m, whereas only approximately 600 m of lifting is required to bring air of 65% relative humidity to saturation. This suggests that if we define the highest layer with $\geq$ 65% relative humidity (which was also not underlain by any lower layer of < 50% mean relative humidity) as the highest potentially cloudy precipitating layer, ℓ_T, it might also be reasonable to define the vertical displacement, Δh_T, of that layer streamline as 600/1500 of the surface streamline displacement, Δh_o (which is assumed to follow either the terrain or the upper surface of the dead layer, whichever is highest). Such a criterion was adopted, but with the following two exceptions. First, if an inversion

TABLE 2

STREAMLINE VERTICAL DISPLACEMENT

STABILITY CLASS	DISPLACEMENT OF "CLOUD TOP" STREAMLINE
(a) INVERSION ABOVE "CLOUD TOP"	0
(b) STABLE 500 MB - 700 MB TEMP. BUT NO INVERSION ABOVE CLOUD TOP	$0.4\Delta h_o$
(c) APPROX. NEUTRAL STABILITY 500 MB TO 700 MB LAYER	$0.7\Delta h_o$ ($1.2\Delta h_o$ OVER HIGHEST TERRAIN)

was noted immediately above layer ℓ_T, streamline displacement of ℓ_T was assumed to be zero (i.e., $\Delta h_T = 0$). On the other hand, if no inversion existed above layer ℓ_T and the environmental lapse rate, as depicted by the 500 mb to 700 mb temperature difference, was near the moist adiabatic value ($\beta \overset{\sim}{\sim} 0$) the streamline displacement Δh_T was set at (0.7) Δh_o, except over the highest terrain where it was defined as (1.2) Δh_o to crudely simulate convective release over the higher ridges. This is the only attempt to consider convection in the model. Displacement, Δh_i, of immediate layers was assumed to vary linearly with pressure between Δh_o and Δh_T. This yields the formula below for Δh_i. Table 2 summarizes the criteria.

$$\Delta h_i = \Delta h_o \left[1 - \left(1 - \frac{\Delta h_T}{\Delta h_o} \right) \left(\frac{P_o - P_i}{P_o - P_T} \right) \right] \tag{4-1}$$

Since $\Delta h_o = Z_{I+1} - Z_I$

$$\Delta h_i = (Z_{I+1} - Z_I)d \tag{4-2}$$

where

$$d = 1 - \left(1 - \frac{\Delta h_T}{\Delta h_o} \right) \left(\frac{P_o - P_i}{P_o - P_T} \right) \tag{4-3}$$

4.2 Orographic Precipitation Computation

Consider the flow depicted in Figure 10 where the flow is two dimensional, steady-state and N_1 and N_2 are streamlines.

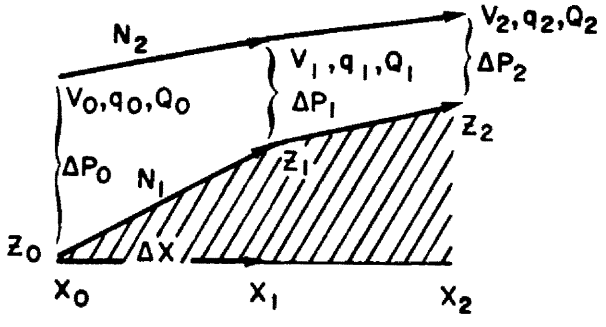

Figure 10. Symbolic two-dimensional flow across a barrier

The atmospheric water balance equation for the region between x_o and x_1 can be written as

$$\bar{\dot{r}}_{0,1} = \frac{1}{\rho_w \Delta x}\left[(q_o + Q_o)\frac{\Delta P_o V_o}{g} - (q_1 + Q_1)\frac{\Delta P_1 V_1}{g}\right] \tag{4-4}$$

where surface evaporation has been neglected, and where

$\bar{\dot{r}}_{o,1}$ = average precipitation rate over the distance, Δx, between grid points 0 and 1

q = layer mean water vapor specific humidity (or $\tilde{\sim}$ mixing ratio)

Q = layer mean cloud water (liquid or solid) specific humidity (or $\tilde{\sim}$ mixing ratio)

ΔP = layer thickness in pressure units

V = mean horizontal velocity of layer

g = gravity

ρ_w = density of water (1g cm $^{-3}$)

However, for two-dimensional steady-state, hydrostatic flow, the continuity equation can be written (when neglecting water substance changes)

$$\frac{\Delta P_o V_o}{g} = \frac{\Delta P_1 V_1}{g} = \frac{\Delta P_2 V_2}{g} \tag{4-5}$$

Therefore, equation (4-4) may be written

$$\bar{\dot{r}}_{o,1} = \frac{V_o \Delta P_o}{\rho_w \Delta x g}\left[(q_o + Q_o) - (q_1 + Q_1)\right] \tag{4-6}$$

Now,

$$\bar{\dot{r}}_{1,2} = \frac{V_1 \Delta P_1}{\rho_w \Delta x g}\left[(q_1+Q_1) - (q_2+Q_2)\right] = \frac{V_o \Delta P_o}{\rho_w \Delta x g}\left[(q_1+Q_1) - (q_2+Q_2)\right] \tag{4-7}$$

or, in general

$$\bar{\dot{r}}_{I,I+1} = \frac{V_o \Delta P_o}{\rho_w g \Delta x} \left[q_I + Q_I - q_{I+1} - Q_{I+1} \right] \tag{4-8}$$

The lifting process is assumed to be moist adiabatic, and, therefore as the parcel moves from point I to I+1,

$$q_{I+1} - q_I = \frac{dq_s}{dz} \Delta h_{I,I+1} \tag{4-9}$$

where

$\frac{dq_s}{dz}$ = the rate of change of parcel saturation water vapor mixing ratio per unit of lift

$\Delta h_{I,I+1}$ = the parcel vertical displacement between point I and I+1.

From section (4.1)

$$\Delta h_{I,I+1} = d(Z_{I+1} - Z_I). \tag{4-10}$$

By continuity,

$$q_I - q_{I+1} = \Delta C_{I,I+1} \tag{4-11}$$

where $\Delta C_{I,I+1}$ is the condensation per unit mass occurring as the parcel moves from I to I+1.

Now, by specifying that a constant fraction, E, of the sum of condensate formed and imported precipitates over the distance Δx, the remaining cloud water, Q_{I+1}, at point I+1 is

$$Q_{I+1} = (1 - E)Q_I + (1 - E)\Delta C_{I,I+1} \tag{4-12}$$

Substitution of eqs (4-11) and (4-12) into eq. (4-8) yields

$$\bar{\dot{r}}_{I,I+1} = \frac{V_o \Delta P_o}{g \Delta x} \left[E(Q_I + \Delta C_{I,I+1}) \right] \tag{4-13}$$

If the parcel descends, evaporation of cloud water contained in the layer is assumed to proceed immediately to maintain the parcel at water saturation so long as $(Q_I + \Delta C_{I,I+1}) \geq 0$. In the event that the descent

is sufficient to evaporate all of the imported cloud water, further descent is still mathematically constrained to be moist adiabatic in order to generate a saturation deficit (negative cloud water content). Under these circumstances,

$$\bar{\dot{r}}_{I,I+1} = 0 \qquad (4\text{-}14)$$

$$Q_{I+1} = Q_I + \Delta CI,I+1 \qquad (4\text{-}15)$$

All computations are made following the parcel (at the pressure midpoint of the layer) by re-initialization of indices to

$$I = I+1$$

$$I+1 = I+2$$

after each computation with the set of equations (4-13), (4-14), and (4-15).

Equations (4-13), (4-14), and (4-15) permit quantitative consideration of the "rain shadowing" effect of upstream barriers on downstream locations by effectively partially removing the parcel water over each barrier, thus raising the cloud base over successive downstream barriers (i.e., requiring greater vertical displacement to attain saturation over each successive downstream barrier). This formulation is very similar to that of Elliott (1969) except that he refers to either the initial cloud base or initial parcel height (whichever is higher) at the upwind edge of the computational area (rather than at the previous grid point) when computing total parcel condensate at any given grid point. A fraction, E, of the condensate is then assumed to precipitate naturally, but by referring the parcel starting height to the upwind edge of the grid, natural "rain shadowing" is not simulated. Computation of the area of cloud-seeding effects with the Elliott model does consider partial parcel

water consumption by artificially nucleated crystals, and thus provides for a downwind decrease of seeding effects.

Equation (4-13) is also similar to the Lagrangian approach of Fraser, et al. (1973) in computing a steady state field of condensate in the x-z plane. They did not allow for partial precipitation of the condensate, however, at each successive downstream grid point. Willis (1970), on the other hand, used a strictly Eulerian framework to compute the field of condensate supply which forced the cloud liquid water to zero at all points where downward vertical motion existed.

4.3 Large-Scale Vertical Motion

Herein, the large scale vertical motion is considered to be linearly additive to the topographic vertical motion. Thus, in equation (4-10) the vertical displacement, $(\Delta Z)_{\ell.s.}$, due to large scale vertical motion over ΔX distance is added to $(Z_{I+1} - Z_I)d$, giving

$$Q_{I+1} = (1-E)\left(-\frac{dq_s}{dz}\left(\Delta h_{I,I+1} + \Delta Z_{\ell.s.}\right)\right) + (1-E)Q_I \qquad (4\text{-}16)$$

when substituting eqs (4-10) and (4-11) into eq (4-9) and inserting the result into eq (4-12).

Large scale vertical motion can, of course, be estimated in a variety of ways. For the large number of historical data runs made, a version of the Bellamy (1949) technique was used (see Section 6.3).

4.4 Layer Computations

Computations as discussed in the previous two sections can be made for any desired number of layers and the results added together. In so doing, however, provision must be made for evaporation of precipitation falling into subsaturated layers. Also, precipitation produced in the

upper layers may not reach the lower levels until the air has moved 50 to 70 km downstream. Thus some form of trajectory computations should perhaps be made.

By including trajectories the water budget bookkeeping task can easily become formidable. To minimize this problem some grossly simplifying assumptions must be made. Experiments were made with the model ignoring the trajectory problem and simply making precipitation computations for each 50 mb layer, and also by including the trajectory computation, but forcing precipitation to fall out at grid points. To do the latter required (a) computation of precipitation in variable depth layers, (b) the restriction that all snow crystals falling through a given layer fall at the same terminal velocity, and (c) allowance for partial (or total) evaporation of precipitation falling into sub-saturated layers.

Tests indicated that the trajectory computations did not add substantially to accuracy, and they were thus eliminated from the final version.

Evaporation of falling precipitation into unsaturated lower layers moistens these strata and decreases the precipitation reaching the ground. Evaporation of precipitation is assumed to occur in layers subsaturated with respect to water. If the lower layer (layer 1) saturation deficit is sufficiently large, all precipitation may evaporate. If so, the lower layer vapor mixing ratio change because of this is

$$(\Delta q_{I,I+1})_{evap_1} = \frac{EV_2\Delta P_2}{V_1\Delta P_1}\left(Q_{I_2} + (\Delta C_{I,I+1})_2\right) \qquad (4\text{-}17)$$

where the ratio $\frac{V_2}{V_1}$ corrects to unit mass of air for layers moving at different speeds (e.g., a faster moving precipitating layer aloft with laminar flow will be more effective in moistening a subsaturated lower

layer than if $V_2 = V_1$. The ratio $\Delta P_2/\Delta P_1$ corrects to unit mass for layers of different thickness. If the lower layer remains subsaturated,

$$(Q_{I+1})_1 = (Q_I)_1 + (\Delta C_{I,I+1})_1 + (\Delta q_{I,I+1})_{evap_1} \tag{4-18}$$

on the other hand, if $(\bar{r}_{I,I+1})_2$ is more than sufficient to saturate layer 1, the precipitation falling through the base of layer 1 is

$$(\bar{r}_{I,I+1})_{BASE_1} = (\bar{r}_{I,I+1})_2 + \frac{V_1 \Delta P_1}{\rho_w g \Delta x} \left((Q_I)_1 + (\Delta C_{I,I+1})_1 \right) \tag{4-19}$$

following which $(Q_{I+1})_1$ is set to zero (i.e., the precipitation from layer 2 above has saturated layer 1 removing its saturation deficit at I+1).

The above formulations are extended to n layers by starting all calculations in the highest layers and working downward.

4.5 Precipitation Efficiency

Natural precipitation efficiency, E, over an orographic barrier, is controlled by the ice nuclei activity spectrum, crystal multiplication processes, the vertical and upwind extent of the cloud, and the prevailing horizontal and vertical wind velocity in the cloud. The process is complex and is probably almost as dependent on the time and space scales of the saturated flow and the mountain geometry as it is on nucleation processes.

Representative values of natural precipitation efficiency have been sought by a number of investigators largely because of the extreme importance of this knowledge for assessing weather modification potential. Elliott and Hovind (1964) estimated that approximately one quarter of the condensate forming over the San Gabriel and Santa Ynez ranges in California precipitated, while for the cap cloud over Elk Mountain in Wyoming

Auer and Veal (1970) obtained a value of $E \tilde{\sim} 0.60$ for several case studies.

Chappell (1970) computed supply rate of condensate by assuming certain mean values of orographic vertical motion and $\frac{dq_s}{dz}$ through the estimated mean cloud depth for Wolf Creek Pass and Climax, Colorado. When comparing observed precipitation at those locations with the computed values of condensate supply, the implication was that E was near 1.0 for the colder clouds but ranged downward to 0.25 - 0.35 for the warmer end of the upper air temperature spectrum. Young (1974), in a case study with his two-dimensional orographic model calculated theoretically a very low E value of 0.0004 for a non-seeded cloud with a top at -13°C temperature.

Many computations of precipitation rates for hydrometeorological purposes routinely set E = 1 (i.e., they equate condensate supply rate to precipitation rate).

Primarily, the studies mentioned above point up the elusiveness of this important factor of precipitation efficiency. Thus in view of its obvious complexity and generally poorly known character, and since routinely available input data is of such poor resolution as to preclude very accurate specification of cloud microphysical characteristics or cloud geometry, a simplest possible approach for determination of E has been used for this study.

A large number of test cases were run using a variety of E values (see Section 6.2). It was found that a functional form of $E = -kT_c$, where

k = a positive constant

T_c = temperature (°C) of the highest layer with $\geq$ 65% Rh

gave satisfactory results (when also preventing E from becoming negative

for $T_c > 0°C$, and setting an upper limit of E = 0.25 for cold T_c values). A reasonable value for k was found to be .01.

It should be pointed out that with the form of the model equations used, precipitation efficiency is necessarily a function of grid interval.

4.6 Initializing the Upwind Borders

In the event the inflowing air was initially unsaturated, the lifting condensation level (LCL) was computed and added to the elevation of the top of the blocked layer to define a minimum elevation (MELV) of terrain over which the air parcel would be required to flow before saturation was reached.

If the elevation at the upwind border of the study area was less than MELV, an initial, negative amount of condensate (saturation deficit) was computed for each layer, ℓ, as

$$(Q_o)_\ell = -\frac{dq_s}{dz}_\ell (z_o - MELV) \qquad (4\text{-}20)$$

This was carried downstream in the usual way through Equation (4-13).

Where elevation at the upwind border was greater than MELV, initial condensate Q_o was generated by assuming an arbitrary terrain up-slope of 0.01 to exist upwind of the border. This, of course, generated condensate as the air climbed the slope, and for some parts of the border produced unrealistically large precipitation values along the upwind edge of the computational area.

4.7 Input Requirements

The model requires at least an estimate of the vertical profiles of wind, temperature, and humidity at the upwind edges of the study area, and preferably an estimate of the large scale vertical motion over the area.

Appendix B describes the methods employed to supply this necessary information in this study for Colorado.

4.8 Model Limitations

Due to numerous simplifying assumptions there are a number of limitations inherent in using this model to simulate the orographic precipitation process. Some of these are listed in Table 3 below for convenience.

TABLE 3

PARTIAL LIST OF MODEL PROCESSES AND SOME RESULTING MODEL LIMITATIONS

MODEL PROCESS	LIMITATION
Blocked Layer Determination	1) No variation along streamline allowed
	1a) No previously existing radiational drainage (i.e., Cold Air Pooling) considered (except at sounding site itself)
	2) Real 3-D phenomenon not necessarily simulated
Streamline Displacement	
a) horizontal	1) No flow-splitting around narrow barriers aligned with wind allowed
	2) No funneling or channeling of any kind allowed
	3) Only one wind direction allowed per computation case to "represent" entire grid and all layers, resulting in only partial simulation of layer water budgets
b) vertical	1) No consideration of lee-wave or other complicating downwind effects on basic current flow or stability
	2) Inadequate simulation of imbedded convection
Precipitation Efficiency Computation	1) Detailed Cloud physics usage prohibited
	2) E must be calibrated to grid interval used
Elimination of Crystal Trajectories	1) Precipitation deposition displacement due to varying windspeed not allowed

5.0 ERROR DISCUSSION

There are a number of inherent errors and limitations in the model formulation, some of which were listed in Section 4.8. By employing real data as input information, numerous additional sources of error are introduced. Some of these arise from instrumental inaccuracies, but larger ones are likely present because of areal or temporal non-representativeness of the upper air sounding.

No routine parallel observations exist for assessing the magnitude of the various errors. Thus systematic consideration of them is not possible. Even so, it is perhaps worthwhile to briefly explore the possible composite effects of all errors over various time scales.

In order to identify the types of errors which should be considered, one can analyze the nature of the main model precipitation equation (4-13) written below as a time integrated precipitation amount

$$R = \int \dot{r} dt = \frac{E}{\rho_w} \int_o^t \frac{V_o \Delta P}{\Delta x g} (Q_I + \Delta C_{I,I+1}) dt \tag{5-1}$$

It is also helpful to recall that

$$\Delta C_{I,I+1} = -\left(\frac{dq_s}{dz}\right)_I \left((Z_{I+1} - Z_I)d + \Delta Z_{\ell.s.}\right) \tag{5-2}$$

and that

$$\frac{dq_s}{dz} = f(T,P).$$

Inspection of each factor in Equation (5-1) indicates that errors arising from the sources listed in Table 3 probably influence the computed precipitation over any given period. Ignoring the question of errors in large scale vertical motion, it can be seen that R is basically

computed as the product of a number of factors, each of which is likely to have an associated error of one type or another. In the case of wind direction, the associated error affects the type of topography traversed by the air, affecting Q_I and $\Delta C_{I,I+1}$, and should thus feed into the error induced by topographic inaccuracies.

According to Barford (1967), the standard random error, $S(\phi)$, of a quantity, ϕ, functionally related to a product of other measured variables (i.e., where $\phi = \alpha\, u^a v^b \ldots y^n$) is

$$\frac{S(\phi)}{\bar{\phi}} = \left(a^2 \frac{S^2(u)}{\bar{u}^2} + b^2 \frac{S^2(v)}{\bar{v}^2} + \ldots n^2 \frac{S^2(y)}{\bar{y}^2} \right)^{\frac{1}{2}} . \qquad (5\text{-}3)$$

Again no corroborative data exists to obtain very accurate estimates of standard random errors of each factor. However, knowledge of the temporal variability of the factors would yield some crude estimates.

Considering precipitation efficiency, E, and cloud depth, ΔP, first, Figures 11,12, and 13 indicate extreme 3 hour variability of relative humidity in upper layers sensed by serial rawinsonde releases in southwestern Colorado at Durango. This is perhaps due to migratory meso-scale banded cloud structures. It thus appears that there is likely an approximately 100mb typical error associated with the designation of cloud depth. Such an error, if primarily occurring in upper layers would introduce about a 25% inaccuracy in model precipitation. The extreme twelve hour variability in model designated "cloud top" temperature in Figure 14 logically follows, considering the relative humidity variability in Figures 11, 12, and 13. From figure 14, approximately two thirds of the cases have 12 hour "cloud top" temperature changes of $\leq$14C. On the other hand if 100mb is a reasonable standard error for cloud depth, the associated "cloud top" temperature

error should be in the vicinity of 8C, giving an error of .08 in precipitation efficiency (See Section 6.2). From figure 19 in section 6.2, if E=0.17 is considered the standard the fluctuation of the precipitation profiles over high terrain induced by setting E=0.25 or E=0.12 is generally < 30%. Over and above the problem of representativeness of the input data is the question of inaccurate formulation for precipitation efficiency, for which the answers are not known.

Some knowledge of the degree of representativeness of wind direction using one observation over a twelve hour period can be obtained by noting the twelve hour variability of 700mb wind direction as shown visually in Figure 15a. Approximately two thirds of the data is within the ±40 degree 12 hour variation bands. Assuming the direction changes occur linearly with time, the one sounding should be able to yield estimates accurate to within ±20 degrees in at least 2/3 of the cases. Figure 15b shows the effect on model precipitation of a ±20 degree error in direction for one point (Aspen Mt.). The value of

$$\sqrt{\sum_{i=1}^{n}\left(r_{d_i} - r_{(d+20)_i}\right)^2 / n} \Big/ \left(\frac{1}{N}\sum_{i=1}^{n} r_{d_i}\right)$$

is 0.52. (r_d is the model precipitation for direction, d; r_{d+20} is model precipitation for direction + 20°; N = number of direction increments considered, and in this case was 24, or every 10° running clockwise from 160° through 030° inclusive). This degree of sensitivity to wind direction is for a single point and would not be quite as extreme for a watershed. Thus, 0.4 appears to be a reasonable estimate of the standard random error combining wind direction and topographic effects.

Wind speed errors affect model output linearly. Figure 16 indicates the standard deviation of twelve hour change in 700mb wind speed to be approximately 4 m/s for the 1961-62 winter season, while the mean speed was 8.8 m/s. This yields an approximate standard random error (s.r.e.) of 0.45. Again, assuming that speed changes linearly with time, the s.r.e. about the observation employed in the model should be in the vicinity of 0.2.

Condensation, $\Delta C_{I,I+1}$, is proportional to $\frac{-dqs}{dz}$ and $\frac{dqs}{dz} = f(T,P)$. Therefore, the representativeness of temperature should be estimated. A comparison of interpolated to observed temperature on constant pressure surfaces showed only a 1.4C average absolute error in the interpolated data. Also, the 12 hour variability ot constant pressure surface temperature is quite small (Figure 17). It thus appears that 3C is a reasonable s.r.e. for temperature representativeness. Figure 18 indicates a resulting reasonable s.r.e. for $\frac{dq_s}{dz}$ (and, therefore, for $\Delta C_{I,I+1}$) is about 0.1.

Finally, the 12 hour duration coefficient of variability was found to be 0.51 for Climax (altitude 11,300 ft. MSL) during the 1961-62 season. However, shorter duration frequently means more peaks and lulls (periods of no precipitation) than with longer, steadier precipitation episodes. Also, the recording weighing bucket gage can only indicate $\geq$ .01" increments per hour so that, if it snows at .0033" per hour for 3 hours, only the third hour would indicate precipitation. This introduces a fictitious additional variability of duration. Consequently the s.r.e. of duration chosen for this error discussion is 0.3.

Inserting the set of rough estimates of standard random errors for the individual vairables in Table 4 into equation (5-3) one obtains

$$\frac{S(\phi)}{\bar{\phi}} \sim 0.7$$

If the errors are random and normally distributed, it is then possible to determine the approximate number of individual computations (one for each sounding time) which would be required to obtain a sum (or sample mean) of a desired degree of accuracy. By standard statistical methods (e.g., Dixon and Massey, 1969), it can be shown that approximately 285 computations would be required to be 95% confident of a sample sum which was within $\pm$ 10% of the true sum. Approximately 100 computations would need to be added together to be 95% certain of $\pm$ 15% sum accuracy. It thus appears that the experimental approach herein might be used to compute reasonably accurate seasonal total values of precipitation over most of the grid, while model values for individual sounding times would be expected to show rather severe departures from observed quantities in a significant fraction of the cases.

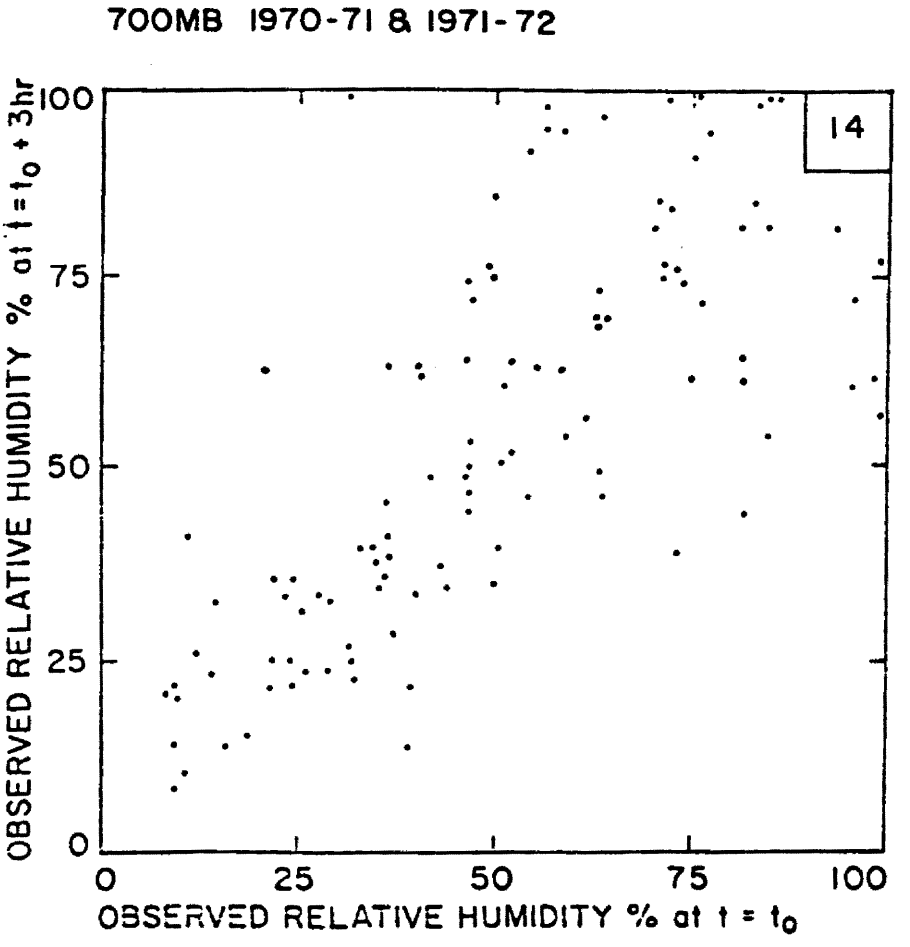

Figure 11. Scatter plot of Durango ,Colo., rawinsonde relative humidity (RH) at time t_o (horizontal axis) and 3 hours later (vertical axis). Box in upper right gives number of RH measurements of >90% at both t_o and $t_o + 3$ hrs.

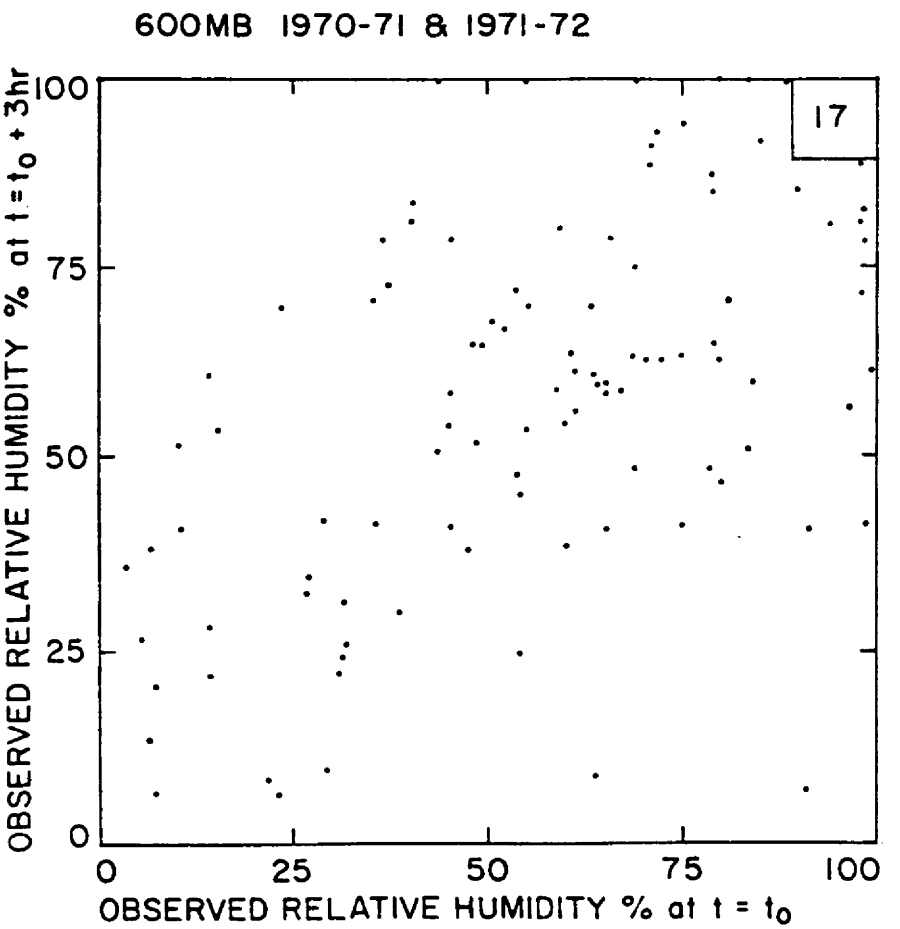

Figure 12. Same as figure 11

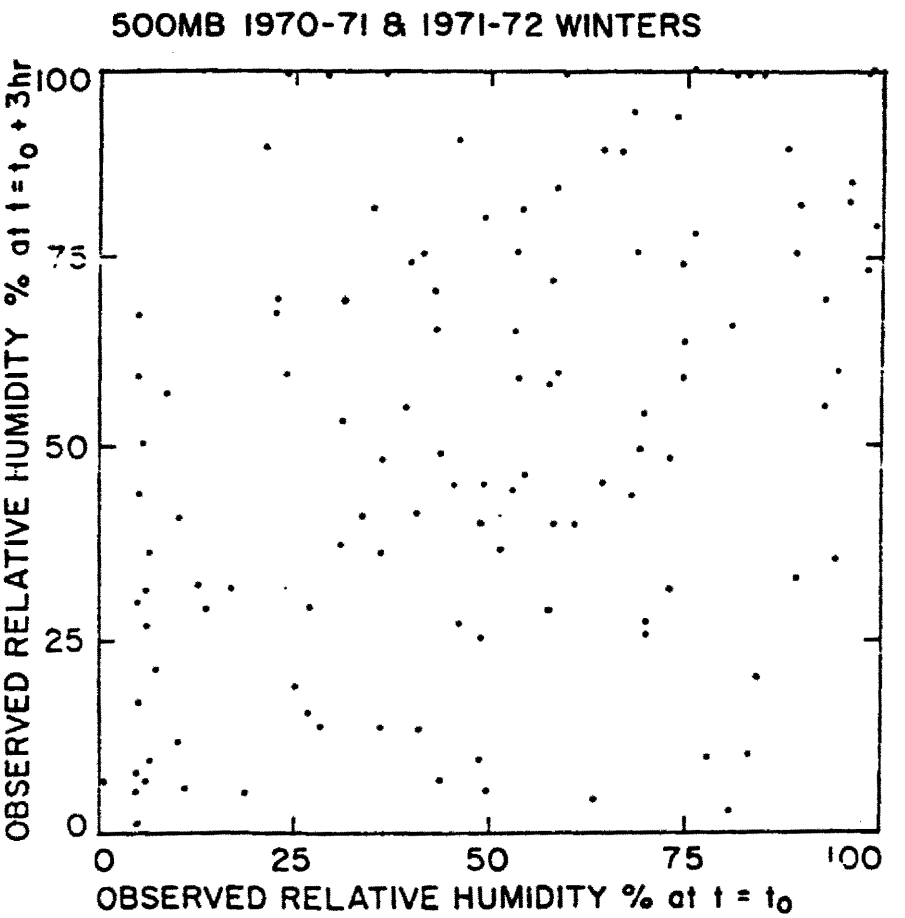

Figure 13. Same as figure 11

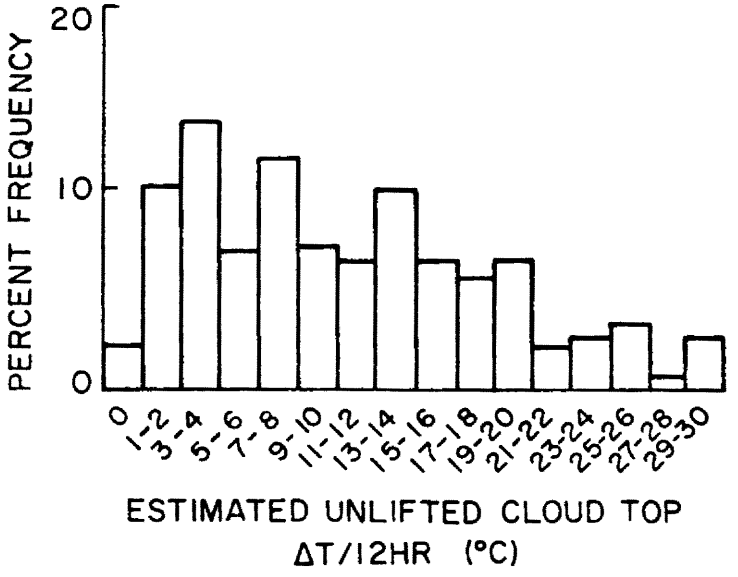

Figure 14. Frequency distribution of 12 hour change of unlifted "cloud top" temperature, T_c, based on 7 winter seasons (1963-1970)

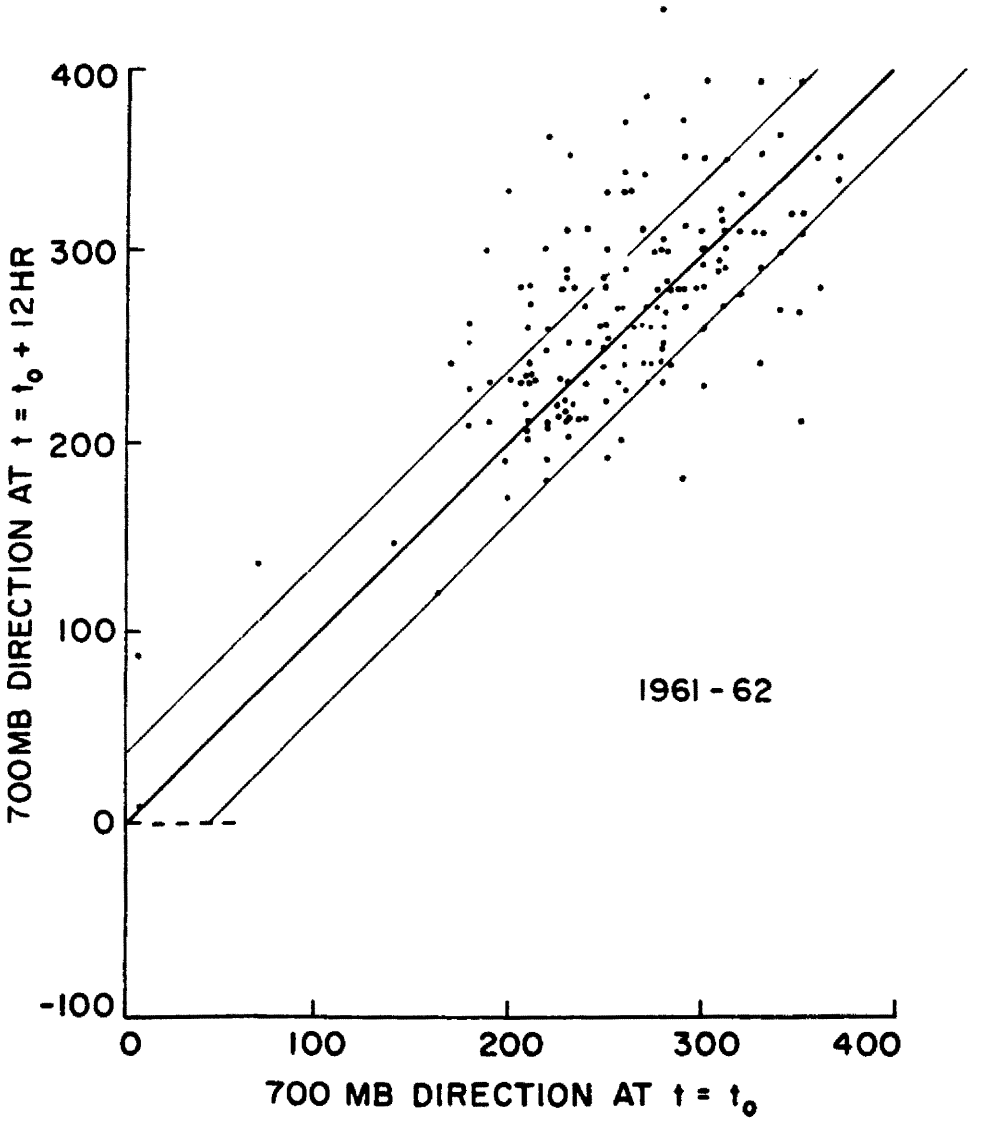

Figure 15a. Scatter plot of interpolated 700mb wind direction (at center of study area) at time t_o and 12 hours later (for period 15 October 1961-30 April 1962)

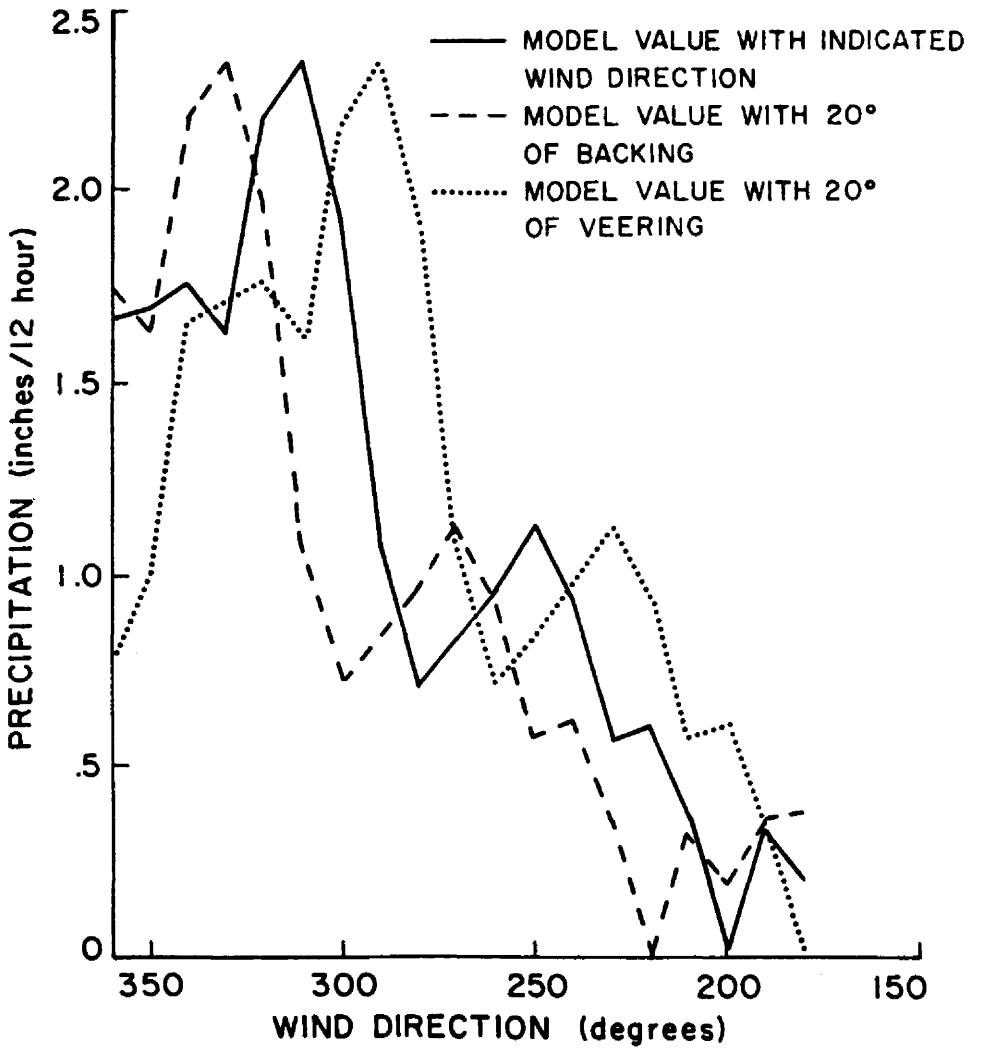

Figure 15b. Example (for Aspen Mountain) of model sensitivity to wind direction

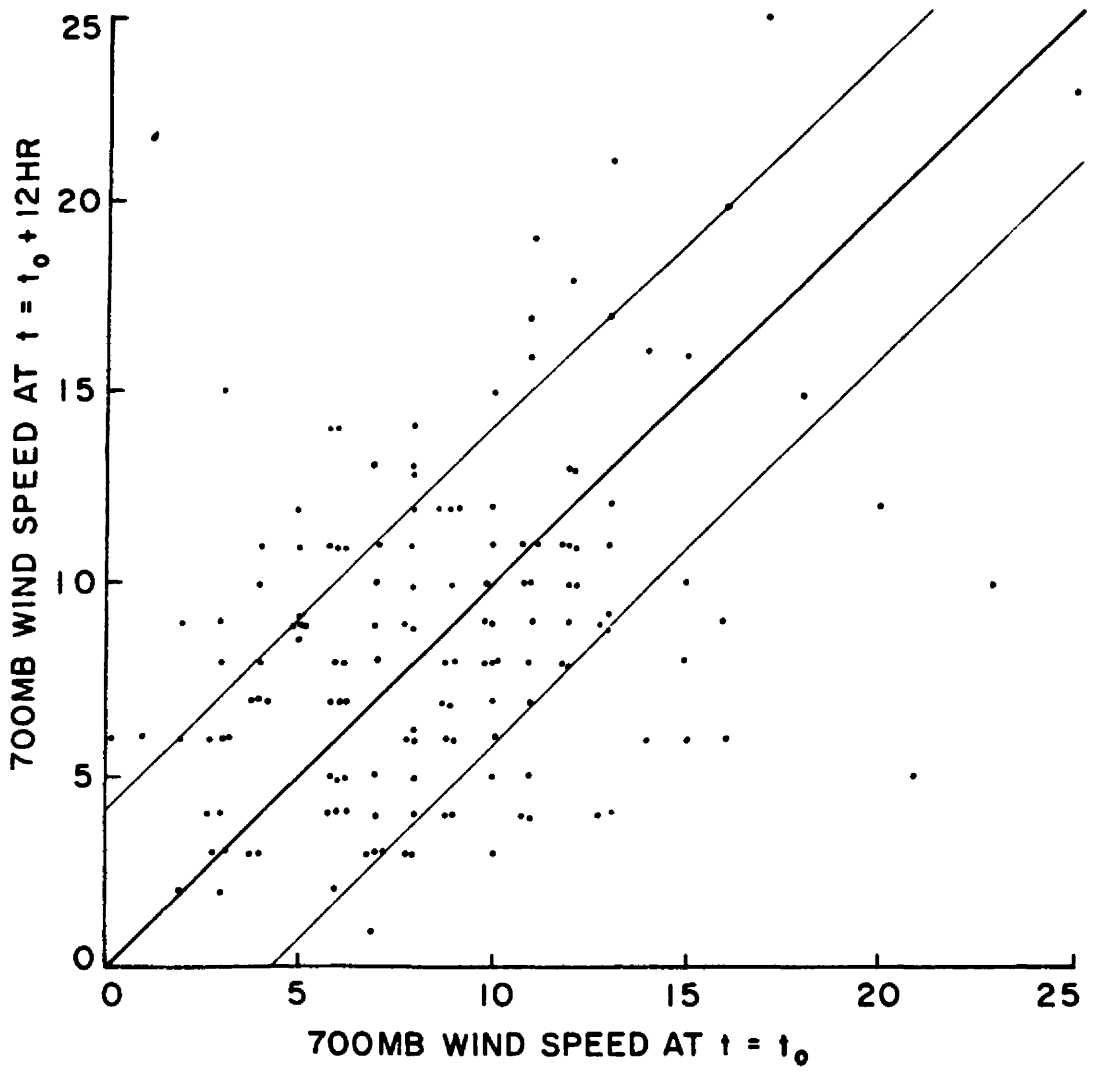

Figure 16. Scatter plot of interpolated 700mb wind speed (at center of study area) at time t_o and 12 hours later (for period 15 October 1961-30 April 1962)

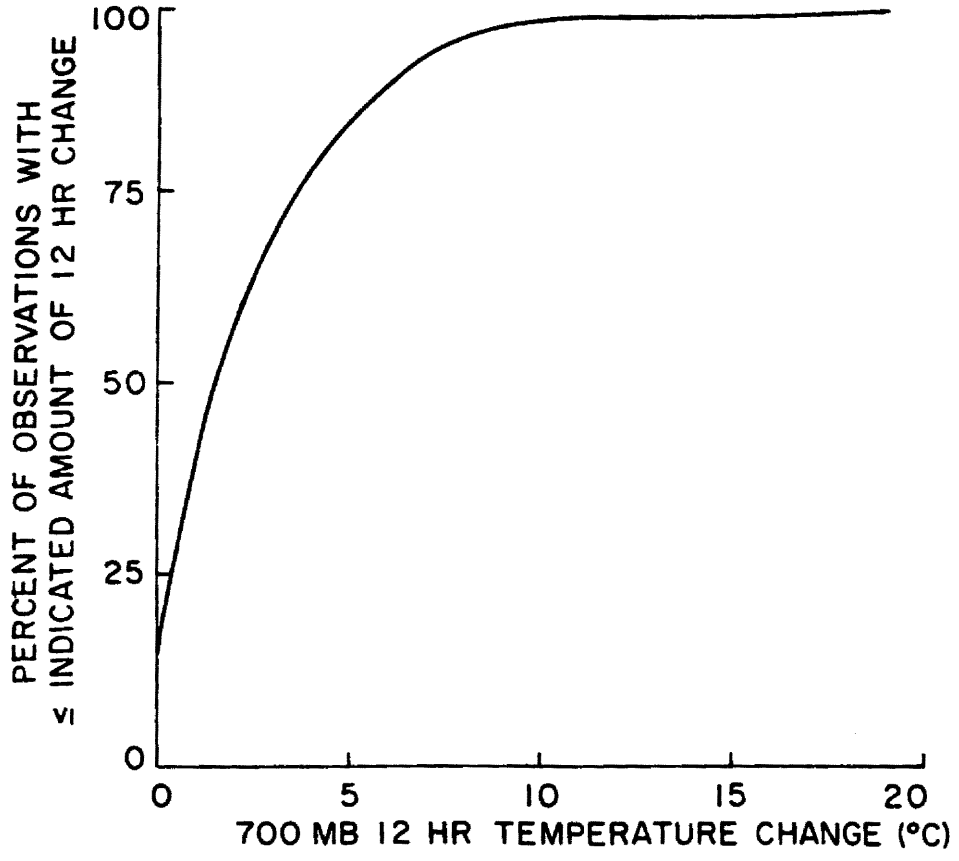

Figure 17. Five year climatology of 700mb 12 hour temperature change at Salt Lake City (SLC) for cases of dewpoint depression $\leq$5C

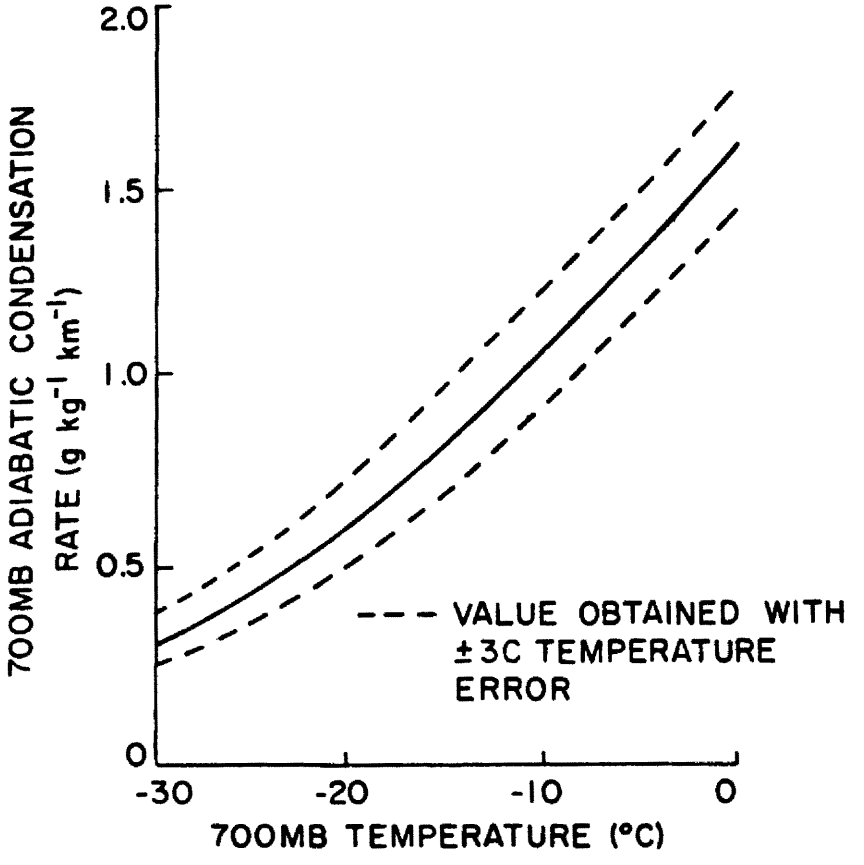

Figure 18. Plot of 700mb level adiabatic condensation rate versus temperature

Table 4

Summary of Model Error Sources and Estimated Error Magnitude

SOURCES OF ERROR	ESTIMATED STANDARD RELATIVE ERROR
MODEL	
Flow	.30
Topography	combined with wind direction
Precipitation Efficiency	.30
UPPER AIR DATA	
Wind Direction	.40
Wind Speed	.20
Temperature (dq_s/dz)	.10
Moisture Depth	.25
DURATION	.30

6.0 PARAMETER CALIBRATION AND SENSITIVITY TESTING

6.1 General

The discussion of errors (section 5.0) implies that output values from rather large numbers of cases should be added together and compared to observation in order to obtain reliable model parameter calibrations, due to probable large and random input data representativeness errors which are of the same order of magnitude as model differences induced by parameter variation.

Snow course and precipitation data from two seasons (1965-66 and 1970-71) were employed to calibrate those model parameters requiring sums of large numbers of model computations. These two years were chosen for their extremely different flow regimes. (The winter of 1965-66 was dominated by southwest flow aloft while that for 1970-71 had an abundance of northwesterly flow and a serious lack of southwesterlies.) Resulting model parameter values or functions which gave the best areal distribution of precipitation were then adopted as standard for all 13 seasons of runs. To maintain the season sample size at 13, these two "calibration" seasons were included in all model evaluation runs. Thus, 2 of the 13 seasons are not independent data. They do not, however, dominate the results.

The primary model parameter requiring calibration is E (precipitation efficiency). However, the output values are sensitive to a number of other model processes as well as input data. Some exploration of these sensitivities has been made.

6.2 Precipitation Efficiency

As mentioned in section 4.6, E is a complex, elusive factor to quantitatively determine. Neither is it theoretically spatially

constant. For clouds of limited geographic extent, E should be negatively correlated to cloud top temperature (i.e., the colder the temperature the greater the number of active ice nuclei) and inversely related to wind speed (i.e., the faster the wind the less the crystal residence time in the cloud for continued growth). In some studies (e.g., Rhea, 1973; Elliott and Shaffer, 1962; Nielsen, 1966) though, orographic precipitation rate, $\dot{r}$, has been found to be directly proportional to wind speed, V, over a wide range of speeds. This implies no strong inverse dependence of E on windpseed, because in simplest terms $\dot{r} = E\dot{c}$, where $\dot{c}$ is condensate supply rate and $\dot{c} \propto V$. In other words, if $E = k_1/V$ and $\dot{c} = k_2 V$, then after substitution V should cancel on the right hand side of the equation $\dot{r} = E\dot{c}$. This does not appear to happen over typical ranges of wind speed.

In view of the above and the requirement for a prohibitively large number of cases in order to empirically study the "cloud top" temperature, T_c, and windspeed dependency of E separately, the primary calibration of E was restricted to a consideration of temperature effects.

One to two full winter seasons (1965-66 and 1970-71) of runs were made for a number of precipitation efficiency functions. Individual examples of the output for various values of E are shown in figure 19. The phenomenon of "shadowing" by upstream barriers becomes rather severe for the higher efficiency values.

In the particular example of figure 19, the shape of the topographic profile causes the maximum precipitation rate to occur about 50 km upwind of the highest topography in response to the greatest vertical displacement between grid points at moderate altitudes where dq_s/dz is still quite large. Relatively flat topography between 170km and 190km

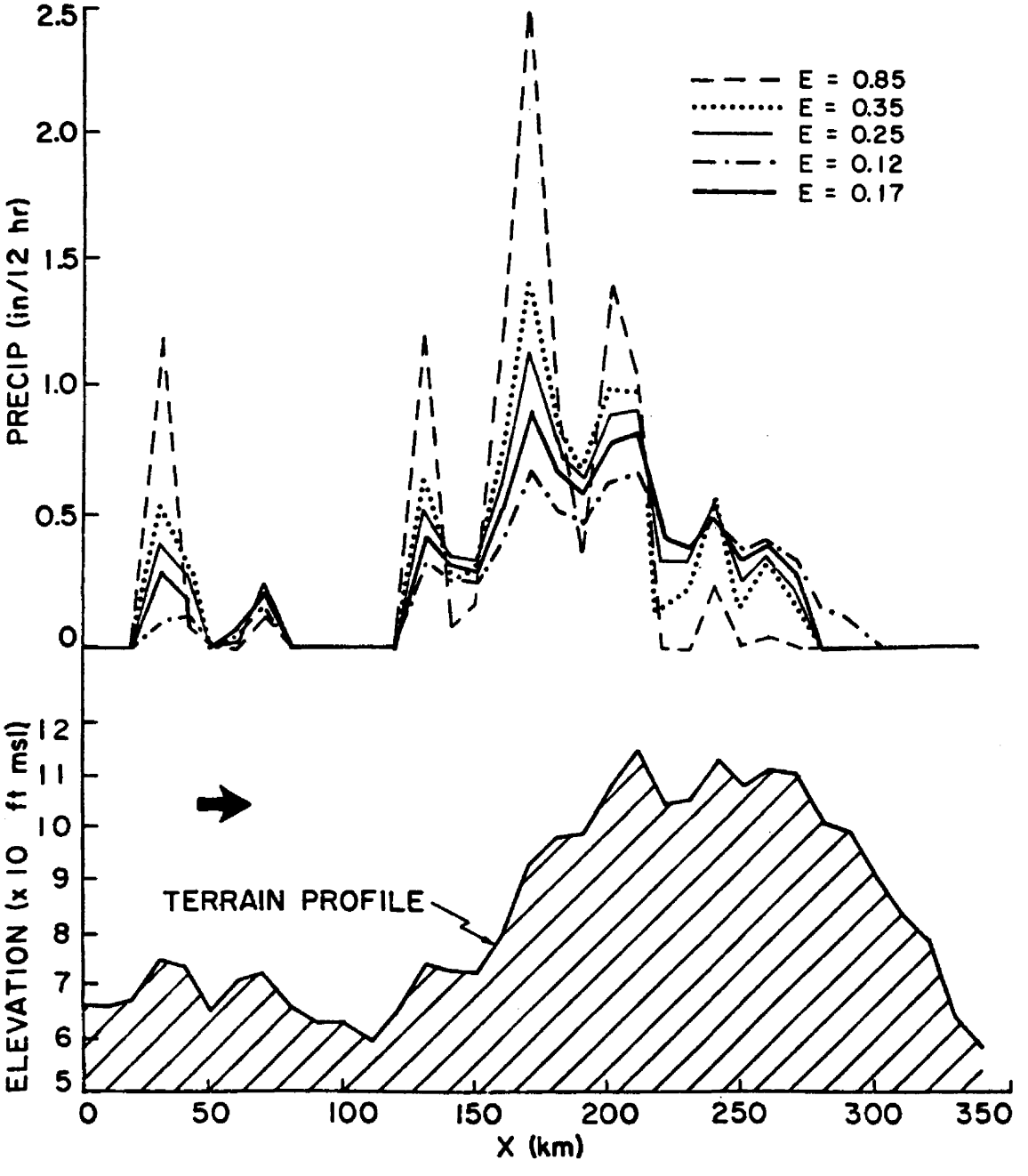

Figure 19. Examples of model sensitivity to precipitation efficiency

fails to generate enough condensate to offset the depletion by upwind precipitation of the imported cloud water. Consequently, precipitation rate decreases. From 190 km to 220 km, moderately strong lift occurs but dq_s/dz is smaller because of colder temperatures and the imported cloud water for precipiation is fairly small.

The equation (where T_c is in degrees C)

$$E = - .01T_c \qquad (6\text{-}1)$$

was found to give the best areal distribution of seasonal precipitation using a group of snowcourses from all regions of the state(for the two test seasons). Consequently, it was adopted for the 13 years of model runs, but with an upper limit of .25 for values of cloud top temperature of $\leq$ -25C to prevent over-shadowing at colder temperatures.

A linear functional form of E is considerably less sensitive to cloud top temperature than are formulations based on diffusional and accretional growth. However, extreme parameter sensitivity is not desirable (considering the crudeness of input data), as was verified by unrealistic results when testing efficiency functions based on microphysical computations.

For the interpolation point at the center of the study area, a 7 winter study (1963-1970) of the frequency of "cloud top" temperature as defined in this paper indicated 33% of the cloud tops were colder than -25C (i.e., E=0.25) while 50% were colder than -20C (i.e.,$E \geq 0.21$). Cold cloud tops implies deep clouds and thus greater atmospheric water flux. It is thus probable that at least 50% of the season moisture flux occurred with model precipitation efficiencies of 0.25 and at least 70% with efficiencies of 0.21 or greater.

6.3 Streamline Displacement

The three classes for streamline vertical displacement permitted by the model (section 4.2.3) represent distinctly different levels of influence. An example of the degree to which these differences affect precipitation is indicated in figure 20. These profiles were constructed by running the model using each of the streamline displacement classes for the same atmospheric sounding (figure 21). For comparison, the model was also run with $d = 1$ (no damping) for all levels.

Comparison of the profiles using the stable but no inversion case as a standard indicates that the existence of an inversion above "cloud top" has a severe damping effect on precipitation over the relatively low hills for this example and diminishes precipitation by 18-25 percent over the higher mountains.

The "unstable" case increases high mountain precipitation by 13-25 percent compared to the standard stable profile, and is only slightly less productive than the case for $d = 1$ at all points.

6.4 Large-Scale Vertical Motion

In this study, large-scale vertical motion, was considered to be additive to that induced by topography. From the nature of the model precipitation computation equation, large-scale vertical motion had to be less effective in overcoming "shadowing" effects for strong wind compared to slower flow cases. Downward values of w would further intensify "shadowing" effects. However, with negative w, restrictions are necessary on the maximum allowable downward parcel displacement (lest the parcels burrow into the ground). Figure 22 gives examples of the effects of w on precipitation profiles.

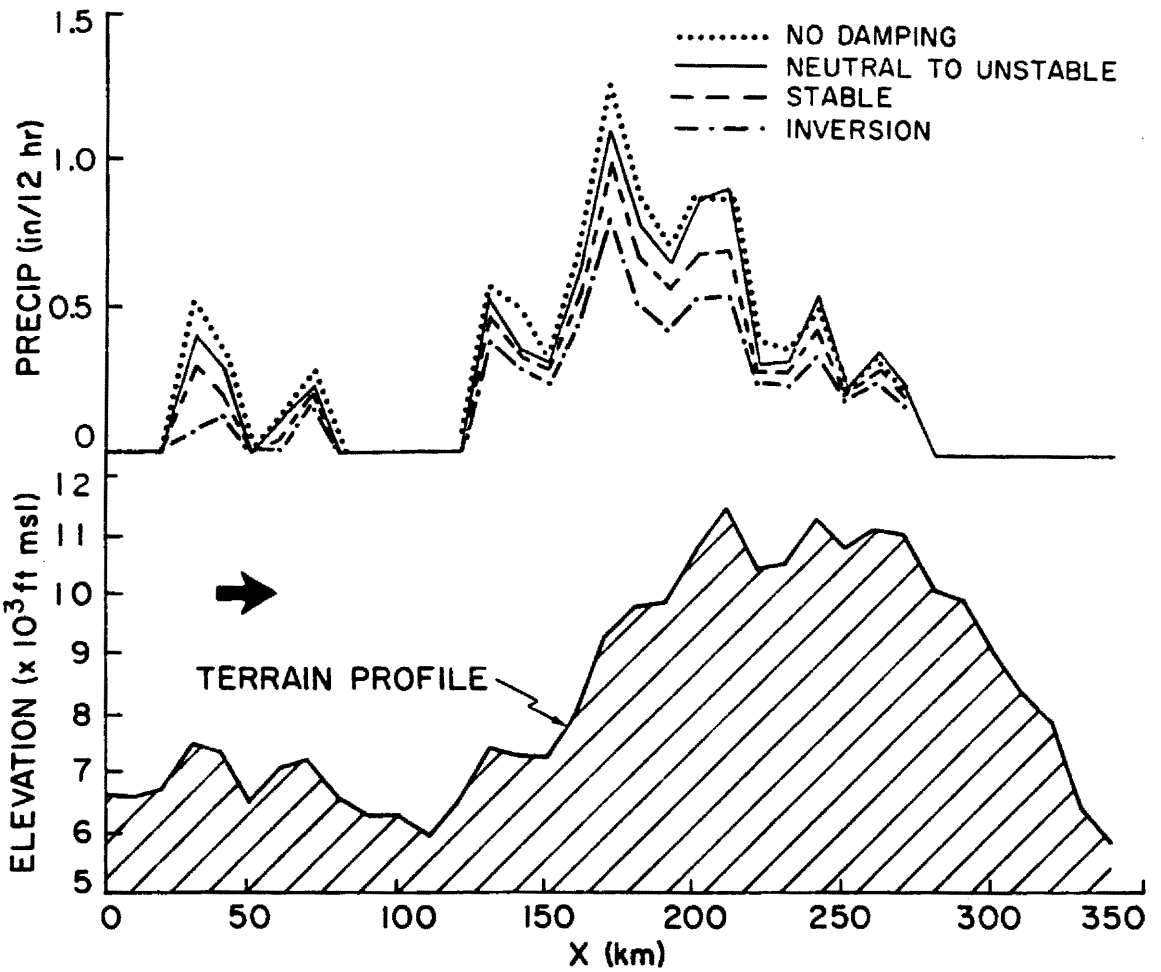

Figure 20. Examples of model sensitivity to streamline vertical displacement classes

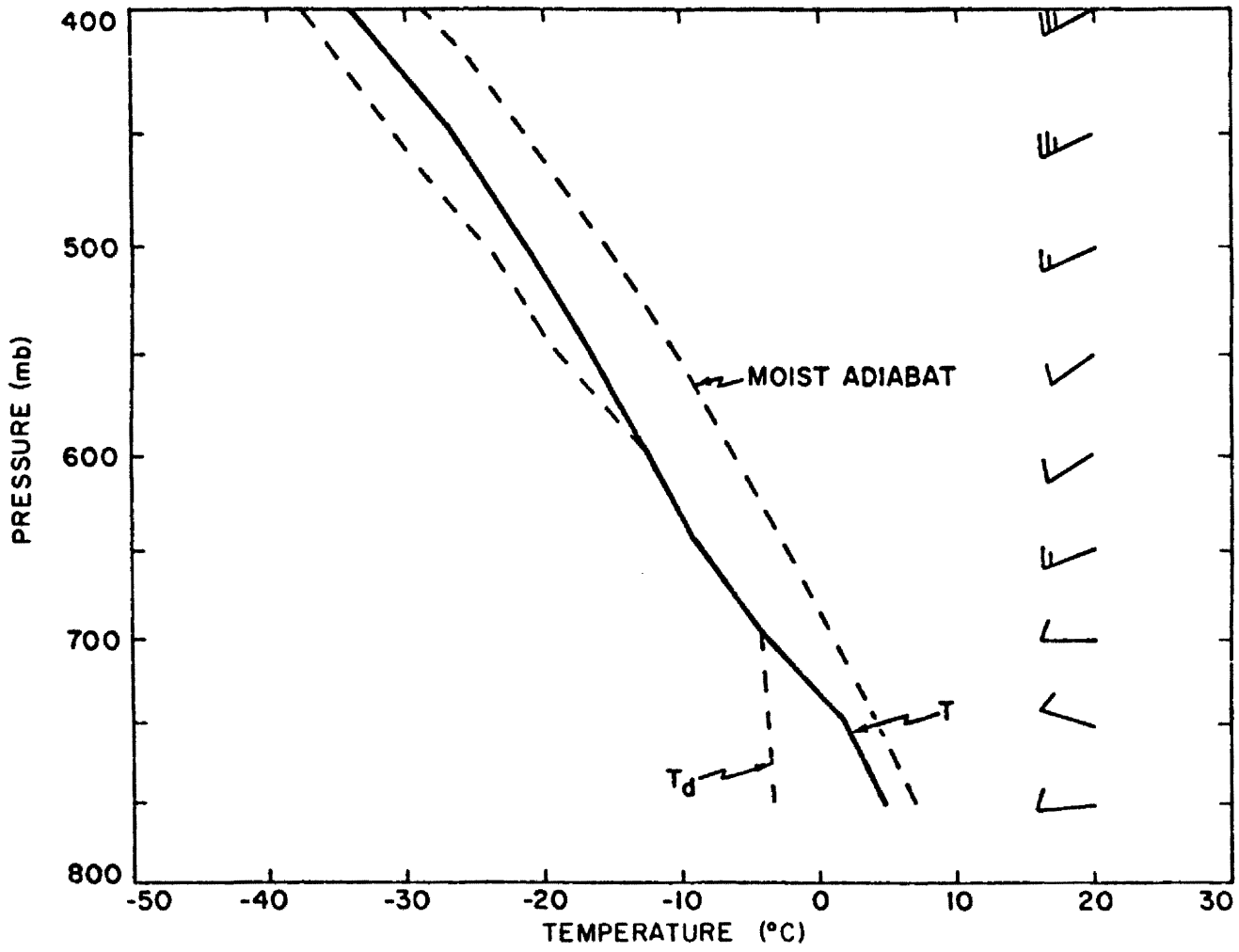

Figure 21. Hypothetical sounding used to make sensitivity tests

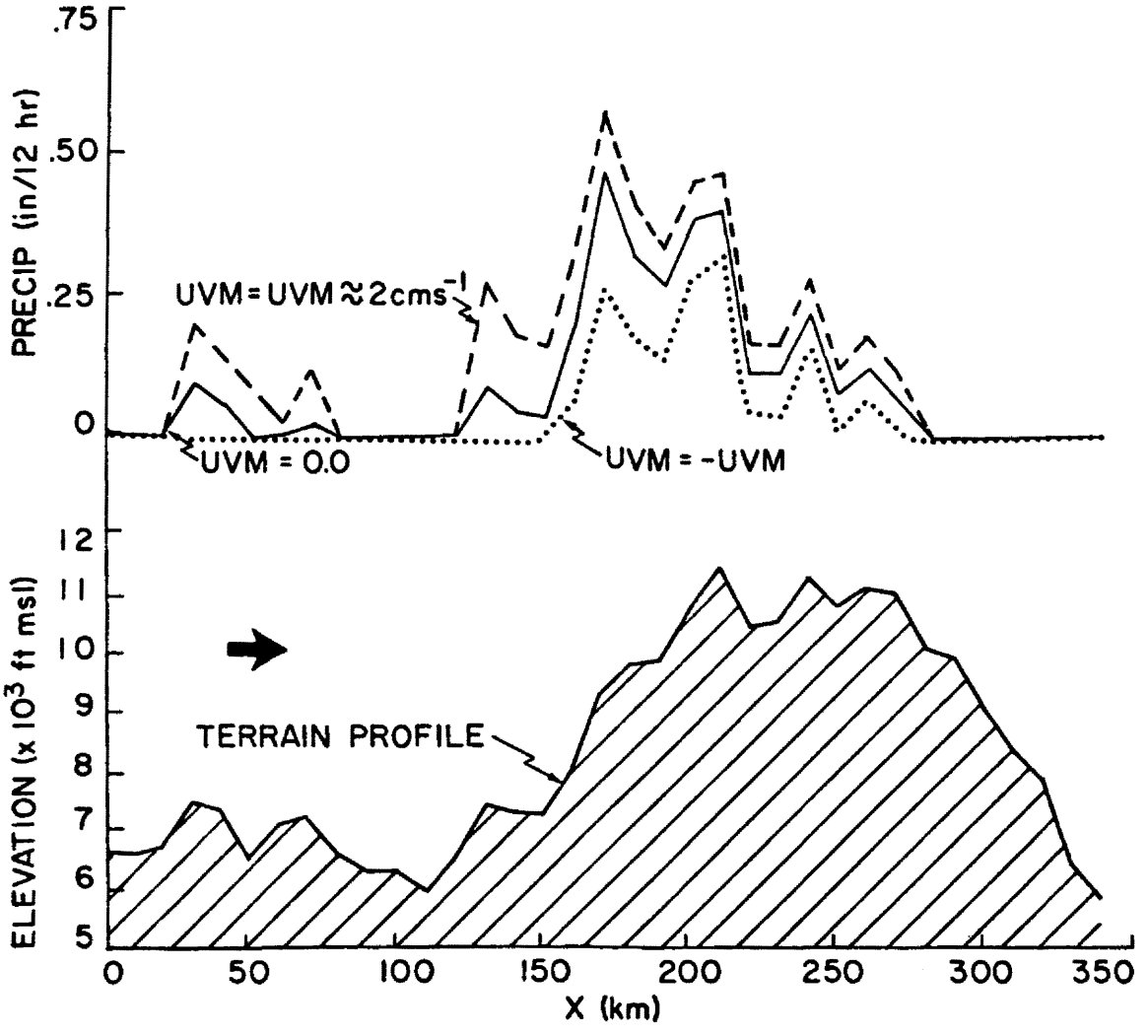

Figure 22. Examples of model sensitivity to large-scale vertical motion

Table 5. Results of a Year of Testing with Various Values of Large-Scale Vertical Motion

A	B	C	D		E	F	
Water-shed no.	Production Run $w \geq 0$ (in.)	Test 1 Run ($w = 0$) (in.)	Test 1 minus Production (in.)	%	Test 2 Run ($w < 0$) (in.)	Test 2 minus Production (in.)	%
15 October-30 April							
1	23.65	20.61	-3.04	-12.8	23.09	-.56	-2.6
2	14.76	12.27	-2.49	-16.9	14.10	-.66	-4.5
3	7.59	5.86	-1.73	-22.3	7.12	-.47	-6.2
4	21.27	18.53	-2.74	0.12.9	20.58	-.69	-3.2
5	28.25	25.44	-2.81	- 9.9	27.59	-.66	-2.3
6	14.10	11.64	-2.46	-17.4	13.09	-1.01	-7.2
7	19.63	17.14	-2.49	-12.7	19.36	-.27	-1.3
8	23.01	20.38	-2.63	-11.4	22.71	-.30	-1.3
9	22.12	19.59	-2.43	-11.0	21.49	-.63	-2.9
10	14.76	12.28	-2.48	-16.8	14.25	-.51	-3.4
11	6.39	4.21	-2.18	-34.1	611	-.23	-4.4
12	6.09	3.84	-2.25	-36.9	5.71	-.38	-6.2
13	13.52	9.68	-3.84	-23.4	12.60	-.92	-6.8
14	11.15	7.31	-3.34	-34.4	10.51	-.64	-5.7
15	11.43	8.30	-3.13	-27.4	10.48	-.95	-8.3
16	4.09	2.43	-1.66	-40.6	3.81	-.28	-6.8
17	8.54	5.80	-2.74	-32.1	7.71	-.83	-9.7
18	24.33	18.66	-5.67	-23.3	22.76	-.57	-2.3
19	8.66	5.62	-3.04	-35.1	7.90	-.76	-8.8
Average			-2.82	-23.0		-.60	-4.9

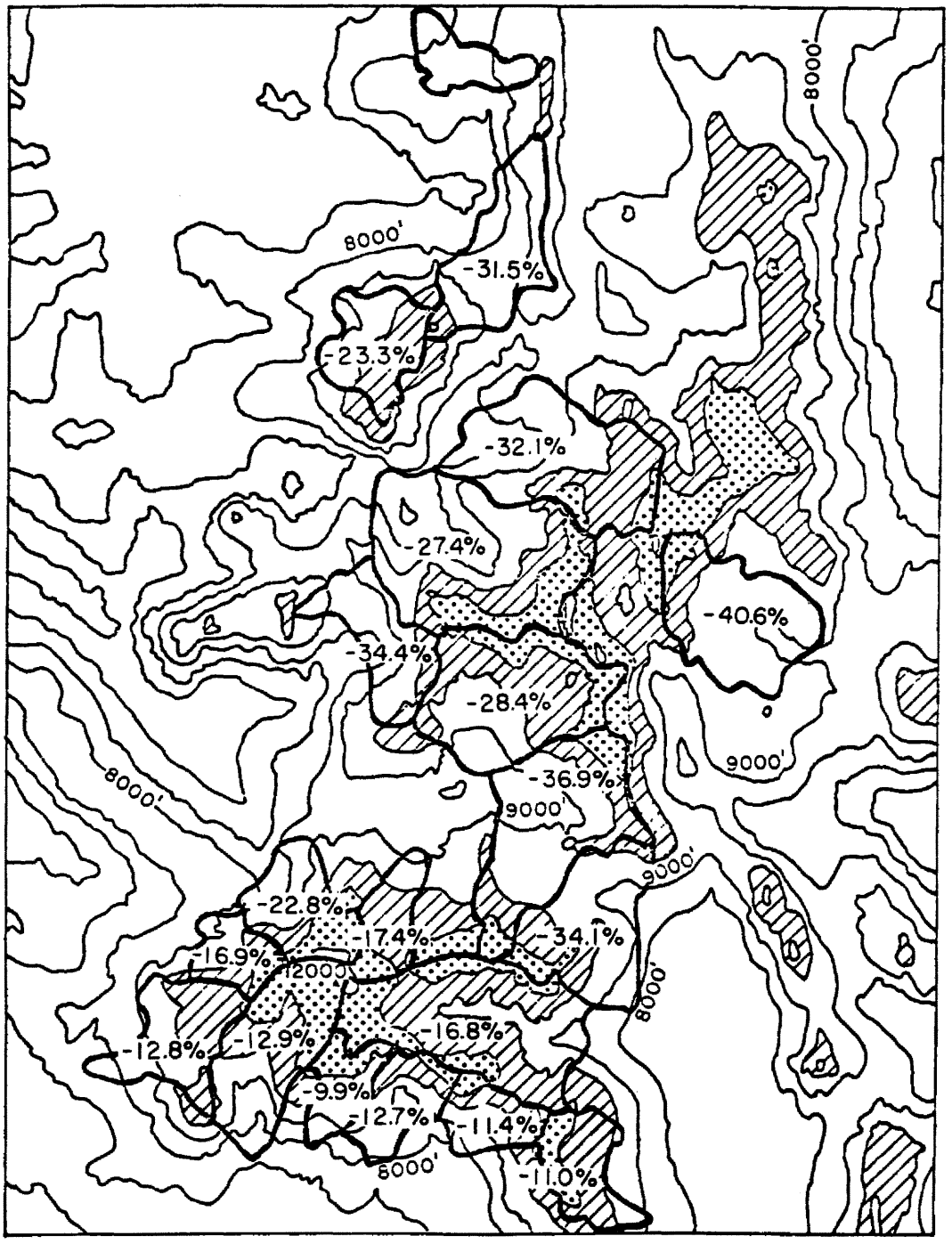

Figure 23. Percent decrease of model precipitation from setting large-scale vertical motion to zero for the period 15 October 1965-30 April 1966. The season was dominated by southwest flow aloft

For the 13-year study, the practice of allowing only zero or upward values of w in model computations was adopted to eliminate the problem of subterranean sinking parcels.

Table 5 indicates the effect of setting $w = 0$ in all cases for the 1965-1966 test season is to decrease precipitation by an average of 23 percent, while a decrease of about five percent occurs when allowing negative as well as positive large-scale vertical motion.

The test year (1965-1966) was dominated by southwesterly flow. Clearly, when studying figure 23, a primary effect from ignoring large-scale vertical motion is to increase the shadowing in areas downstream from southwest Colorado. In other words, in this model, the large-scale upward vertical motion field appears to be quite important in lifting parcels back to saturation following passage of the airsteam over an initial high barrier.

6.5 Sensitivity to Grid Interval

Precipitation in mountainous terrain is observed to vary markedly over distances as small as 2 to 5 km. However, considering the time scale of snow crystal growth, and typical windspeeds, 10-20 km should be near the lower horizontal scale limit of the orographic precipitation process (e.g., Sawyer, 1956). As a compromise between observation and theory, test computations in this study were made for 5 km and 10 km grid intervals.

Figure 24 gives examples of precipitation profiles for each of the grid resolutions. The 5 km grid interval allows more realistic simulation of precipitation regimes for very local deep valleys surrounded by rugged terrain. However, since the model does not permit air to blow around small-scale flow obstructions, this finer topographic

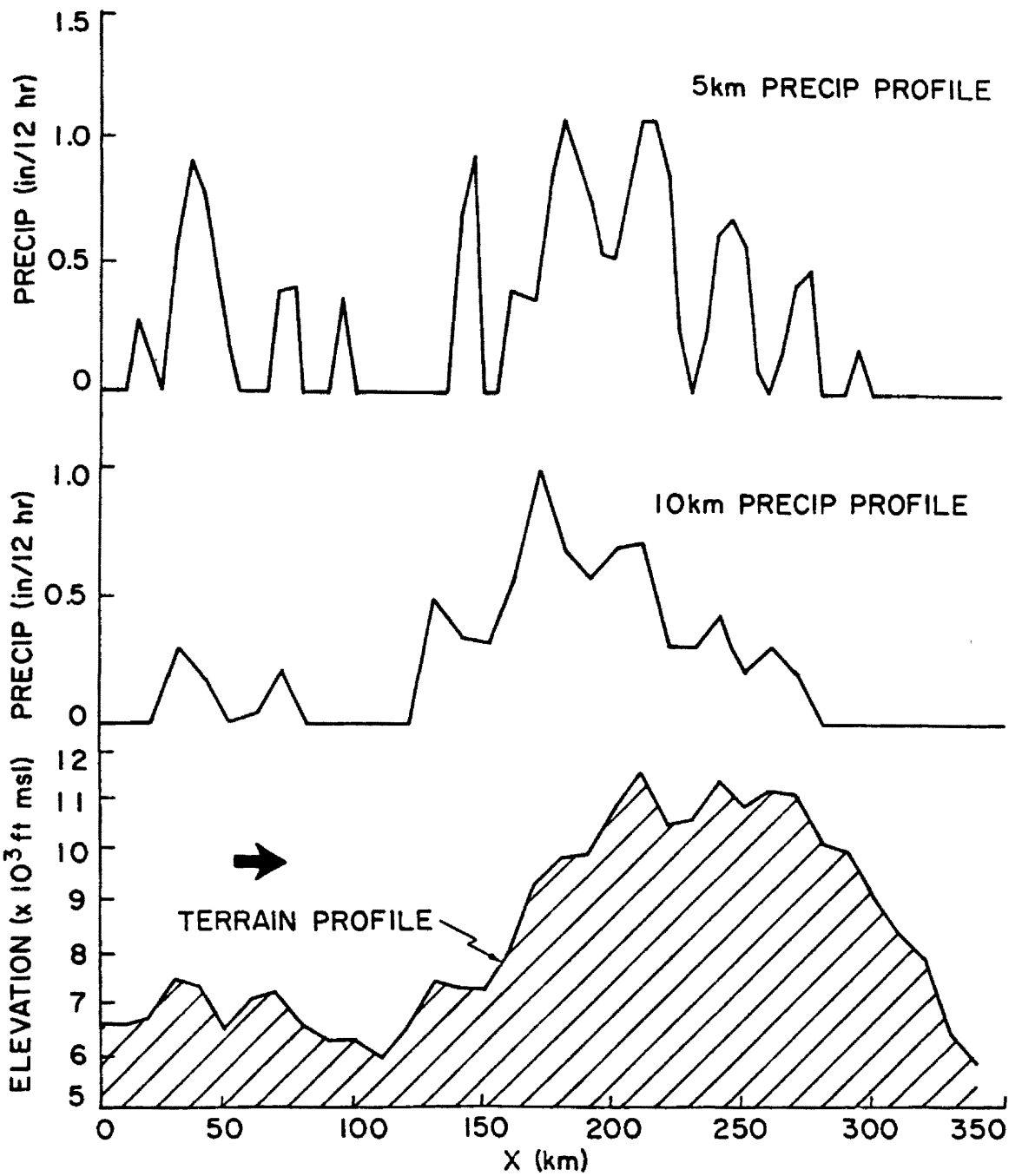

Figure 24. Comparisons of model precipitation profiles for 10km and 5 km grid intervals

resolution very likely erroneously puts too much snow on the highest peaks. Furthermore, running time quadruples using this fine-mesh grid. In view of the latter, and the questionable gain in overall areal-total precipitation accuracy, the larger-scale 10 km grid mesh was chosen for the 13-year study.

6.6 Relative Humidity

As described in Appendix B, a major change in radiosonde relative humidity sensors was made during the 13-year study period. Corrections for errors with both types of sensors were attempted. It is thus desirable to determine model sensitivity to relative humidity values.

Tests of the effect of increasing as well as decreasing all relative humidity values by 10 percent were made for the 1965-1966 season (Table 6). Results indicated rather extreme model sensitivity to humidity values. One reason for the sensitivity is that, if the profile of relative humidity does not contain a layer of $\geq$ 65 percent value, the sounding was considered too dry for precipitation (in agreement with historical observation) and precipitation computations were not made. Thus altering the relative humidity by $\pm$10 percent significantly changed the number of cases for which precipitation computations were made. In addition to the above, though, the model is truly rather sensitive over low to moderately high terrain to relative humidity variations as can be seen from Figure 25.

The primary conclusion to be drawn from these tests is that the relative humidity corrections that were made to the 13-year record of input data (Appendices C and D) must have reasonably rectified the errors for each sensor type. Otherwise, the latter nine years of model

Table 6. Results of Relative Humidity Sensitivity Test for 1965-1966 Season

Production Run		Test 1 RH = RH + 10%		Test 2 RH = RH - 10%	
	(in.)	(in.)	Percent Change	(in.)	Percent Change
1	23.65	32.26	36.4	14.09	-40.4
2	14.76	20.06	35.9	9.80	-33.6
3	7.59	10.19	34.3	5.31	-30.0
4	21.27	28.66	34.7	13.94	-34.5
5	28.25	37.77	33.7	19.33	-31.6
6	14.10	18.73	32.8	10.21	-27.6
7	19.63	25.12	33.1	12.42	-36.7
8	23.01	31.64	37.5	14.73	-36.0
9	22.12	33.47	51.3	15.21	-31.2
10	14.76	18.54	25.6	10.37	-29.7
11	6.39	7.66	19.9	4.38	-31.3
12	6.09	8.00	31.4	4.31	-29.2
13	13.52	16.19	34.5	9.27	-31.4
14	11.15	14.69	31.7	7.07	-36.6
15	11.43	15.93	39.8	7.30	-36.1
16	4.09	5.59	36.7	2.86	-30.1
17	8.54	12.56	47.1	5.53	-35.2
18	24.33	33.77	38.8	15.20	-37.5
19	8.66	13.07	50.9	5.14	-40.6

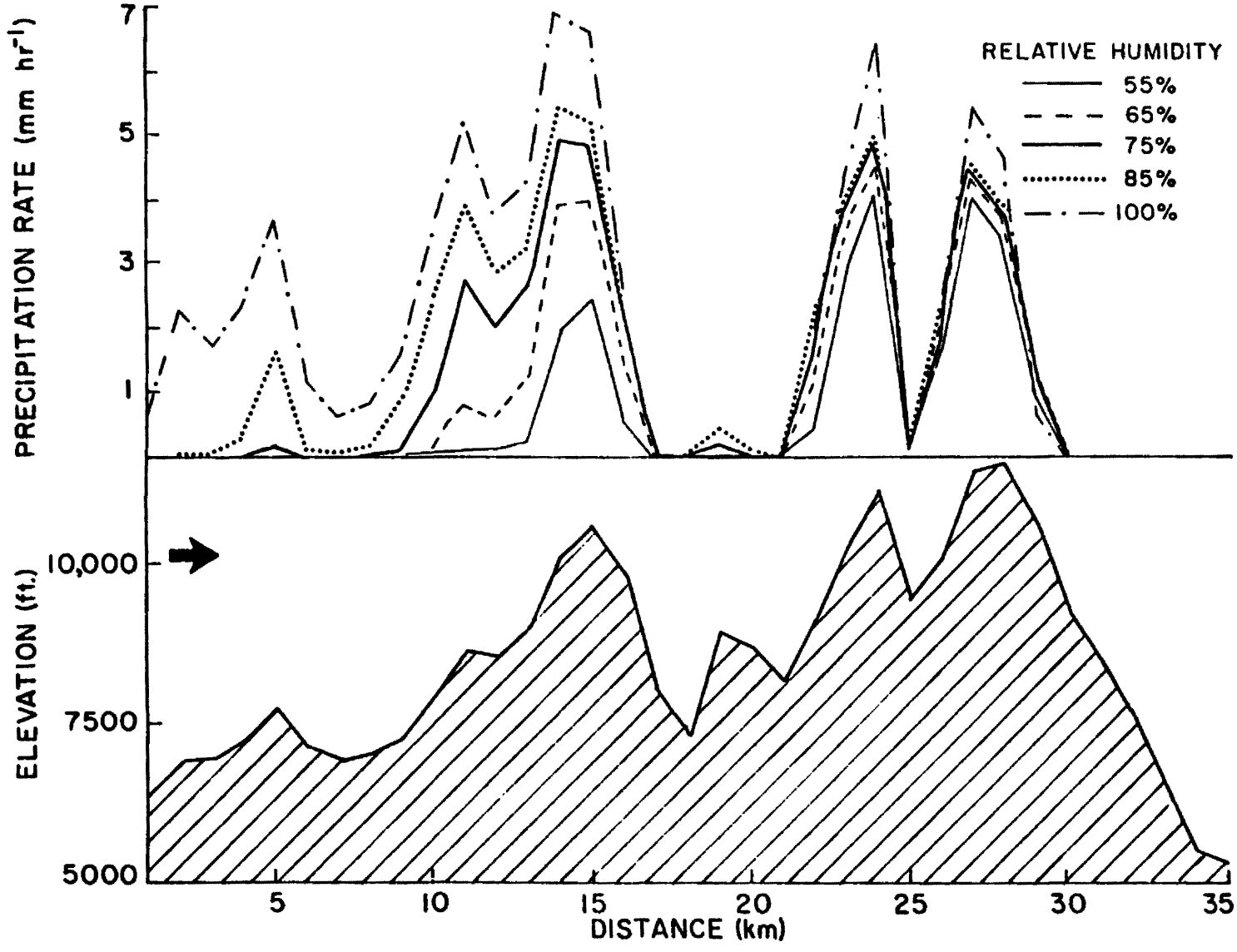

Figure 25. Example of model sensitivity to the input profile of relative humidity for deep moisture and V = 30 m/s

computations would have given substantially different results from the earlier years.

6.7 Blocking

The criteria for blocking were described in Section 4.1.2. Tests were run using those rules and interpolated large-scale sounding data. Primarily two modifications in procedure were found necessary. First, it was necessary to consider the layer below the 800 mb level to be blocked in all cases. (Most of the upper air stations were at approximately the 840 mb surface pressure level.) Not to do so resulted in over-predictions of precipitation on barriers rising abruptly from deep broad river valleys (e.g., the Grand Mesa in figure 26). Second, for west and west-northwest flow, the blocked layer top was forced to always be 800 mb for border points 3, 4, and 5 (see figure 1 of section 3.3).

The second of the above required modifications is largely a problem of the upper air interpolation inaccuracy. Frequently, in conditions of west to west-northwest flow aloft, moderate to strong sea level pressure gradient develops across Wyoming and extends into northern Colorado while very weak flow is observed over central and southern Colorado. The Grand Junction (GJT) radiosonde under these conditions frequently indicates either temperature inversions or isothermal vertical structure with light and variable winds to approximately 700 mb. The upper air interpolation scheme weights this stagnant GJT condition too heavily when computing the wind and temperature profiles for border points 3, 4, and 5, resulting in unrealistically deep blocked layers.

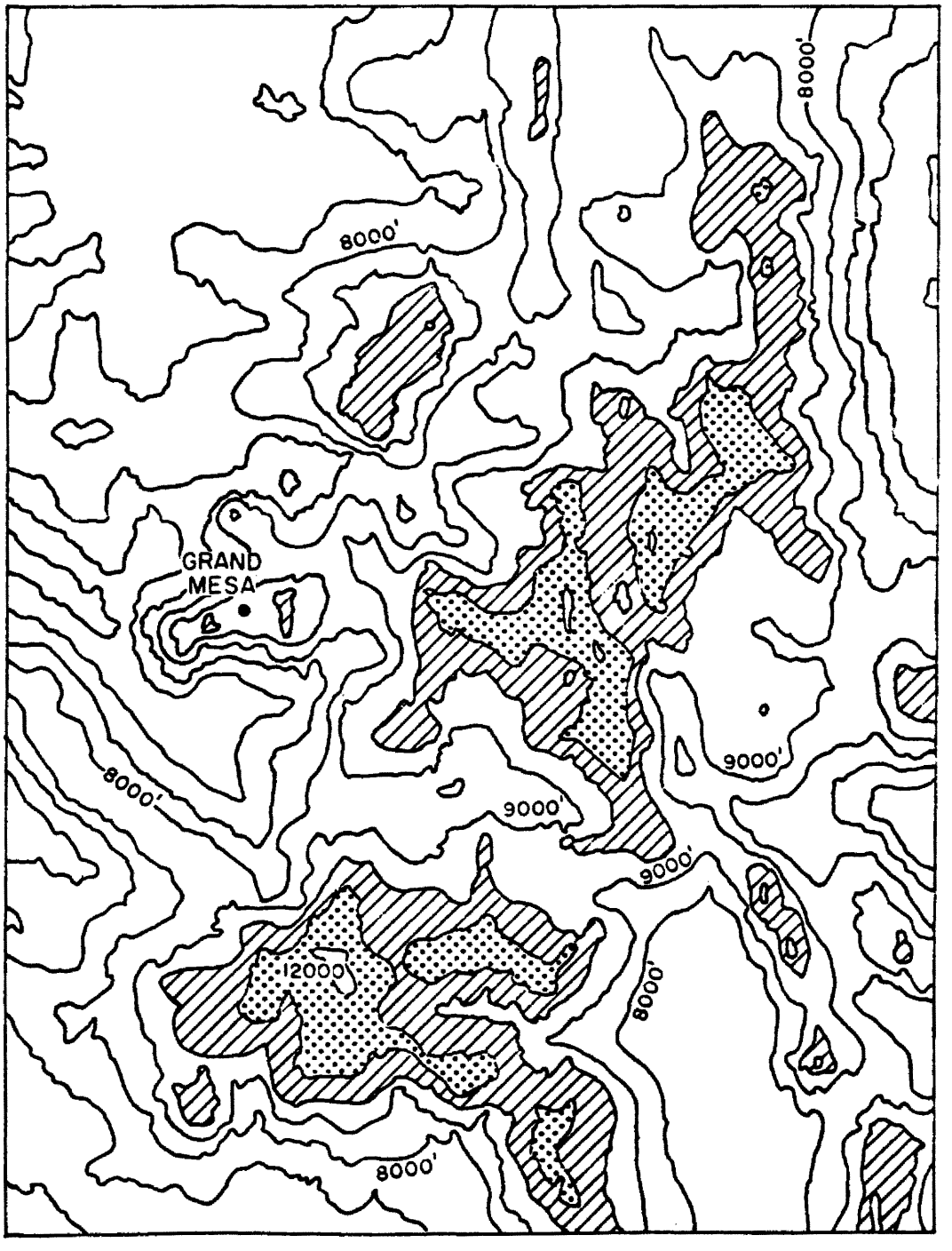

Figure 26. Model topography with the Grand Mesa indicated

7.0 TESTING THE MODEL

7.1 Historical Computations

Computations of precipitation for each grid point at each sounding time were made for the period 15 October-30 April for each of 13 seasons from 1961-1962 through 1973-1974.

To prevent over-prediction, the period of representativeness of each sounding was assumed to be 10 hours. Summations of computed precipitation were made for each season.

Figures 27 through 39 show the model isohyetal patterns for each season. Marked variations occur from year to year in totals over the area as a whole as well as in regions of relatively heavy and light precipitation. For instance 1964-1965 was indicated to be a very heavy precipitation season over the whole area (with over 50 inches or 1270 mm in some locations) while 1962-1963 was quite light generally. Observations agreed well with model indications. In 1970-1971 large values were indicated and observed in the northern mountains with below normal in the south, while the reverse trend was both indicated and observed in 1965-1966 with near normal values in the south and very low quantities in the north. Hence, even with a cursory look, the model's ability to describe both the interseasonal and areal variations in precipitation is evident.

The following sections give more detailed comparisons between model and observed values, areally and temporally.

7.2 Comparison to Snowcourses

Groups of snowcourses were selected for comparison to model precipitation computations in each of 21 areas (see figure 40). Areally averaged 15 October-30 March model precipitation was then

Figure 27. 1961-1962 season isohyetal map of model precipitation (inches). Topography is indicated by shading

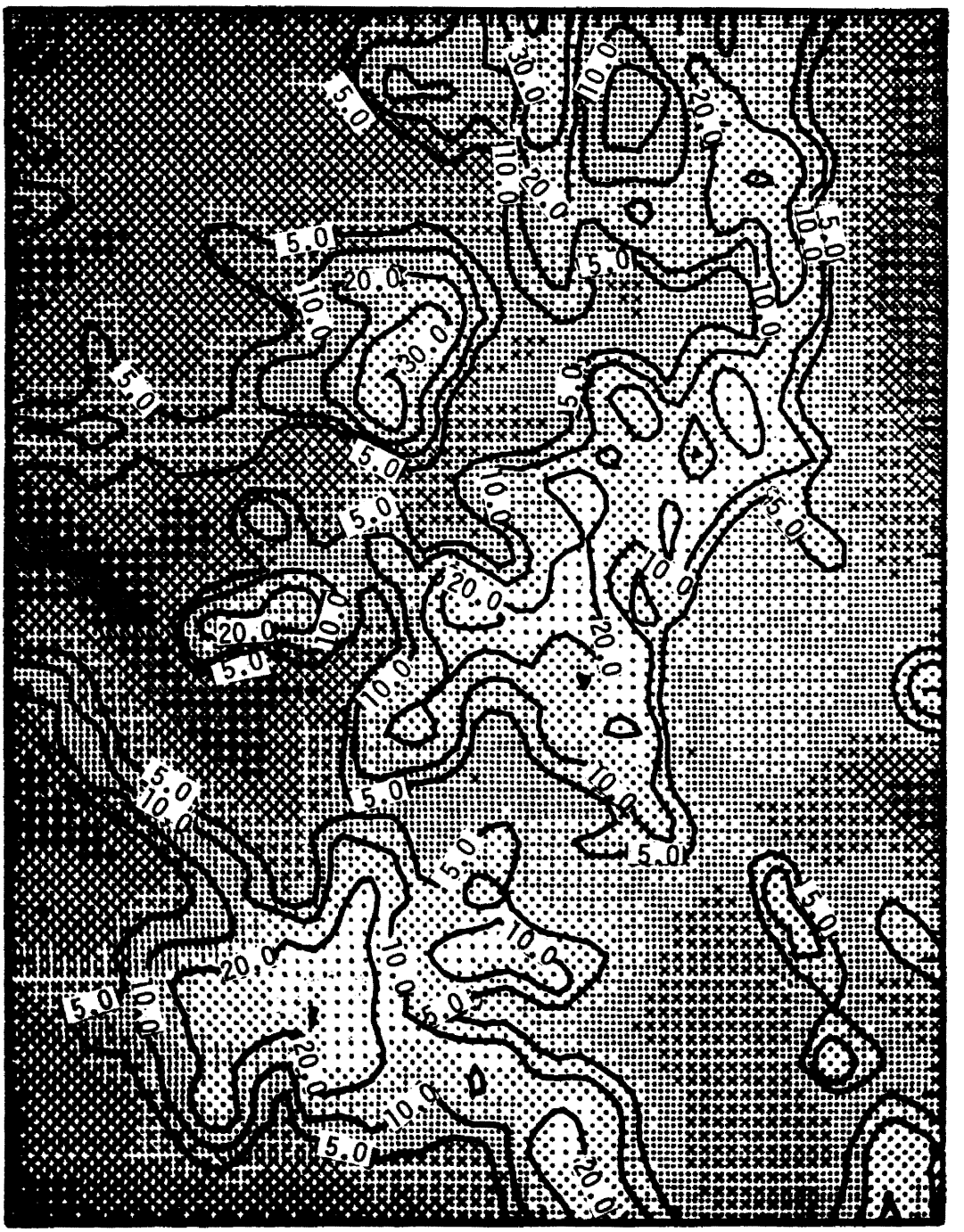

Figure 28. 1962-1963 season isohyetal map of model precipitation (inches). Topography is indicated by shading

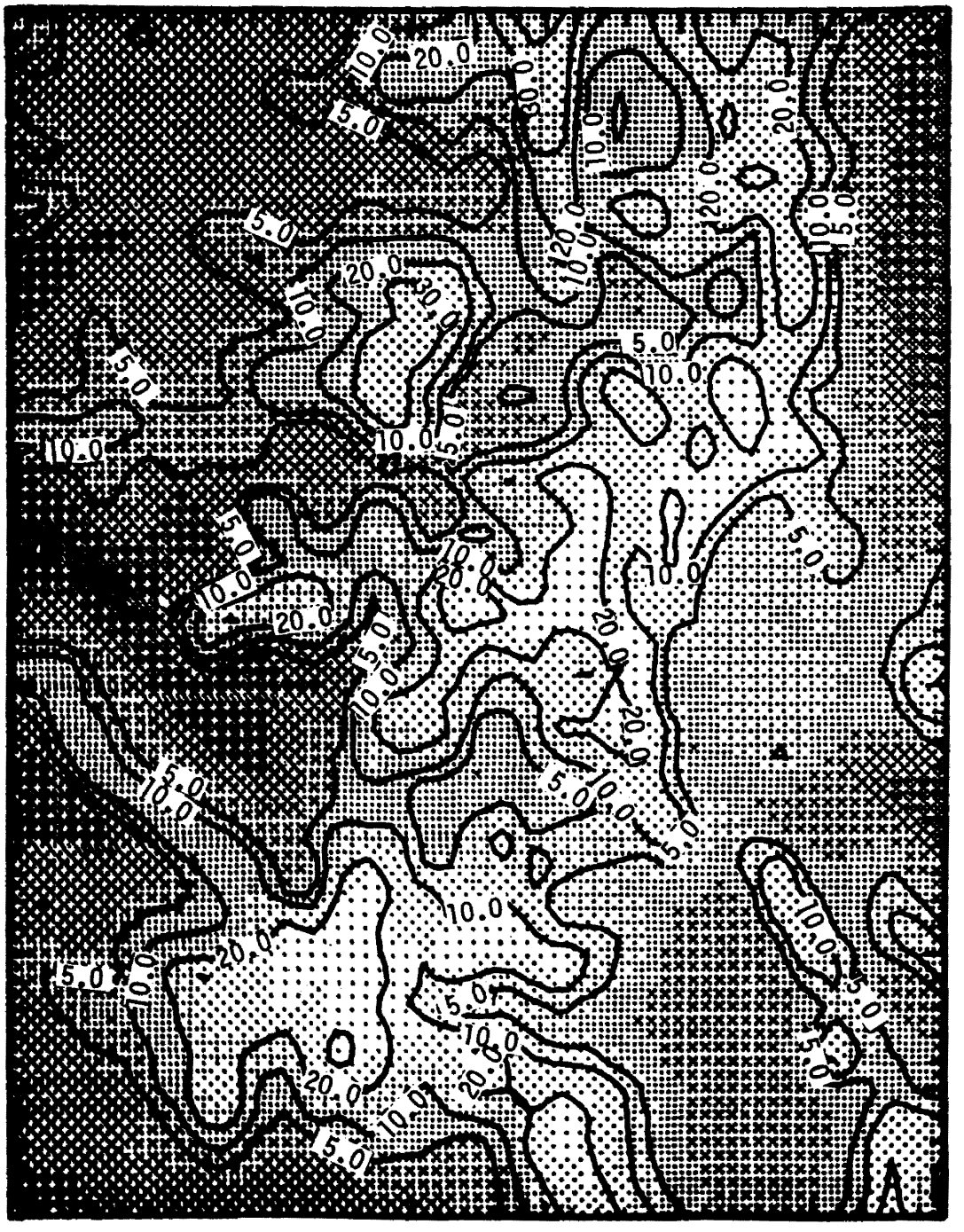

Figure 29. 1963-1964 season isohyetal map of model precipitation (inches). Topography is indicated by shading

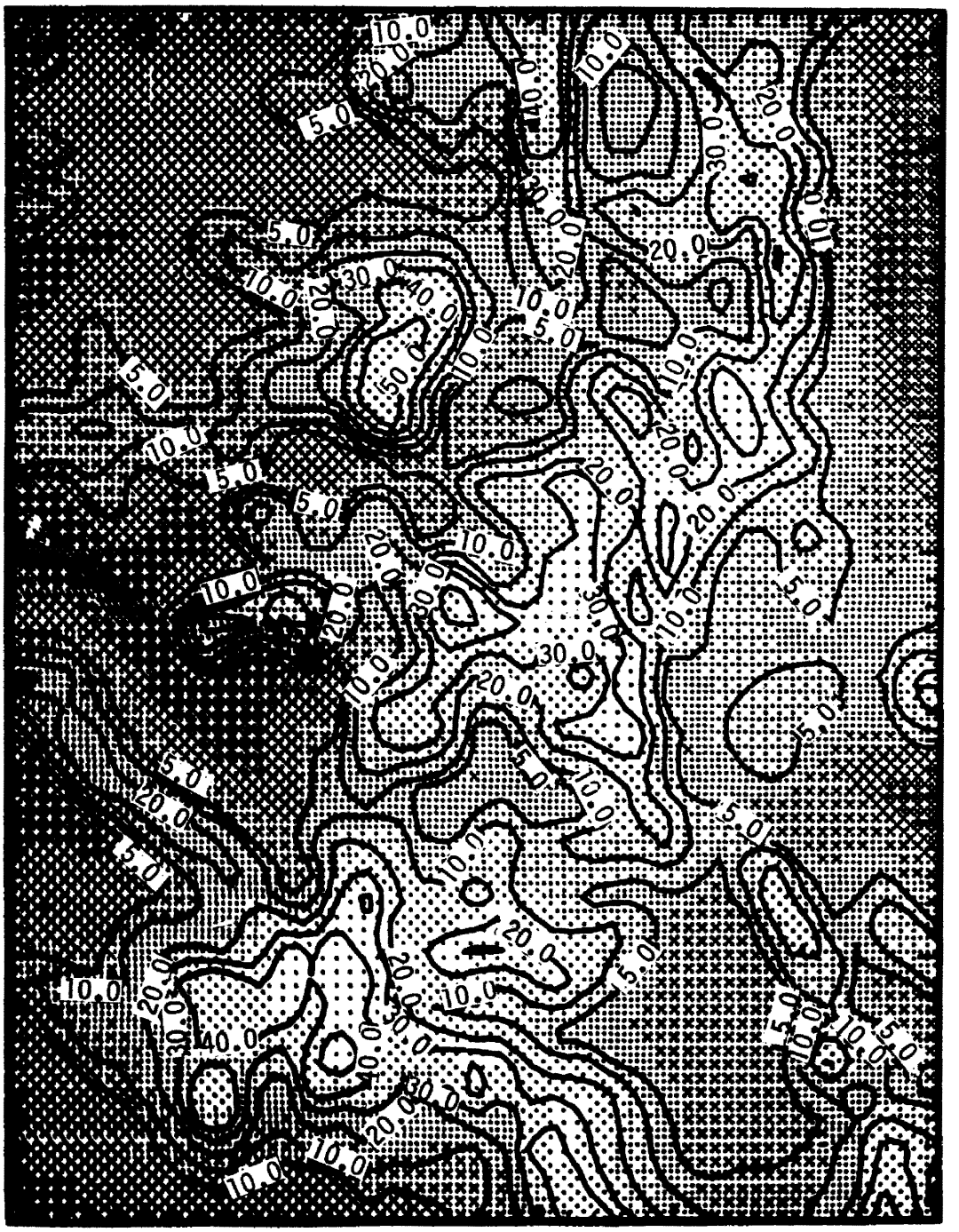

Figure 30. 1964-1965 season isohyetal map of model precipitation (inches). Topography is indicated by shading

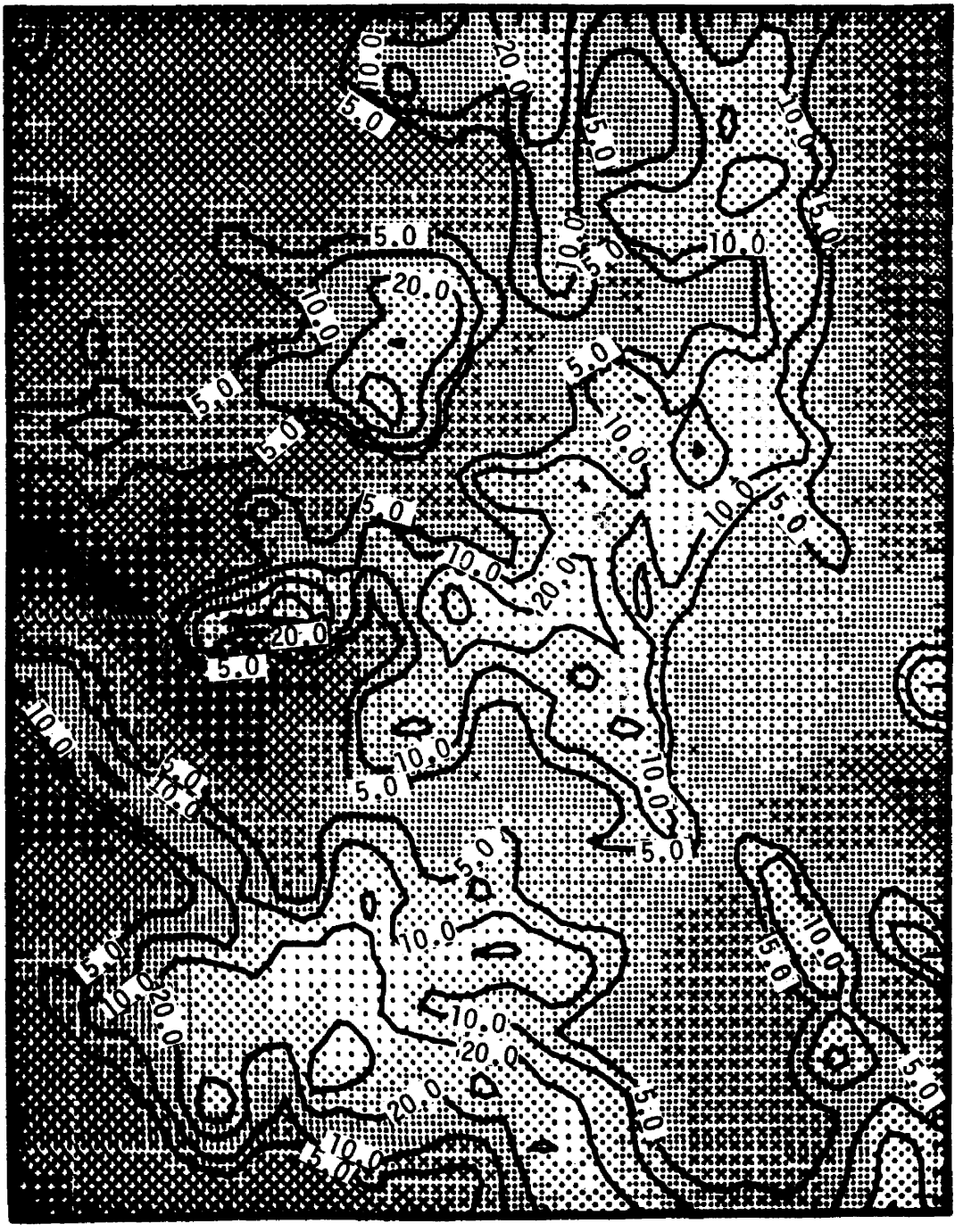

Figure 31. 1965-1966 season isohyetal map of model precipitation (inches). Topography is indicated by shading

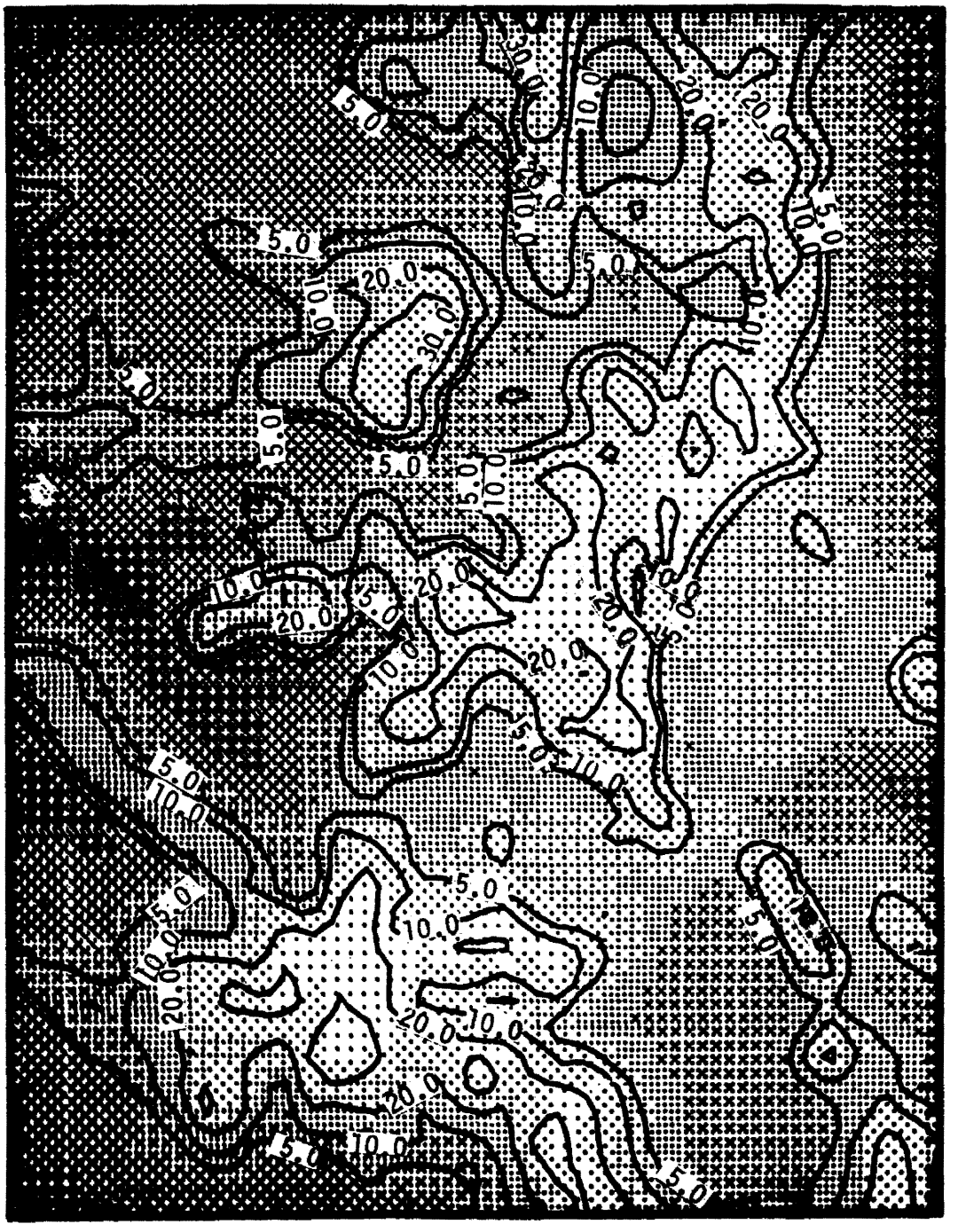

Figure 32. 1966-1967 season isohyetal map of model precipitation (inches). Topography is indicated by shading

Figure 33. 1967-1968 season isohyetal map of model precipitation (inches). Topography is indicated by shading

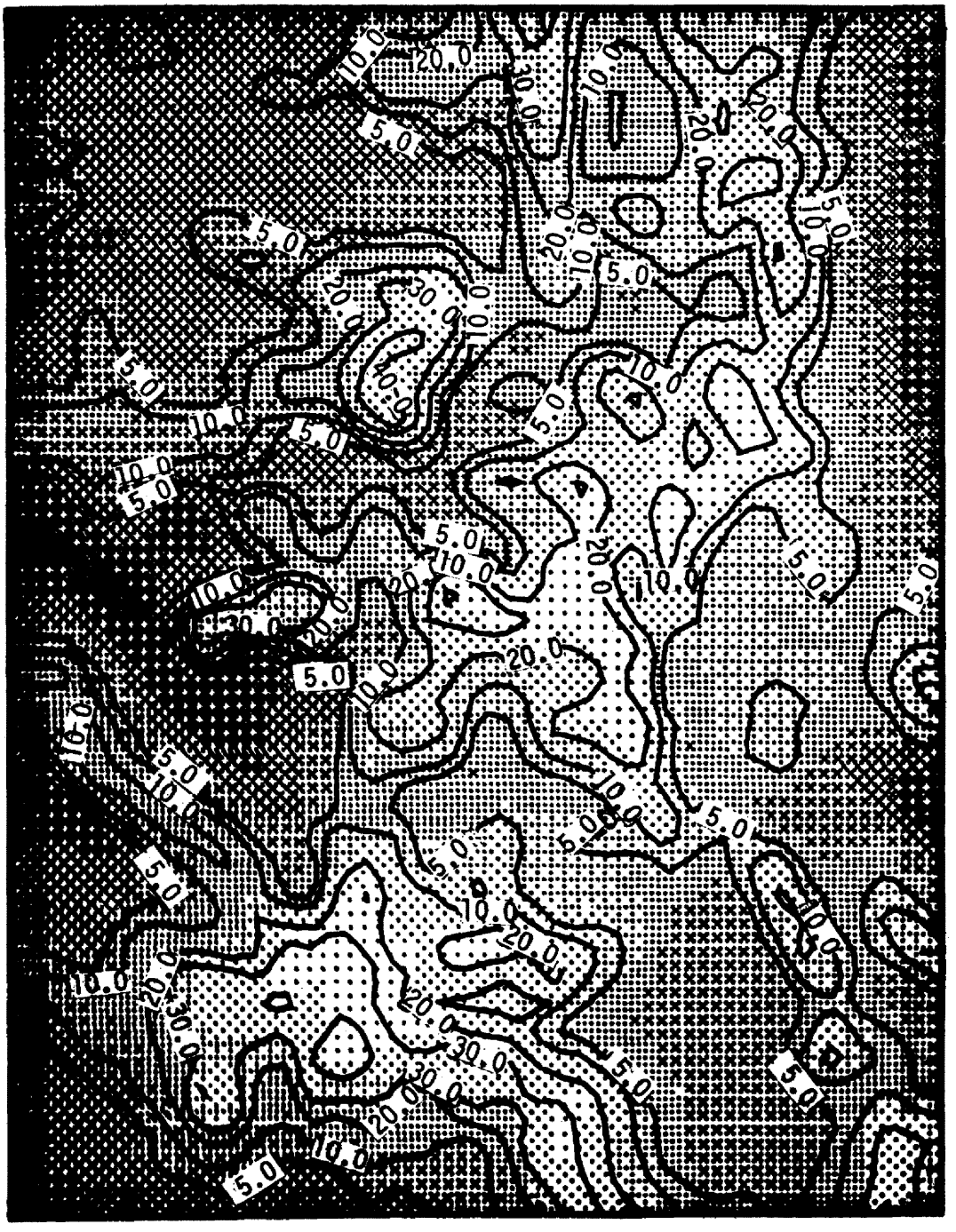

Figure 34. 1968-1969 season isohyetal map of model precipitation (inches). Topography is indicated by shading

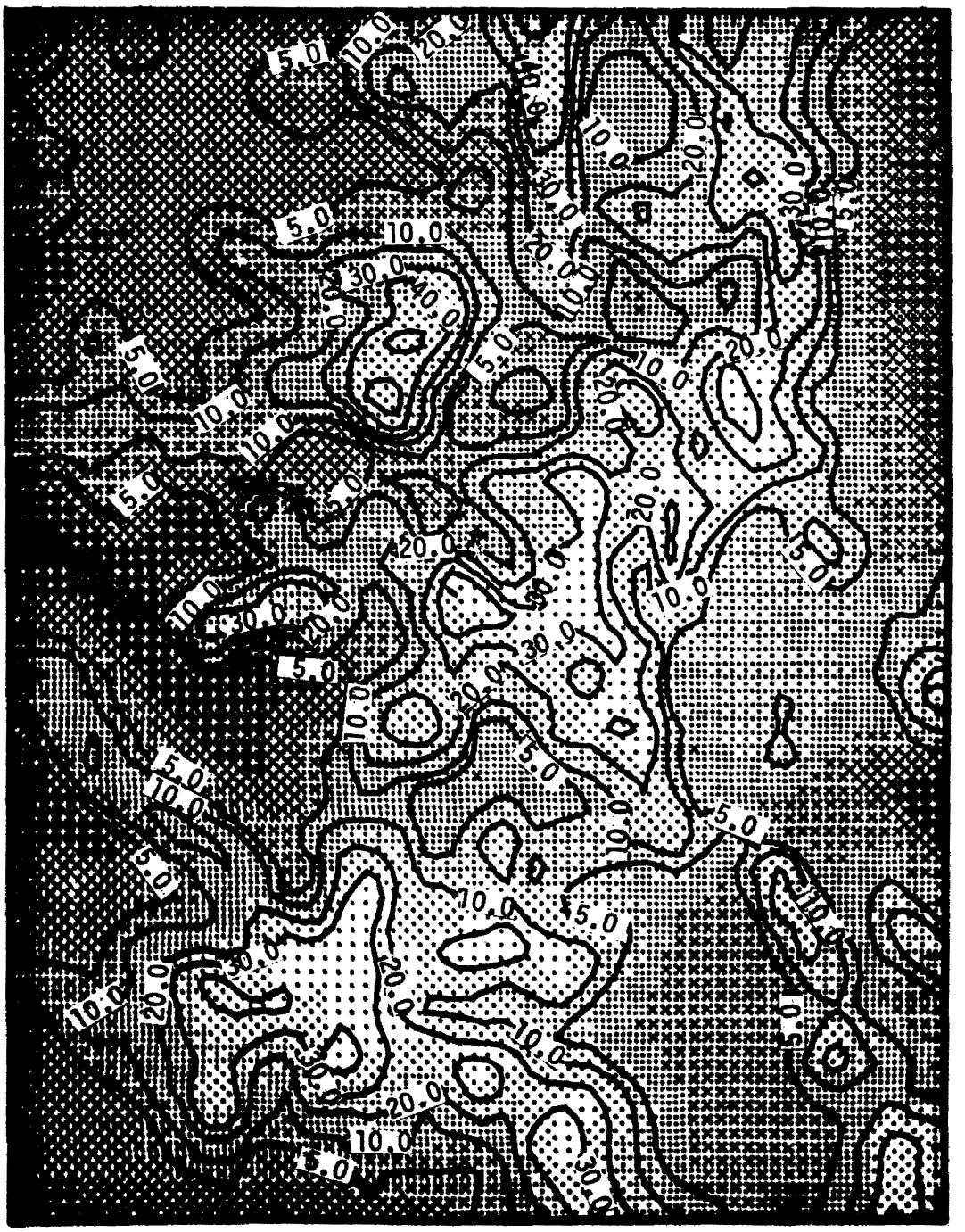

Figure 35. 1969-1970 season isohyetal map of model precipitation (inches). Topography is indicated by shading

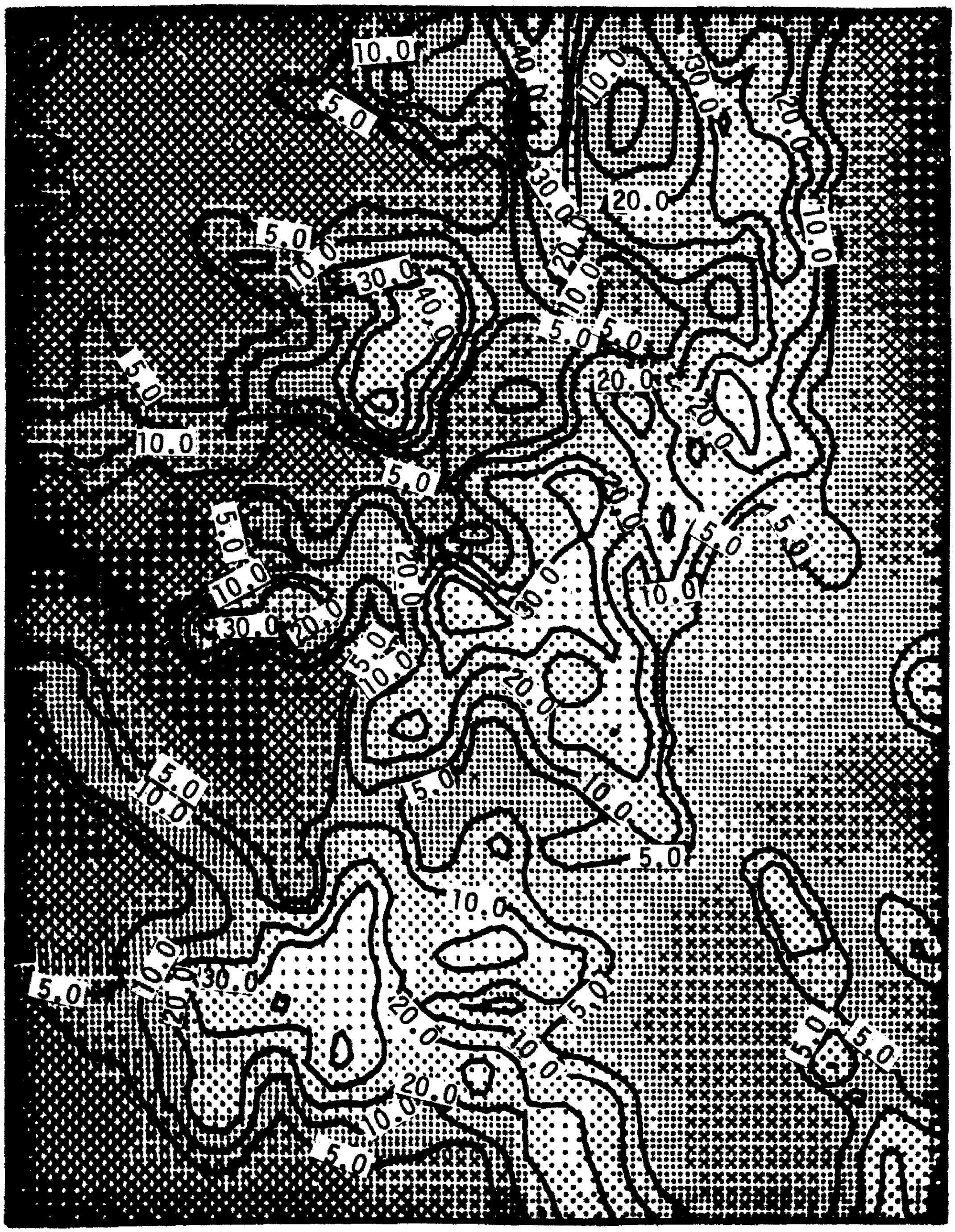

Figure 36. 1970-1971 season isohyetal map of model precipitation (inches). Topography is indicated by shading.

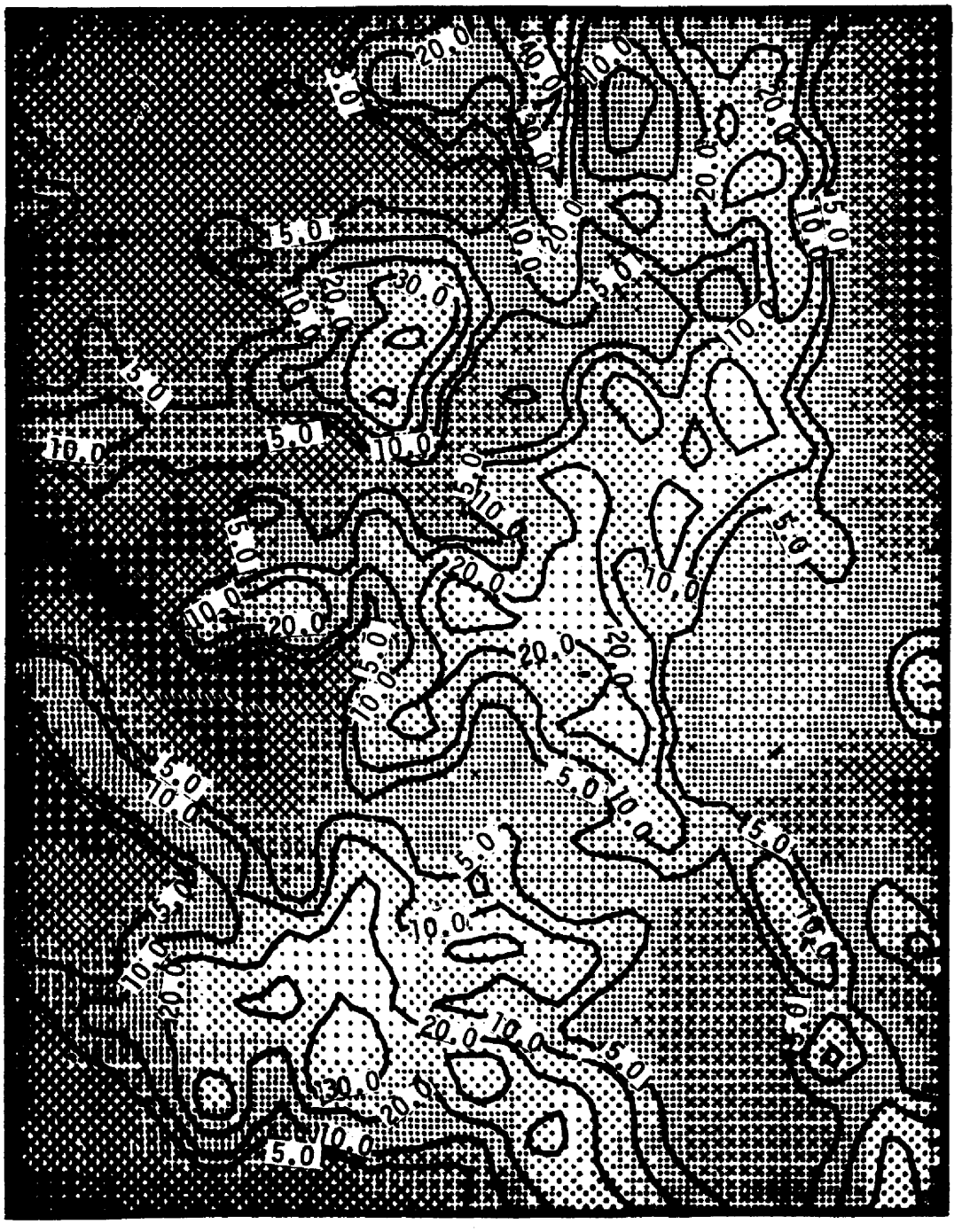

Figure 37. 1971-1972 season isohyetal map of model precipitation (inches). Topography is indicated by shading

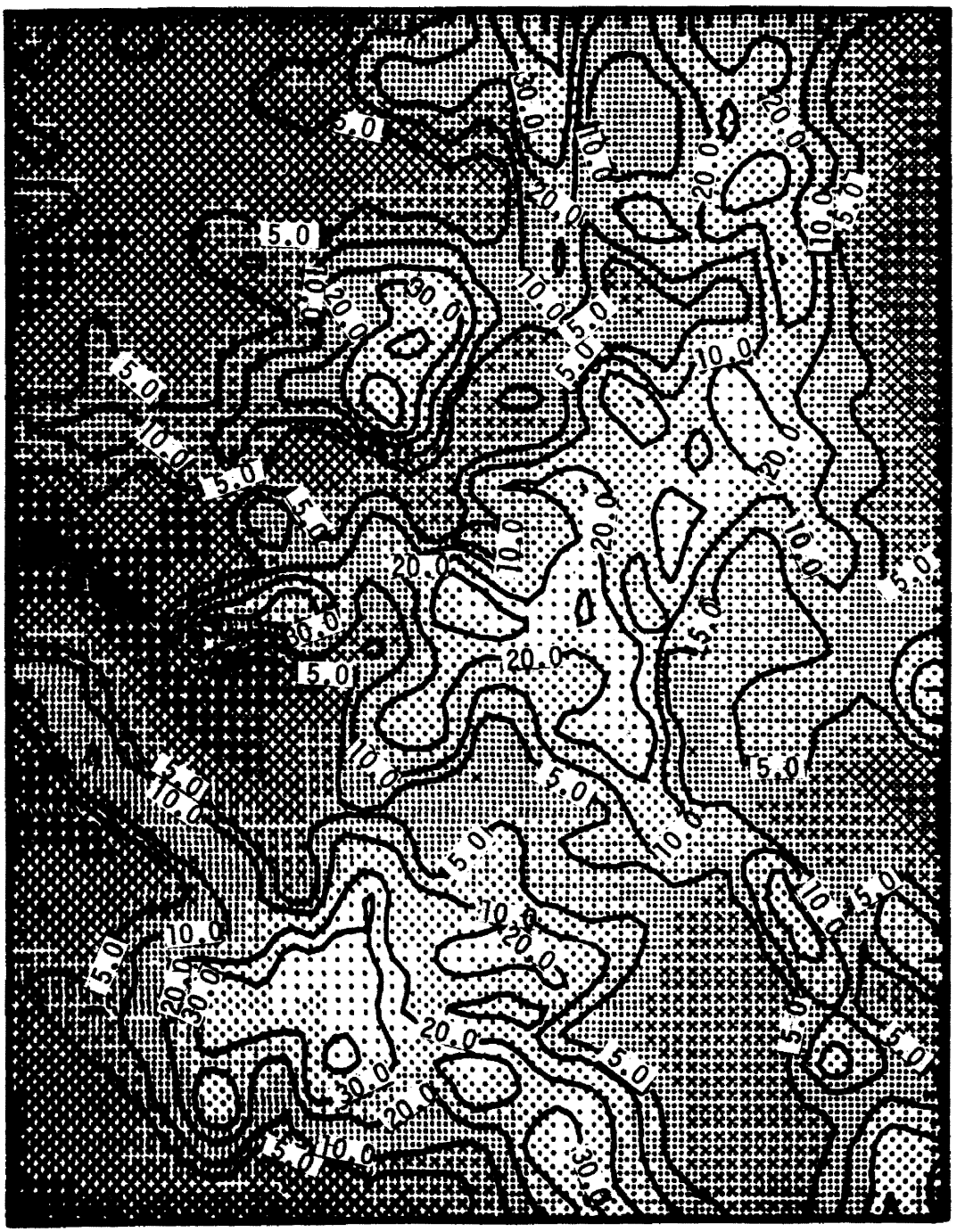

Figure 38. 1972-1973 season isohyetal map of model precipitation (inches). Topography is indicated by shading

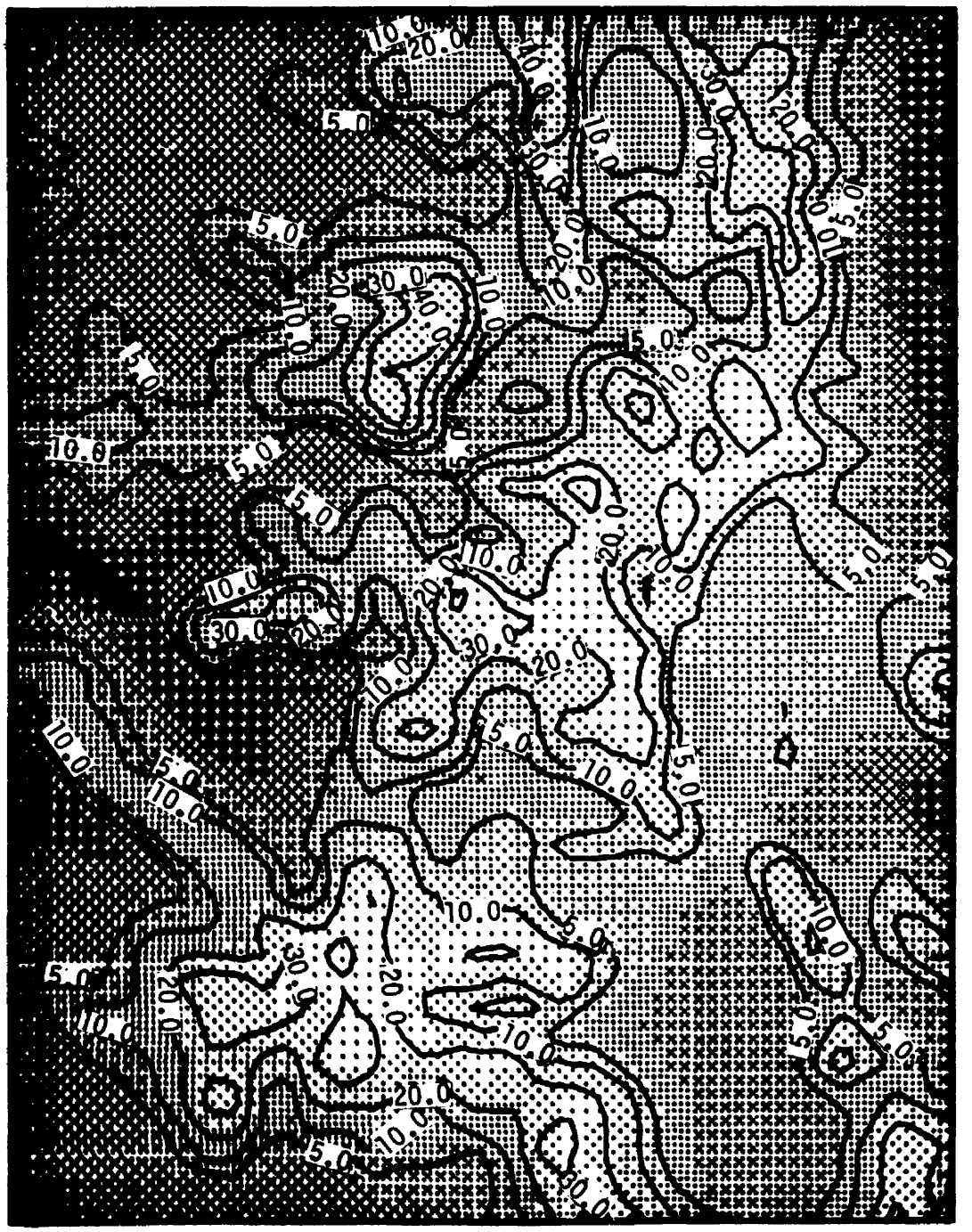

Figure 39. 1973-1974 season isohyetal map of model precipitation (inches). Topography is indicated by shading

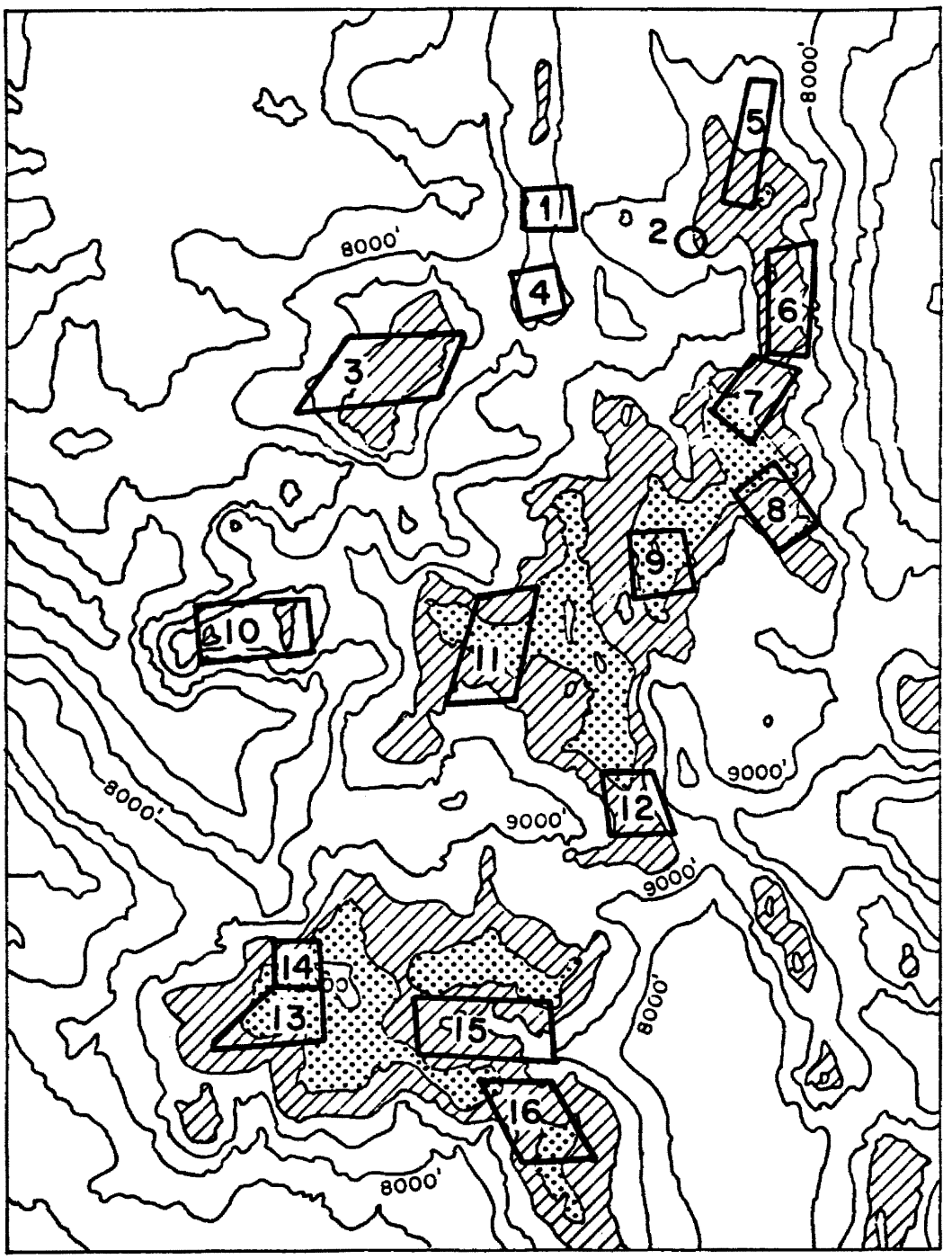

Figure 40. General location of snowcourse areas used for model validation

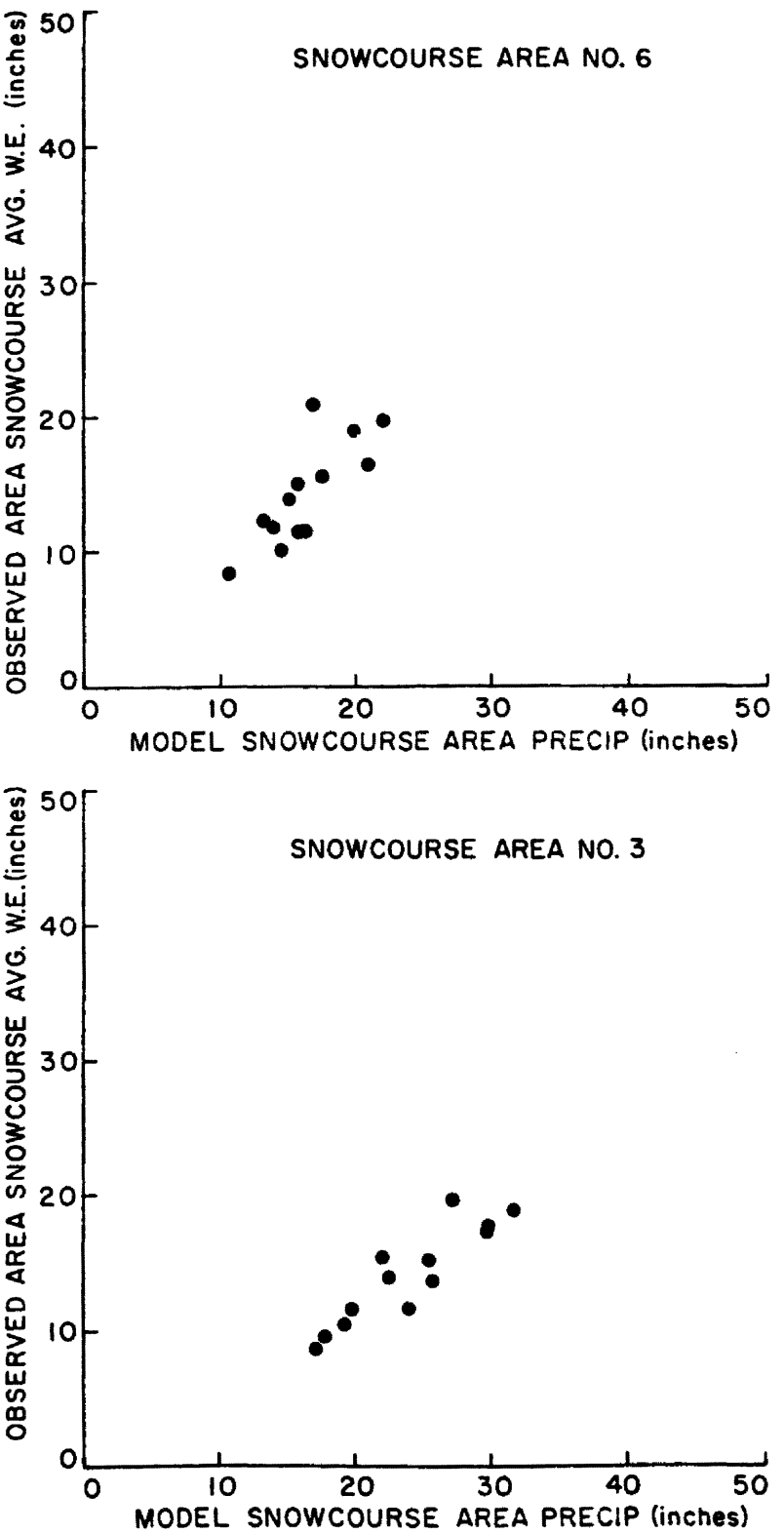

Figure 41. Examples of correlation between model precipitation and observed snowcourse values in northern sections of the study area

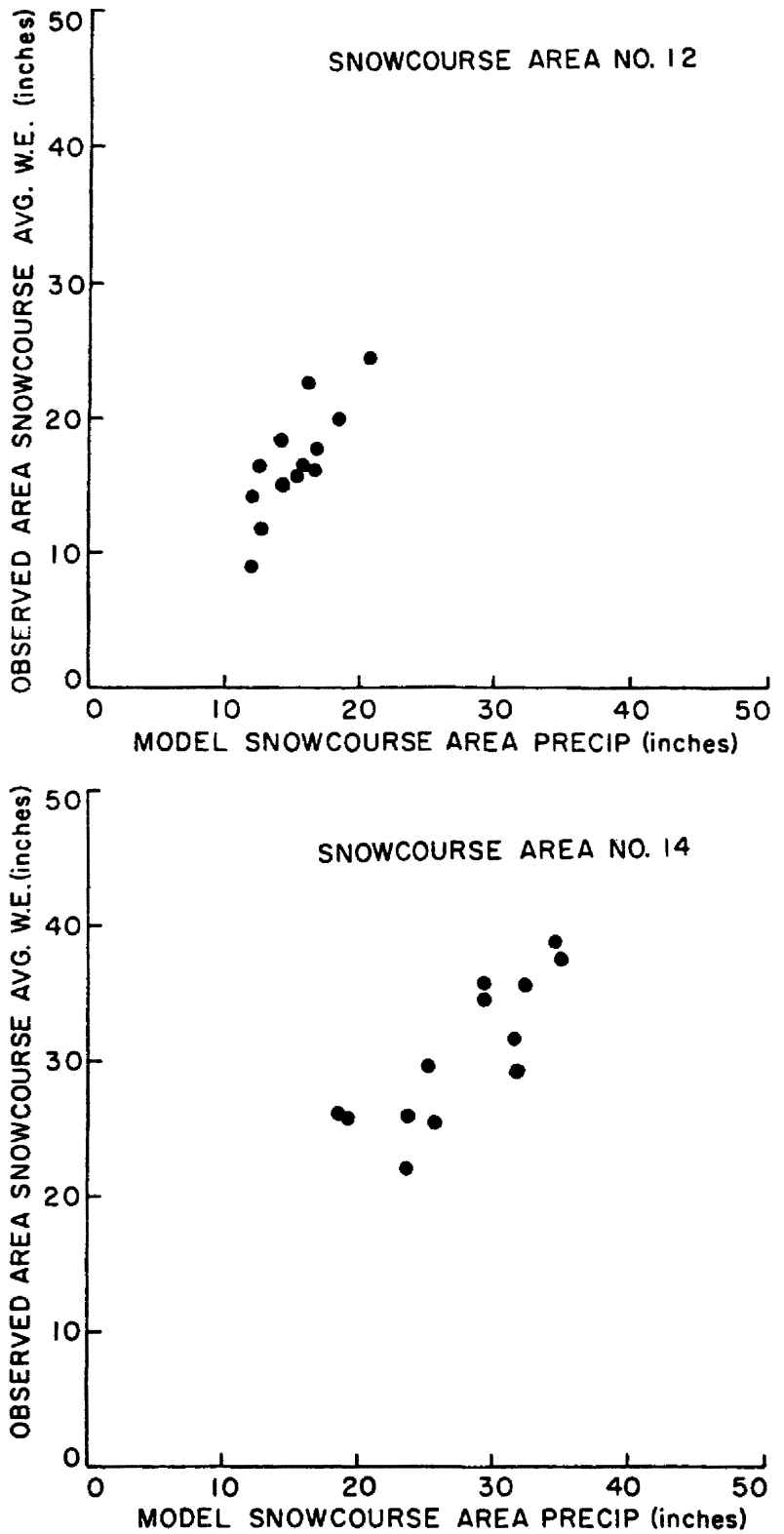

Figure 42. Examples of correlation between model precipitation and observed snowcourse values in southern sections of the study area

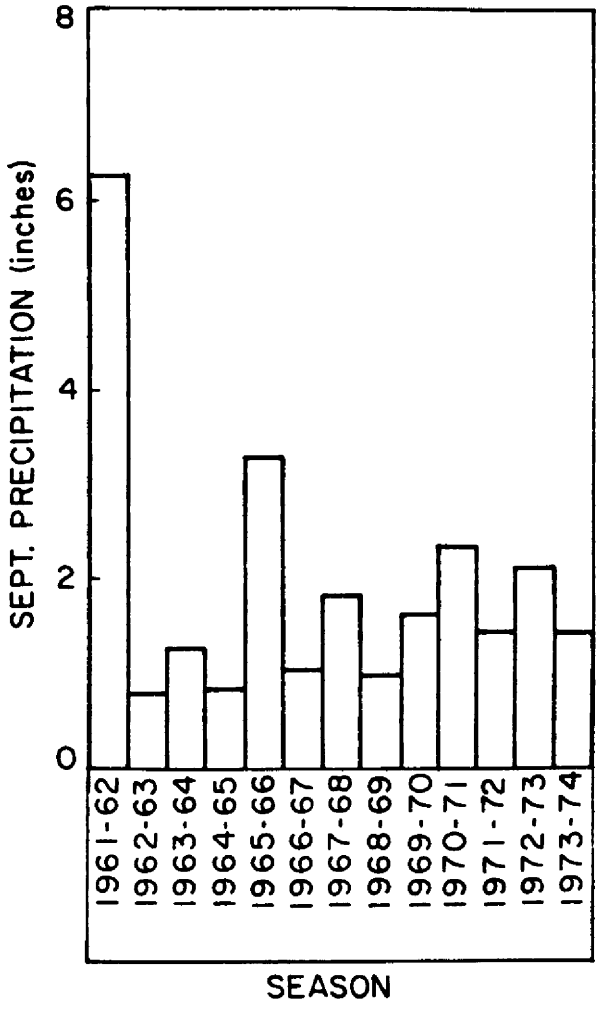

Figure 43. Average September precipitation for 5 central and northern Colorado climatological stations showing the exceptionally wet September of 1961

Table 7. Summary of Comparisons to Snowcourses

Snowcourse	Area No.	Correlation Coeff.	Variance Explained %
Park Range	1	.89	79
Willow Creek	2	.71	50
Flat Tops	3	.91	83
Gore-Lynx Pass	4	.82	67
Cameron-Deadman	5	.87	76
Indian-Lango Peak	6	.80	64
Berthoud-Loveland	7	.92	85
Kenosha-Geneva Park	8	.51	26
Climax	9	.87	76
Grand Mesa	10	.84	71
Aspen-Crested Butte	11	.85	72
Monarch Pass	12	.83	69
Western San Juan 1A	13	.77	59
Western San Juan 1B	14	.83	69
Upper Rio Grands Valley	15	.58	34
Eastern San Juan	16	.77	59

compared to the observed 1 April water equivalent values for the appropriate snowcourse group.

Examples of results are shown in figures 41 and 42. In general for higher average area elevation, better statistical agreement between model and observed values was found. In the case of 1961-1962 extremely heavy snows fell in the very cold September of 1961 in the central and northern mountains (see figure 43) with resulting underpredictions by the model for those regions.

Since the snowcourse measurements do not quantitatively reflect areal average precipitation, it is not surprising tc find departures of the regression line slopes from 45°.

Table 7 summarizes the statistical relations obtained and the amount of variance explained by the model computation. Fourteen of the 16 linear correlation coefficients are significant at the five percent level.

7.3 Inter-Area Comparisons

As is evident from the seasonal model isohyetal maps (figures 27 through 39 of section 7.1), there is considerable variation of the seasonal precipitation regime from one area to the next on different years. To study the validity of these variations, model indicated precipitation in one region was divided by that for another region. The resulting model precipitation ratios were compared to observed snowcourse ratios as in figures 44 and 45 or to observed runoff ratios as in figures 46 and 47 Linear correlation coefficients are printed on each figure.

For the thirteen years of study, the computations explained between 50 and 70 percent of the variance in snowcourse or streamflow

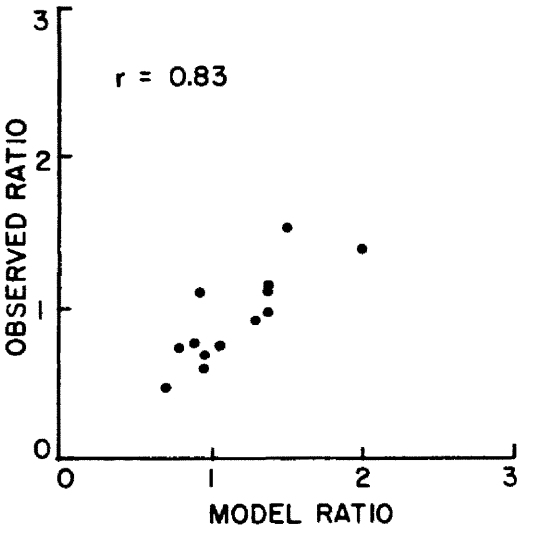

Figure 44. Scatter plot of observed seasonal ratios (Snowcourse area 16/Snowcourse area 1) of snowcourse readings versus model precipitation ratios to test model ability in determining areal gradations in seasonal precipitation

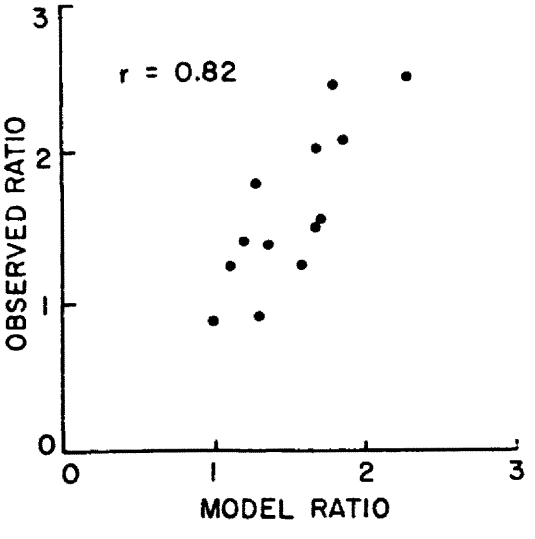

Figure 45. Same as figure 44 but with area 16/area 7

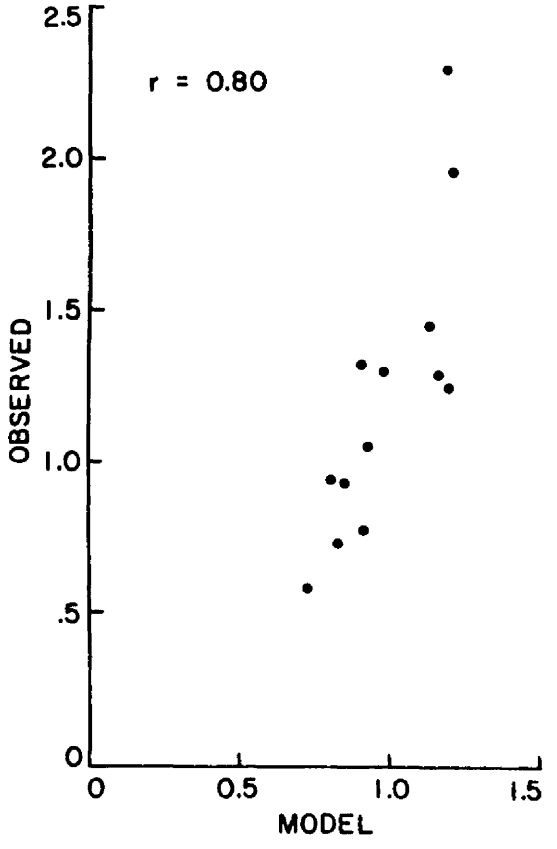

Figure 46. Scatter plot of observed ratios of March-July runoff versus model watershed precipitation ratios to test model ability in determining areal gradations in seasonal precipitation (Regional basin 2/Regional basin 5)

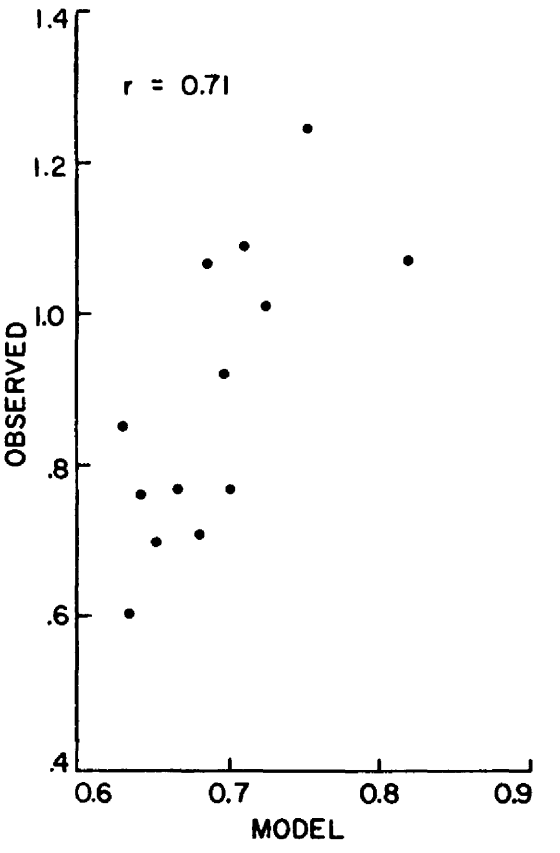

Figure 47. Same as figure 46 but for Regional basin 1/Regional basin 3

readings between the northern and southern edges of the study area.

The important question of areally accurate distribution of precipitation amounts over the whole region by the model is not easily answered because of (1) a lack of comparative data quantitatively representing areal precipitation and (2) the smoothing of terrain over the 10 km grid interval, thus precluding the ability of the model to adequately represent point values of precipitation at specific measurement sites. The latter problem is particularly severe if the measurement site resides in a locally low area surrounded by nearby higher ridges.

However, in a first attempt to assess the overall areal distribution accuracy groups of (and in some instances, individual) snowcourse stations were selected from 22 regions of the study area. These were selected based on their locations in either locally high areas or broad flat regions (and therefore, their relative freedom from sub-grid scale topographic complications). Figure 48 indicates the geographic distribution of these areas.

Model computations were summed and averaged for 15 October-31 March for each of these groups of points each season. The resulting scatter plots of model versus observed values for each year are shown in figures 49 through 52. When plotting all points on one graph (figure 53), a linear correlation coefficient of 0.89 was obtained. This result should not be over-emphasized however, as only a relatively small number of measurement locations were employed.

Generally, the model severely overestimated for narrow mountain valleys and underpredicted in the intermontaine broad valleys, particularly

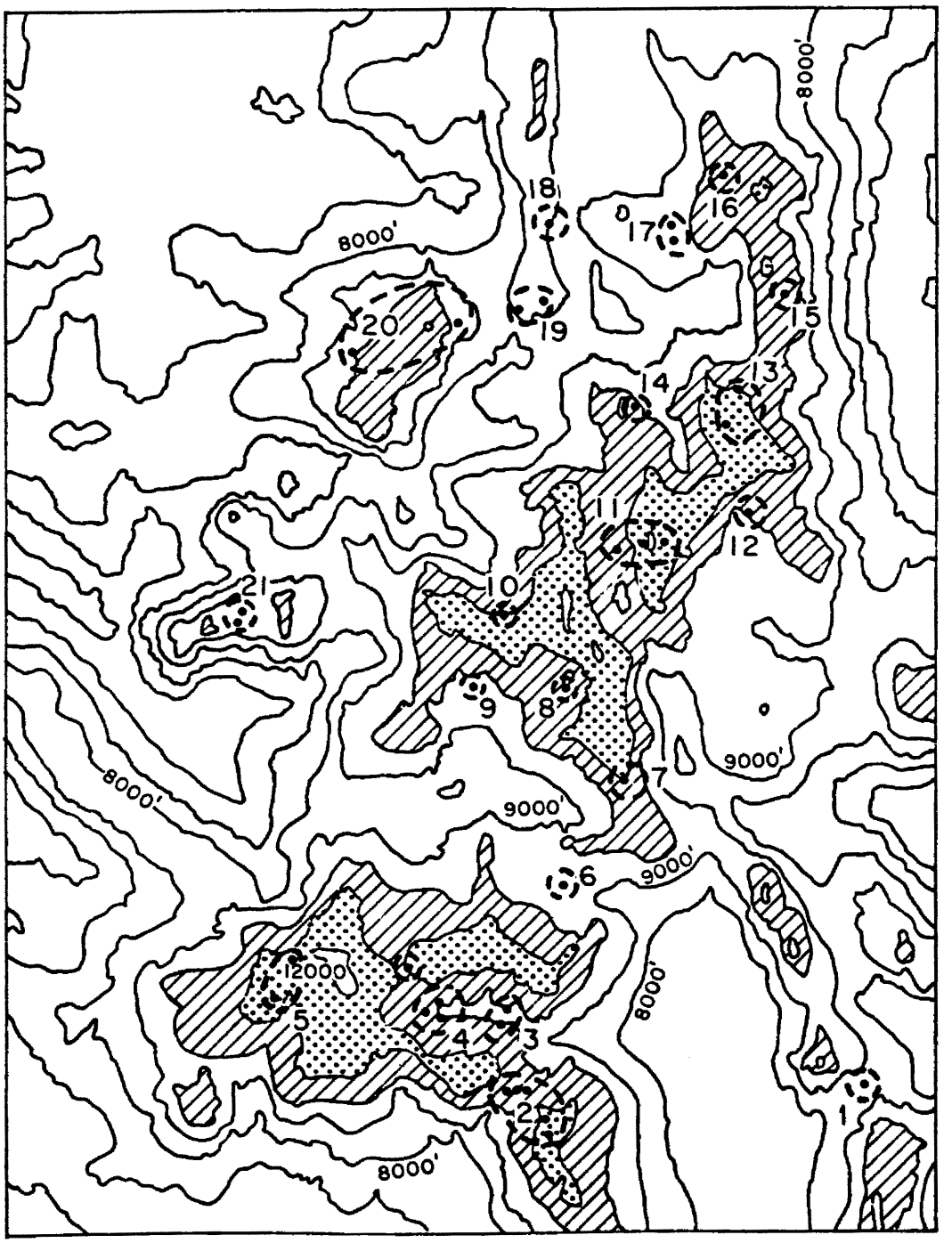

Figure 48. General location of snowcourse groups used in study of model areal distribution accuracy

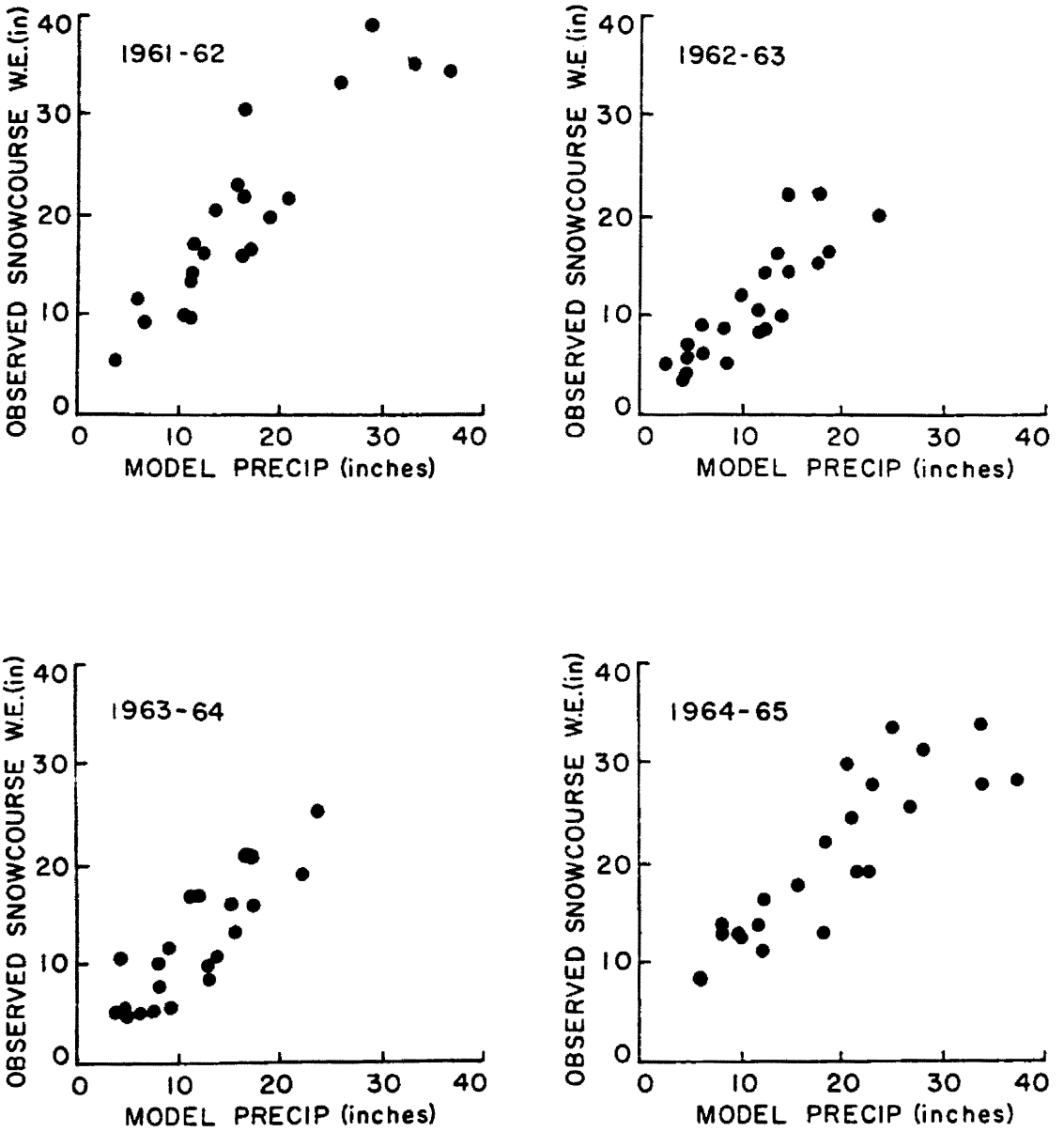

Figure 49. Scatter plots of 1 April snowcourse group (from Figure 48) values versus model 15 October-31 March precipitation

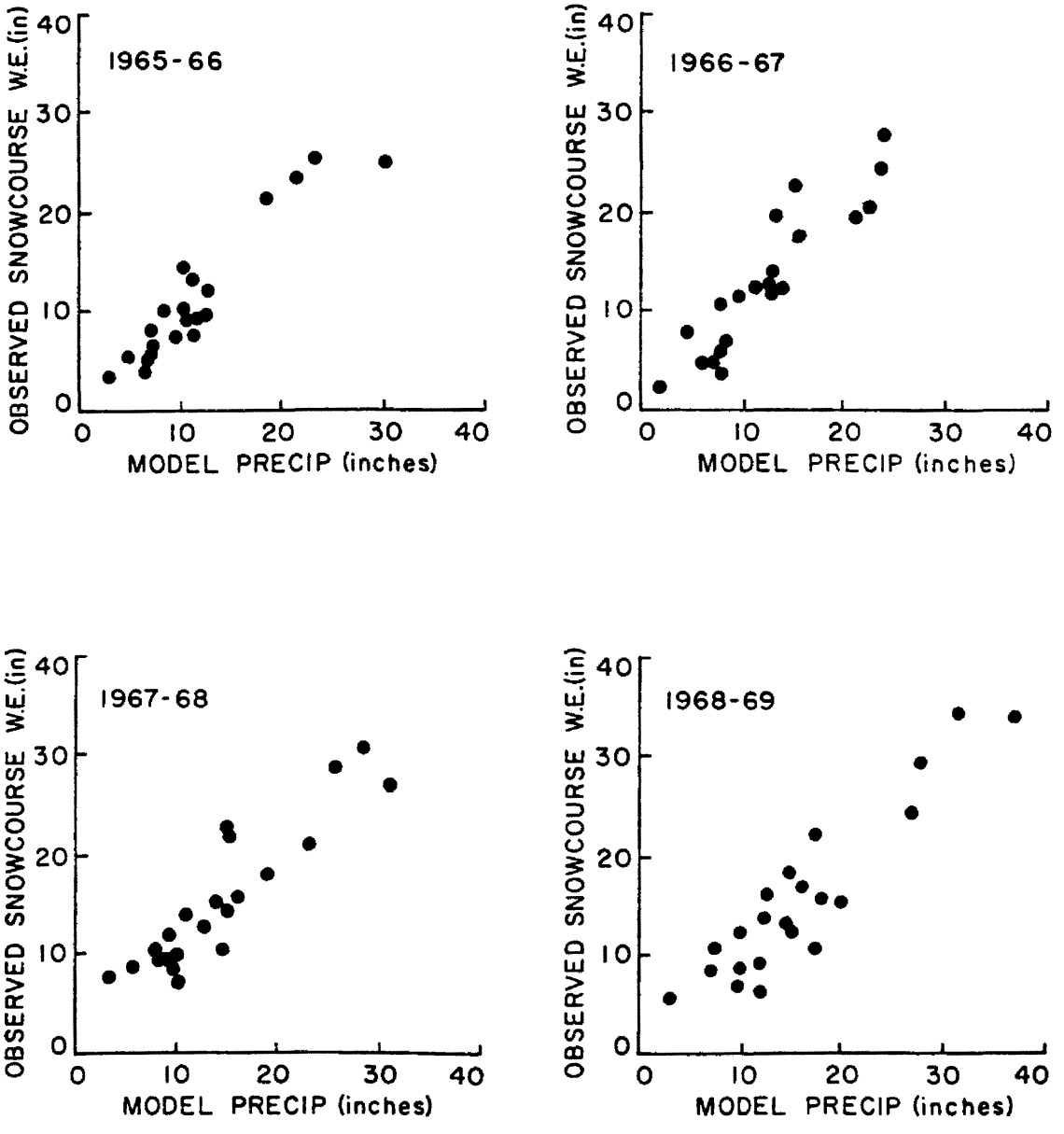

Figure 50. Same as figure 49

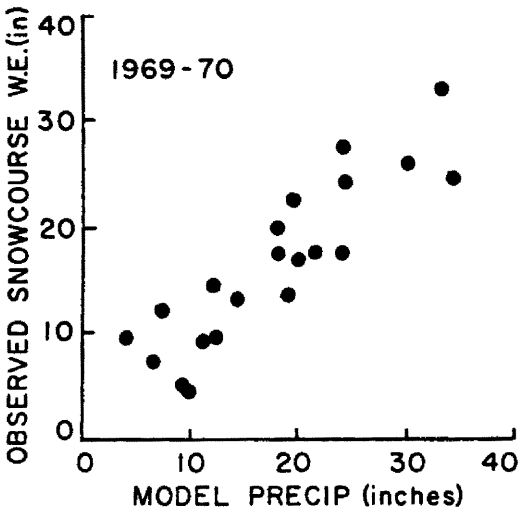

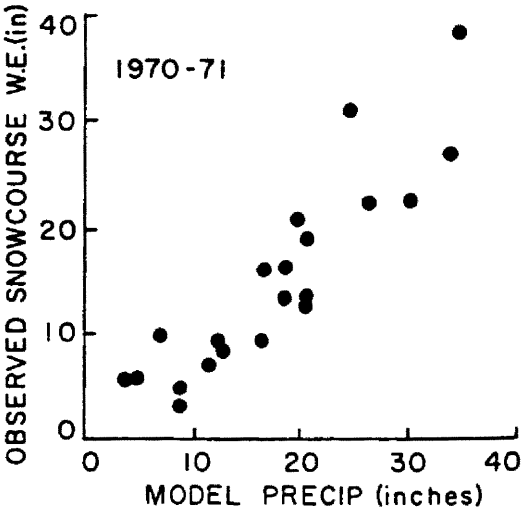

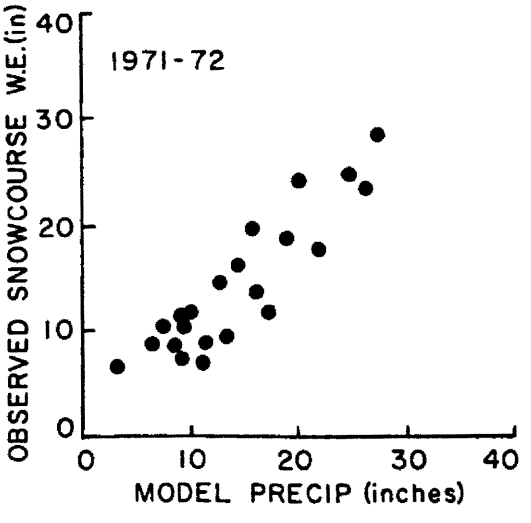

Figure 51. Same as figure 49

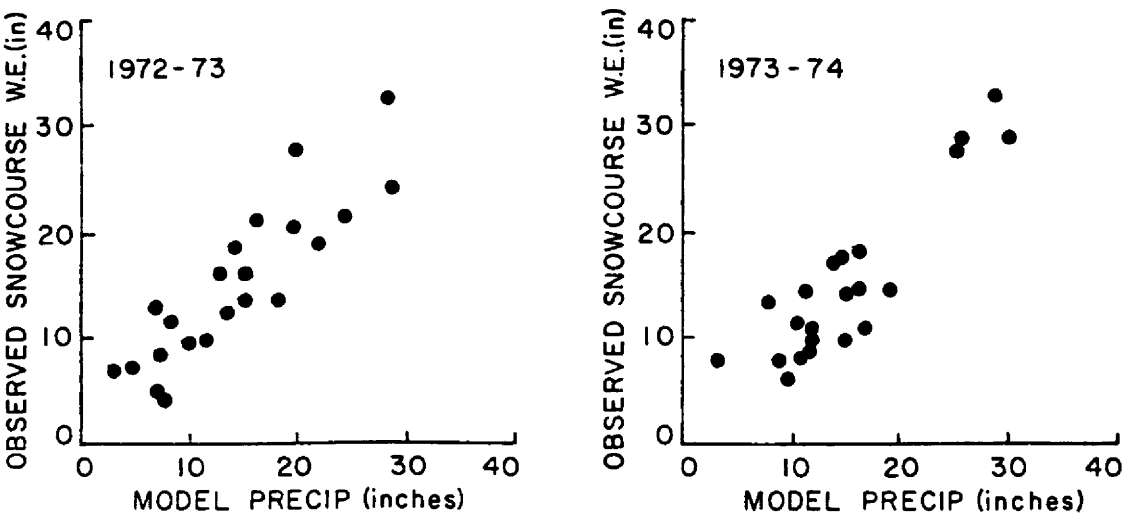

Figure 52. Same as figure 49

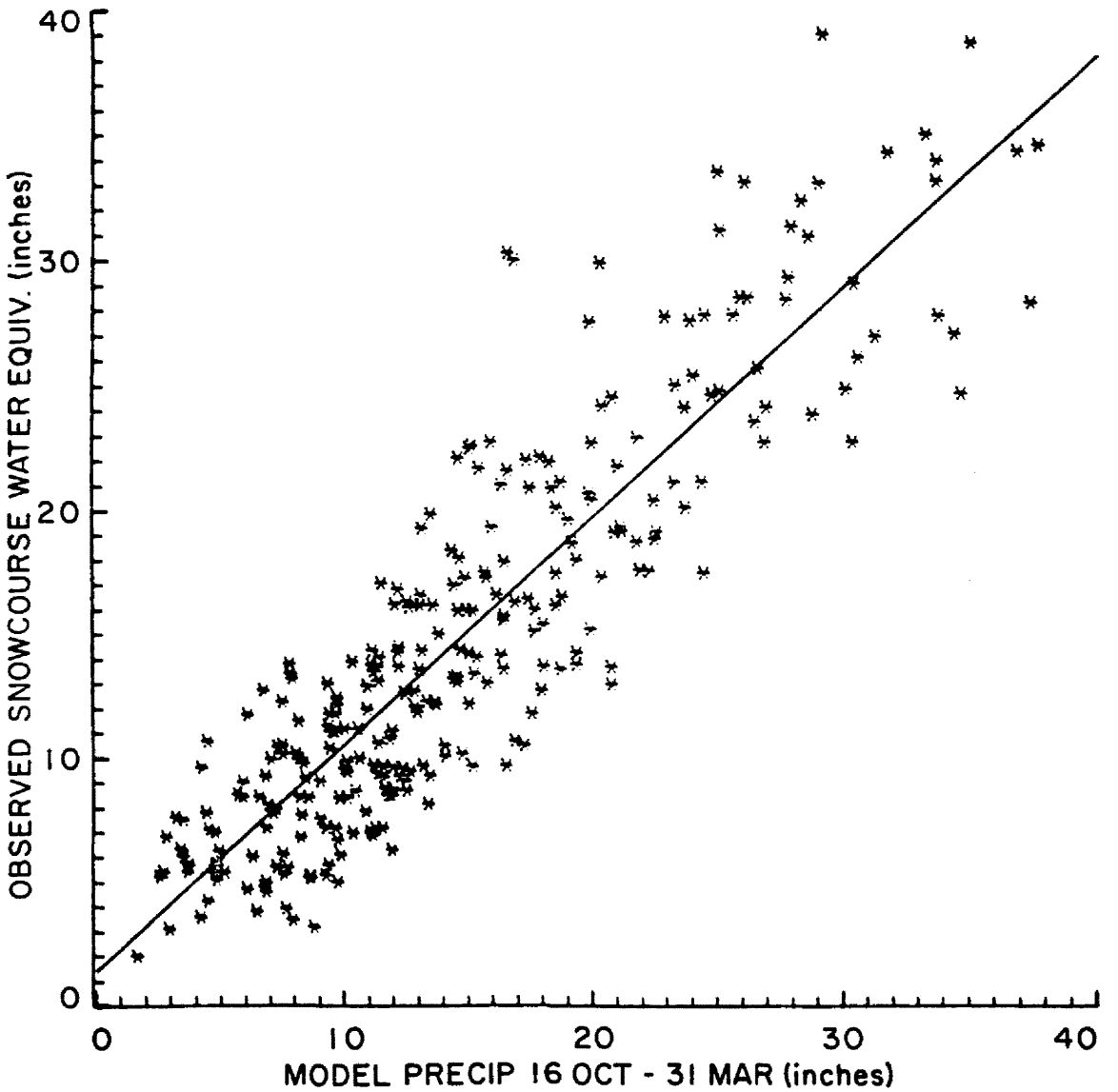

Figure 53. Scatter plot of 1 April snowcourse group (from Figure 48) values versus model 15 October- 31 March precipitation for each of 13 seasons

for those areas below about 7300 ft (2225m), indicating the restriction of model utility to ridges and high plateaus.

There are at least four probable reasons for the under-predictions in the inter-mountain valleys. First, it is probable that the non-orographic vertical motion fields were under-estimated. Second, since the model is not three-dimensional, meso-scale valley convergence fields due to channeling are not considered. Third, in the model, evaporation of falling precipitation began as water subsaturation was encountered. Delay of evaporation until ice-subsaturated conditions were encountered would have allowed some additional precipitation to reach the ground over relatively low topography. Fourth, Figure 25 of section 6.6 indicates rather extreme sensitivity of model precipitation at low altitudes as relative humidity changes from 85% to 100%. Thus, an underestimate of the frequency of existing 100% relative humidity layers could result in serious under-prediction of valley precipitation.

7.4 Comparison to Runoff

The streamflow records for the watersheds shown in figure 9 (Section 3.4.2) were used in various ways and combinations to evaluate model performance. Each of the studies relating model winter precipitation indications to observed spring and summer runoff is discussed in detail in the following sections.

7.4.1 Small Basins

Volume model precipitation (15 October-30 April) was computed for most of the watersheds in figure 9 and compared to the observed runoff totals for March through July (minus five times the February flow to roughly correct for the baseflow hydrograph component).

Before interpreting the results it should be restated that the very wet and cold September of 1961 in the central and northern portions of Colorado contributed significantly to the 1961-1962 winter snowpack whereas model computations did not start until 15 October. For 1972-1973, record October (1972) precipitation occurred on the southern slopes of the San Juan Mountains in southwest Colorado and these heavy amounts also affected the Grand Mesa. Much of this precipitation was quite convective in nature and drenched the valley areas with as much as 11 inches of precipitation (see figure 54 for Durango). The orographic model is not capable of simulating strong convection over the ridges or especially over the valleys. Thus, comparisons between model and observations were made with and without these two years.

Figures 55 through 59 visually depict the relations between model volume precipitation and observed runoff for selected watersheds. The nonlinear character of the relations probably arises from effects of evapotranspiration and soil moisture recharge. Tables 8, 9, 10, and 11 summarize the statistics for all watersheds with and without the two problem years of 1961-1962 and 1972-1973. Fifteen of the 18 correlation coefficients are significant at the one percent level for all years, while all are significant at the five percent level. With the problem years deleted all of the correlation coefficients attain the one percent significance level.

Marked variations in regression line slope occurs from one watershed to another. This is partially due to differing basin runoff characteristics (determined by numerous other variables not considered here, such as vegetation, microclimatic conditions, soil characteristics, and basin geology). To some extent, though, they probably

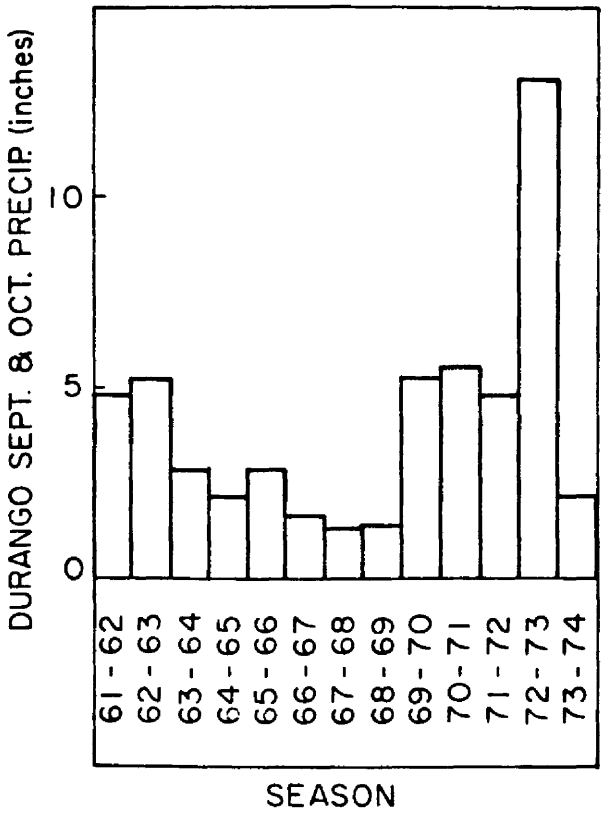

Figure 54. Durango (see Fig. D1) September and October precipitation for each winter season, showing the excessive autumn rains of October, 1972

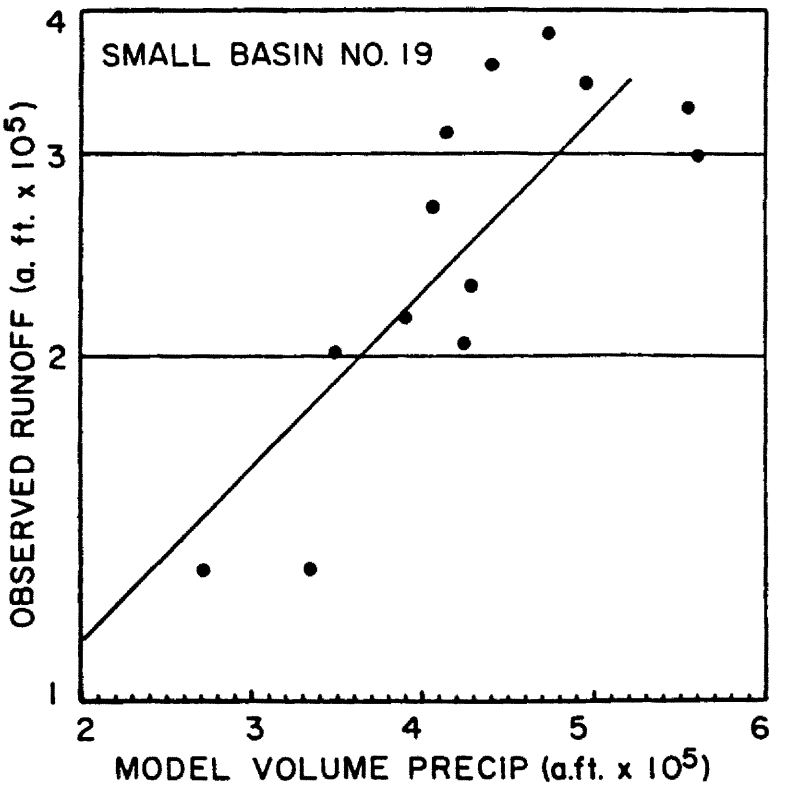

Figure 55. Example of model watershed volume precipitation correlation to observed March-July (minus baseflow) runoff

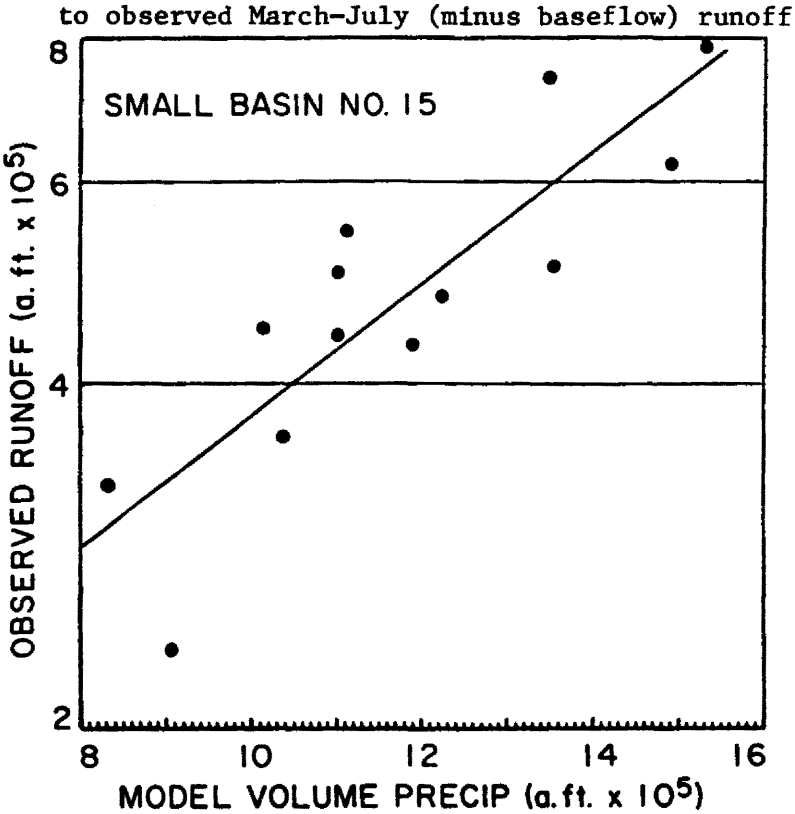

Figure 56. Same as figure 55

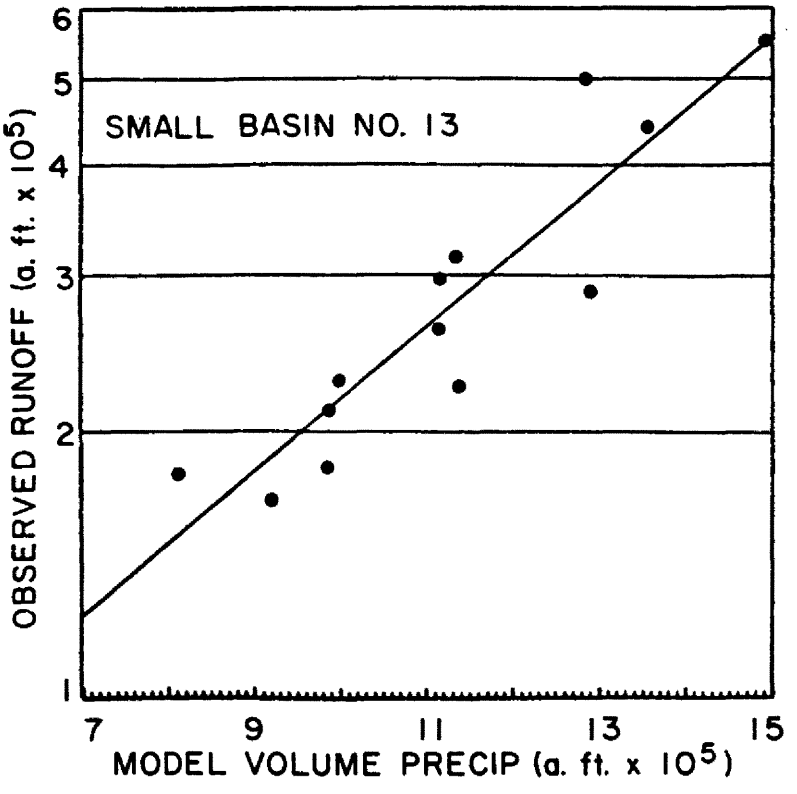

Figure 57. Same as figure 55

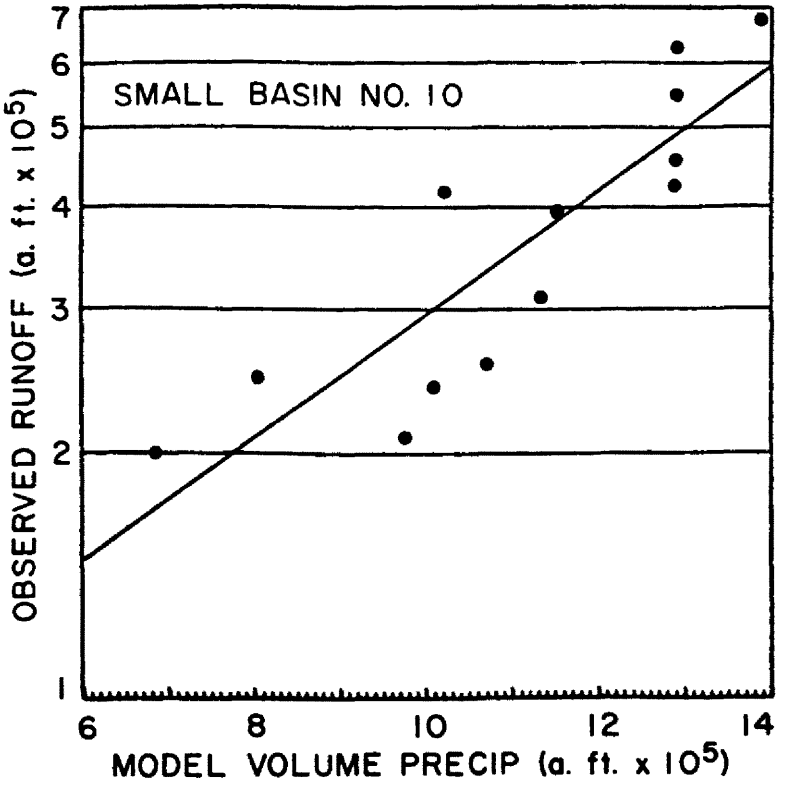

Figure 58. Same as figure 55

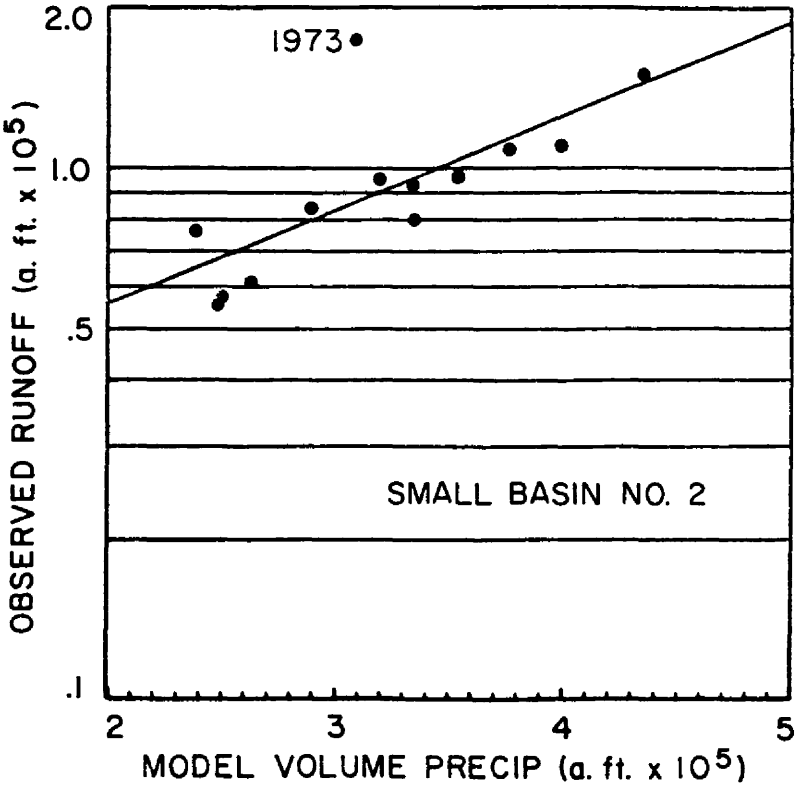

Figure 59. Same as figure 55

Table 8

Summary of Comparisons of Model to Individual Watershed and Small Basin Groups for 13 seasons (1961-1962 through 1973-1974)

Regional Basin	Watershed (s)	Correlation Coefficient r	Correlation Coefficient r^2	Average % Absolute Error
1	18 + 19 + 20	0.85	.72	13.3
2	15 + 17	0.84	.71	11.7
3	3 + 6 + 12 + 13 + 14	0.90	.81	11.7
4	9 + 10 + 11	0.91	.83	13.2
5	1 + 2 + 4 + 5 + 7 + 8	0.71	.50	15.9
	1	.62	.38	18.2
	2	.63	.40	14.4
	3	.62	.38	21.2
	4	.74	.55	16.5
	5	.64	.41	14.0
	6	.89	.79	10.7
	7	.88	.77	14.5
	8	.72	.52	23.9
	9	.82	.67	16.5
	10	.88	.77	18.2
	12	.73	.53	30.9
	13	.91	.83	12.0
	14	.74	.55	15.8
	15	.86	.74	14.2
	17	.82	.67	16.1
	18	.82	.67	14.5
	19	.70	.49	18.0
	20	.80	.64	11.6

Table 9

Summary of Comparisons of Model to Individual Watersheds and Small Basin Groups for 12 Seasons (1972-1973 omitted)

Regional Basin	Watershed	Correlation Coefficient r	r^2	Average % Absolute Error
1	18 + 19 + 20	0.88	.77	12.1
2	15 + 17	0.85	.72	11.5
3	3 + 6 + 12 + 13 + 14	0.95	.90	9.2
5	9 + 10 +11	0.93	.86	11.7
4	1 + 2 + 4 + 5 + 7 + 8	0.92	.85	11.7
	1	.89	.79	13.2
	2	.94	.88	9.3
	3	.88	.77	17.3
	4	.93	.86	13.2
	5	.87	.76	10.2
	6	.92	.85	9.9
	7	.88	.77	14.5
	8	.78	.61	20.5
	9	.87	.76	15.5
	10	.88	.77	17.3
	12	.83	.69	28.6
	13	.92	.85	12.2
	14	.86	.74	14.2
	15	.88	.77	13.5
	17	.82	.67	16.1
	18	.84	.71	14.1
	19	.73	.53	16.9
	20	.80	.64	12.3

Table 10

Summary of Comparisons of Model to Individual Watersheds and Small Basin Groups for 12 Seasons (1961-1962 omitted)

Regional Basin	Watershed	Correlation Coefficient r	Correlation Coefficient r^2	Average % Absolute Error
1	18 + 19 + 20	0.88	.77	11.9
2	15 + 17	0.87	.76	11.3
3	3 + 6 + 12 + 13 + 14	0.90	.81	10.6
5	9 + 10 + 11	0.91	.83	12.9
4	1 + 2 + 4 + 5 + 7 + 8	0.71	.50	16.7
	1	.63	.40	18.7
	2	.64	.41	14.7
	3	.63	.40	22.1
	4	.75	.56	17.2
	5	.63	.40	15.0
	6	.88	.77	11.6
	7	.88	.77	16.0
	8	.71	.50	25.8
	9	.84	.71	16.0
	10	.87	.76	18.6
	12	.74	.55	31.8
	13	.95	.90	11.2
	14	.73	.53	15.2
	15	.88	.77	13.3
	17	.84	.71	15.1
	18	.82	.67	14.1
	19	.75	.56	16.5
	20	.81	.66	11.9

Table 11

Summary of Comparisons of Model to Individual Watersheds and Small Basin Groups for 11 Seasons (1961-1962 and 1972-1973 omitted)

Regional Basin	Watersheds	Correlation Coefficient r	Correlation Coefficient r^2	Average % Absolute Error
1	18 + 19 + 20	0.92	.85	10.9
2	15 + 17	0.89	.79	10.8
3	3 + 6 + 12 + 13 + 14	0.97	.94	8.5
5	9 + 10 + 11	0.93	.86	11.5
4	1 + 2 + 4 + 5 + 7 + 8	0.92	.85	12.5
	1	.89	.79	13.9
	2	.95	.90	9.4
	3	.89	.79	17.4
	4	.93	.86	13.7
	5	.85	.72	10.7
	6	.90	.81	10.6
	7	.88	.77	16.0
	8	.76	.58	21.3
	9	.90	.81	14.4
	10	.86	.74	16.8
	12	.85	.72	28.6
	13	.95	.90	11.3
	14	.89	.79	13.0
	15	.91	.83	12.1
	17	.90	.81	14.0
	18	.85	.72	13.4
	19	.79	.62	15.1
	20	.81	.66	12.7

reflect the sign of precipitation model inaccuracies. For instance, the model appears to severely overpredict the runoff for the White River drainages in the Flat Tops area of northern Colorado. On the other hand, it underpredicts somewhat for the Yampa (see figure 9 and Table 1). To a certain extent the latter logically follows given the overprediction in the first case. This is so because portions of the Yampa drainage are downwind from the Flat Tops so that with overprediction of Flat Top precipitation, rainshadowing downstream would be unrealistically severe. It is suspected that the Flat Tops present a sufficiently narrow cross section to southwesterly flow that considerable flow splitting occurs with significant flow around rather than over this barrier. The current model formulation does not consider this phenomenon.

The Soil Conservation Service (SCS) of the USDA routinely makes predictions of April through August runoff based upon historical multiple linear regression relationships between certain snowcourse water equivalent readings and observed runoff. Table 12 summarizes SCS predictions for the 13 years for several of the watersheds used in this study. Comparing Tables 8 and 12, it is noted that approximately 62 percent to 94 percent of the runoff variance was explained by SCS regression techniques utilizing observed snow water equivalent values, while the orographic model explained 38 percent to 83 percent of it by using upper air data and the topographic grid as input to compute the watershed precipitation.

The success of the SCS in using key snowcourse readings for predicting runoff suggests the possibility of using model indicated point precipitation values for runoff computations. Figures 60a and 60b give sample trials of this method. Figures 61a and 61b supply the

Table 12

Summary of Correlation Between Predicted and Observed Runoff from Selected Watersheds Using USDA Soil Conservation Service Snowcourse-Runoff Regression Equations

No.	Watershed Name	Correlation Coefficient, R	R^2	Avg. Absolute Error (%)
1	Dolores	.91	.82	12.7
4	Animas at Durango	.91	.82	13.2
5	Los Pinos	.78	.62	12.6
10	Rio Grande	.96	.93	8.8
13	Gunnison	.93	.87	13.4
14	N. Fork Gunnison	.94	.88	7.1
15	Roaring Fork	.96	.93	5.8
3	Uncompahgre	.94	.88	9.8
18	White	.94	.89	5.6
19	Yampa	.97	.93	5.3

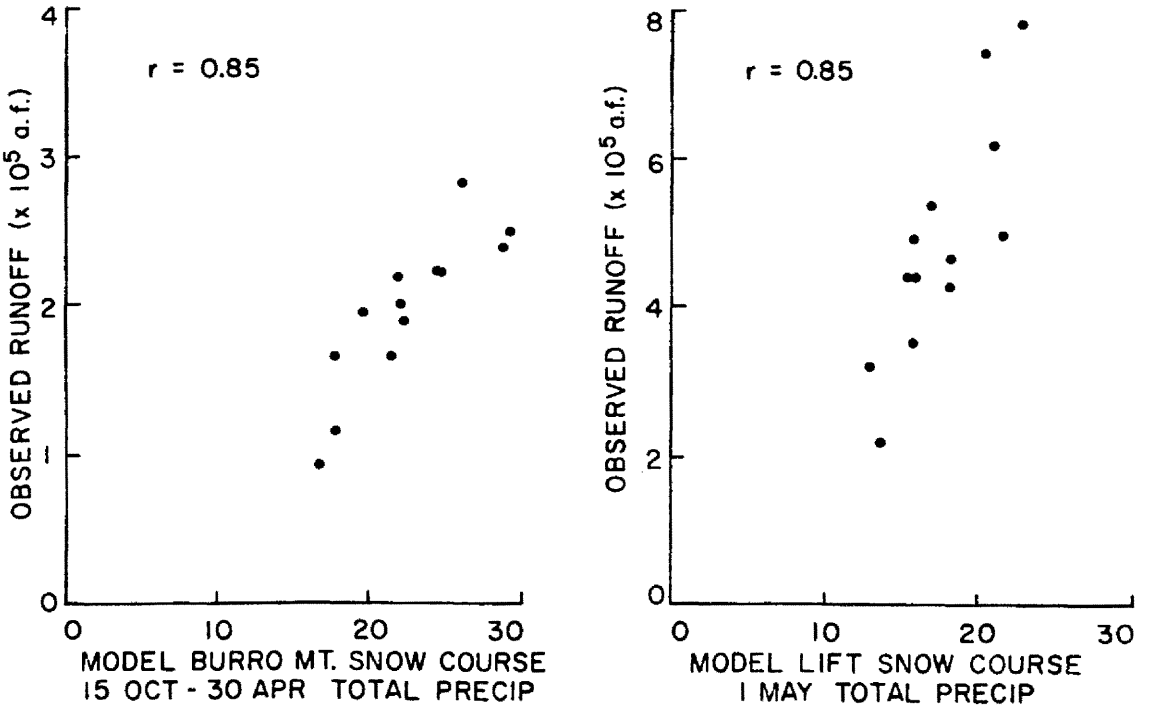

Figure 60. Examples of ability of model point seasonal computation s to predict spring and summer runoff

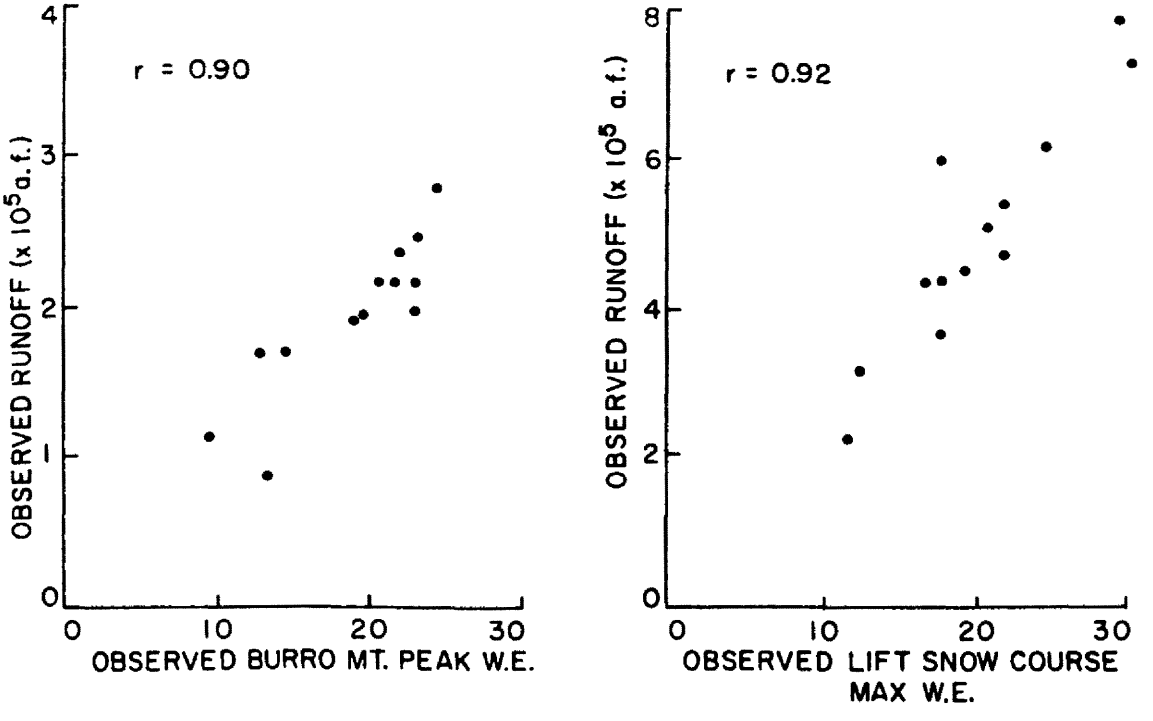

Figure 61. Examples of actual point snowcourse measurement (corresponding to points used in figure 60) for predicting spring and summer runoff

comparative information using the actual snowcourse readings. The method appears to hold some promise, but a more successful prediction could probably be derived by inter-facing the orographic model with a hydrologic process model.

7.4.2 Larger Basins

Both model precipitation and observed runoff data were summed over groups of small watersheds to yield yearly data for the five resulting larger regional basins shown in figure 62.

The relations between model and observations for each of these larger basins are depicted in figures 63 through 67 and summarized statistically in Tables 8 through 11. Somewhat tighter relationships are generally noted as compared to those between model and observed for the smaller basins. The problem season of 1972-1973 is again extremely obvious for the San Juan region. By eliminating 1972-1973, explained runoff variance percentages ranged from 72 percent to 90 percent. With 1972-1973 considered, all but the San Juan area exhibited quite good agreement. Comparative SCS runoff regression equations do not exist for this composite of basins.

7.4.3 Integration over all Watersheds

Summation of the relevant data over all the watersheds used in this study and then comparing model to observations resulted in the scatter plot of figure 68 with approximately 77% of the runoff variance explained. This includes 1972-1973. Omitting that year, the explained variance increases to over 80 percent.

Considering only the northern three larger basins as a summation region (figure 69), statistics indicate 83 percent of the variance was accounted for by the model precipitation. Soil Conservation Service

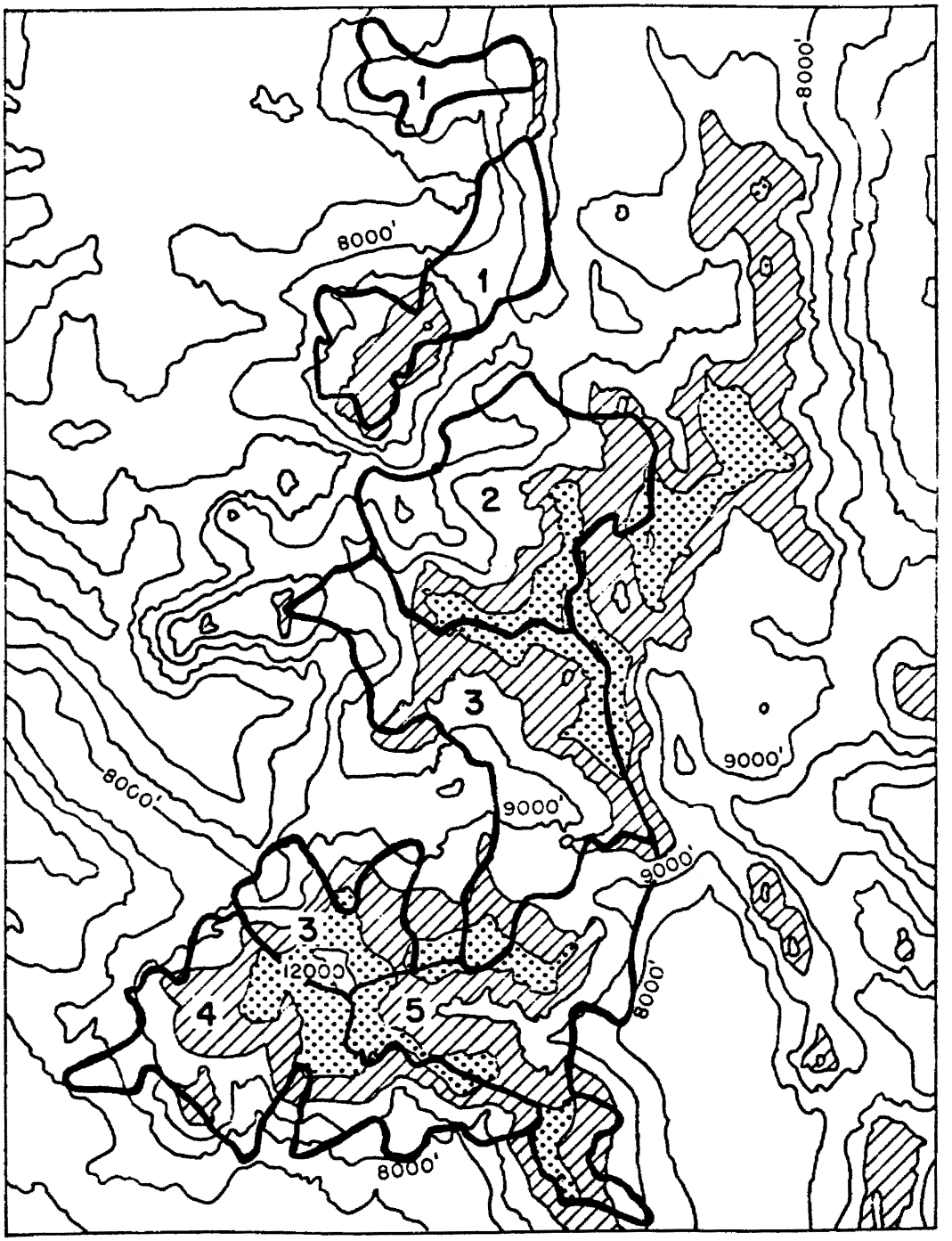

Figure 62. Regional drainage basins used for model validation

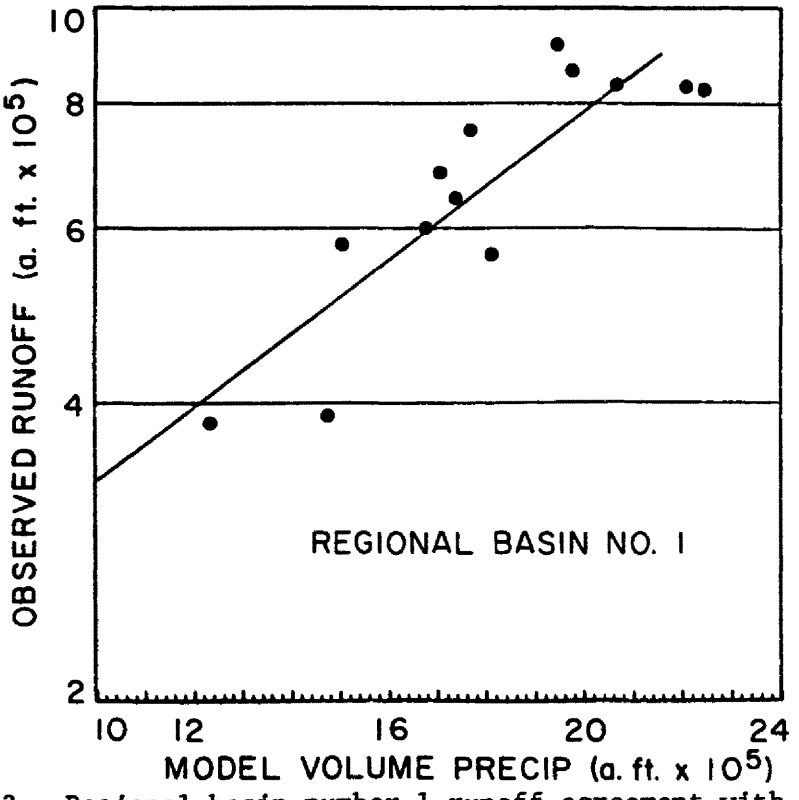

Figure 63. Regional basin number 1 runoff agreement with model volume 15 October-30 April precipitation

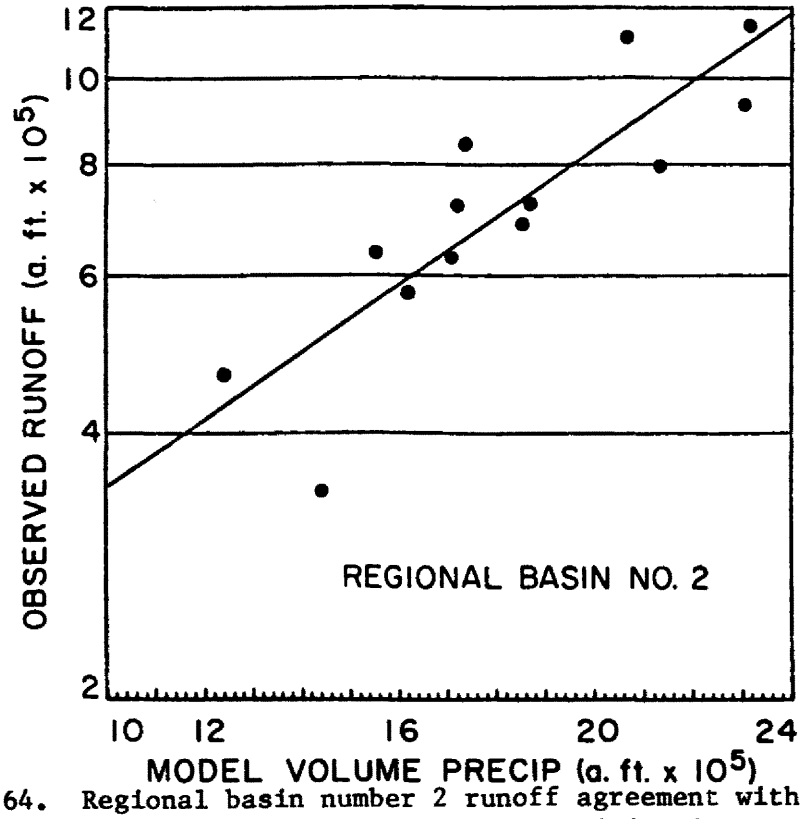

Figure 64. Regional basin number 2 runoff agreement with model volume 15 October- 30 April precipitation

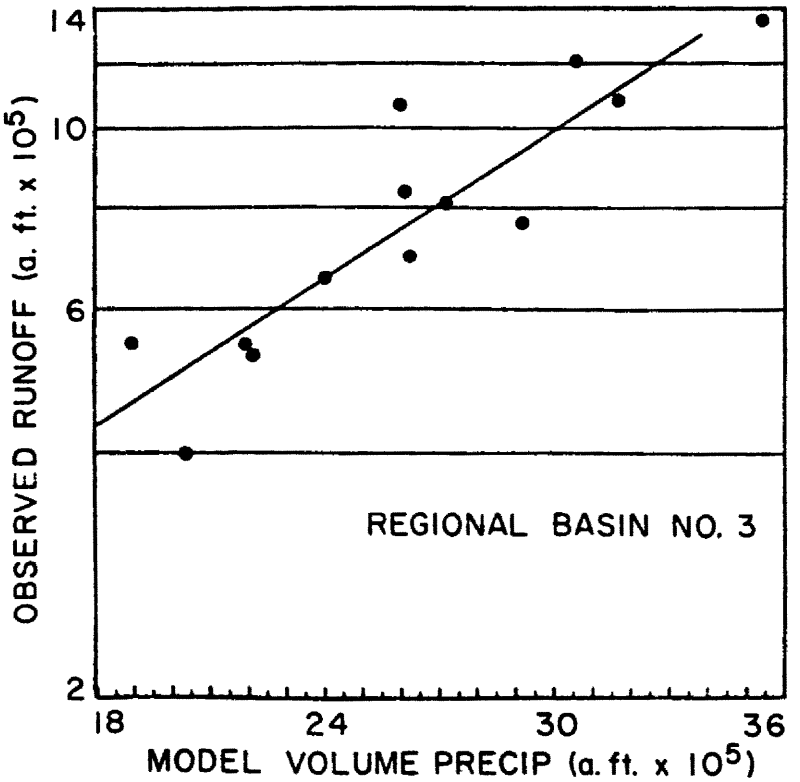

Figure 65. Regional basin number 3 runoff agreement with model volume 15 October- 30 April precipitation

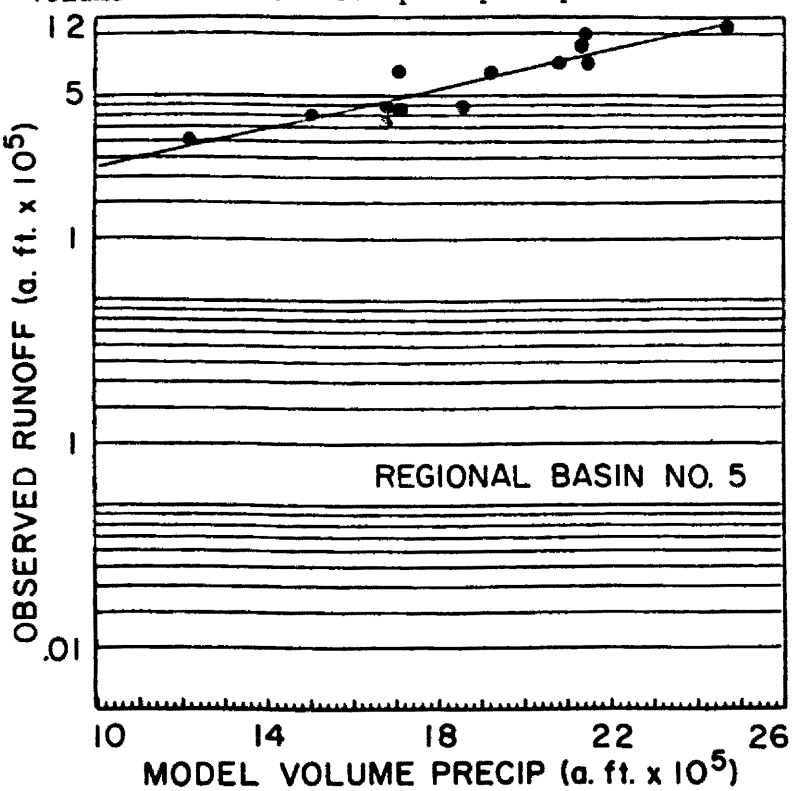

Figure 66. Regional basin number 5 runoff agreement with model volume 15 October- 30 April precipitation

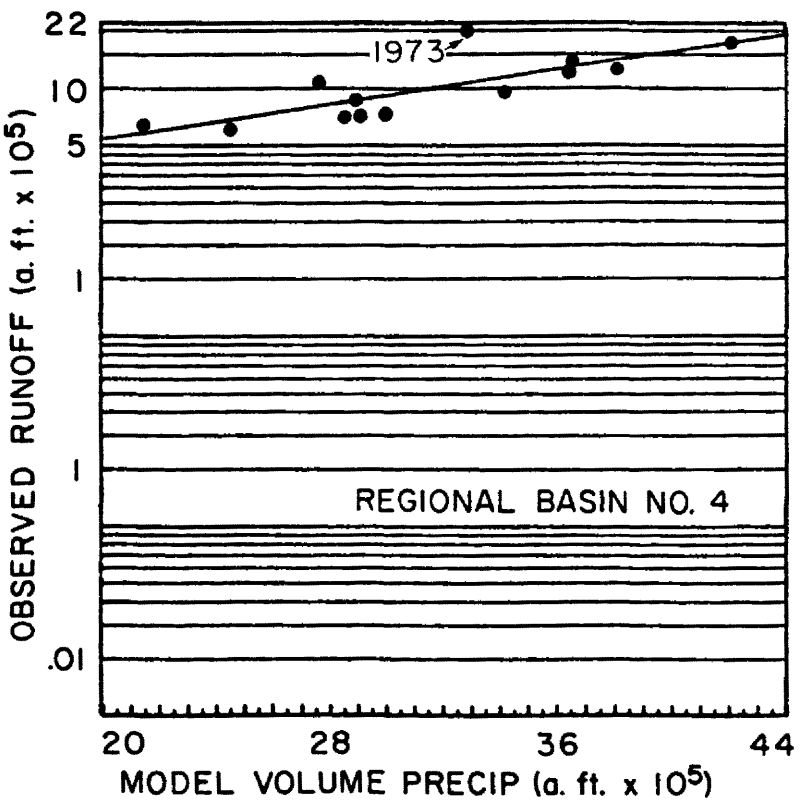

Figure 67. Regional basin number 4 runoff agreement with model volume 15 October- 30 April precipitation

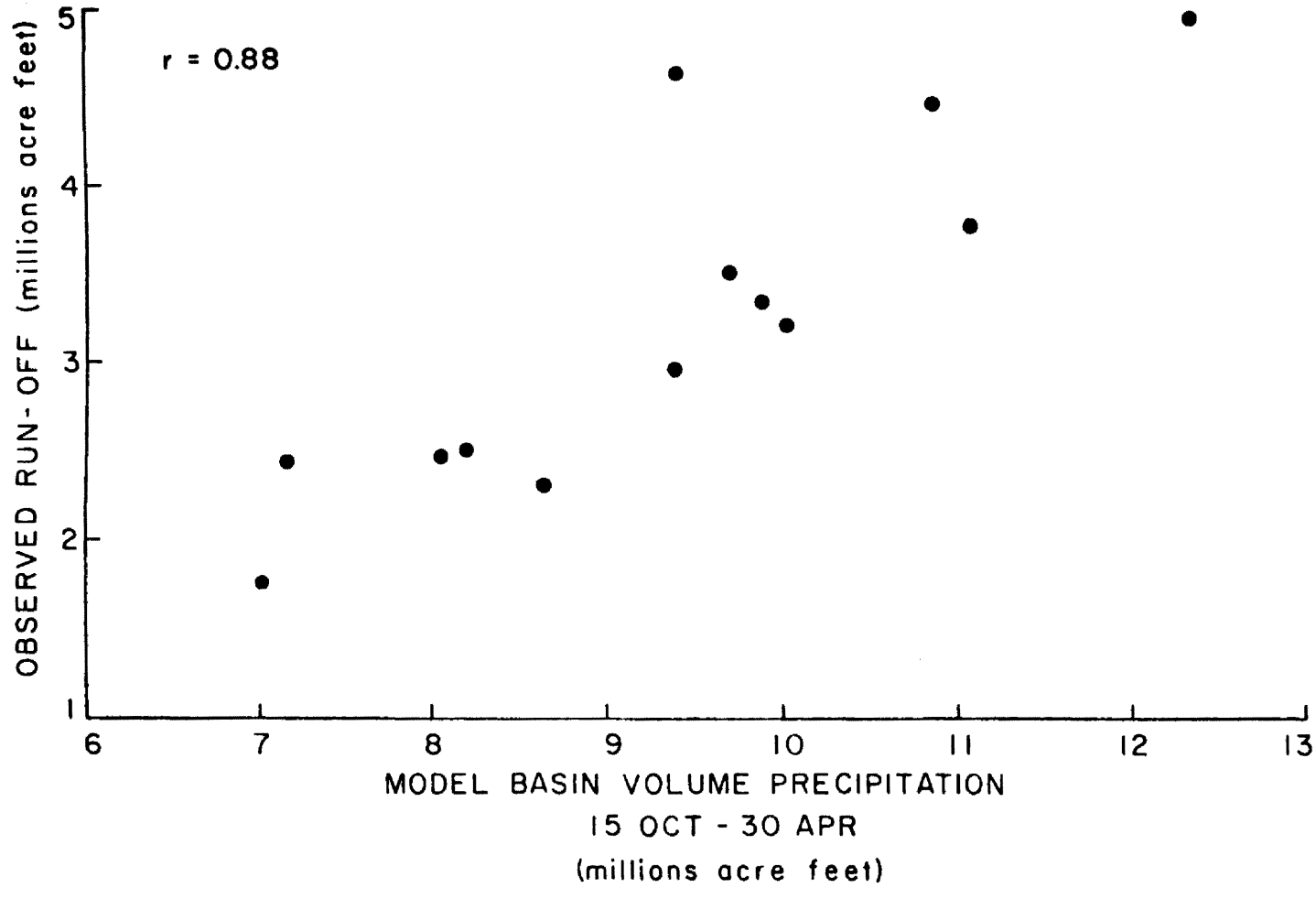

Figure 68. Runoff versus model volume 15 October - 30 April precipitation for sum of regional basins 1, 2, 3, and 4

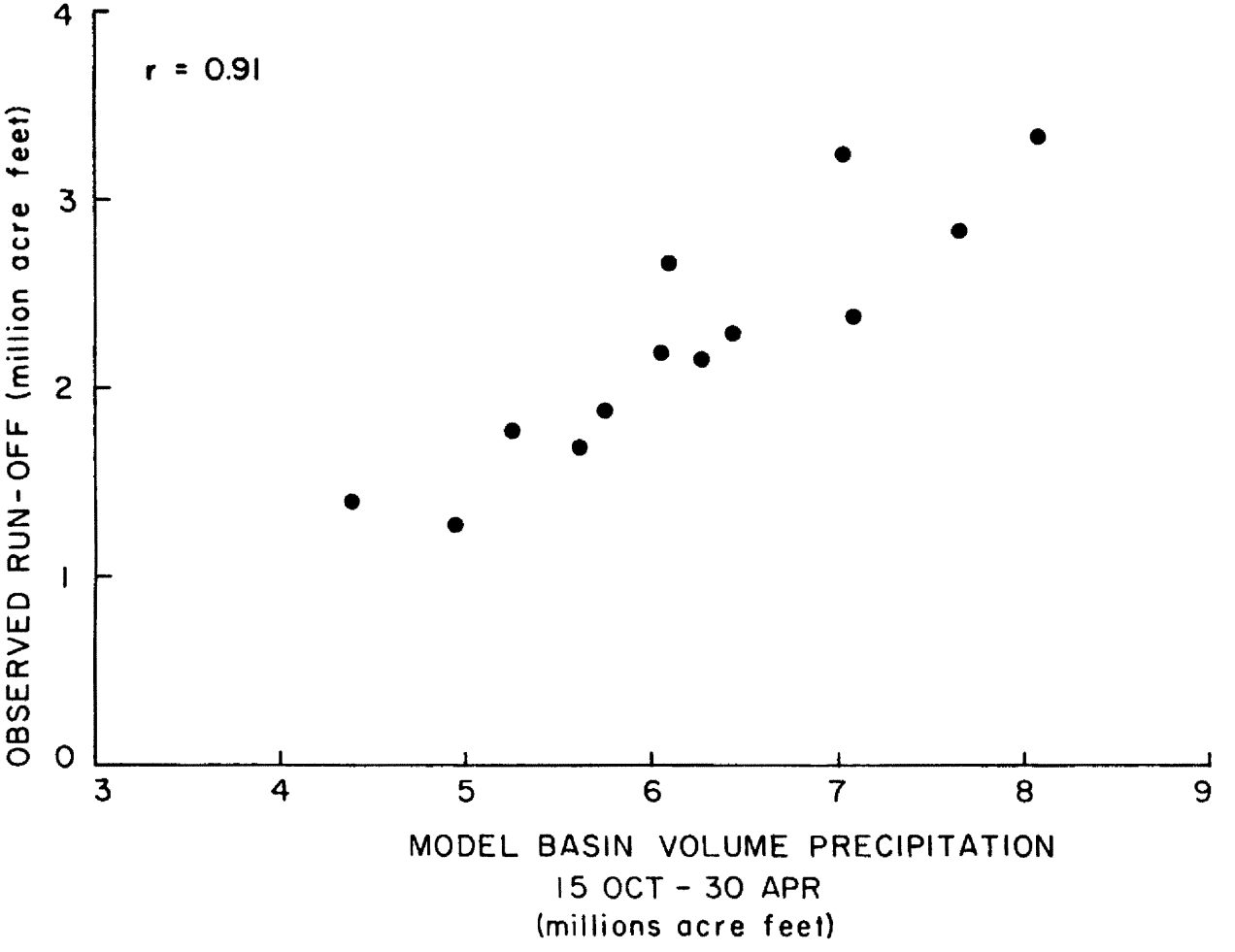

Figure 69. Runoff versus model volume 15 October- 30 April precipitation for sum of regional basins 1, 2, and 3

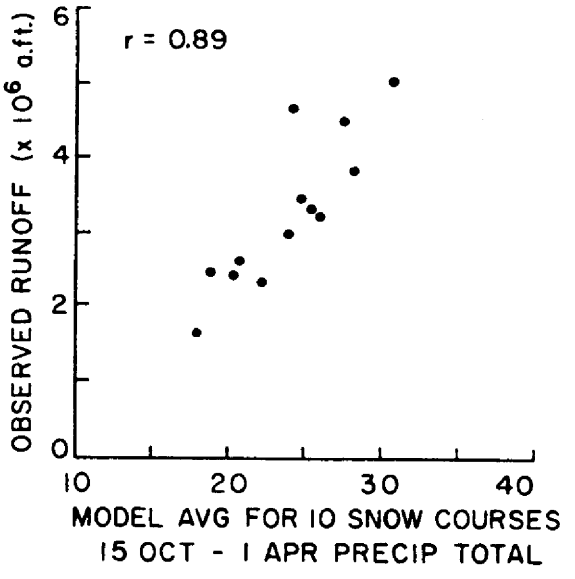

Figure 70. Test of ability to predict spring and summer runoff from sum of regional basins 1, 2, 3, and 4 using average model 15 October- 30 April precipitation for 10 regional snowcourse locations

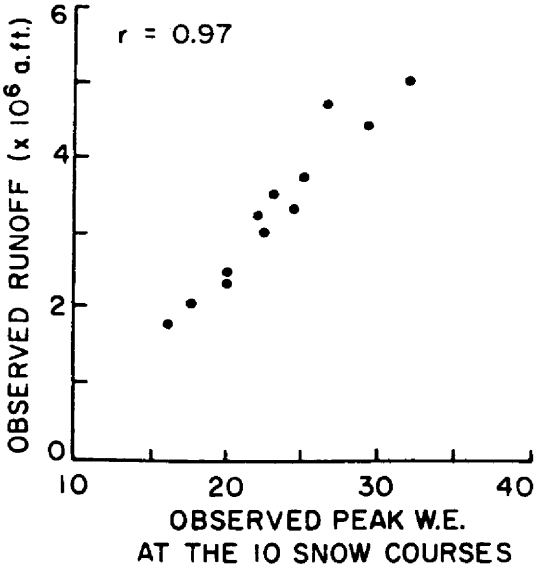

Figure 71. Test of ability to predict spring and summer runoff from sum of regional basins 1, 2, 3, and 4 using observed peak water equivalent at the 10 regional snowcourses of figure 70

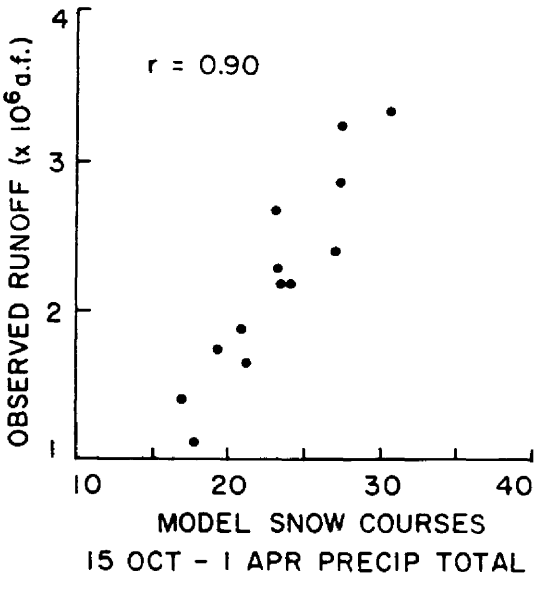

Figure 72. Test of ability to predict spring and summer runoff from sum of regional basins 1, 2, and 3 using model volume precipitation from 8 regional snowcourse locations

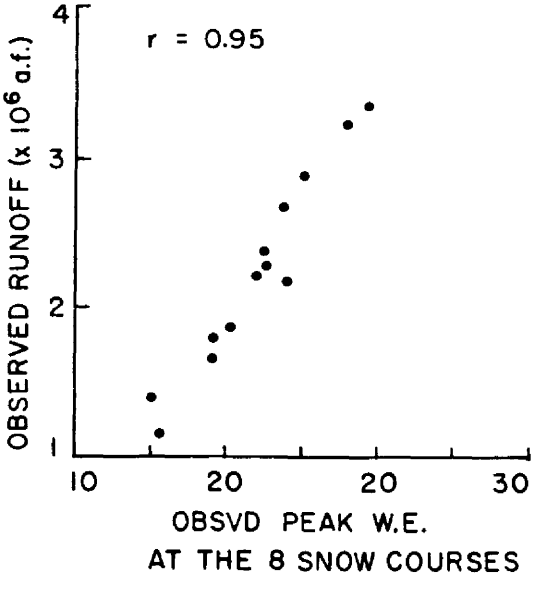

Figure 73. Test of ability to predict spring and summer runoff from sum of regional basins 1, 2, and 3 using observed peak water equivalent at the 8 regional snowcourse locations of figure 72

regression equations over this particular composite of basins do not exist for comparison.

As a further test of the feasibility of using key point precipitation values as runoff indicators over an area, the size of this composite of basins, model computation of point precipitation for 10 snowcourse locations were made and summed. These sums were plotted against observed runoff for the integrated basins having Colorado River drainage. Figure 70 shows the results.

Seventy-nine percent of the runoff variance was explicable by this method, compared to about 94 percent when using the observed peak water equivalent values at the 10 snowcourse sites (figure 71). When deleting the San Juan Region from the basin composite and dropping the two appropriate model snowcourses from the snowcourse group, figure 72 resulted, with about 80 percent of the variance explained. This compares to about 91 percent explained variance using the actual peak water equivalent readings as runoff indicators (figure 73).

7.4.4 Climatological Areal Distribution

As a further test of the areal distribution accuracy of the model, the 13-year average observed March through July (minus fives times the February flow) runoff (converted to equivalent uniform depth) for each watershed was scatter plotted against the corresponding model 15 October-30 April precipitation. The results in figure 74 at first glance show a considerable amount of scatter. However, since no watershed hydrologic parameters (other than model precipitation) were considered, such scatter might be expected. Inspection of Table 13 reveals substantial differences among watersheds in the fraction of annual runoff occurring

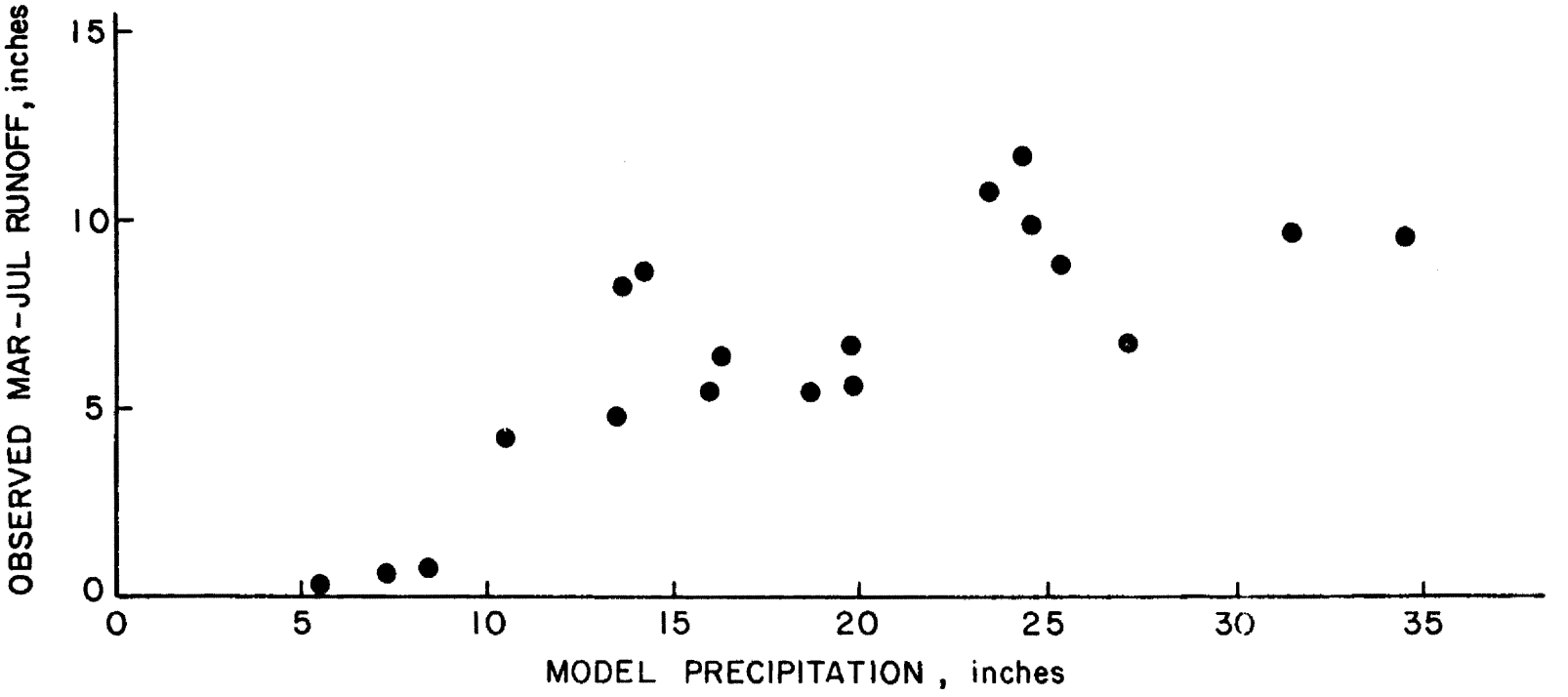

Figure 74. Scatter plot of 13 year average model watershed precipitation versus observed mean March-July (minus baseflow) runoff for individual basins

Table 13

Fraction of Annual Runoff Occurring During March-July (With Five Times the February Flow Subtracted) and Resulting Normalizing Factor

Watershed	f_i Fraction of Annual Runoff Occurring in March-July Minus 5 Times the Feb. Flow	$N_i = \bar{f}_i / f_i$ Normalizing Factor
1	.74	.85
2	.61	1.03
3	.58	1.08
4	.61	1.03
5	.56	1.12
6	.68	.92
8	.72	.87
9	.71	.88
10	.67	.94
11	.48	1.31
12	.45	1.40
13	.57	1.10
14	.77	.82
15	.57	1.10
16	.51	1.23
17	.61	1.03
18	.51	1.23
19	.77	.82
20	.81	.78
	$\bar{f}_i$ = .628	

in the March through July period. If these runoff timing differences are all attributed to differences in watershed hydrologic characteristics (other than warm season precipitation) a normalizing factor, N_i, to partially rectify these differences can be computed by

$$N_i = \frac{\bar{f}}{f_i} \tag{7-1}$$

where

f_i = fraction of annual runoff occurring during the March through July period for watershed i

$$\bar{f} = \frac{1}{k} \sum_{L=1}^{k} f_i .$$

The March-July runoff, F_i, for watershed i can then be adjusted to

$$(F_i)_{adj} = N_i F_i \tag{7-2}$$

Figure 75 shows the results of these adjustments. The linear correlation coefficient from the data is 0.89. The main disagreement between model precipitation and observed runoff is with watershed Number 1 (figure 9) which is the Dolores River above Dolores. Inspection of figure 9 shows this watershed to have smoothed topography features which would promote flow around rather than over the watershed for most wind directions. Further inspection of figure 9 reveals that none of the other watersheds appear as topographically prone to this phenomenon over as many flow directions as does the Dolores above Dolores.

From the general areal distribution agreement when using adjusted runoff, it thus appears that orographic model precipitation can be used in combination with some knowledge of watershed hydrologic characteristics to obtain a first approximation to climatological values of runoff in currently ungauged areas of greater than about 250 square

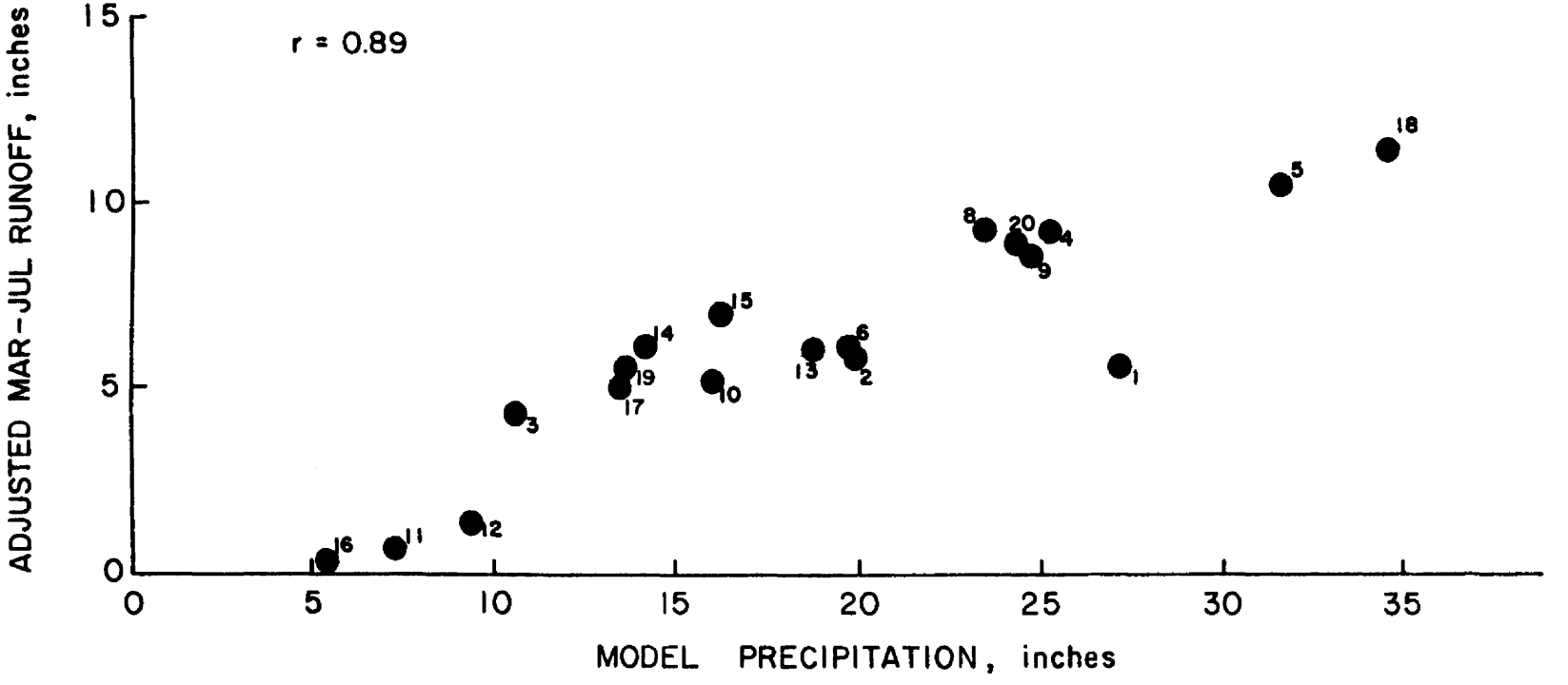

Figure 75. Scatter plot of 13 year average model watershed precipitation versus observed mean March-July (minus baseflow) adjusted for other watershed factor differences

miles with the accuracy of runoff estimate partially dependent on the degree to which hydrologic processes are considered.

7.5 Comparison to Precipitation Stations

As mentioned earlier there are very few high mountain precipitation stations in Colorado with an adequate period of record for model evaluation. However, some comparisons were made to data from a few stations.

Monthly sums for model and selected precipitation stations are scatter plotted in figures 76 through 79. As expected from the error discussion in section 7, only modest agreement is observed. Seventy-five percent of the most severe model underpredictions for Berthoud Pass and Climax occurred in March or April while these months constitute only about 30 percent of the data sample of 15 October through 30 April. This reflects the increase in convective precipitation in these months and the inability of the model to adequately simulate that process. Similarly, for Bonham Reservoir three of the five most serious model underpredictions occurred in March and/or April, while one was for October 1972, when 4.75 inches (121 mm) of precipitation fell in one day, again signifying significant convection.

On a daily basis the scatter increases even more, again in accordance with expectations considering the serious random error for individual cases. Figure 80, however, indicates the model computes approximately the proper frequency distribution of daily precipitation classes with the exception of the .01-0.10 in. (0.25-2.5 mm) where it significantly overpredicts. These comparative frequencies were taken from a compilation of four winter seasons of data for Wolf Creek

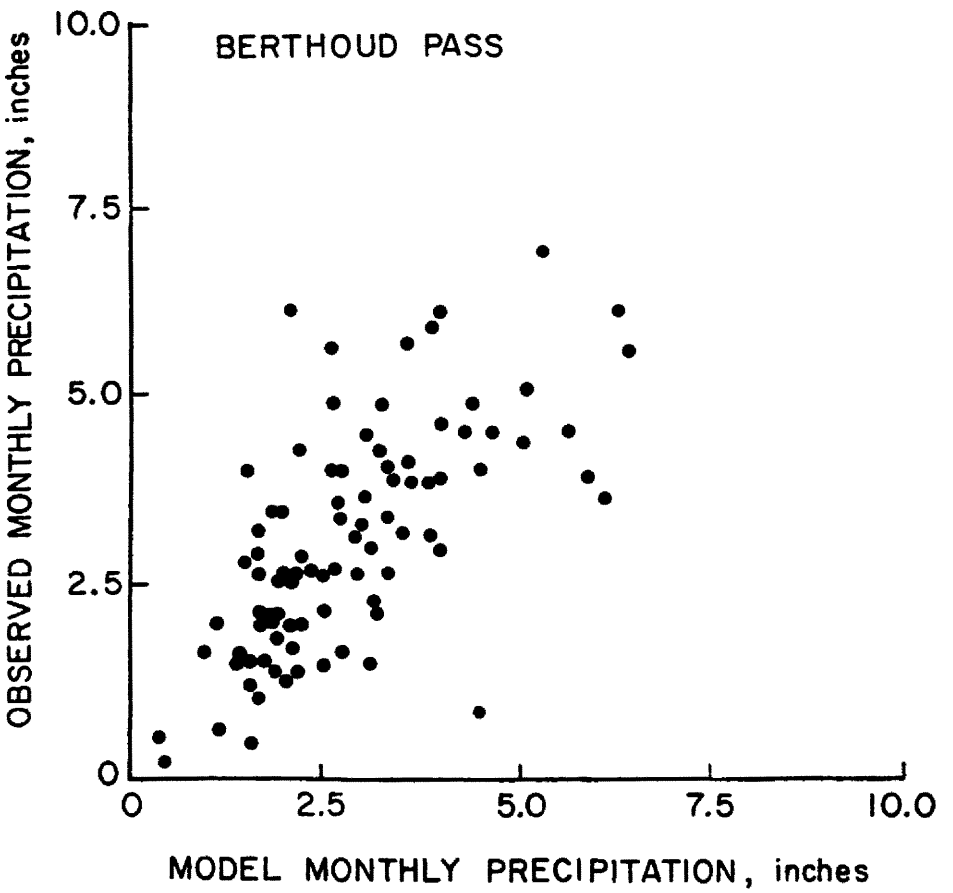

Figure 76. Example of agreement between model and gauge-measured monthly precipitation at a point in the northern mountains

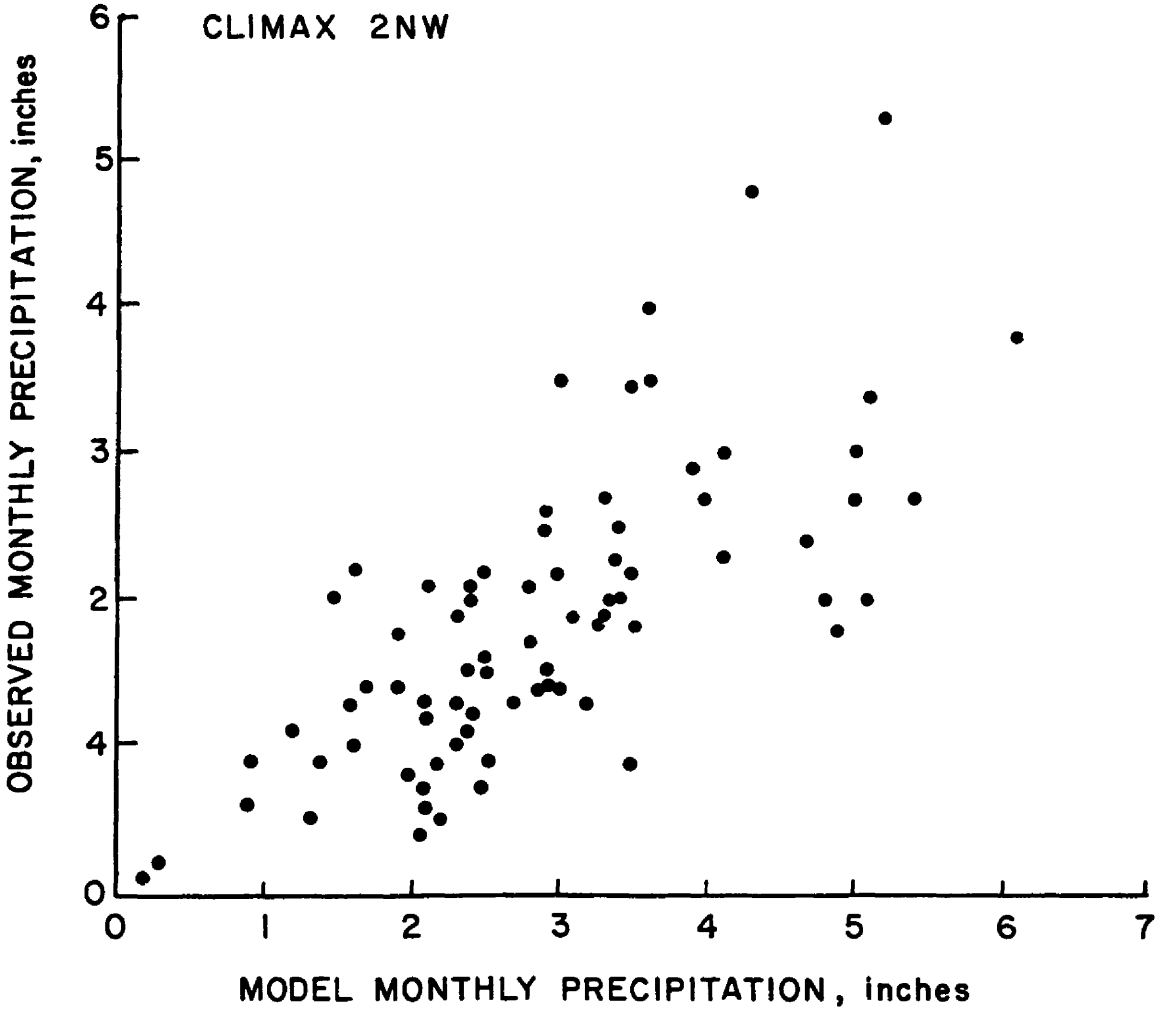

Figure 77. Example of agreement between model and gauge-measured monthly precipitation at a point in the central mountains

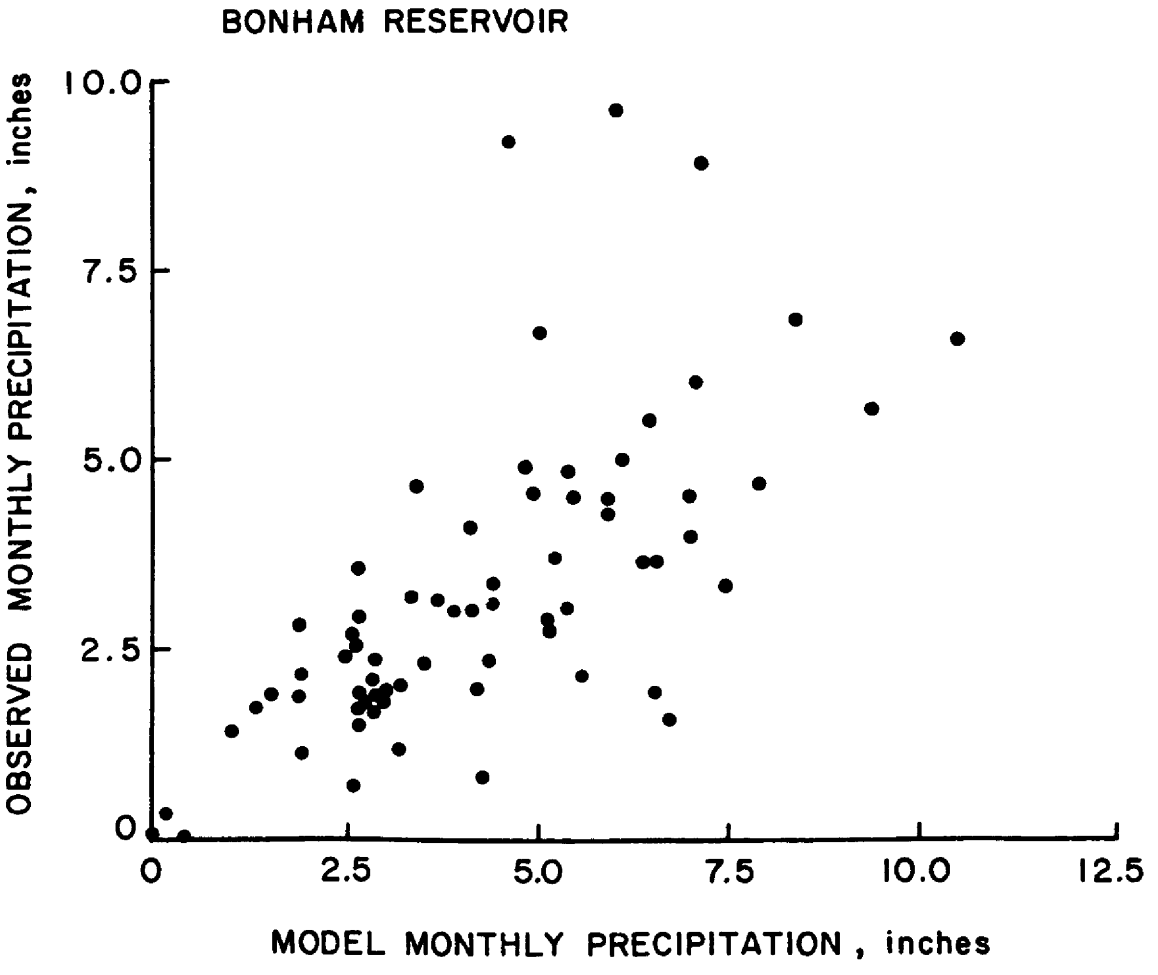

Figure 78. Example of agreement between model and gauge-measured monthly precipitation at a point on the Grand Mesa

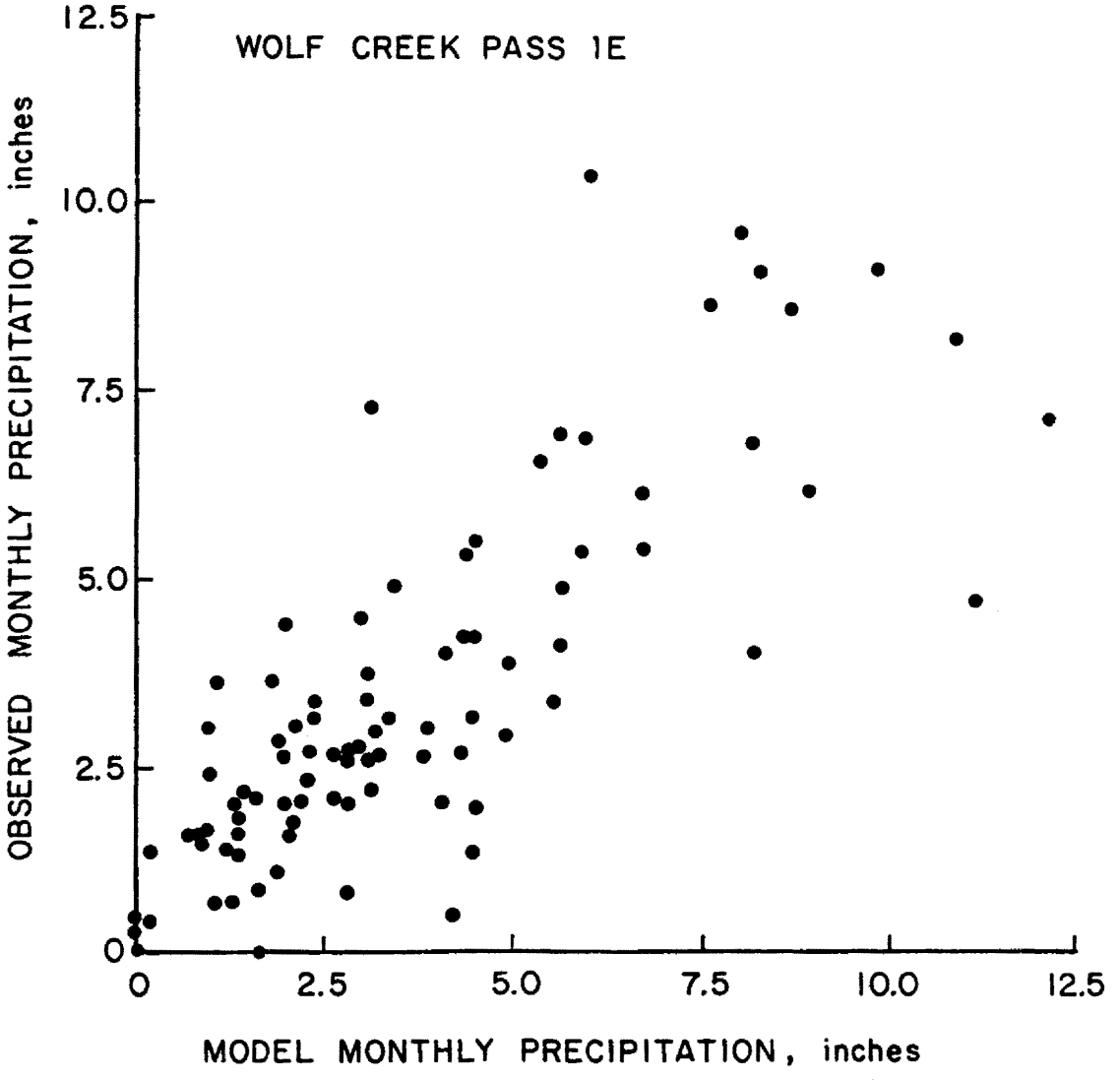

Figure 79. Example of agreement between model and gauge-measured monthly precipitation at a point in the San Juan Mountains in southwestern Colorado

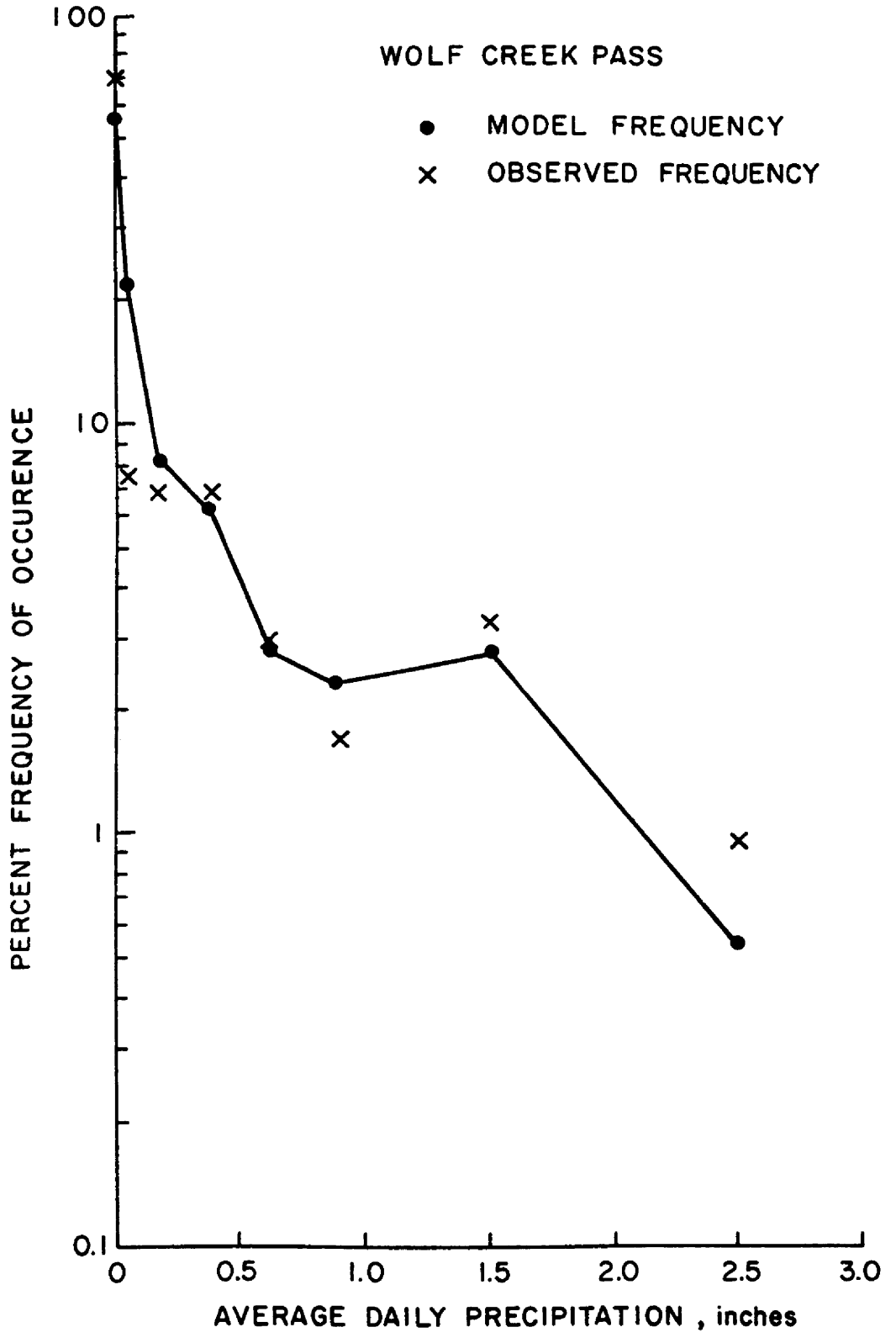

Figure 80. Comparison of model to observed frequency distribution of daily precipitation amounts

Table 14

Chi-Square Table of Model Historical Performance for computing Daily Values of Precipitation at Wolf Creek Pass

Predicted		Observed		
		Zero or Trace	.01-.50"	>.50"
	Zero or Trace	394	40	6
	.01-.50"	133	101	23
	>.50	3	19	39

Table 15

Examples of Probability of Observed Precipitation Amounts at Wolf Creek Pass for Given Model Computed Values

Model Precip. (inches)	Actual Precip. (inches)	≥.01"	.10"	.25"	.50"	.75"	>1.0"	>2.0"
	Zero	10.0	4.7	2.3	1.1	0.9	0.3	0.3
	Trace	22.2	17.5	7.9	3.1	0.0	0.0	0.0
	.01-.10	37.7	24.7	14.9	3.9	1.9	1.9	0.6
	.11-.25	55.2	46.6	20.7	8.6	5.2	1.7	0.0
	.26-.50	75.6	64.4	51.1	26.7	22.2	11.1	0.0
	.51-.75	95.0	75.0	70.0	50.0	30.0	25.0	5.0
	.76-.99	88.2	88.2	76.5	52.9	23.5	17.6	0.0
	1.00-1.99	100.0	95.0	90.0	90.0	65.0	55.0	15.0
	≤2.00	100.0	100.0	100.0	100.0	100.0	100.0	50.0

Pass in southwestern Colorado. The contingency table (Table 14) has a chi-square value of 892 with much less than .001 probability that the model daily computations bear no relation to those observed. The model's skill score (Panofsky and Brier, 1954) for being within the class of the observed value is 0.43. (Zero would indicate no skill while 1.00 corresponds to perfect predictions.)

While the scatter between daily model computations and observed values is large, these historical computations could be used to derive probability estimates for occurrence of greater than specified quantities of precipitation given that the model computed a certain amount. An example is given in Table 15.

7.6 Comparisons to Previous Studies

The 13 seasons of model runs were summed and averaged for each grid point. Figure 81 shows the resulting "climatological" map of 15 October-30 April model precipitation. For comparison an isohyetal map of October-April precipitation constructed by ESSA of the U.S. Department of Commerce by the method of Peck and Brown (1962) using the 1931-1960 precipitation measurements and statistical correlation to physiographic features was available (figure 82). There is, of course, less model detail since the model grid interval was 10 km, and the model obviously underpredicts over most valley areas. However, inspection of the two figures reveals quite close agreement, in general, in positioning of local maxima and frequently even in amount. It is interesting that the ESSA map (based on real precipitation data and empirical correlation to local physiographic features) and the orographic model map (based only on upper air data, topography, a parcel-following water budget equation, and model parameters calibrated with 2 of the 13 seasons

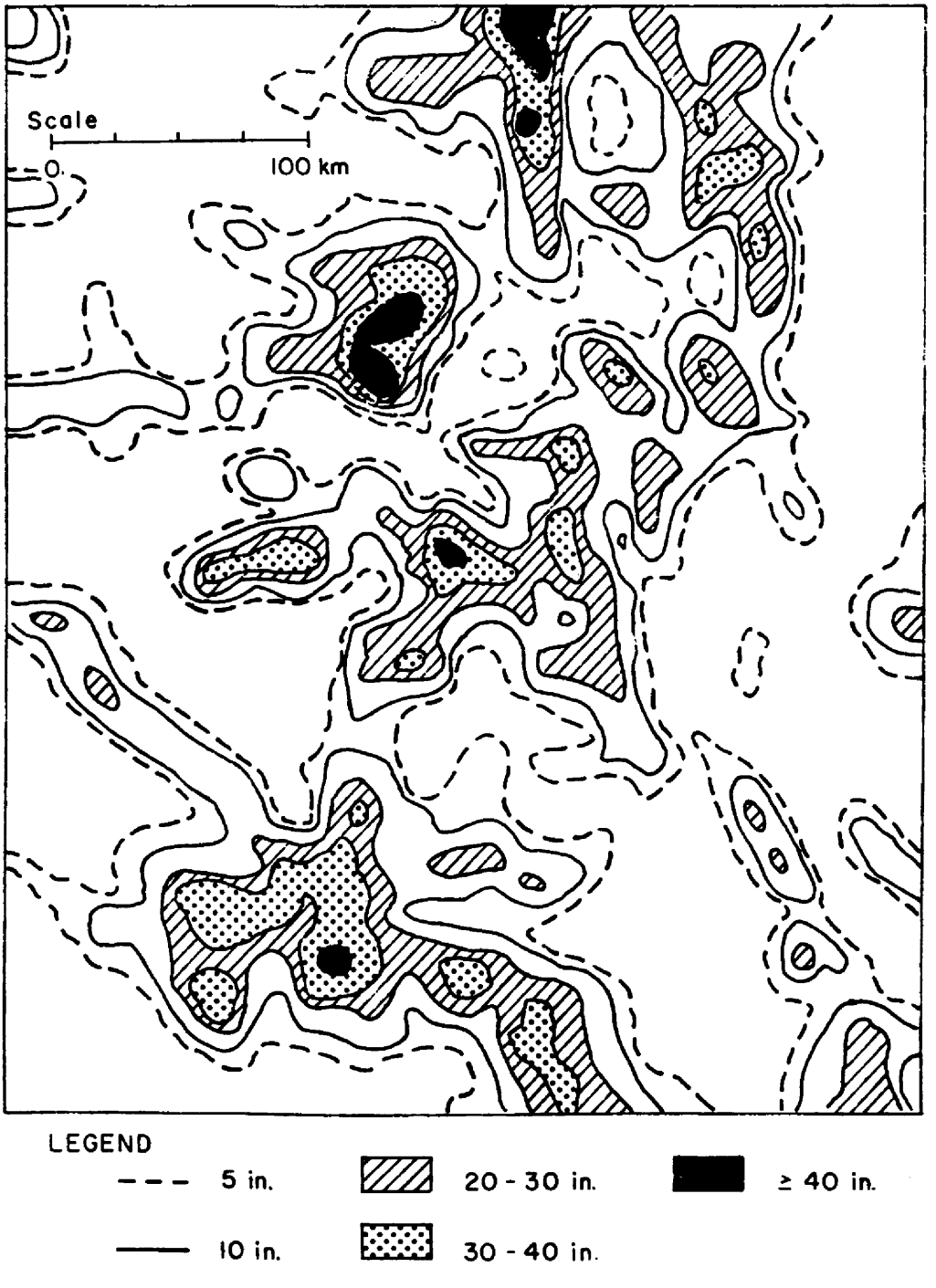

Figure 81. Isohyetal map of 13 year model average 15 October - 30 April precipitation

LEGEND: SAME AS FIGURE 70.

Figure 82. Isohyetal map of normal October-April precipitation based on climatological data for 1931-1960 and correlation of precipitation to physiographic features by the method of Peck and Brown (1962)

employed in obtaining Figure 81) agree so well. Apparently, on the one hand, local precipitation measurements are sufficiently indicative of the upstream barrier shadowing effects to allow construction of the ESSA map, while the orographic model which was specifically designed to consider the rainshadow phenomenon is also depicting the shadowing to almost the same degree.

From this comparison and the numerous more detailed comparisons in earlier sections, it thus appears that it is possible to assess the average magnitude of topographic effects on winter precipitation using only upper air input data, a fine mesh topographic grid, and a simple, parcel-following orographic precipitation model.

7.7 Test Quantitative Precipitation Forecasting (QPF)

One of the objectives of this study was to determine the utility of the approach as an objective quantitative precipitation forecast tool. To the end, test quantitative precipitation forecasts were made from mid-November 1975 through March 1976. These forecasts were then communicated by 1000 MST to the U.S. Forest Service avalanche forecasters.

To incorporate objective QPF aids from the orographic model, "pattern maps" with orographic precipitation isohyets were constructed for each 30° wind direction class by using a time integrated form for model precipitation and a reference hypothetical sounding (subscripted m) as input such that

$$\bar{r}_{M_{I,\ I+1}} = \frac{E_M V_M \Delta P_M}{\rho_w g \Delta x} \left(Q_I + \Delta C_{I,I+1} \right)_M \Delta t_M \qquad (7-3)$$

Figures 83, 84, and 85 give examples of the strong pattern control by wind direction.

The QPF task then became one of calibrating the isohyets for the forecast period. Inspection of equation (7-3) plus the assumption of approximate moist adiabatic stratification and a reference 700 mb temperature of 0°C results in the number and type of correction factors in Table 16. The forecast isohyetal values are then obtained by multiplying the reference isohyets by the total correction factor.

The use of calibrated pattern maps rather than full model runs using a complete set of input data for each prediction period greatly simplifies the use of the method but at the same time eliminates considerable detail that would otherwise be available from actual model runs (provided adequately accurate input data existed). This simplification and loss of model detail for use in QPF forecasting is consistent with the accuracy of available prognostic input information though, as will be seen in this section.

Of the correction factors listed in Table 16, DEP and ECOR present the most difficulty. DEP is fairly sensitive to both temperature and pressure. Further, the vertical position and depth of moist layers is not very well predicted. The efficiency correction factor cannot validly be invoked because a change in efficiency in an actual model run would result in a different areal precipitation pattern. As a first approximation, though, ECOR could be used to index the general effect of differing efficiencies.

The windspeed factor, VCOR, is referenced to the 700 mb wind since 700 mb direction and speed serve as a good index of orographic effects to expect over the study area. From Figure 18 in Section 5, the

Figure 83. Model precipitation pattern map for 210 degree flow

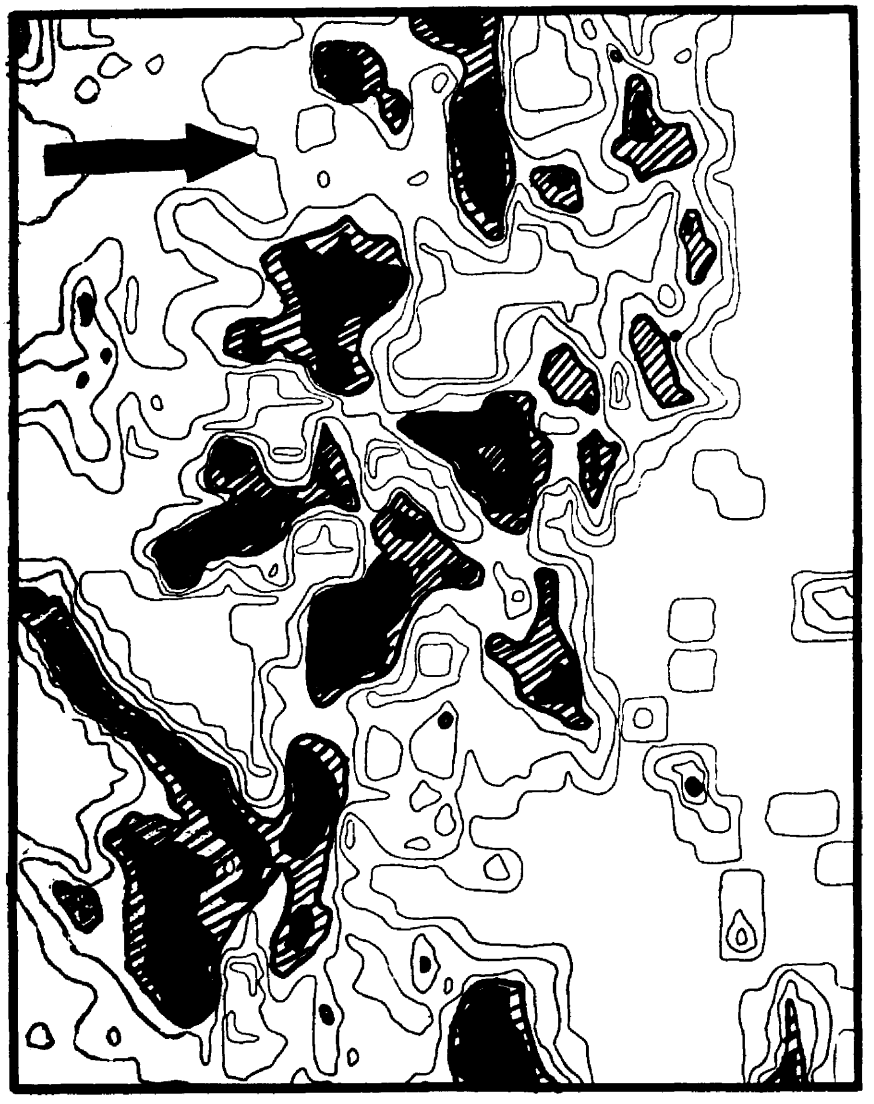

Figure 84. Model precipitation pattern map for 270 degree flow

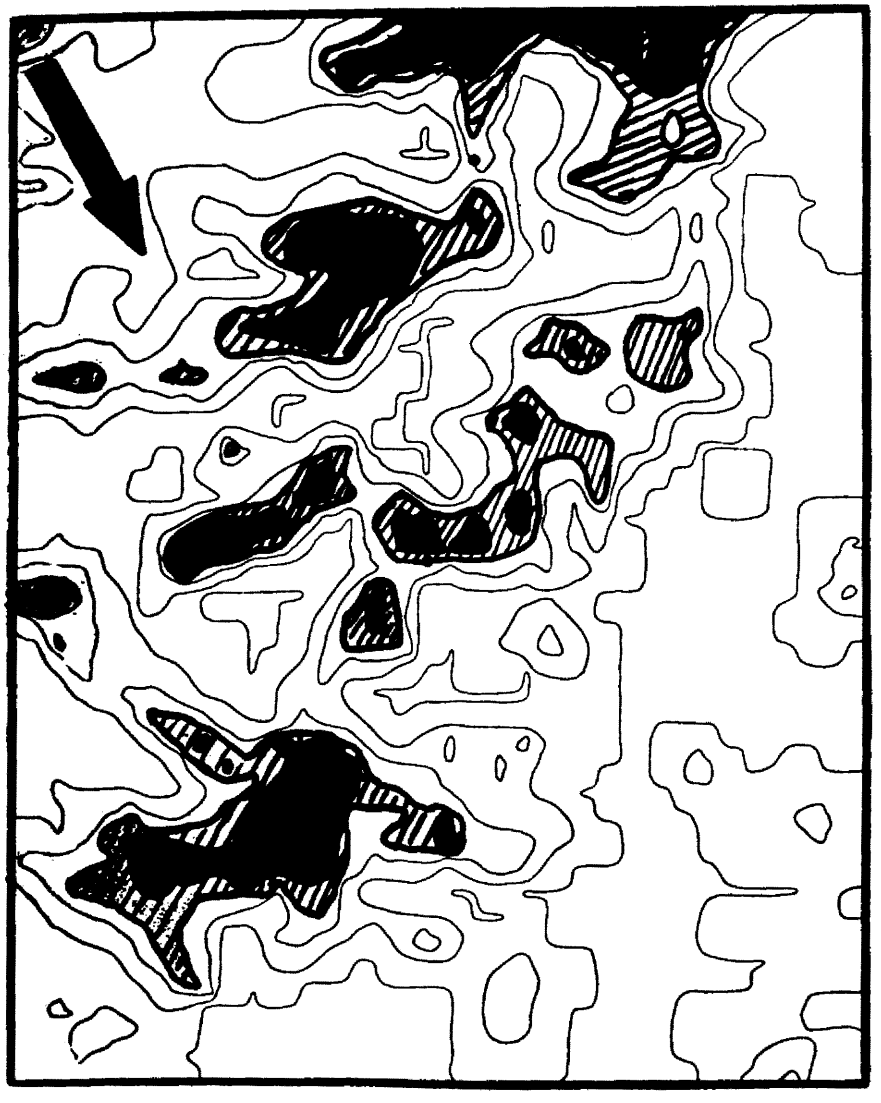

Figure 85. Model precipitation pattern map for 330 degree flow

Table 16

FACTORS FOR CALIBRATION OF PATTERN MAP VALUES

Name and Form	Remarks
1. DURATION FACTOR $DUR = \frac{\Delta t}{\Delta t_M}$	Δt = expected duration
2. TEMPERATURE FACTOR (CONDENSATION PER LIFT) $TF = 1 + \frac{T700}{30}$	T700 = expected 700MB Temperature
3. CLOUD DEPTH FACTOR $DEP = \frac{\left(\overline{\frac{dq_s}{dz}}\right)_{\Delta P, T}^{\Delta P}}{\left(\overline{\frac{dq_s}{dz}}\right)_{\Delta P_M, T}^{\Delta P_M}}$	
4. WIND SPEED FACTOR $VCOR = V700/V_M$	V700 = expected 700MB windspeed
5. PRECIPITATION EFFICIENCY $ECOR = E/E_M$	
6. TOTAL CORRECTION FACTOR $TOTCOR = (DUR)(TF)(DEP)(VCOR)(ECOR)$	
7. CALIBRATED ISOHYETS $R_j = TOTCOR(R_M)_j$ $R_{j+1} = TOTCOR(R_M)_{j+1}$ $\vdots \quad\quad \vdots$ $R_{j+n} = TOTCOR(R_M)_{j+n}$	

Table 17

INFORMATION AVAILABLE FOR MAP CALIBRATION

1. CURRENT SOUNDINGS

2. 12-HR PROGNOSTIC GRIDDED FIELD DATA

   (a) FIELD VARIABLES
   - Temperature
   - Dew point
   - Windspeed
   - Wind Direction

   (b) PRESSURE LEVELS

   850, 700, 500, 400 MB

3. USUAL FAX PRODUCTS

temperature related decrease of condensation per unit lift of about 3% per degree C was employed to arrive at the equation for TF (based on the 700 mb reference temperature, $T700_m$, of 0°C).

Information available for making the map calibrations is summarized in Table 17.

Accuracy of the NMC objective 12 hr LFM and 24 hr PE gridded field prognostic data available through the U.S. Bureau of Reclamation's Environmental Data System is indicated in figures 86-88. Figure 86 indicates quite useful information is available for wind direction assessment. On the other hand, both wind speed and humidity prognoses depart markedly from the observed values as revealed in figures 87 and 88, respectively.

Pattern map 24-hour calibrations (QPF's) were made using a combination of all the aids available in Table 17 including generally strict adherence to the 12-hour LFM gridded fields as a primary input. A major deficiency in available prognostic data was the lack of sufficient vertical and temporal resolution of the expected humidity profile, with a prevailing serious need for an additional forecast level near 600 mb. Figure 13 (Section 5) also implies a serious need for more frequent rawinsonde measurements. Main subjective forecast factors included: (1) estimation of duration of moist flow, (2) determination of vertical positioning and depth of clouds, and (3) fine-scale delineation of areal coverage of the moist flow pattern. In practice, the efficiency correction factor was seldom invoked, and the depth correction estimates were generally either 1, 0.7, or 0.5 for deep, medium and shallow clouds.

Results for a strong southwesterly flow case which dumped large quantities of snow in southwest Colorado but with severe shadowing of

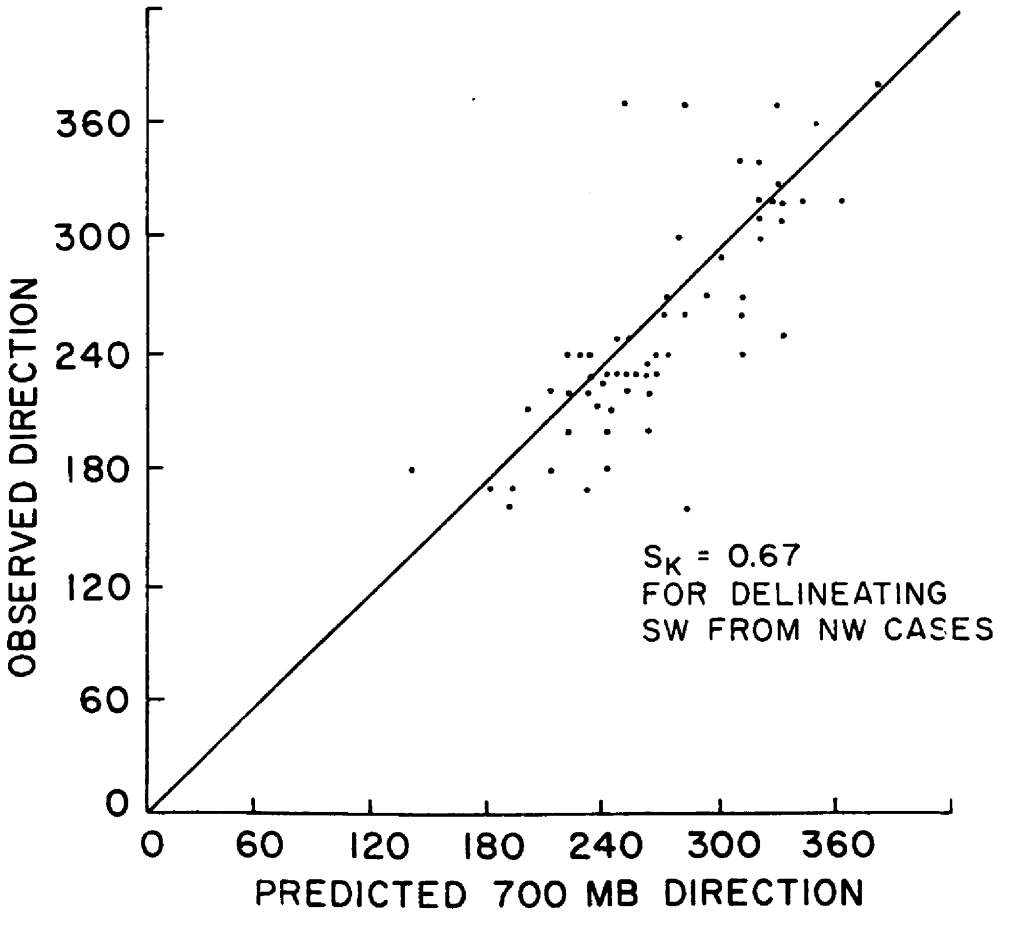

Figure 86. 12 hour LFM and/or 24 hour PE NWS model-predicted versus observed Grand Junction (GJT) 700mb wind directions

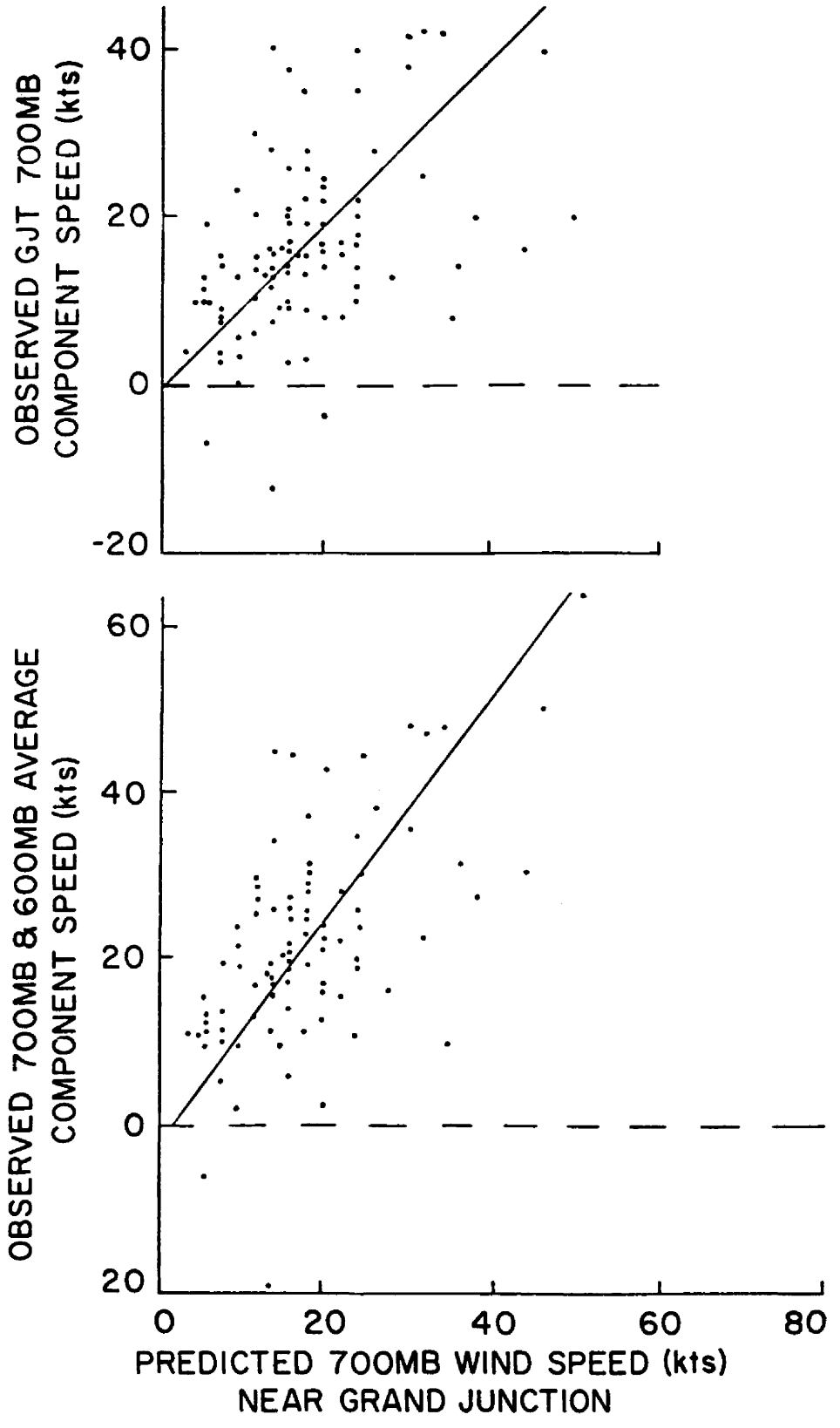

Figure 87. 12 hour LFM and/or 24 hour PE NWS 700mb predicted versus observed GJT component speed (along the predicted direction)

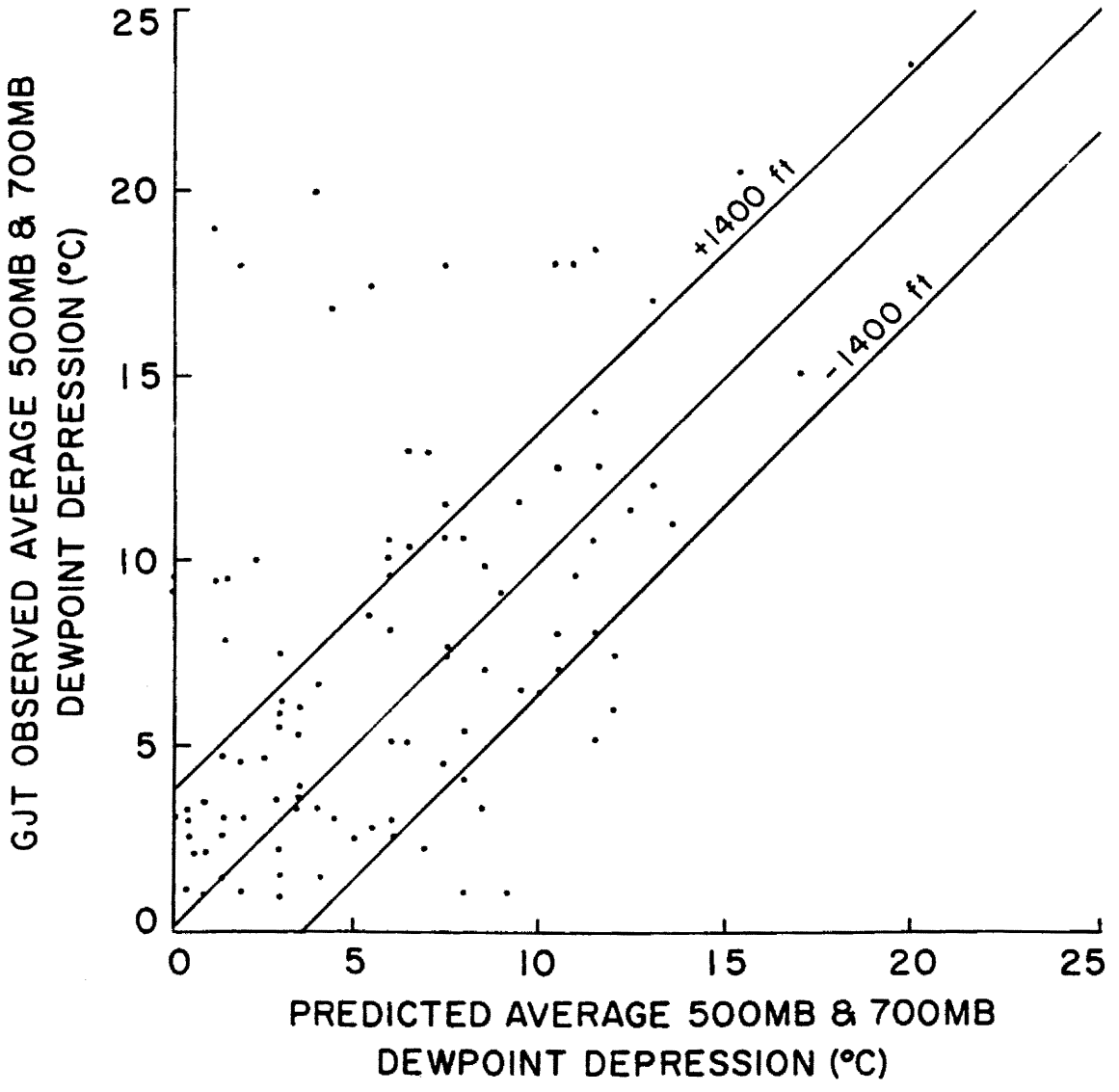

Figure 88. Comparison of predicted to observed dewpoint depression. Lines labled plus or minus 1400 ft. are 3.5C removed from the 45° line and represent a 1400 ft. error of the lifting condensation level

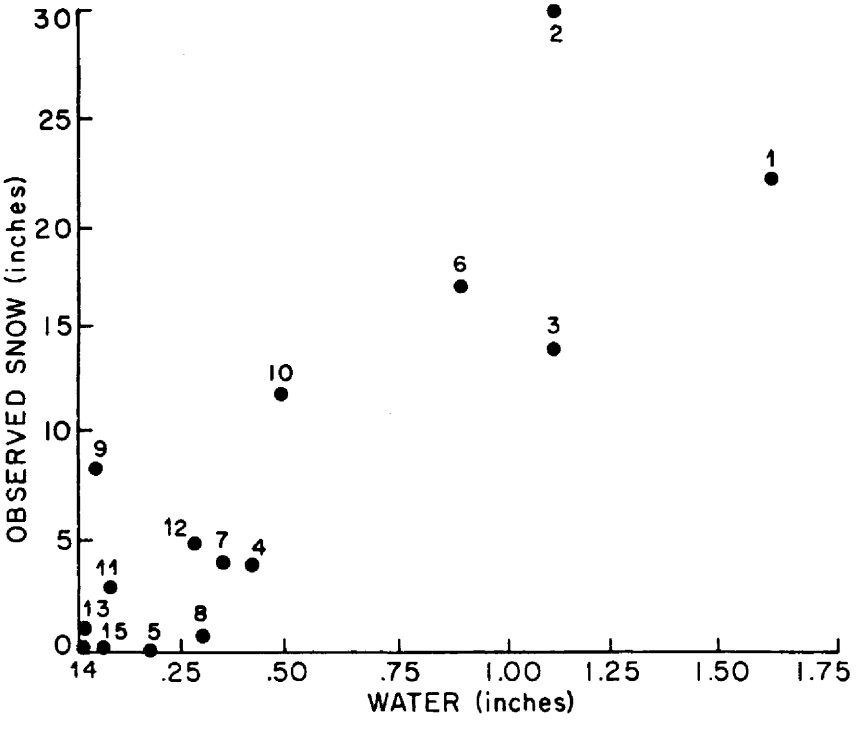

Figure 89. Scatter plot of 24 hour QPF (inches of water) point values versus observed snowfall (inches)

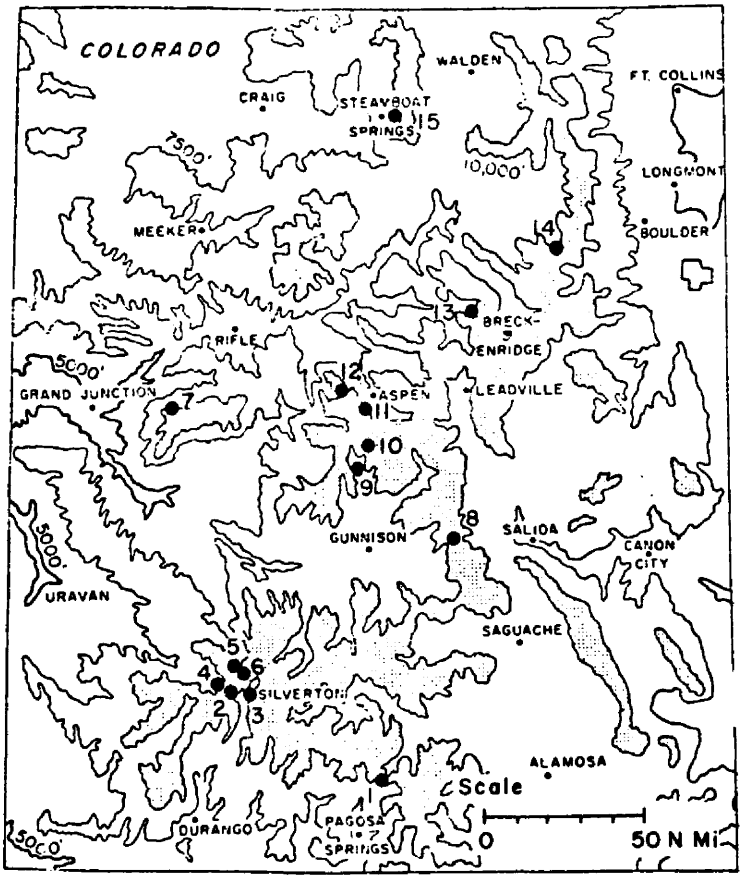

Figure 90. Location of numbered points in Figure 89

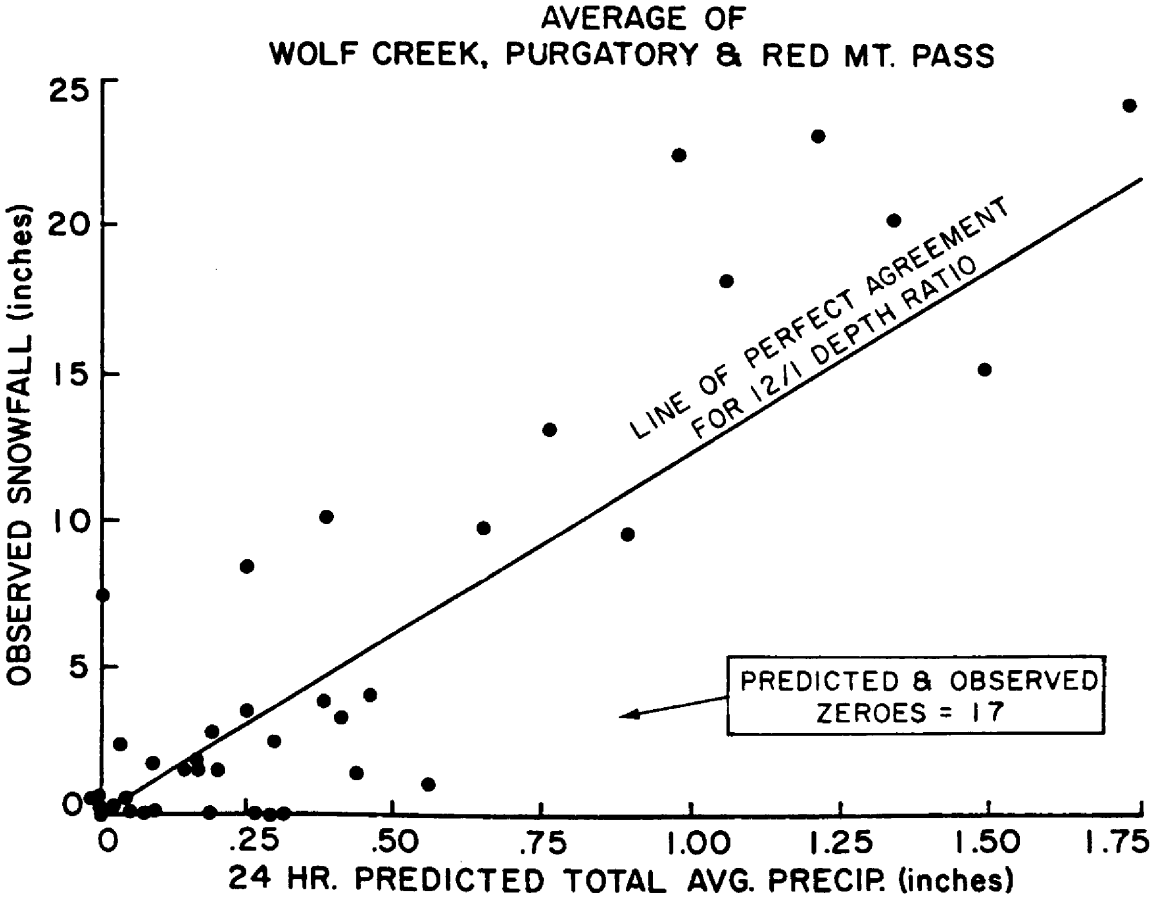

Figure 91. Examples of QPF accuracy for the San Juan Mts. in southwest Colorado using orographic model objective aids

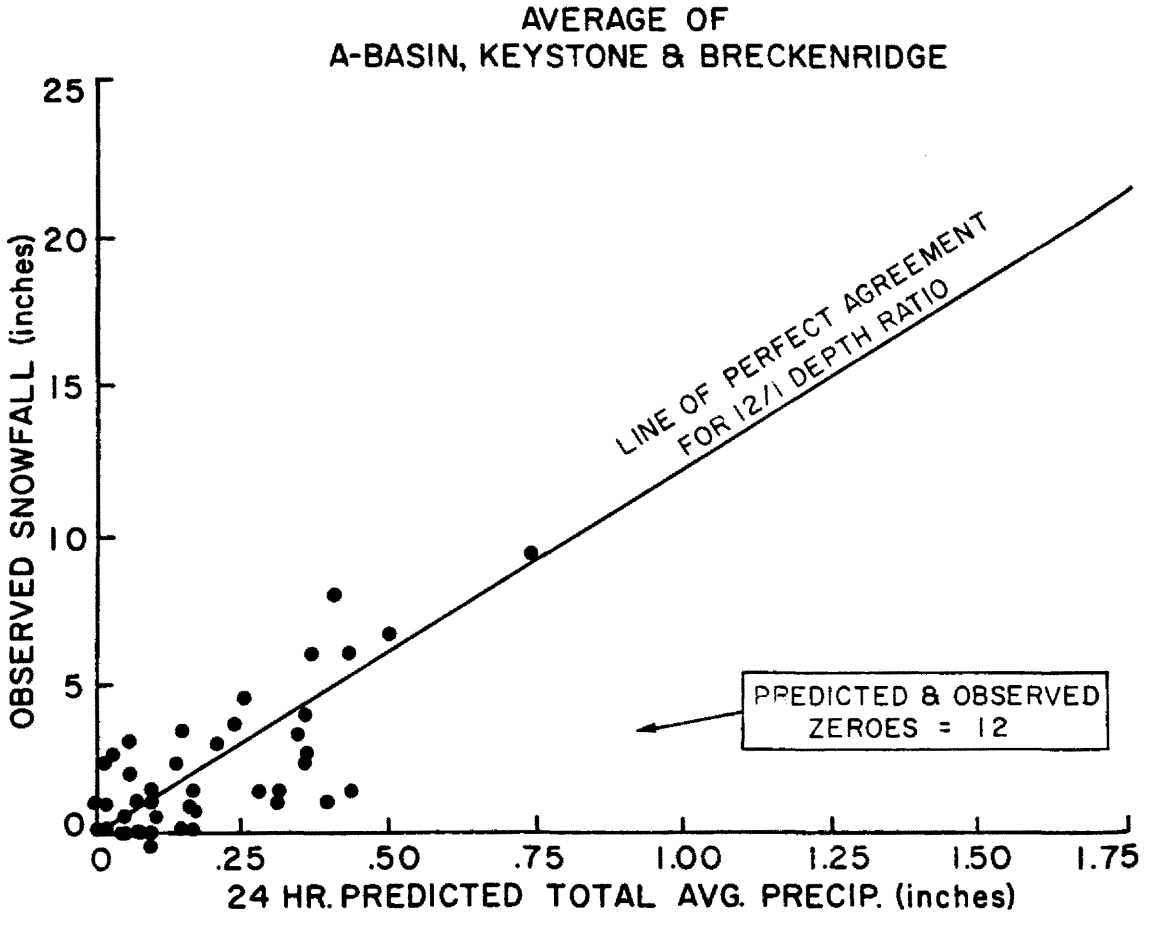

Figure 92. Example of QPF accuracy for a group of ski areas west of Denver using orographic model objective aids

Table 18

24-HOUR QUANTITATIVE SNOWFALL PREDICTION (VERIFICATION)

NOVEMBER 1975 - MARCH 1976 USING OBJECTIVE MODEL AIDS

STATION GROUP	CRITICAL AMOUNT	POD	FAR	S_K	SAMPLE SIZE
SAN JUANS	6"	0.75	0.10	0.78	57
ELK MTS	5"	0.67	0.40	0.56	56
VAIL/COPPER	4"	0.88	0.11	0.87	57
A-BASIN - BRECKEN-RIDGE - KEYSTONE	4"	0.86	0.45	0.61	56
BERTHOUD PASS	3"	0.69	0.36	0.58	63
STEAMBOAT MIDWAY	5"	0.82	0.44	0.59	67
		0.78	0.31	0.67 AVG	

the northern mountains are shown in figures 89 and 90. Figure 90 gives the station locations while the forecast and observed values for each site are scatter plotted in figure 89.

New snow reports from ski areas (via Ski Country USA) were used extensively in this example and throughout the verification of QPF results. Other important verification data came from reporting stations on the U.S. Forest Service's Avalanche Warning network in Colorado. Without the above special information sources, reasonable verification would not have been possible due to a paucity of high mountain precipitation stations.

To reduce the scatter from both point forecast and measurement errors, measurements were averaged for regional station groups of one to five. Figures 91 and 92 show the scatter plots of predicted versus observed 24-hour values for the San Juans in southwest Colorado and a group of ski areas west of Denver, respectively. Table 18 summarizes the prediction scores for each regional group. The varying "critical amounts" were necessary in order to obtain a meaningful sample size delineating "light" from "heavy" in some of the areas. The POD value is the "probability of detecting" (forecasting) the occurrence of an amount equal to or greater than the "critical amount", while the FAR (false alarm rate) is a measure of the frequency of overprediction of large amounts (Donaldson, 1975). The usual skill score (Brier and Panofsky, 1954) is denoted by s_k. There were numerous dry days for which snow was not expected that were not included in the sample used for vertification.

Table 18 indicates skill scores ranging from 0.56 to 0.87 while the degree of overprediction of large amounts ranged from 10 percent

to 45 percent. The fraction of all observed heavier snows that were also forecast averaged 78 percent. In the case of the Vail/Copper Mountain station pair there was only one occurrence of $\geq$ four inches of snow which was not forecast and only one forecast of more than four inches which failed to materialize.

The skill scores in Table 18 represent forecast skill obtained by a combined man-machine effort. Purely objective forecasts for the corresponding forecast periods were not routinely available as only the 12 hour LFM gridded field data was available by forecast decision time. However, three years of 24-hour model computations were made using "perfect progs" with 50 mb vertical resolution. The skill score for delineating < .5" from $\geq$ .5" at Wolf Creek Pass was 0.54. It is thus estimated that purely ogjective model skill scores using prognostic data would have been near 0.35 to 0.4. As an experienced forecaster it can be stated that the model pattern maps were very helpful objective aids in preparing the QPF's. From this QPF study, it can be concluded that:

1. Large QPF errors can frequently arise due to a serious deficiency of vertical resolution in predicted profiles of humidity for mountain precipitation forecast purposes.
2. There is sufficient error in LFM or PE predicted wind speed component (along the wind direction predicted) to frequently give a QPF error of at least $\pm$60 percent and to therefore require forecasts to be phrased in terms of a range of expected values.
3. The calibrated model "pattern maps" are a very valuable objective aid for making short period quantitative precipitation forecasts in mountainous areas.

8.0 SUMMARY AND CONCLUSIONS

8.1 Summary

8.1.1 Model Development and Calibration

An operationally-oriented steady-state orographic precipitation model was developed for hydrometeorological and climatological use. It was designed to run with highly realistic topography. It has the flexibility of using topographic grid meshes as small as 2.5 km on a side, but the testing has been with either a 10-km or a 5-km grid interval.

The model follows the interactions of air layers with the underlying topography by allowing forced vertical displacement of the air column. It keeps track of the condensate or evaporation resulting from these vertical displacements. As the layers flow across the region, part of the condensate precipitates. That which does not moves downstream to the next grid point where a fraction of it and the condensate generated as a result of topographic lift precipitates. In the case of sinking motion, part or all of the parcel cloud water evaporates. Precipitation falling into a layer from above partially (or totally) evaporates when encountering subsaturated conditions. Eventually, precipitation generated in the highest layers reaches the ground provided it does not totally evaporate.

With the foregoing stipulations plus a coordinate framework which follows the parcels, and the further assumptions of steady-state, two-dimensional flow and spatially constant precipitation efficiency, E, the computational formula for precipitation rate, $\bar{r}_{I,I+1}$, along grid interval, Δx, is, from an atmospheric water budget viewpoint

$$(\bar{\dot{r}}_{I,I+1})_{\ell} = \frac{EV_{\ell}\Delta P_{\ell}}{\rho_w g \Delta x} (Q_I + \Delta C_{I,I+1})_{\ell} \qquad (1)$$

where

ℓ = computational layer in question

V = the horizontal wind speed in the x direction at the upwind edge of the computational grid

ΔP = pressure thickness of the inflowing layer at the upwind edge of the computational grid

Q_I = cloud water content (mixing ratio) of liquid or solid at grid point I

$\Delta C_{I,I+1}$ = additional condensation (or evaporation) due to vertical displacement between points I and I+1. (In the event that $\Delta C_{I,I+1}$ is evaporation and is numerically greater than Q_I, precipitation is zero.)

E = precipitation efficiency.

ρ_w = density of water (1 g cm^{-3})

This formulation provides for the shadowing effects of upstream topography when combined with the requirement for a separate topographic grid for each prevailing wind direction.

Model sophistication was designed to be consistent with the routinely available input data resolution. Input requirements are flexible and provision is made for considering variable moisture profiles across the computation area.

The primary objective was to maintain sufficient simplicity (and therefore fast running time) to (a) allow large numbers (thousands) of historical cases to be processed and summed over various time and space

intervals for climatological and hydrological purposes, and to permit the use of model excerpts as objective short term forecast aids.

Prevailing wind direction (and, therefore, choice of topographic grid to be used for each computation case) was determined by the 700 mb direction at the center of the study area.

Blocked flow (i.e., the existence of a "dead layer") was assumed in those strata if either the mean layer transbarrier wind was less than 2.5 ms^{-1} or $\frac{\partial T}{\partial P} < 0.45K/50$ mb provided that all lower layers also met these criteria.

In view of the operationally-oriented nature of the model and the desire to use real upper data as input, three very simple classes of streamline vertical displacement were defined based upon stability and humidity characteristics of the "undisturbed" airstream. These are shown in Table 19 where "cloud top" is defined as the highest layer whose relative humidity is $\geq$ 65% and which is not undercut by a layer of < 50% relative humidity, and where Δh_o is the displacement of the surface streamline. For the approximately neutral stability class, the increase with height of streamline displacement over the highest ridges represents the only attempt in this study to even crudely simulate convection. Using the "stable but no inversion" case as a standard, it was found that the inversion above "cloud top" case decreased precipitation by 18-25% over the higher mountains, while the neutral to unstable case increased it by 13-25%.

In this study large scale vertical motion was considered to be additive to that induced by topography, and only upward large scale vertical motion (computed by the Bellamy method) was permitted. It was found for one test year that if large scale vertical motion was ignored

TABLE 19

STREAMLINE VERTICAL DISPLACEMENT

STABILITY CLASS	DISPLACEMENT OF "CLOUD TOP" STREAMLINE
(a) INVERSION ABOVE "CLOUD TOP"	0
(b) STABLE 500 MB - 700 MB TEMP. BUT NO INVERSION ABOVE CLOUD TOP	$0.4\Delta h_o$
(c) APPROX. NEUTRAL STABILITY 500 MB TO 700 MB LAYER	$0.7\Delta h_o$ ($1.2\Delta h_o$ OVER HIGHEST TERRAIN)

completely, average precipitation over the area was decreased by 23%, while allowing negative as well as positive large-scale vertical motion produced about a 5% decrease in area-average precipitation.

A primary model parameter requiring calibration is precipitation efficiency. One to two full winter seasons of runs were made for each of several temperature-dependent efficiency functions. The phenomenon of "shadowing" by upstream barriers was rather severe for the higher efficiency values. Of the several functions tried (for the 10 km grid interval topography) the equations

$$E = -.01\ T_c$$

or

$$E = 0.25 \text{ (for } T_c \leq -25C)$$

where T_c is the designated unlifted "cloud top" temperature in °C gave the best areal distribution of seasonal precipitation when compared to a group of snow courses from all regions of the state.

Due to numerous simplifying assumptions there are a number of limitations inherent in this model. Some of these are listed in Table 20 for convenience.

In addition to the errors inherent in the model itself, numerous additional sources of error are introduced when employing real data as input. The data errors are largely of a random nature, arising due to the areal and temporal non-representativeness of the upper air information. The magnitude of all the errors is sufficient to produce rather large discrepancies between model and observation for short period computations. Cancellation of random errors when summing computations over a season would be expected to allow reasonable agreement, however.

Table 20

Partial List of Model Processes and Some Resulting Model Limitations

Model Process	Limitation
Blocked Layer Determination	(1) No variation along streamline allowed (1a) No previously existing radiational drainage (i.e., cold air pooling) considered (except at sounding site itself) (2) Real 3-D phenomenon not necessarily simulated
Streamline Displacement (a) Horizontal	(1) No flow-splitting around narrow barriers aligned with wind allowed (2) No funneling or channeling of any kind allowed (3) Only one wind direction allowed per computation case to "represent" entire grid and all layers, resulting in only partial simulation of layer water budgets
(b) Vertical	(1) No consideration of lee-wave or other complicating downwind effects on basic current flow or stability (2) Inadequate simulation of imbedded convection
Precipitation Efficiency Computation	(1) Detailed cloud physics usage prohibited (2) E must be calibrated to grid interval used
Elimination of Crystal Trajectories	(1) Precipitation deposition displacement due to varying windspeed not allowed

8.1.2 Testing the Model

With the above limitations and sources of error in mind, and using the model parameters as described earlier, computations of precipitation for each grid point at each sounding time were made for the period 15 October - 30 April for each of 13 seasons. The period of representativeness for each sounding was assumed to be 10 hours. Summations of model precipitation were made for each season for (a) grid points, (b) over selected watersheds, (c) at selected snowcourse measurement sites, and (d) at selected precipitation measuring sites. The computational area consisted of the mountainous area of Colorado west of 105°W longitude with dimensions of 340 by 440 km.

Model input information consisted of interpolated upper air data along the inflow (upwind) borders of the computation grid. This was obtained by the objective analysis method of Panofsky (1949) using six rawinsonde stations within and/or surrounding the computational area. Large-scale vertical motion was estimated by the Bellamy (1949) method with a correction by O'Brien (1970).

For west or westnorthwest flow, it was necessary to override the objective analysis scheme and use the actual sounding from only one upstream sounding station as input data for border points in northwest and northern Colorado due to unrepresentativeness (due to local topography) of the other surrounding soundings. This points up the difficulty of indexing the large scale moisture field with only a few measuring sites in complex terrain.

It was found necessary to make sensor lag corrections to profiles of relative humidity from each sounding prior to areal interpolation to obtain useable estimates of humidity profiles for model input. Changes

in the humidity sensors in use were made during the historical period of data used for model testing, necessitating differing sets of correction procedures dependent on the instrument in use. Reasonable rectification of humidity errors was apparently accomplished, as no marked differences in model output characteristics were observed for the early period compared to later years.

In general, resulting year-to-year model precipitation pattern variations agreed quite well with those observed. An example of the areal contrast accuracy is given in Figure 93.

Correlation coefficients between model and actual snowcourse values ranged from 0.51 to 0.91 with 14 of the 16 correlation coefficients significant at the 1% level.

Volume model precipitation for each year was compared to observed March - July runoff from each of 18 watersheds of varying size selected from all across the computation grid. For the sample size of 13 years, correlation coefficients between model and observation for the 18 watersheds ranged from 0.62 to 0.91 with 14 of the 18 above 0.70. Elimination of one year (1972-1973) which had record-breaking October precipitation (with strong embedded convection) in southwest Colorado brought the least correlation coefficient up to 0.73 with 16 of the 18 above 0.80 and all significant at the 1% level. Summation of model volume precipitation for larger basins and the resulting comparisons to observed March-July runoff yielded correlation coefficients of 0.85, 0.88, 0.95, 0.93, and 0.92, respectively for 5 composited basins located from the northern part of the area progressively further south. Summation over all watersheds used yielded a correlation coefficient between model and observation of 0.88 with the problem year of 1972-73 included and 0.92 by omitting it.

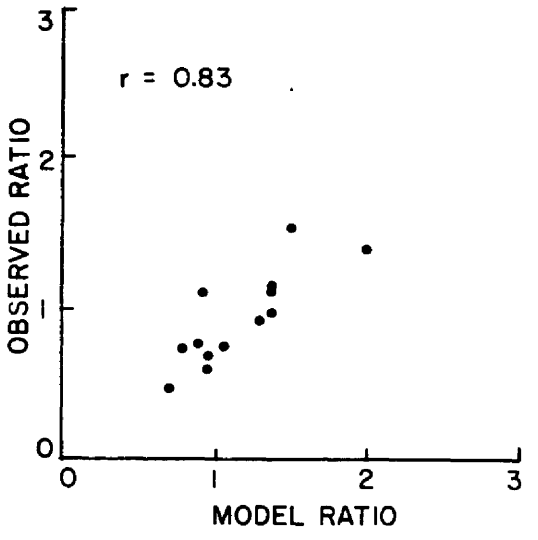

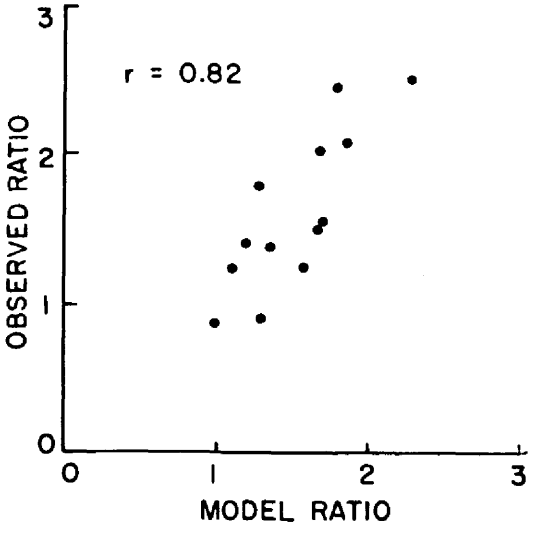

Figure 93. Scatter plots of observed seasonal ratios of snowcourse readings versus model precipitation ratios to test model ability in determining areal gradations in seasonal precipitation

Correlation between model values for a group of 8 snowcourses (used as an index of precipitation for all but the San Juan Mountains area) and observed runoff was 0.90. This compares quite closely with a correlation coefficient of 0.92 when replacing model values with real snowcourse readings.

As a measure of the areal distribution accuracy of the model, the 13-year average value of model precipitation depth was computed for each of 19 watersheds of > 250 mi^2 in area over the computation area. The correlation coefficient between these values and observed runoff depth was 0.89.

A comparison of the model-derived 1961-62 through 1973-74 mean precipitation map with a similar isohyetal map by ESSA of the U.S. Department of Commerce based on the 1931-1960 precipitation data and empirical correlation to local physiographic features (Peck and Brown, 1962) showed remarkably close agreement over mountainous regions. Model precipitation in the valleys was unrealistically low.

Only a few high mountain point precipitation stations were available for comparisons with the model. Also model topography is sufficiently smoothed to prevent an expectation of 1 to 1 correspondence between model and observed point precipitation. Modest agreement was observed on a monthly basis, however. The scatter increased markedly on a daily basis, but the frequency distribution of model daily amounts was very similar to that for observed precipitation with the exception of a higher than observed incidence of light (0.01 - 0.10 inch) amounts.

Finally, in response to the last objective of this study, test quantitative precipitation forecasts were made (and communicated daily to the U.S. Forest Service) from November, 1975,through March, 1976,

using wind direction-dependent pattern maps from the model as objective aids. Isohyets on these pattern maps were calibrated using forecast values of wind speed, moisture depth, duration and areal coverage, and cloud temperature. Skill scores for 24 hour quantitative precipitation amounts ranged from 0.56 to 0.87.

8.2 Conclusions

From this study a number of conclusions can be drawn and these are listed below.

1. It has been demonstrated that it is feasible to assess the average magnitude and the inter-season variation of topographic effects on winter season precipitation in the mountainous section of Colorado using only routinely available upper air information, a fine mesh topographic grid, and a simple orographic precipitation model.
2. Computations of model volume precipitation over various watersheds in the study area show strong positive correlation to observed spring and summer runoff. Thus the method has substantial potential for providing input to hydrologic process models for streamflow forecasting, especially for watersheds of greater than 250 square miles . This input could consist of computed areal and temporal distributions of winter precipitation using only routinely available upper air data as soon as it is collected.
3. The employment of model wind-direction dependent pattern maps of precipitation as objective aids to quantitative precipitation forecasting in mountainous areas is quite useful and should be continued.

4. The basic model should be transferable to other mountainous areas which are not dominated by convective precipitation. Parameter re-calibration would be required depending on such things as latitude, altitude, terrain scale-size and micro-physical characteristics of the moist air masses.

5. Historical orographic precipitation computations using real upper air information as model input require corrections for humidity sensor lag if meaningful model results are to be obtained.

8.3 Model Utilization Suggestions

Model patterns of precipitation are sufficiently realistic to suggest several immediately useful applications. Some of these are briefly discussed below.

First of all, the skill scores attained from the 1975-76 winter of test quantitative precipitation forecasting (QPF) are sufficiently high to warrant the construction and use of model pattern maps for QPF aids in other topographically complex areas as well as the continued use of the method for Colorado.

A second endeavor which would likely yield useful results would involve the interfacing of this orographic precipitation model to models of hydrologic processes and blowing snow to obtain runoff estimates. Snowcourses and precipitation gauge data for adjusting the model volume watershed precipitation should be incorporated in the method, while then using the adjusted precipitation model output to define the areal relative distribution of precipitation over the watershed. Adaptation of the blowing snow model by Schmidt (1972) for use with interpolated winds aloft

data is recommended as a technique for estimating sublimative water losses from blowing snow in the alpine zone.

The combined usage of the orographic precipitation model and a blowing snow model naturally suggests the incorporation of the resulting output into an avalanche dynamics model currently being developed by the U.S. Forest Service. Related to this, but more empirical in nature would be a climatological study of the model-indicated frequency of conditions conducive to avalanche occurrence utilizing model precipitation and upper air wind information.

Historical upper air information attending previous record point snowfalls could be input to the model for the construction of maps of "project snowstorms", an exercise which should be useful for structural planning purposes.

The gridded arrays of model output for each wind direction would be immediately useful for identifying widely separated points having a high degree of correlation between their precipitation values over a wide range of wind directions. Such information could be utilized for selection of precipitation measurement sites for use as weather modification target and control areas. The technique could also be employed to strategically locate gauges in a hydrometeorological network to maximize the information gained from a minimum number of gauges.

With adequate spatial and temporal resolution of upper air soundings, model output would be a quite useful data set for direct use as a covariate (equivalent to a control area precipitation station) for reducing the unexplained variance in weather modification target area precipitation and thus minimizing the required duration of the experiment for obtaining meaningful results.

Finally, the rather dramatic visual and quantitative depiction of terrain shadowing effects in model output suggests that qualitative insight into the possible downwind effects of weather modification might be gained from a series of model sensitivity tests employing spatially variable precipitation efficiency values.

While results from this simple approach to the orographic precipitation problem are encouraging and point to its immediate utility for certain purposes, limitations inherent in both the model simplicity and in the input data should be kept in mind. Based on this study and those of several other investigators referenced herein, accuracy limits even with adequate input data for computing precipitation over periods of 6 hours or less should be near a value of 0.7 for the correlation coefficient between model and measurement. Summation of these short period computations over 24 hour periods might attain a correlation coefficient of approximately 0.8. Seasonal summations can be expected to attain peak correlation of near or just slightly above 0.9.

Accuracy beyond that stated above will likely require (1) consideration of three-dimensional effects on airflow, (2) markedly improved knowledge of precipitation efficiency, (3) improved parameterization of meso-scale banded precipitation phenomena, and (4) better temporal and spatial resolution of upper air moisture profiles.

8.4 Recommendations for Further Research

Continued pursuit of the problem of seasonal orographic precipitation estimation is recommended along the lines discussed in this study. In particular the implications from Section 7.4.4 suggest an attempt to quantify effects from (a) terrain funneling, (b) ridges aligned with the wind, or (c) isolated peaks might be profitable. Objective precipitation

corrections for these effects might logically be sought by comparing the fields of either horizontal perturbation velocity or vertical motion obtained from a three-dimensional flow model to those from the current computation scheme.

The regression relationships obtained between model precipitation and observed runoff should be tested for stability for several subsequent years. In particular tests should be made using data from any available extremely dry or wet years.

Also, it would be instructive to test the approach for other areas including topographically complex regions dominated by stratiform rain.

Much more effort should be expended to understand the nature of and quantify precipitation efficiency.

An attempt should be made to fine tune the model to even finer resolution topography. This should include studies employing nested topographic grids with resolution of the inner-most grid of 2.5 km. The crystal trajectory subroutine of the model should be turned on for this research. Empirical fine-tuning relations could also be sought by developing correction factors for current model output by considering model and actual station elevations and precipitation. These correction factors might then be useful over a limited area to estimate precipitation on the sub-grid scale.

Finally, the model should be combined with an atmospheric water balance box model such that the box model water balance specifies the box volume quantity precipitation minus evaporation while the orographic model is utilized to areally distribute the precipitation. Extensive usage of interpolated upper air temperature, wind, and humidity data should be made in this study not only for model computations but also

to test the utility of these interpolated data for developing relations to indicate periods of high mountain evaporation through both blowing snow sublimation and from the stationary snow cover. Insight into the areal and temporal distribution of evaporation should be one outcome of this research.

The extreme short period variability of relative humidity profiles observed in this study suggests the need for additional research into the causes for such with end goals of (a) arriving at improved ways of considering the effects of mesoscale banded structures (including convection bands) and (b) a determination of the minimum sampling frequency of upper air moisture fields required to significantly improve precipitation estimates.

REFERENCES

Auer, A.H.,Jr., and D.L. Veal, 1970: An investigation of liquid water-ice content budgets within orographic cap clouds, J. de Recherches Atmospheriques, pp 59-64.

Barford, N.C., 1967: Experimental Measurements: Precision, Error, and Truth, Addison-Wesley Publishing Co., Inc., London.

Bellamy, J.C., 1949: Objective calculations of divergence, vertical velocity, and vorticity. Bull. Amer. Meteor. Soc., 30, 45-49.

Betts, A.K., 1973: A composite mesoscale cumulonimbus budget, J. Appl. Meteor., 30, 597-610.

Brousaides, F.J. and J.F. Morrissey, 1974: Residual temperature-induced humidity errors in the National Weather Service radiosonde. Final report, AFCRL-TR-74-0111, Instrumentation Papers, No. 215.

Chappell, C.F., 1970: Modification of cold orographic clouds, Ph. D. Dissertation, Colorado State University, Atmospheric Science Paper No. 173.

Colton, D.E., 1975: Precipitation analysis for operational streamflow forecasting - the use of mesocale numerical modeling to enhance estimation of precipitation in mountainous areas. Proceedings of AGU Conference on Precipitation Analysis for Hydrologic Modeling, Davis, California, June.

Colton, D.E., 1976: Numerical simulation of the orographically induced precipitation distribution for use in hydrologic analysis. J. Appl. Meteor:,15, 1241-1251.

Dixon, W.J., and F.J. Massey, Jr., 1969: Introduction to Statistical Analysis, 3rd Edition, McGraw-Hill Book Co., New York, 638 p.

Donaldson, R.J., R.M. Dyer, and M.J.Kraus, 1975: An objective evaluation of techniques for predicting severe weather events. Proceedings of AMS Conference on Severe Local Storms.

Elliott, R.D., and R.W. Shaffer, 1962: The development of quantitative relationships between orographic precipitation and airmass parameters for use in forecasting and cloud seeding evaluation, J. Appl. Met., Vol. 1, 218.

Elliott, R.D., and E.L. Hovind, 1964: On convective bands within Pacific Coast storms and their relation to storm structure. J. Appl. Met., Vol. II, 143-228.

Elliott, R.D., 1969: Cloud seeding area of effect numerical model: Aerometric Research, Inc., Report to Fresno State College Foundation, Aerometric Research, Inc., Goleta, California.

Fraser, Alistair B., R.C. Easter, and P.V. Hobbs, 1973: A theoretical study of the flow of air and fallout of solid precipitation over mountainous terrain, Part I, Airflow Model: J. Atm. Sci., Vol. 30, No.5, 801-812.

Hjermstad, L.M., 1970: The influence of meteorological parameters on the distribution of precipitation across central Colorado mountains. Master's Thesis, Colorado State University, Atmospheric Science Paper No. 163.

Middleton, W.E.K., and A.F. Spilhaus, 1953: Meteorological Instruments, University of Toronto Press, Toronto.

Morrissey, J.F., and F.J. Brousaides, 1970: Temperature induced errors in the ML-476 humidity data. J. Appl. Meteor., 9, 805-808.

Myers, V.A., 1962: Airflow on the windward side of a ridge. J. Geophy. Res., 67, 4267-4291.

Nickerson, E.D., C.F. Chappell, and E.L. Magaziner, 1976: Effects of cold orographic clouds, Atm. Physics and Chemistry Lab Report, NOAA, Boulder, Colorado.

Nielsen, B.C., 1966: A technique for forecasting the rate of snowfall at Ata, Utah. Alta Avalanche Study Center, Project D, Progress Report No. 1, U.S.Dept. of Agriculture, Forest Service, Wasatch National Forest, 15 p.

O'Brien, J.J., 1970: Alternative solutions to the classical vertical velocity problem, J. Appl. Meteor., 9, 197-203.

Ostapoff, F., W.W. Shinners, E. Augstein, 1970: Some tests on the radiosonde humidity error. NOAA Tech. Rept. ERL 195-AOML 4.

Panofsky, H.A., 1949: Objective weather map analysis. J. Meteor., 6, 386-392.

Panofsky, H.A., and G.W.Brier, 1958: Some Applications of Statistics to Meteorology, Pennsylvania State University Press, University Park, Pa. 224 p.

Peck, E.L., and M.J. Brown, 1962: An approach to the development of isohyetal maps for mountainous areas. J. Geophy. Res., Vol. 67, 681-694.

Peck, E.L., and P. Williams, Jr., 1962: Terrain influences on precipitation in the intermountain west as related to synoptic situations. J. Appl. Met., Vol. 1, 343-347.

Plooster, M.N., and N. Fukuta, 1974: Numerical model of seeded orographic snowfall. AMS Proceedings of Fourth Conference on Weather Modification, Fort Lauderdale, Florida, November.

Rhea, J.O., P. Willis and L.G. Davis, 1969: Park Range atmospheric water resources program. Final report to Bureau of Reclamation (Contract No. 14-06-D-5640), EG&G, Inc., Boulder, Colorado

Rhea, J.O., 1973: Interpreting orographic snowfall patterns. Colorado State University, Atmospheric Science Paper 192, January, 74 pp.

Rhea, J.O., 1975: A simple orographic precipitation model for hydrological and climatological use. Proceedings of AGU Conference on Precipitation Analysis for Hydrologic Modeling, Davis, California, June.

Rhea, J.O., and L.O. Grant, 1974: Topographic influences on snowfall patterns in mountainous terrain, Advanced Concepts and Techniques in the Study of Snow and Ice Resources, Nat'l. Academy of Sci., Washington, D.C., pp 182-192.

Rogers, C.F., 1970: A mountain precipitation study, Master's Thesis, University of Nevada, Reno.

Sarker, R.P., 1967: Some modifications in a dynamical model of orographic rainfall, Monthly Weather Review, Vol. 95, No. 10, 673-684.

Sawyer, J.S., 1956: The physical and dynamical problems of orographic rain, Weather, 11, 375-381.

Schermerhorn, V.P., 1967: Relations between topography and annual precipitation in western Oregon and Washington. Water Resources Research, 707-711.

Schmidt, R.A., Jr., 1972: Sublimation of wind transported snow - a model, USDA Forest Service Research Paper RM-90, Rocky Mt. Range and Forest Experiment Station, Ft. Collins, Colorado.

Spreen, W.C., 1947: A determination of the effect of topography upon precipitation, American Geophysical Union Trans., Vol. 28, No. 2, 285-290.

Wexler, Arnold, 1949: Low temperature performance of radiosonde electric hygrometer elements, J. Research NBS, 43.

Willis, P., 1970: A parameterized numerical model of orographic precipitation, Report to U.S. Bureau of Reclamation, Contract 14-06-D-5640, EG&G, Inc., Enviromental Service Operation, Boulder, Colorado.

Wilson, J.W., and M.G. Atwater, 1972: Storm rainfall variability over Connecticut. J. Geophy. Res., 77, (21), 3950-3956.

Young, K.C., 1974: A numerical simulation of wintertime orographic precipitation: Part I. Description of the model microphysics and numerical techniques. J. Atm. Sci., 31, (7), 1735-1748.

APPENDIX A

EQUATION DERIVATON

A.1 Computational Formula for dq_s/dz

The available upper air data for model usage consists of values of temperature, geopotential height, relative humidity, wind speed, and wind direction at 50-mb pressure increments. It would thus be convenient to develop an expression for the parcel change (along a moist adiabat) of saturation water vapor mixing ratio with height, dq_s/dz, in terms of pressure and temperature only. This development proceeds below.

The first law of thermodynamics for a moist process with phase change of water supplying the only diabatic effect can be written

$$-Ldq_s = c_p dT - \alpha dP \tag{A1}$$

Expressed as derivatives with respect to height eq (A1) becomes

$$\frac{dq_s}{dz} = -\frac{c_p}{L}\frac{dT}{dz} + \frac{\alpha}{L}\frac{dP}{dz} \tag{A2}$$

For the moist adiabatic process in a hydrostatic atmosphere Equation (A2) can be expressed as

$$\frac{dq_s}{dz} = \frac{c_p}{L}\gamma_m - \frac{g}{L} = \frac{c_p}{L}(\gamma_m - \gamma_d) \tag{A3}$$

An expression for γ_m is

$$\gamma_m = \frac{g}{c_p}\left[\frac{1 + \frac{L}{R_d}\frac{q_s}{T}}{1 + \frac{\varepsilon L^2 q_s}{c_p R_d T^2}}\right] \tag{A4}$$

Substitution of Equation A4 into Equation A3 gives

$$\frac{dq_s}{dz} = \frac{gq_s}{R_d T}\left(1 - \frac{\varepsilon L}{cpT}\right) \Big/ \left(1 + \frac{\varepsilon L^2 q_s}{cpR_d T^2}\right) \tag{A5}$$

Strictly speaking,

$$q_s = \varepsilon e_s/(P - e_s) \tag{A6}$$

but with negligible error for practical purposes

$$q_s \simeq \frac{\varepsilon e_s}{P} \tag{A7}$$

The Clapeyron equation may be used in combination with Equation A5 and Equation A7 to express dq_s/dz only in terms of P and T.

Writing the Clapeyron equation in the integrated form (when T is in °K and e_s is in mb)

$$\ell n\left(\frac{e_s}{6.11}\right) = \frac{\varepsilon L}{R_d}\left(\frac{1}{273} - \frac{1}{T}\right) \tag{A8}$$

or

$$e_s = 6.11 \exp\left[\frac{\varepsilon L}{R_d}\left(\frac{1}{273} - \frac{1}{T}\right)\right] \tag{A9}$$

and substituting Equation A9 into Equation A7 yields

$$q_s \simeq \frac{(\varepsilon)(6.11)}{P} \exp\left[\frac{\varepsilon L}{R_d}\left(\frac{1}{273} - \frac{1}{T}\right)\right] \tag{A10}$$

Insertion of Equation A10 into Equation A5 yields (after units conversions to express dq_s/dz in $\left[g_{H_2O}\, g_{AIR}^{-1}\, cm^{-1}\right]$, when T is in °K and P is in mb) the desired computational formula

$$\frac{dq_s}{dz} = [.0013T - 2.037]/\left[\frac{PT^2}{\exp\left(20.099 - \frac{5489.9}{T}\right)} + 0.526 \times 10^8\right] \tag{A11}$$

is obtained.

APPENDIX B

OBTAINING THE INPUT DATA

B.1 Relative Humidity Corrections

A study designed to compute quantitative precipitation values from atmospheric soundings requires reasonably good estimates of the vertical profile of relative humidity over given periods in the area of interest. Thus, it was necessary to explore the reliability of such humidity measurements before performing the model validation study. This proved to be no simple task, as there were no less than three significant changes either in relative humidity elements or humidity element housing design during the 13-year period covered in the study.

The response characteristics of the lithium chloride hygristors (in use prior to late 1964) were neither quantitatively well known nor well-behaved under the variety of atmospheric conditions to which they were routinely exposed. Wexler (1949) made the most extensive study of the time lag characteristics for this element type under controlled laboratory conditions for a realistic range of temperature and humidity by keeping temperature constant and suddenly changing relative humidity. His results are shown in Figure B1. The data shown in this figure represent averages of from 2 to 8 elements per point. Variations of 30% from element to element were observed for the same ambient conditions.

For the present study, a set of empirical curves crudely depicting similar lag constants to Figure B1 were constructed. Examples are given in Figure B2. Comparing this to Figure B1 it can be seen that for relative humidities of less than 75% these lag constants are somewhat less than those of Wexler while for higher humidity they are higher.

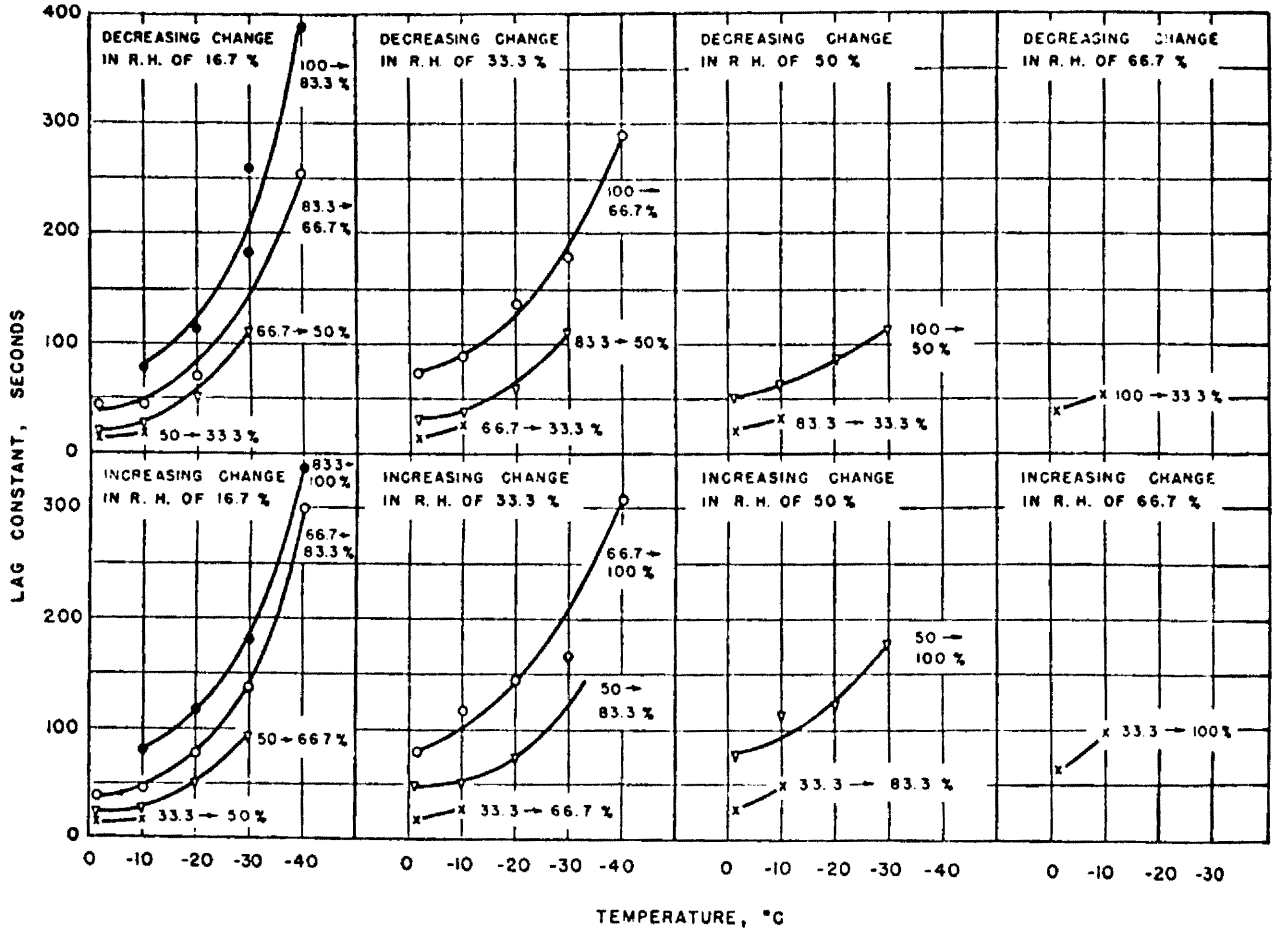

Figure B1. Lag constants from the lithium chloride relative humidity sensor (Wexler, 1949)

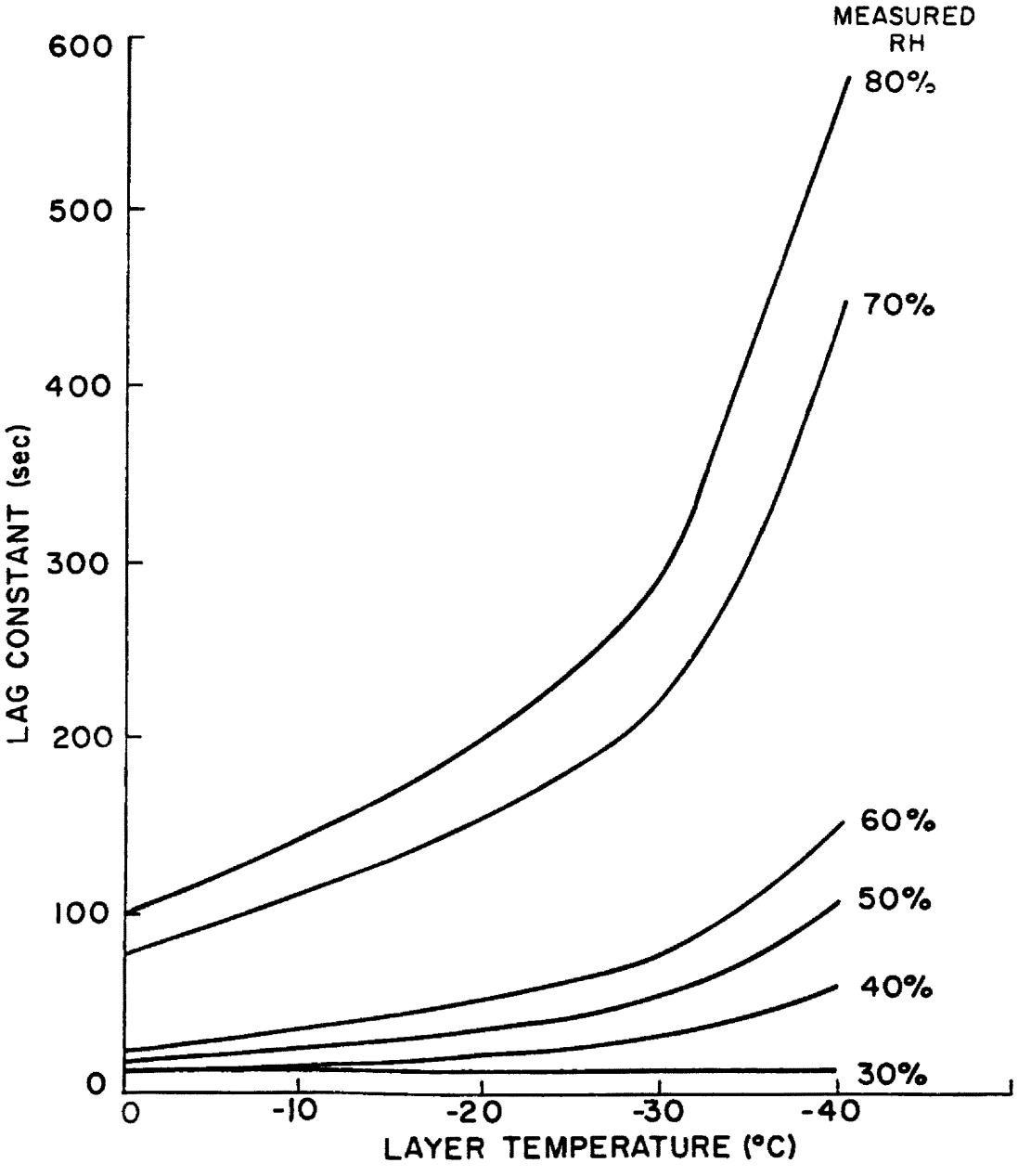

Figure B2. Lag constant curves used for correcting the lithium chloride sensor-measured relative humidity

Using the lag constants from the empirical curves, corrections to the relative humidity profile were made through the equation (see Appendix C for derivation)

$$r_e = \left[r_s - \left(r_{s_o} - r_{e_o}\right)e^{-t/\lambda} - r_{e_o}\,\frac{\lambda}{t}\,(1-e^{-t/\lambda})\right] \Big/ \left(1 - \frac{\lambda}{t}\,(1-e^{-t/\lambda})\right) \qquad \text{(B1)}$$

where

r_e = correct environmental relative humidity after rise time, t

r_s = sensor reading of relative humidity after rise time, t

r_{s_o} = initial sensor relative humidity at the next lower level

r_{e_o} = initial environmental relative humidity at the next lower level

λ = lag constant of humidity sensor

t = time required for radiosonde to rise from reference level below to measurement level in question.

This equation assumes a linear change in relative humidity between 50-mb constant pressure level increments as well as a constant balloon ascension rate of 5 m sec^{-1}. To obtain corrections to the humidity at each 50-mb level a program was written which allowed insertion of the corrected value for the next lower level as an estimate of r_{e_o}, thus permitting solution of equation (B1).

Appendix C shows results of a year of testing the corrected and non-corrected relative humidity profiles against observed cloud cover at radiosonde observation release time for Grand Junction, Colorado.

In approximately late 1964, (documentation on the changeover is fragmentary) the carbon relative humidity element replaced the much slower responding lithium chloride sensor and uncorrected relative humidity profiles improved considerably (at least for night-time

soundings). Rather severe errors were introduced during periods of high sun angle, and element ventilation rates proved to be considerably less than the balloon ascension rate. For purposes of the study herein, standard release times at 12Z and 00Z from November to April at 40°N are either before sunrise or very near sunset, thus minimizing the insolation-induced errors in the carbon element. Thus, corrections to this set of relative humidity profiles consisted of (a) a blanket correction factor of 1.09 applied to each humidity value at each level (Morrissey and Brousaides, 1970) and (b) the use of Equation B1 with a lag constant of 20 seconds (Ostapoff et al.,1970). Appendix C gives results of a year of testing this correction scheme.

In 1972 the housing design for the carbon element was changed, permitting better ventilation and markedly less insolational error (Brousaides and Morrissey, 1974; Betts, 1973). Thus corrections were so small as to be unwarranted following this improvement.

B.2 Areal Interpolation of Upper Air Data

B.2.1 Main Interpolation Scheme

This is required for initializing the orographic precipitation model. Sounding stations used were LND, GJT, SLC, DEN, INW, and ABQ (Figure B3). Data was read from tape for each 50-mb level from 850 mb to 300 mb.

It was assumed that any variable, $\psi(x,y)$, on each constant pressure surface could be expressed by a quadratic surface (Panofsky, 1949) such that

$$\psi(x,y) = a_o + a_1x + a_2x^2 + a_3xy + a_4y^2 + a_5y \qquad \text{(B2)}$$

To evaluate coefficients, six data points were required (the six sounding stations). This allowed determination of a function, $\psi(x,y)$, for temperature, relative humidity, and wind at each pressure level.

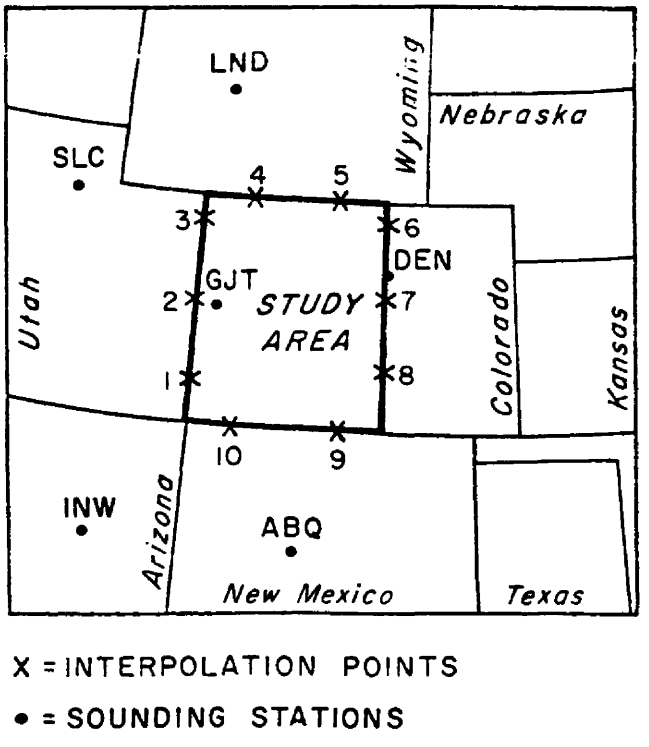

Figure B3. The study area and available upper air stations

Insertion of interpolation point coordinates, (x,y), to the function yielded values of the desired meteorological variable at each point of interpolation (see Figure B3).

B.2.2 Provision for Missing Stations

In the event of one or more missing upper air stations for any given constant pressure level, interpolation proceeded via the use of inverse distance-squared upper-air station weighting.

Appendix D shows results of comparing interpolated to observed relative humidity for Durango in southwestern Colorado.

B.3 Provision for Station Biases

When generating mesoscale upper air information from the large-scale observation network, questions of representativeness and bias of the original soundings arise. This is particularly true in regions of complex terrain. Such biases should be identified and corrections made (if possible).

Considering possible local biases in station humidity data, the sign but not the magnitude can be readily deduced by considering nearby topographic featuers in relation to large-scale flow. For example, for a west-northwest flow of moist air, LND and DEN would be expected to indicate lower relative humidity than SLC due to partial precipitation of the atmospheric water content upon lifting over the mountain barriers upwind of each of these stations, while SLC humidity should be biased toward high values because water is yet to be removed over intervening high terrain between that location and the northwest Colorado border.

This presents a dilemma of what inflow humidity profile to use for model computations, particularly when coupled with the frequent phenomenon of WNW moist flow extending only as far south as the northern

third of Colorado, leaving GJT dry. In such cases either of the interpolation schemes would be expected to bias northwest and northern border point humidity toward low values. Forecast experience for the northern Colorado mountains indicates the SLC sounding to be more representative than any of the other three under such circumstances. Provision was thus made to simply use the SLC sounding for border points 3, 4, and 5 under conditions of moist west through west-northwest flow (especially since preliminary calculations without such provision indicated a serious dry bias by the usual interpolation schemes).

The necessity for invoking such corrections based on local experience points up substantial inadequacies in the ability of the large-scale sounding network to represent large areas in regions of complex terrain.

B.4 Border Point Selection

Once vertical profiles of temperature, humidity, and wind are obtained, the model then selects (dictated by the 700 mb wind direction at the center of the computation area) either the 2, 3, or 5 appropriate upwind border point soundings for computational use.

B.5 Large Scale Vertical Motion Computation

The same set of six sounding stations as above was utilized. Vertical motion profiles were computed for each of 5 triangles formed by the sounding stations by first computing horizontal divergence by the Bellamy technique (Bellamy, 1949) and then using the continuity equation to obtain vertical motion at 50 mb increments. Corrections were then made to vertical velocity by the method of O'Brien (1968) by assuming a linear correction to divergence with pressure and by further assuming

that vertical motion (large-scale) is zero at the lower boundary and at the top of the highest layer of calculations (275 mb).

The Bellamy technique consists of computing the proportionate rate of change of triangle areas due to horizontal divergence, which is

$$\nabla_H \cdot \vec{V} = \frac{1}{A_{ABC}} \frac{d(A_{ABC})}{dt} \tag{B3}$$

where

A_{ABC} = area of triangle ABC formed by balloons located at each of three upper wind measurement sites

ΔA_{ABC} = the change in area of triangle formed by the three balloons (moving horizontally) after time, Δt.

Triangle areas may be found by Heron's formula

$$A_{ABC} = \sqrt{S(S - \overline{AB})(S - \overline{BC})(S - \overline{CA})} \tag{B4}$$

where

$$S = (\overline{AB} + \overline{BC} + \overline{CA})/2 \tag{B5}$$

Leg lengths $\overline{AB}$, $\overline{BC}$, $\overline{CA}$ can be found by noting that

$$\overline{AB} = \sqrt{x_{AB}^2 + y_{AB}^2} \tag{B6}$$

and

$$x_{AB} = (\lambda_B - \lambda_A) \cos\left(\frac{\phi_B + \phi_A}{2}\right) \tag{B7}$$

$$y_{AB} = \phi_B - \phi_A \tag{B8}$$

where

ϕ = latitude

λ = longitude

The change in λ and ϕ in time Δt can be shown to be

$$\Delta\lambda = \frac{-|\vec{V}| \cos(270 - \beta)}{.017453\ r \cos((\phi_o + \phi_o + \Delta\phi)/2)} \quad \text{(B9)}$$

$$\Delta\phi = |\vec{V}| \sin(270 - \beta)/.017453\ r \quad \text{(B10)}$$

where

r = earth radius

β = conventional wind direction

Then assuming a linear variation of velocity, V, over the triangle, it is possible to compute a new area of the triangle after passage of time, Δt, by noting that

$$x_{A'B'} = (\lambda_B' - \lambda_A') \cos\left(\frac{\phi_{o_A} + \phi_{o_B}}{2}\right) \quad \text{(B11)}$$

$$y_{A'B'} = \phi_B' - \phi_A' \text{ , etc.} \quad \text{(B12)}$$

Once divergence is computed for each 50-mb layer, vertical motion, ω, can be computed from the continuity equation

$$\frac{\partial\omega}{\partial P} = -\nabla_H \cdot \vec{V} \quad \text{(B13)}$$

or

$$\omega_{P_{TOP}} = \omega_{P+\Delta P_{BOTTOM}} + \overline{(\nabla_H \cdot \vec{V})}\ \Delta P \quad \text{(B14)}$$

O'Brien's correction gives corrected vertical motion values, ω_P', as

$$\omega_P' = \omega_P - (\omega_K - \omega_T)\ k(k + 1)/K(K + 1) \quad \text{(B15)}$$

where

K = total number of layers

k = the layer number in question

ω_K = the uncorrected vertical velocity at the top of the highest layer (275 mb)

ω_T = forced (by assumption) corrected value of vertical motion at the top (275 mb) and taken to be zero.

For a given layer, the resulting 5 values of vertical motion are averaged together and then applied in Equation (4-16) of Section 4.3 for precipitation computations.

APPENDIX C

RELATIVE HUMIDITY CORRECTIONS

C.1 Discussion

The basic need for correcting the relative humidity profiles from radiosondes was discussed in Appendix B and will not be repeated here. Rather, correction equation derivation will be presented as will results of testing the corrected values against cloud observations.

C.2 Equation Derivation

A meteorological sensor exposed to the atmosphere does not respond instantaneously to indicate the true environmental reading of the quantity it is sensing. According to Middleton and Spilhaus (1953) the differential equation describing sensor response is given as

$$\frac{d\theta_s}{dt} = -\frac{1}{\lambda}(\theta - \theta_e) \qquad (C1)$$

where θ_s is the sensor reading at time, t, θ_e is the true environmental value and λ is known as the "lag constant" (a function of the sensor response characteristics).

If we consider a relative humidity sensor borne upward by a balloon rising at a constant rate and moving through a linearly varying humidity field, we can rewrite Equation (C1) as

$$\frac{dr_s}{dt} = -\frac{1}{\lambda}(r_s - r_e) + \frac{dr_e}{dt} - \beta \qquad (C2)$$

where

$$\beta = \frac{dr_e}{dt} \qquad (C3)$$

Re-arranging terms we obtain the first order non-homogeneous differential equation:

$$\frac{d}{dt}(r_e - r_s) + \frac{1}{\lambda}(r_e - r_s) = \beta \tag{C4}$$

The characteristic solution of Equation C4 is

$$r_e - r_s = C_1 e^{-t/\lambda} \tag{C5}$$

while a particular solution is

$$r_e - r_s = e^{t/\lambda} \int \beta e^{t/\lambda}\, dt$$

or

$$r_e - r_s = \beta\lambda \tag{C6}$$

Therefore

$$r_e - r_s = \beta\lambda + C_1 e^{-t/\lambda} \tag{C7}$$

To evaluate the arbitrary constant, we note that at t=0, (where $r_e = r_{e_o}$ and $r_s = r_{s_o}$)

$$r_e - r_{s_o} = \beta\lambda + C_1 \tag{C8}$$

and, thus

$$C_1 = r_{e_o} - r_{s_o} - \beta\lambda \tag{C9}$$

Insertion of Equation C9 into Equation C7 completes the solution as

$$r_e = r_s + \beta\lambda + (r_{e_o} - r_{s_o})e^{-t/\lambda} - \beta\lambda e^{-t/\lambda} \tag{C10}$$

Considering a constant balloon ascension rate and a linearly varying environmental relative humidity field, we can re-arrange Equation C10 further. First, we can write

$$r_e = r_{e_o} + \beta t \tag{C11}$$

and thus

$$\beta = (r_e - r_{e_o})/t \tag{C12}$$

Substitution of Equation C12 into Equation C10 gives (after some rearrangement)

$$r_e = \left[r_s-(r_{s_o}-r_{e_o})e^{-t/\lambda}-r_{e_o}\frac{\lambda}{t}(1-e^{-t/\lambda})\right] \Big/ \left(1-\frac{\lambda}{t}(1-e^{-t/\lambda})\right) \quad \text{(C13)}$$

By starting at the bottom of the sounding and working upward, estimates of $r_{e,i}$ (where i is the level in question) can be obtained by considering $r_{s_o} = r_{s,i-1}$ and $r_{e_o} = r_{e,i-1}$ (i.e., by assuming the corrected value of r_e at the next lower level is the true ambient value at that level.

C.3 Comparison of Corrected Relative Humidity to Cloud Observations

Through the use of Equation C13 and the set of lag constants from Appendiz B, corrections were made to the 0000Z relative humidity profile (as depicted at 50 mb intervals) for Grand Junction, (GJT). Corrected profiles were then compared to the 0000Z surface observation of cloud heights and amounts at that site for the period October - April of two years (1961-62 and 1970-71) which encompassed both the lithium chloride and carbon element usage periods. It was not feasible to make the same kind of comparison to the 1200Z radiosonde due to darkness and unreliable sky observations.

To make the comparison, the following criteria were established:

1. Since the object was to compare relative humidity to visible clouds further conversion of the relative humidity values to relative humidity with respect to ice was made for layer temperatures below -24°C and with correction to values intermediate between ice and water for -13°C to -24°C temperatures.
2. The humidity profiles were searched to determine the distinct layer or layers with maximum or secondary maximum values of

relative humidity (see Figure C1 as an example). The humidity, layer height, and layer temperature were recorded.

3. The surface observation at GJT was used to determine existence of clear, scattered, broken, or overcast conditions at the approximate heights of layers of relative maxima of relative humidity. Remarks of existing precipitation at the station or of visible mountain precipitation were also noted.
4. Data points were then scatter-plotted on a layer relative humidity, layer temperature plane as in Figure C2 with points labeled as to sky condition for that layer.

Results are shown for each of the two years in Figures C2 and C3. Apparently most of the temperature dependent lag effects, particularly troublesome with the LiCl sensor, have been removed by the corrections. Further, there appear to be few events of less than broken to overcast when the corrected layer relative humidity is greater than about 92%. Also, there are very few remarks of mountain precipitation (and, from a further check not shown here, very few recorded measurable quantities of mountain precipitation at mountain stations) when the maximum relative humidity on the entire profile was less than 65%.

Comparing Figure C2 with Figure C3, it appears that the basic sensor response differences have been reasonably well corrected.

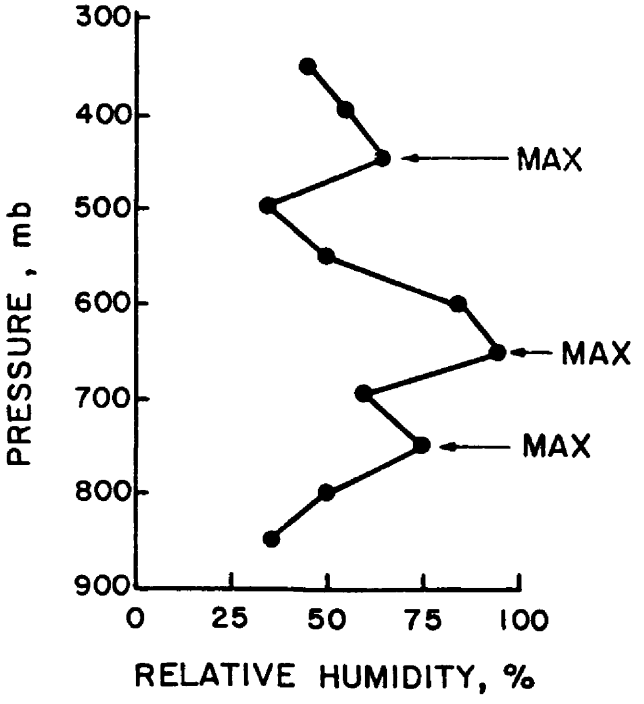

Figure C1. Example of method for designating relatively moist layers

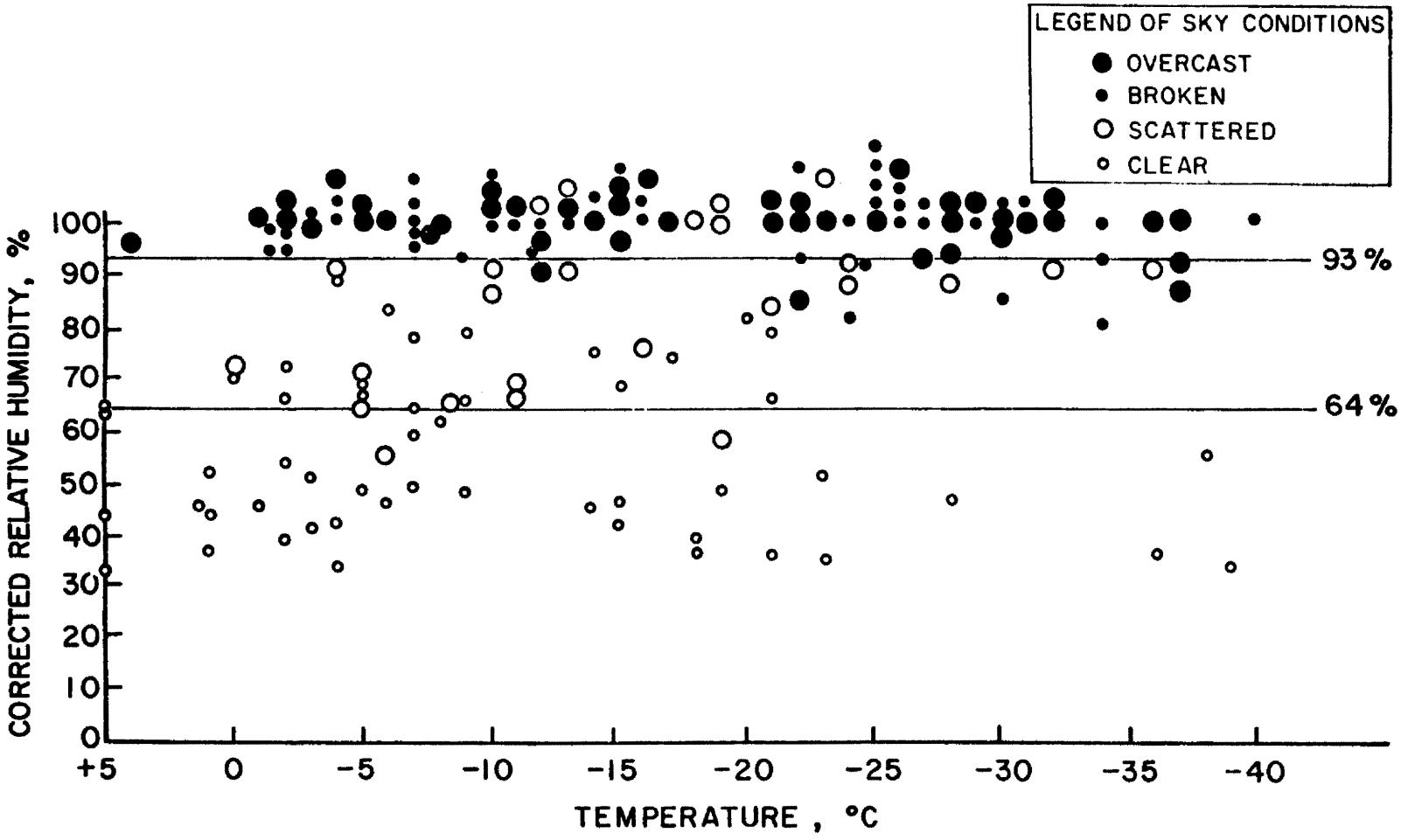

Figure C2. Plot of layer cloud cover conditions on a temperature-corrected relative humidity plane indicating the removal of a temperature-dependent "critical relative humidity" for designating cloud layers using the lithium chloride sensor

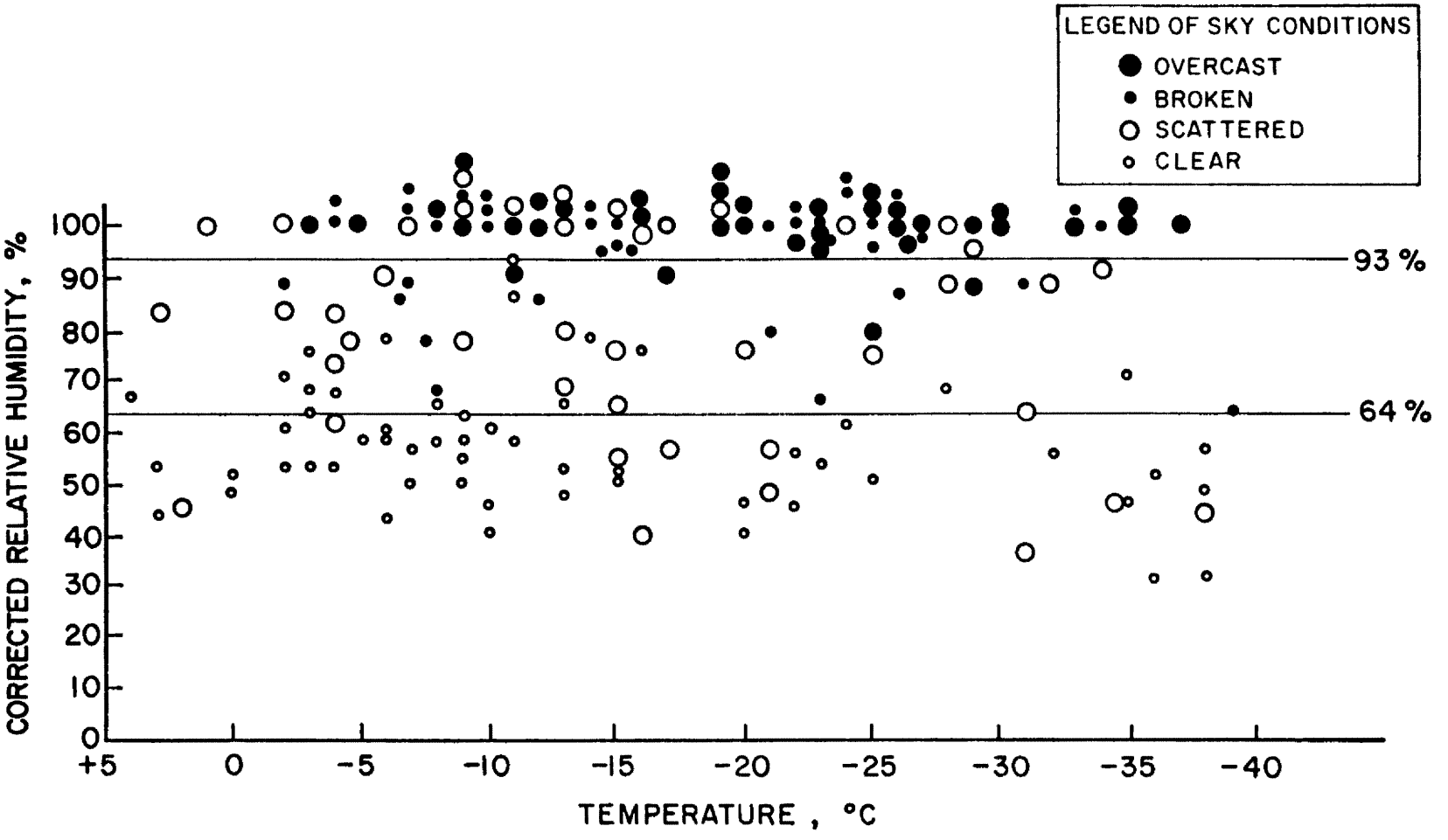

Figure C3. Same as figure C2 except humidity sensor used was the carbon element

APPENDIX D

COMPARISONS OF INTERPOLATED TO OBSERVED RELATIVE HUMIDITY FOR DURANGO, COLORADO

A season of rawinsonde information from Durango in southwestern Colorado was available for comparison to the interpolated values for that point. Since reasonably good relative humidity values are vital for obtaining useable model computations, a study was performed to test the agreement between interpolated and observed humidity values for Durango.

To obtain meaningful data sets for comparison it was necessary to consider the expected terrain influence on the Durango relative humidity profile as the site is quite close to rather large topographic features (see Figure D1). From the nearby terrain features, three classes of flow were designated. First if the mean flow below 600 mb was from a direction of less than 240°, upslope motion was presumed to exist and observed humidity would be expected to be higher than the interpolated value. For flow from 270° through 070° downslope should prevail and with lower observed than interpolated relative humidity. Only in the narrow sector of 240° - 270° flow direction could one perhaps expect reasonably close agreement between interpolated and observed values.

Figures D2 and D3 bear out the reality of the above expectations. While for the 240 - 270° class, the average observed is approximately equal to the interpolated value, there is around a $\pm$ 20% departure to be expected for a given case.

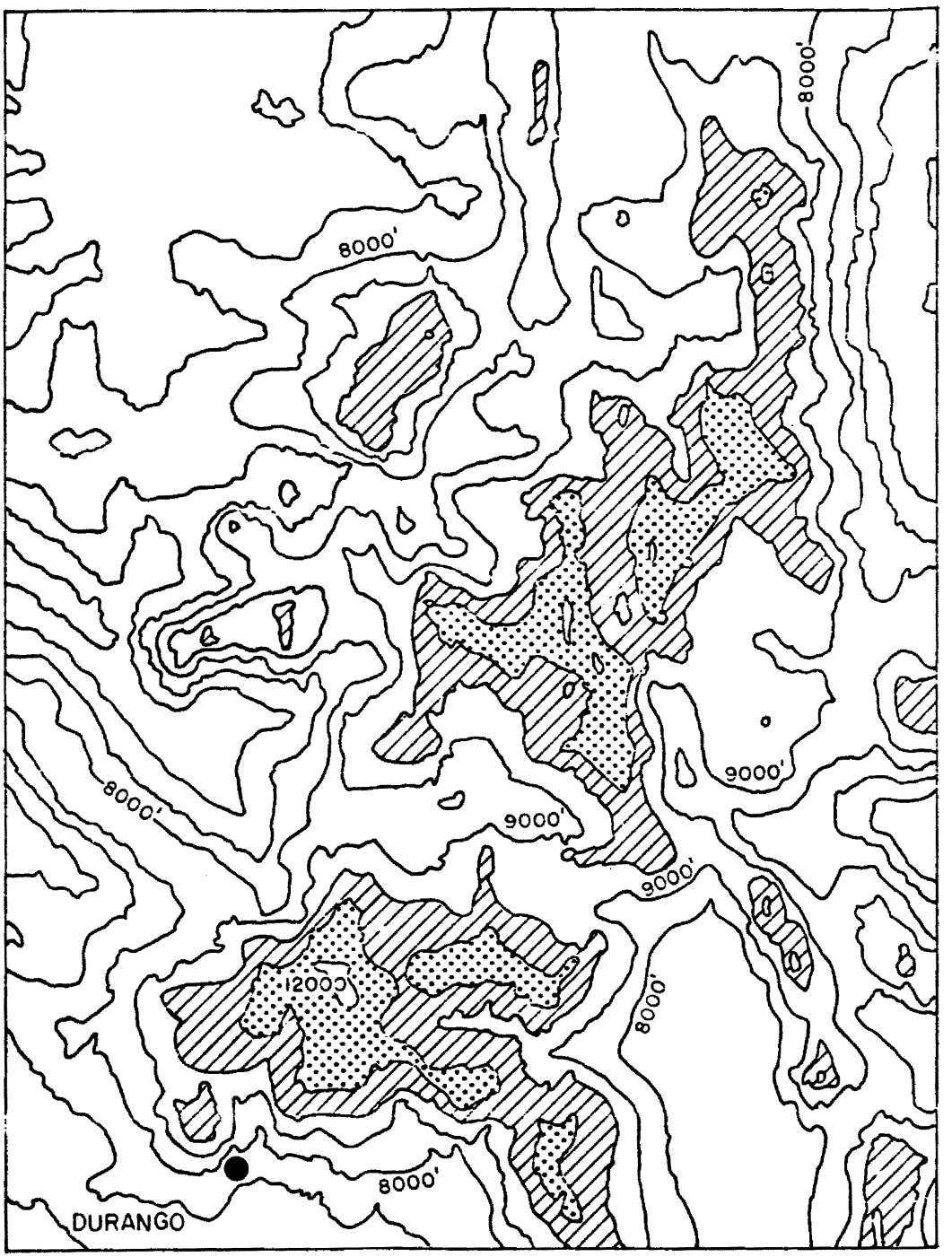

Figure D1. Topographic map with the location of Durango indicated

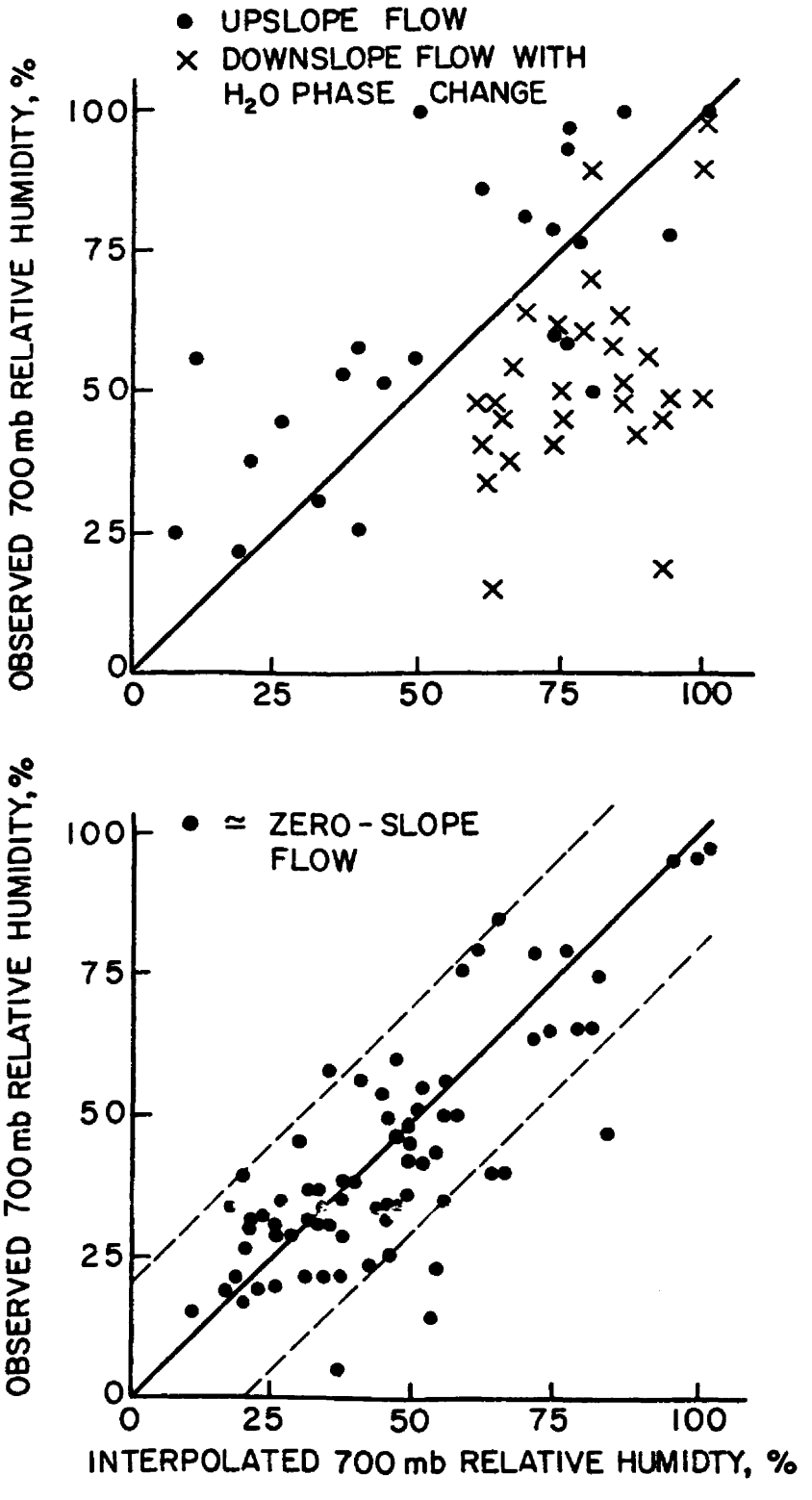

Figure D2. Scatter plot of interpolated versus observed 700mb relative humidity for Durango showing the effects of nearby topography on the degree of agreement

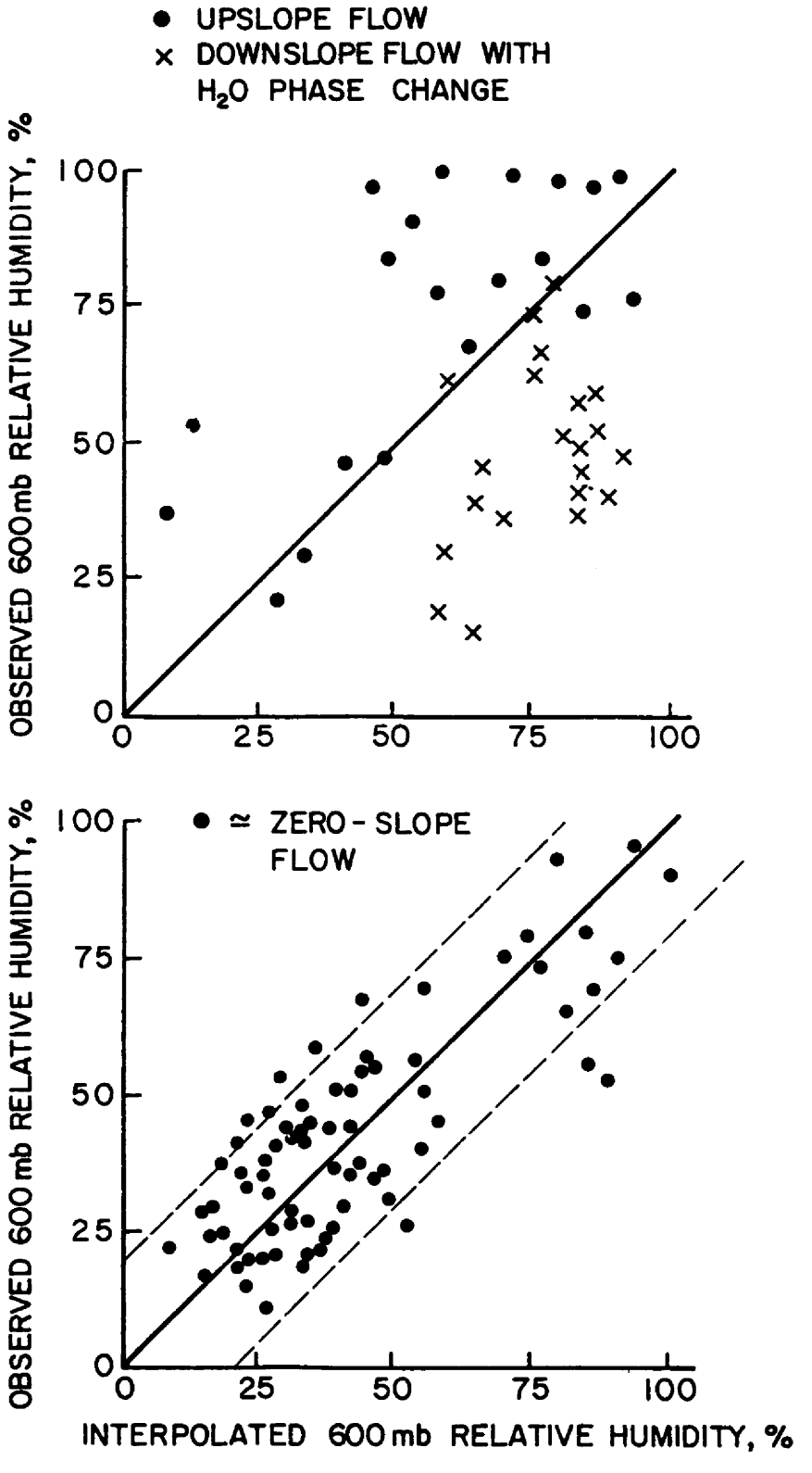

Figure D3. Same as figure D2 for the 600mb level

BIBLIOGRAPHIC DATA SHEET	1. Report No. CSU-ATSP- 287	2.	3. Recipient's Accession No.

4. Title and Subtitle

Orographic Precipitation Model for Hydrometeorological Use

5. Report Date: March, 1978

6.

7. Author(s): J. Owen Rhea

8. Performing Organization Rept. No. CSU-ATSP- 287

9. Performing Organization Name and Address
Dept. of Atmospheric Science
Colorado State University
Foothills Campus
Ft. Collins, Colorado 80523

10. Project/Task/Work Unit No.

11. Contract/Grant No.: Cooperative Agreements 16-332-CA & 16-547-CA

12. Sponsoring Organization Name and Address
U.S.D.A. Forest Service
Rocky Mountain Forest & Range Experiment Station
240 West Prospect
Fort Collins, Colorado 80521

13. Type of Report & Period Covered: Ph.D. Thesis

14. Apr. Jul. 1973-1977

15. Supplementary Notes: This report consists in its entirety of a Ph. D. dissertation by the author, completed and accepted in July, 1977.

16. Abstracts

Research was performed to determine the ability to diagnose the effect of topography on winter precipitation for western Colorado over various time periods for differing wind regimes, employing upper air data and a fine-mesh (10 km grid interval) topographic grid.

To accomplish the objectives, a simple, operationally-oriented orographic precipitation model was developed. The model is two-dimensional, steady state, and multi-layer. It follows parcels at layer mid-points through topographically-induced ascents and descents. Layer budgets of water substance are calculated by (a) allowing precipitation of a constant fraction of the total of local condensation plus imported cloud water, (b) carrying the remainder downstream where it and additional condensate can partially precipitate, and (c) permitting evaporation of cloud water upon descent and of precipitation falling into subsaturated layers. A key feature of this approach is its representation of precipitation shadowing by upstream barriers (when used with a different topographic grid for each wind direction). Effects of large scale vertical motion are added to those of topography.

The model was tested using 13 winter seasons of twice daily upper air measurements as input. Results were summed seasonally and compared to observed spring and summer runoff from watersheds of varying size. Correlation coefficients ranged mainly between 0.75 and 0.94.

A 13 year model mean precipitation map agreed quite well in mountainous areas with one prepared by ESSA (U.S. Department of Commerce), but model estimates in broad valleys were low.

Test quantitative precipitation forecasts (QPF's) were made for one season, using wind direction-dependent model pattern maps as objective aids. Skill scores for 24 hour QPF's ranged from 0.56 to 0.87.

The method should be transferable to other topographically complex areas which are dominated by stratiform precipitation.

17a. Descriptors

Orographic Precipitation Computation; Snowpack Runoff Estimation; Quantitative Precipitation Forecasting; Winter Mountain Snowfall; Hydrometeorology, Mesoscale Climatology; Rainshadow Effects

17c. COSATI Field/Group

18. Availability Statement	19. Security Class (This Report) UNCLASSIFIED X	21. No. of Pages 221
	20. Security Class (This Page) UNCLASSIFIED	22. Price